Structure and Function of DNA Topoisomerase II Beta

Elise Marie Ling

Thesis submitted for the degree of

Doctor of Philosophy

Newcastle University Biosciences Institute

Faculty of Medical Sciences

August 2022

Abstract

Human topoisomerase II beta (TOP2B) is a type II topoisomerase enzyme that modulates DNA topology using the energy from ATP hydrolysis. During catalysis a transient DNA double strand break is made so that another DNA duplex can be passed through the break relieving torsional strain. TOP2B is a homodimer comprising an N-terminal ATPase domain, a breakage reunion core and a C-terminal domain.

The current study investigated the tertiary structure of the ATPase domain of TOP2B and the conformational changes that occur during ATP hydrolysis. The ATPase domain (45-444) was crystallised in the presence of the non-hydrolysable ATP analogue AMPPNP and the ATP hydrolysis product ADP. Moreover, as bisdioxopiperazines are clinically relevant catalytic inhibitors of topoisomerase II that target the ATPase domain, the structure was determined bound to ICRF193, the most potent bisdioxopiperazine. The TOP2B structures reported here lacked the complete N-terminal strap, starting at residue 45. As the strap is the most variable region of the ATPase domain, biochemical characterisation of the full-length ATPase domain (1-444) and the alternative splice variant (1-449) was performed which revealed the strap is inhibitory to ATP hydrolysis.

An increasing number of TOP2B mutations, causative for disease are being identified. Patients can exhibit varying phenotypes from B-cell immunodeficiency to neurological defects like autism. Mutations have been identified throughout the protein, though many concentrate within the TOPRIM domain of the breakage reunion core. Moreover, TOP2B mutations can confer resistance to topoisomerase II targeting drugs. Therefore, to understand the impact of these mutations on enzyme activity, biochemical analysis was performed utilising an *in vivo* yeast complementation system and *in vitro* analysis of the purified proteins (45-1621). Generally, conservative residue changes were tolerated although not all patient mutations were functional *in vivo.* The *in vitro* catalytic activity was variable with some mutations more detrimental than others, potentially accounting for the different phenotypes observed clinically.

Acknowledgements

Firstly, I would like to express my immense gratitude to my supervisors Professor Caroline Austin, Dr Ian Cowell, Professor Tim Blower and Professor Bert van den Berg for their guidance and support throughout my PhD research. Their encouragement and enthusiasm gave me the confidence to explore my own research ideas and develop as a scientist. I would also like to give special thanks to Dr Arnaud Baslé for his invaluable advice and training during the protein purification and crystallisation work. Dr Baslé's guidance allowed me to carry out the structural biology research during the pandemic, for which I am extremely grateful.

I also thank members of the Lakey laboratory in particular, Professor Jeremy Lakey, Dr Helen Waller and Dr Daniel Peters for their help and advice during the bacterial protein expression work. In addition, I would like to thank the members of the Austin laboratory for their friendship over the last four years.

I would like to acknowledge the BBSRC for funding this project, as well as supporting me with further funding to complete a two-month research trip at Sickkids Hospital, Toronto. This visit was part of a collaboration with Dr Michael Wilson, whose laboratory has generated a murine model containing two of the TOP2B mutations I studied *in vitro.*

Finally, I thank all my family and friends who have encouraged and supported me every step of the way. I am hugely grateful for their constant moral support throughout all the highs and lows of the project. In particular, I give a special mention to my parents, Anne-Marie and Stephen, who have supported and helped me endlessly to ensure my research studies went as smooth as possible. I would also like to thank Liam and Matthew for being there to listen to the challenges I faced and encouraging me through the difficult times. And lastly, my three younger sisters who always put a smile on my face! I could not have done it without you!

Declaration

The experiments included in this thesis were performed solely by me, with the exception of the ATPase data for the mutated protein M1 V23S in Chapter 3, Sections 3.8.1 and 3.8.2. These experiments were performed by Will Berry.

Some of the research included in this thesis led to the publication of the following paper:

Ling EM, Baslé A, Cowell IG, van den Berg B, Blower TR, Austin CA. “A comprehensive structural analysis of the ATPase domain of human DNA topoisomerase II beta bound to AMPPNP, ADP, and the bisdioxopiperazine, ICRF193.” Structure. 2022 30(8):1129-1145.e3. PMID: 35660158.

Table of Contents

Abbreviations

Å:	Angstrom
ADP:	Adenosine 5’ diphosphate
ANOVA:	Analysis of Variance
AMPPNP:	5’ adenylyl imidodiphosphate
APS:	Ammonium persulphate
ATP:	Adenosine 5’ triphosphate
BSA:	Bovine serum albumin
ChIP:	Chromatin immunoprecipitation
CTCF:	CCCTC-binding factor
DACA:	N-[2-(dimethylamino) ethyl] acridine-4-carboxamide
dCTP:	Deoxycytidine 5’ triphosphate
dGTP:	Deoxyguanosine 5’ triphosphate
DMSO:	Dimethyl sulphoxide
DNA:	Deoxyribonucleic acid
DNA-PK:	DNA-dependent protein kinase
DSB:	Double strand break
DTT:	Dithiothreitol
ECL:	Enhanced chemiluminescence
EDTA:	Ethylenediaminetetraacetic acid
G-DNA:	Gate DNA
g:	Gram

GUGLA:	Glucose, ura-, glycerol, lactic acid
GyrA:	Gyrase A
GyrB:	Gyrase B
IC_{50}:	50% maximum inhibitory concentration
IPTG:	Isopropylthio-β-galactoside
Kb:	Kilo base
kDa:	Kilo dalton
kDNA:	Kinetoplast DNA
L:	Litre
LA:	Lithium acetate
LB:	Luria bertani
M:	Molar
mAMCA:	Methyl-N-[4-(9-acridinylamino)-2-methoxyphenyl] carbamate hydrochloride
mAMSA:	Amsacrine
MW:	Molecular weight
NES:	Nuclear export sequence
NLS:	Nuclear localisation sequence
OD:	Optical density
PCR:	Polymerase chain reaction
PEG:	Polyethylene glycol
P_i:	Inorganic phosphate

PDB: Protein data bank

PKC: Protein kinase C

PMSF: Phenylmethylsulfonyl fluoride

PTMs: Posttranslational modifications

SDS: Sodium dodecyl sulphate

SDS-PAGE: Sodium dodecyl sulphate polyacrylamide gel electrophoresis

SUMO: Small ubiquitin like modifier

TAE: Tris, acetate, EDTA

TBS: Tris HCl buffered saline

T-DNA: Transport DNA

TEMED: N, N, N', N' -tetramethylethylene diamine

TOP2: DNA topoisomerase II

TOP2A: Human DNA topoisomerase II alpha

TOP2B: Human DNA topoisomerase II beta

TOPIV: DNA Topoisomerase IV

ts: Temperature sensitive

TTBS: Tween, tris HCl buffered saline

Ura-: Synthetic nutrient mixture without uracil

UGLA: Ura-, glycerol, lactic acid

v/v: Volume/volume

w/v: Weight/volume

YPDA: Yeast extract, peptone, glucose, adenine sulphate

List of Figures

List of Tables

Chapter 1 Introduction

1.1 DNA Topology

DNA is a double helical structure composed of two complementary, antiparallel DNA strands that are wrapped around one another into a right-handed structure called B-DNA. The backbone of each strand contains a chain of alternating deoxyribose sugars and phosphate groups. Attached to each sugar is one of the four bases: adenine (A), cytosine (C), guanine (G) or thymine (T) that point inwards to the center of the helix and stack upon each other. Hydrogen bonds occur between the two strands through the bases which keeps the DNA molecule intact. The sequence of bases determines the order of amino acids necessary during the production of proteins. In particular, three consecutive bases determines a single amino acid.

The double helical nature of DNA is essential for the accurate transmission of genetic information but it raises topological issues. To prevent DNA from becoming tangled, eukaryotic DNA is packaged around octamers of histone proteins forming an array of nucleosomes. 145-147 base pairs of DNA are wrapped around two copies of the four core histone proteins: H3, H4, H2A and H2B. Histone H1 acts as a linker histone wrapping another 20 base pairs of DNA around the histones to form the basis of the nucleosome (Kornberg and Lorch 1999). The nucleosomes are then further condensed into chromatin fibers and higher order structures, which gives rise to the final chromosome structure (Wang 1996, Wang 2002, Espeli and Marians 2004, Bates and Maxwell 2005). However, rotation and unwinding of the DNA double helix during cellular processes such as DNA replication and transcription induces torsional stress within the DNA. The double helix twists to accommodate this motion, although because chromosomal DNA ends are fixed in space, the number of turns in the helix remains the same. Therefore, the turns become compressed into a shorter section of DNA impacting DNA topology. The twin domain model of supercoiling (Liu and Wang 1987) where the double helix is converted to either the underwound or overwound state (Bauer, Crick et al. 1980, White and Cozzarelli 1984, Vologodskii and Cozzarelli 1994, Espeli and Marians 2004, Bates and Maxwell 2005) was proposed to describe this characteristic. Underwound or negatively supercoiled DNA has fewer base pairs per helical turn than average whereas overwound or positively supercoiled DNA has more base pairs than average per helical turn (Liu and Wang 1987, Gilbert and Allan 2014).

While negative supercoiling is largely not detrimental, positive supercoiling inhibits most DNA-dependent processes (Gartenberg and Wang 1992, Parvin and Sharp 1993). Positive supercoiling makes it more difficult to separate the individual strands of the double helix during transcription and DNA replication, therefore restricting access to affected genes if left unresolved (Wang 2002, Espeli and Marians 2004, Bates and Maxwell 2005, Falaschi, Abdurashidova et al. 2007, Travers and Muskhelishvili 2007, Gilbert and Allan 2014). Consequently, to regulate and relieve torsional stress, a physical break in the DNA helix must occur allowing strand passage to take place (Wang 1996, Wang 2002, Bates and Maxwell 2005, Leppard and Champoux 2005, Falaschi, Abdurashidova et al. 2007). While torsional stress can be relieved either by single stranded breaks and DNA rotation or by strand passage through a double stranded break, the resolution of knots and tangles requires the presence of double strand breaks in the DNA backbone. DNA topoisomerases are ubiquitous enzymes (EC 5.99.1.3) (Wang 1996) that are vital to catalyse these changes in DNA topology.

1.2 DNA Topoisomerases

DNA topoisomerases have been categorised into two groups depending on whether they catalyse the cleavage of a single DNA strand or a DNA duplex. Type I DNA topoisomerases make a single DNA strand break and pass the opposite strand through the break to remove torsional strain in an ATP independent process (Wang 1996). As such, type I topoisomerases alter the linking number of DNA by +1 or -1. Type I topoisomerases can be further divided into two subfamilies (type IA or type IB) depending on the type of DNA complex they form as a transient intermediate in their reaction cycle. Type IA and type IB topoisomerases are found within all domains of life however, they are structurally unrelated and differ in reaction chemistry. Prokaryotic DNA topo I and III, and eukaryotic DNA topo III are members of the type IA subfamily, introducing a single strand break through the formation of a 5' phosphotyrosine intermediate, and require a divalent metal ion to relax negatively supercoiled DNA (Kirkegaard and Wang 1985, DiGate and Marians 1989, Wallis, Chrebet et al. 1989). By contrast, type IB enzymes (eukaryotic DNA topo I, poxvirus topo I, and archaeal topo V) form a 3’ phosphotyrosine intermediate via an ATP-independent swivel mechanism, where the cleaved strand is rotated around the intact strand. In addition,

type IB topoisomerases can relax both negatively and positively supercoiled DNA (Champoux and Dulbecco 1972, Shuman and Moss 1987, Slesarev, Stetter et al. 1993, Roca 1995, Slesarev, Belova et al. 2001).

In contrast, type II topoisomerases make a double stranded DNA break by cleaving both DNA strands sequentially and become transiently linked to the 5' end of the double strand break through a phosphotyrosyl linkage. Another DNA duplex is then passed through the break, altering the linking number of DNA by +2 or -2 in an ATP dependent process (Brown and Cozzarelli 1979). Like the type I enzymes, type II topoisomerases can be further subdivided into type IIA or type IIB enzymes according to their structure and reaction mechanisms (Gadelle, Filée et al. 2003). The type IIA family relax both positive and negative DNA supercoils through a four base stagger in the opposite DNA strand breaks. Type IIA enzymes include *E. coli* DNA topo IV, eukaryotic DNA topo II and bacteriophage T4 topoisomerase. Bacterial DNA Gyrase is also a type IIA enzyme but possesses the unique feature whereby it can introduce negative supercoils into DNA and remove negative supercoils in the absence of ATP (Reece and Maxwell 1991, Wang 1998). Type IIB enzymes do not share significant structural similarity with type IIA enzymes and lack a protein dimer interface known as the C-gate. Moreover, type IIB enzymes induce a two base stagger between opposite DNA strand breaks (Bergerat, Gadelle et al. 1994). Whereas type IIA topoisomerases are ubiquitous in bacteria and eukaryotes, type IIB members are mostly present in archaea and plants with examples including topo VI and topo VIII (Champoux 2001, Corbett and Berger 2004). Lower eukaryotes such as yeast and *Drosophila* express only one type II topoisomerase, whereas two isoforms have been identified in vertebrates termed topoisomerase II alpha (TOP2A) and topoisomerase II beta (TOP2B) (Tan, Dorman et al. 1992).

1.3 Discovery of DNA Topoisomerases

The first DNA topoisomerase was discovered in 1969 by identification of extracts from *E. coli* that possessed the ability to relax negatively supercoiled DNA (Wang 1969). This activity was later attributed to a single protein termed ω (omega), capable of both DNA strand breakage and religation (Wang 1971). Eight years later the ω protein was renamed *E. coli* DNA topoisomerase I belonging to the type IA family of enzymes (Wang and Liu 1979). In the meantime, eukaryotic DNA topoisomerase I from mouse

extracts was discovered in 1972, possessing a distinct mechanism to *E. coli* DNA topoisomerase I and now belongs to the type IB topoisomerase group (Champoux and Dulbecco 1972). The first type II topoisomerase was discovered in 1976 from *E.coli* and is now known as DNA Gyrase (Gellert, Mizuuchi et al. 1976). Since then type I and type II DNA topoisomerases have been identified in all eukaryotic and prokaryotic cells, in addition to numerous phage and animal viruses (Corbett and Berger 2004).

During the purification of topoisomerase II in 1987 it became apparent that mammals possessed two type II topoisomerase enzymes. Two bands of different molecular weights were observed on an SDS polyacrylamide gel. One band was observed at 170 kDa (p170) and the other was present at 180 kDa (p180). Moreover, different cleavage products were detected after partial proteolysis of the two proteins with *Staphylococcus* V8 protease, suggesting that p170 and p180 were discrete isoforms. Additionally, the two isoforms were immunologically distinct, with antibodies recognising either p170 or p180, disproving the hypothesis that p170 (now known as TOP2A) was a proteolytic fragment of p180 (TOP2B) (Drake, Hofmann et al. 1989). Subsequently, chromosomal mapping confirmed the two isoforms were genetically distinct with the human *TOP2A* gene located on chromosome 17q21-22 (Tsai-Pflugfelder, Liu et al. 1988, Tan, Dorman et al. 1992) and the human *TOP2B* gene on chromosome 3p24 (Tan, Dorman et al. 1992, Davies, Jenkins et al. 1993). In fact, when the *TOP2B* gene was cloned (Austin, Sng et al. 1993) it was determined that *TOP2B* is a paralog of *TOP2A* having originated from a recent ancestral gene duplication event, thought to have occurred in the early chordate lineage (Chung, Drake et al. 1989, Austin and Fisher 1990, Sng, Heaton et al. 1999).

1.4 Biological Roles of DNA Topoisomerase II

DNA topoisomerases are vital for conserving genome integrity and are involved in almost every cellular event that involves DNA. In addition to modulating DNA supercoiling, type II topoisomerases are essential for faithful DNA replication and have fundamental roles in transcription, chromatin remodelling and chromosome segregation. Moreover, type II topoisomerases comprise part of the chromosome scaffold (DiNardo, Voelkel et al. 1984, Holm, Goto et al. 1985, Uemura, Ohkura et al. 1987, Wang 1996). Additionally, topological changes resulting from topoisomerase activity are necessary to increase the accessibility of DNA to the enzymes involved in

recombination (Gangloff, Lieber et al. 1994). Cells lacking type II topoisomerases are non-viable and show major defects in chromosome segregation (DiNardo, Voelkel et al. 1984, Holm, Stearns et al. 1989). Vertebrate cells lacking TOP2A cannot survive, whilst TOP2B null cells grown in culture are viable, but have altered transcriptional profiles (Khazeem, Cowell et al. 2020, Austin, Cowell et al. 2021, Khazeem, Casement et al. 2022).

1.4.1 DNA Replication

DNA topoisomerases are essential enzymes for the initiation of DNA replication, where the DNA substrate must be in a negatively supercoiled state (Wang 1996). In prokaryotes, Gyrase performs this function by introducing negative supercoils in the DNA helix providing the open DNA structure necessary for initiation of replication. Replicative helicases then increase the amount of unwound DNA, required during the initial priming of DNA replication (Nitiss 1998). During this process, the helicase generates positive supercoils ahead of the replication fork as DNA is subject to topological barriers that prevent the free rotation of the DNA duplex around its axis. Consequently, the supercoiling cannot be removed by diffusion along chromatin fibres. Similarly, the advancement of replication forks during the elongation phase of DNA replication generates positive supercoils as the parental strands are separated. Therefore, for DNA replication to continue, a topoisomerase enzyme is required to relieve the positive supercoiling. In prokaryotes, DNA Gyrase, topo III, or topo IV perform this function (Hiasa, DiGate et al. 1994, Hiasa and Marians 1994). Whilst in eukaryotes either topo I or topo II, are necessary as both enzymes can remove positive and negative supercoils (Goto and Wang 1985, Holm, Goto et al. 1985, Brill 1987). However, after elongation, a type II topoisomerase is specifically required to separate the newly replicated molecules and ensure accurate chromosome segregation (Fachinetti, Bermejo et al. 2010). In prokaryotes, topo IV is more effective than DNA Gyrase during this reaction and is most likely the topoisomerase that is required at this stage (Adams, Shekhtman et al. 1992, Zechiedrich, Khodursky et al. 1997), whereas topoisomerase II decatenates the two interlocked double helices in eukaryotes. Studies with Δ topo II yeast cells have fully replicated plasmids, but accumulate as catenated dimers indicating topoisomerase II is essential during the separation of replicated chromosomes (DiNardo, Voelkel et al. 1984).

1.4.2 Transcription

In eukaryotes, transcription occurs in discrete foci known as transcription factories, which are concentrated with large multi subunit RNA polymerases, transcription factors and transcription units (Jackson, Hassan et al. 1993, Wansink, Schul et al. 1993). However, the complexity and size of transcription factories impedes their ability to rotate and accommodate torsional stress during progression along the DNA molecule (Bartlett, Blagojevic et al. 2006, Mitchell and Fraser 2008, Cook and Marenduzzo 2018). Instead, it appears that the template DNA is spooled though a relatively static RNA polymerase complex. Consequently, analogous to replication, the process of transcription generates positive supercoils ahead of the transcription machinery and negative supercoils behind it (Figure 1-1) (Liu and Wang 1987). Thus, in the absence of a functional topoisomerase, supercoils accumulate inhibiting the progression of transcription. Studies with yeast topoisomerase mutants have shown that either a topoisomerase I or topoisomerase II enzyme can efficiently provide the topoisomerase activity necessary for transcription (Schultz, Brill et al. 1992, Cavalli, Bachmann et al. 1996). Furthermore, topoisomerase I and topoisomerase II can act redundantly when enhancing the recruitment of RNA polymerase II to the promoter of highly transcribed genes in yeast (Sperling, Jeong et al. 2011). However, the DNA substrate may play an important role in determining the requirement of topoisomerase activity for successful transcription. For example, a study showed that TOP2A activity was essential for the transcription of chromatin templates but less important for histone-free naked DNA. Upon addition of the topoisomerase II targeting drugs, etoposide or ICRF193, transcription was blocked on chromatin templates whilst transcription on naked DNA was less affected (Mondal and Parvin 2001).

TOP2B also appears to have a role as a gene regulator. TOP2B can introduce transient double strand breaks at promoter regions of specific genes that are crucial to activate gene expression in response to ligand (Ju, Lunyak et al. 2006, Perillo, Ombra et al. 2008, Wong, Chang et al. 2009, Haffner, Aryee et al. 2010, Madabhushi, Gao et al. 2015). Typically, addition of the ligand (e.g., oestrogen or retinoic acid) removes a repressor that is bound to a promoter allowing an activation complex to form. The activation complex can function by looping DNA which brings other regions and enhancers within proximity to the promoter. In some cases, TOP2B is present within these promoter activation complexes in complex with DNA PK and PARP (Austin, Cowell et al. 2021). A double strand DNA break (DSB) has also been identified in these

complexes, which may facilitate the recruitment of other proteins to the promoter, such as chromatin-remodelling enzymes that are necessary for the reorganisation of the chromatin around the transcription start site. Consequently, a TOP2B mediated DSB would lead to more efficient transcriptional activation and implicates TOP2B in the regulation of transcription (Trotter, King et al. 2015).

Additionally, ChIP seq analysis in humans (Manville, Smith et al. 2015) and mouse (Uusküla-Reimand, Hou et al. 2016, Canela, Maman et al. 2017) have identified interactions throughout the genome between TOP2B and regions of open chromatin such as transcription factor binding sites. TOP2B binds to CTCF and peaks of TOP2B and CTCF binding across the genome substantially overlap. CTCF is involved with cohesin in the looping of DNA, however it is not yet understood what function TOP2B has at these sites. TOP2B may modulate DNA supercoiling at the base of loops and at topologically associated domain (TAD) boundaries to facilitate the formation of loop extrusions, and loop anchors consisting of CTCF/cohesin may lead to accumulation of the supercoils as an elongating polymerase approaches them. Consequently, a topoisomerase enzyme associated with the loop anchor may be required to relieve the accumulated supercoils. Moreover, genome-scale location analysis in post mitotic neurones revealed TOP2B binding at methylated lysine 4 of histone H3 sites (H3K4me) suggesting enrichment at promoter regions (Tiwari, Burger et al. 2012). Enhanced binding of TOP2B at highly transcribed genes and promoter regions, supplies further evidence that TOP2B likely plays a regulatory role in the transcriptional activation of certain genes (Uusküla-Reimand, Hou et al. 2016).

TOP2B has been associated with the expression of long genes, likely through its ability to resolve positive supercoiling caused during transcription (Schultz, Brill et al. 1992, King, Yandava et al. 2013, Naughton, Avlonitis et al. 2013, Yu, Davenport et al. 2017). When topoisomerase II was inactivated in yeast, the transcription of long genes was adversely affected, and the number of long transcripts was reduced. The decrease in expression of long genes was attributed to a stall in the progression of RNA polymerase II after transcribing between 2-3 kb, rather than failure to initiate transcription. Indeed, evidence shows that TOP2B is involved in the pause release mechanism to allow a paused RNA polymerase to continue along its pathway in response to activation. In the context of pause release it is hypothesised that a TOP2B DSB recruits the DNA repair machinery which is necessary for continuation of

elongation (Khazeem, Casement et al. 2022). Therefore, expression longer transcripts requires a specific role of topoisomerase II that cannot be compensated for by topoisomerase I (Joshi, Piña et al. 2012).

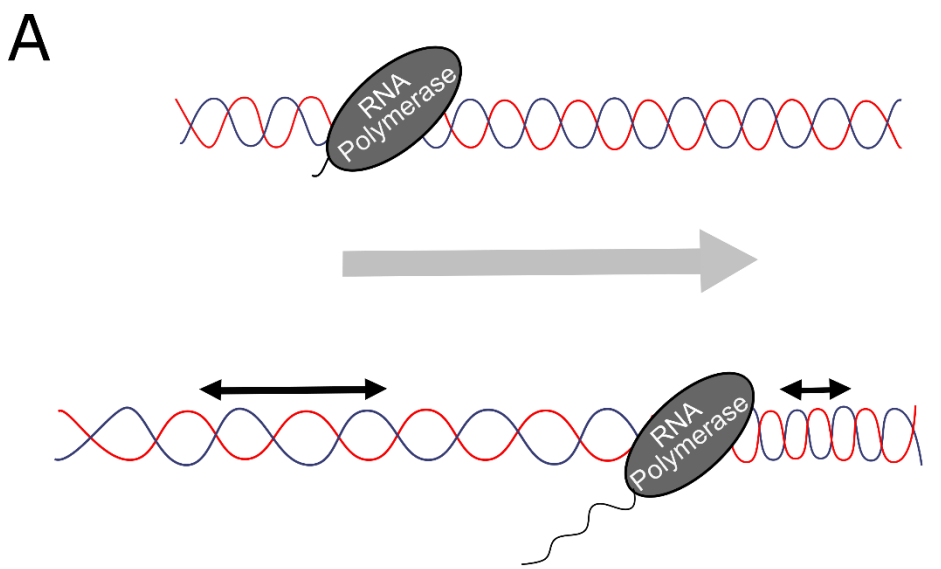

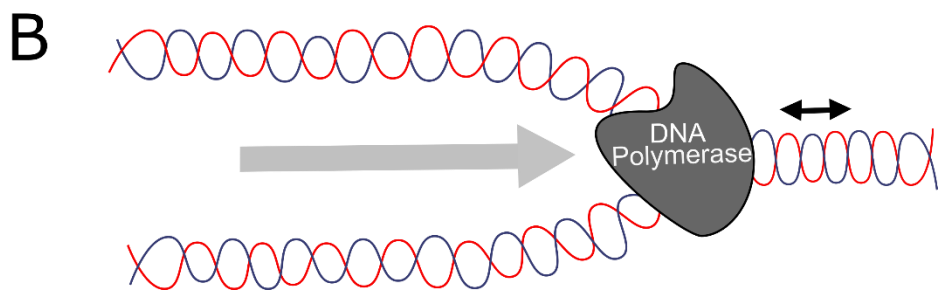

Figure 1-1: Supercoiling in DNA

(**A**) During transcription, RNA polymerase generates positive supercoils ahead of the machinery and negative supercoils behind the machinery. (**B**) During DNA replication, DNA polymerase generates positive supercoils ahead of the machinery, although the newly replicated daughter strands possess the correct topology.

1.4.3 Recombination

The DNA strand passage reactions catalysed by DNA topoisomerases are mechanistically very similar to the breakage and re-joining reactions catalysed by recombinases during site specific recombination (Craig 1988, Landy 1989). Although, topoisomerase enzymes re-ligate the same nucleotides back together that were originally broken in the first transesterification step to maintain genetic integrity. During recombination strand switching occurs to introduce genetic variability. The 3' end of the cleaved top strand is re-joined to the 5' end of the cleaved bottom strand and vice versa during recombination. However, because the chemical mechanisms are very similar between DNA topoisomerases and recombinases, in specific circumstances topoisomerase enzymes can catalyse recombination (Been and Champoux 1981, Tse-Dinh 1986). In addition, topoisomerases can influence recombination by altering the topological state of DNA which determines the accessibility of recombinase enzymes to the DNA substrate (Wang, Caron et al. 1990, Gangloff, Lieber et al. 1994). Furthermore, the relaxation activities of topoisomerases can prevent intertwining of inappropriately paired DNA strands that could otherwise undergo recombination (Dröge 1994).

1.4.4 Chromosome Segregation

The discovery that topoisomerase II is involved in chromosome segregation has largely been achieved from studies of *S. cerevisiae* and *S. pombe topo II* conditional mutants. Both organisms contain a single topoisomerase II gene that is essential for cell viability (Goto and Wang 1984, Uemura and Yanagida 1984). Studies of temperature-sensitive yeast *topo II* mutants at the non-permissive temperature has shown that a functional topoisomerase II enzyme is vital for chromosome segregation during mitosis and meiosis (Uemura, Ohkura et al. 1987, Rose and Holm 1993). In *topo II* yeast mutants, accumulation of intertwined, catenated chromosomes are observed after just one round of DNA synthesis resulting from newly replicated circular plasmids not being separated (DiNardo, Voelkel et al. 1984). Consequently, failure to segregate intertwined DNA molecules causes cell death during mitosis when the cell attempts to divide. Therefore, only mutant cells that are actively progressing through the cell cycle are inviable and when mitosis is inhibited the lethal phenotype is rescued (Holm, Goto et al. 1985). Thus, DNA topoisomerase II is essential during daughter chromosome segregation and without a functional type II topoisomerase increased levels of

chromosome breakage and nondisjunction occur, eventually causing cell death (Holm, Goto et al. 1985, Holm, Stearns et al. 1989).

In addition to its role in chromosome segregation, topoisomerase II is required for efficient nuclear division during meiosis. *S. cerevisiae* and *S. pombe topo II* mutant cells can undergo the initial events in meiosis I such as pre-meiotic DNA synthesis and recombination however cell cycle arrest occurs during the first meiotic cell division (Rose, Thomas et al. 1990, Rose and Holm 1993, Hartsuiker, Bähler et al. 1998). Consequently, topoisomerase II is required to resolve DNA entanglements and intertwining that arise between recombinant homologs at meiosis I (Hartsuiker, Bähler et al. 1998).

In vertebrates, TOP2A is the predominant isoform involved in chromosome segregation. Specifically, TOP2A is vital during G2/M phase of the cell cycle where it facilitates the separation of DNA catenanes. Indeed, deletion of murine TOP2A leads to severe defects in nuclear division and embryonic lethality (Akimitsu, Adachi et al. 2003). Likewise, silencing TOP2A expression in a human cell line inhibited anaphase and cytokinesis causing cell death due to polyploidy (Carpenter and Porter 2004). Similarly, mutations in zebrafish TOP2A have been identified that cause mitotic spindle defects and incompletely decatenated chromosomes during metaphase (Dovey, Patton et al. 2009). Consequently, TOP2A has an essential function in chromosome segregation that cannot be compensated for by the TOP2B isoform.

1.4.5 Chromosome Condensation

Topoisomerase II was the first protein identified in chromosome condensation, which is a fundamental eukaryotic process that involves folding of the chromatin fiber into mitotic chromosomes (Uemura, Ohkura et al. 1987). Since then, the function of topoisomerase II in chromosome condensation has been investigated *in vivo* and *in vitro,* the results of which remain conflicting. Indeed, chromosome morphologies are impacted to varying extents when topoisomerase II is inactivated in different organisms (Baxter and Aragón 2012).

The use of temperature-sensitive yeast mutants have demonstrated topoisomerase II is necessary for chromosome condensation in *S. pombe* (Uemura, Ohkura et al. 1987) but not in *S. cerevisiae* (Lavoie, Hogan et al. 2002). Whilst immunodepletion experiments implicate topoisomerase II in chromatin condensation in chicken

erythrocytes (Newport and Spann 1987, Adachi, Luke et al. 1991). However, inactivating topoisomerase II activity after the completion of chromosome condensation had little effect on the chromosome morphology (Hirano and Mitchison 1993, Cuvier and Hirano 2003). Likewise, when the only topoisomerase II enzyme in *Drosophila* cells was knocked down, chromosomes had a 2.5-fold decrease in chromosome compaction and were morphologically abnormal. However, the overall process of chromosome condensation during mitosis could progress in the absence of topoisomerase II (Chang, Goulding et al. 2003).

Studies using mammalian cells have demonstrated that the decatenation activity of topoisomerase II is not necessary for chromosome condensation and instead, topoisomerase II has a non-enzymatic function whereby interactions with condensin are important (Cuvier and Hirano 2003, Samejima, Samejima et al. 2012). Moreover, a conditional knockout of TOP2A in a human cell line showed TOP2A is essential for chromosome segregation but generally has a redundant function during chromosome condensation (Carpenter and Porter 2004). Instead, chromosome condensation is more severely impacted in cells with a double knockdown of TOP2A and TOP2B. Metaphase chromosomes had ~10% reduction in axial compaction although the chromosomes were still morphologically recognisable. Consequently, mammalian topoisomerase II plays a less important role in chromosome condensation than originally suggested with only minor abnormalities in chromosome structure in the absence of a type II topoisomerase enzyme (Sakaguchi and Kikuchi 2004).

1.4.6 Chromosome Scaffold Protein

Topoisomerase II is proposed to have a structural function in the organisation of metaphase chromosomes. During metaphase in vertebrates chromatin is organised in loops of 50-100 kb bound to a proteinaceous scaffold extending through the chromosome (Laemmli, Käs et al. 1992). The chromosome scaffold is defined as the residual assembly of proteins that remain after DNA and histones are removed from the mitotic chromosomes (Adolph, Cheng et al. 1977). Topoisomerase II is a major component of the chromosome scaffold, with the TOP2A isoform performing this function in human cells (Berrios, Osheroff et al. 1985, Earnshaw and Heck 1985, Chaly and Brown 1996, Rattner, Hendzel et al. 1996). On average there are three TOP2 enzymes per DNA loop at specific DNA sequences termed scaffold attachment regions (SARs) (Gasser, Laroche et al. 1986, Gasser and Laemmli 1986). Other proteins that

comprise the chromosome scaffold, such as cohesin and condensin, have a function in organising interphase chromosome territories and chromatin loops into topologically associated domains (TADs) (Dixon, Selvaraj et al. 2012, Rao, Huntley et al. 2014, Fudenberg, Imakaev et al. 2016). TADs are thought to form partly as a result of cohesin and CTCF-mediated chromatin loop extrusion and represent distinct genome compartments that are physically separated from each other. Accordingly, interactions between regions within the same TAD occur more often than interactions between different TADs (Dixon, Selvaraj et al. 2012, Nora, Lajoie et al. 2012, Sexton, Yaffe et al. 2012).

1.5 Catalytic Mechanism of DNA Topoisomerases

Type II topoisomerase enzymes use the energy from ATP hydrolysis to add or remove DNA supercoils and either introduce or remove DNA tangles and knots. These topological changes rely on a multistep catalytic mechanism following the two-gate model determined by biochemical and structural studies described below (Roca and Wang 1992, Berger, Gamblin et al. 1996, Wang 1998, Champoux 2001, Corbett and Berger 2004). Type II topoisomerase enzymes bind two DNA helices, a gate DNA (G-DNA) at the protein core gate and a transport DNA (T-DNA) at the ATPase domain that dimerises upon ATP binding (Figure 1-2) (Osheroff 1986, Wigley, Davies et al. 1991, Roca and Wang 1992, Berger, Gamblin et al. 1996, Olland and Wang 1999, Campbell and Maxwell 2002, Schmidt, Osheroff et al. 2012). Conformational changes occur in the enzyme caused by ATP hydrolysis which opens the central gate where a transient double strand break (DSB) on the G-DNA is created. This DSB is necessary to allow the passage of the other DNA duplex (T-DNA) through the break and alleviate torsional stress. To produce the DSB, the topoisomerase II dimer first associates with the G-DNA through positively charged residues in the WHD, tower, and TOPRIM domains of the enzyme. A pair of active site tyrosine residues, one from each topoisomerase II monomer, then initiate a transesterification reaction on two phosphodiester bonds on opposite DNA strands four base pairs apart. This gives rise to the “TOP2 cleavage complex” (Liu, Rowe et al. 1983, Worland and Wang 1989) which harbours the “DNA-gate”. At this stage the 5’ phosphoryl groups of the cleaved G-DNA are covalently attached to the phenolic oxygens of the tyrosine residues, leaving a pair of free 3’ hydroxyl groups. The DNA gate then undergoes a closed to

open conformational change in which the tyrosine linked 5’ DNA ends of the cleaved G-DNA separate to create a physical gap for the passage of T-DNA (Lindsley and Wang 1991, Roca and Wang 1992). Upon completion of strand passage, the DNA-gate must return to the original closed conformation to allow religation of the G-DNA by reversing the transesterification reaction. Subsequently, a second ATP molecule is hydrolysed and the inorganic phosphate released which causes a further conformational change to occur whereby the bottom C-terminal gate is opened. To ensure the T-DNA exits the enzyme through the C-terminal gate the upper gate remains closed (Wei, Ruthenburg et al. 2005). Finally, the enzyme is reset for another round of catalysis by re-opening the N-gate dimer interface to its original conformation (Figure 1-2) (Harkins, Lewis et al. 1998, Chen, Huang et al. 2018).

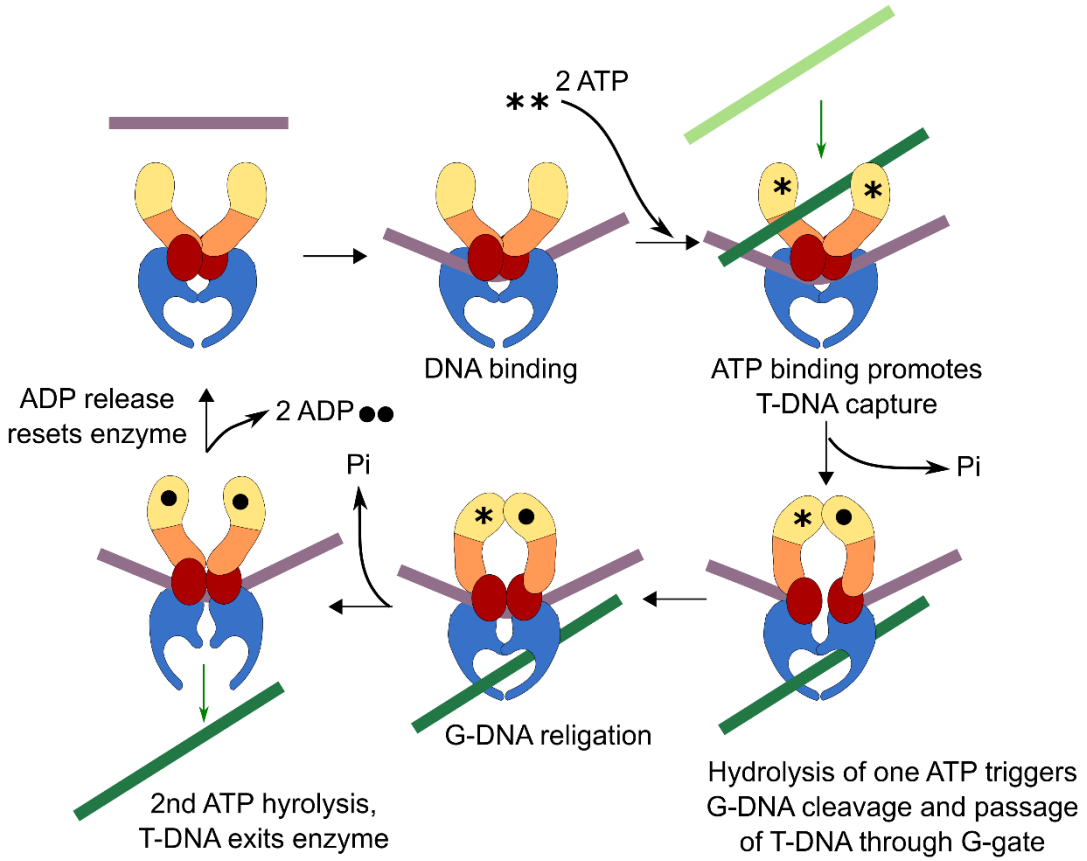

Figure 1-2: Catalytic mechanism of type II topoisomerase enzymes

In the absence of bound G-DNA and ATP the enzyme is in an 'open' conformation with the ATPase (yellow and orange) domains from each monomer separated. When the DNA which is to be cleaved, G-DNA (purple) binds a conformational change occurs which brings the active-site tyrosine's within the A' domain (blue) into the conformation for DNA cleavage. Next, ATP (denoted by *) binds and the ATPase domains dimerise causing a further conformational change in the enzyme. During ATPase domain dimerisation, a second DNA duplex, T-DNA (green) is captured and passed through the break in the G-DNA into the central cavity of the enzyme. Once the T-DNA has entered the central cavity religation of the G-DNA can occur. A linked conformational change opens the C-gate through which the T-DNA exits as described in the two-gate model (Roca, Ishida et al. 1994, Berger, Gamblin et al. 1996, Wang 1998). ATP hydrolysis is necessary to reset the enzyme back to its original conformation for another round of catalysis. Figure adapted from (Schmidt, Osheroff et al. 2012).

1.5.1 DNA Binding

The first step of catalysis requires a DNA substrate to bind to the topoisomerase II enzyme. Two DNA helices bind to topoisomerase II, the G-DNA at the enzyme core and the T-DNA at the ATPase domain. It is necessary for topoisomerase II to bind two DNA helices at the same time in order to perform its essential function during segregation of intertwined chromosomes at mitosis, and in anchoring chromatin loops to the chromosome scaffold.

The process of DNA binding to topoisomerase II does not require divalent cations or ATP (Osheroff 1986, Osheroff 1987, Hung, Luo et al. 1996). In fact, increasing the salt concentration has a negative effect on DNA binding, with maximum DNA binding occurring at low salt concentrations (Osheroff 1986, Osheroff 1987, Lee, Sander et al. 1989, West and Austin 1999). This suggests electrostatic interactions are important for DNA binding to topoisomerase II (Shelton, Osheroff et al. 1983). In addition, the pH impacts interactions between topoisomerase II and DNA, with maximum DNA binding occurring at a low pH (Lee, Sander et al. 1989). Studies with *Drosophila* topoisomerase II revealed both DNA helices bind to topoisomerase II independently and the G-DNA binds with a greater affinity than the T-DNA (Corbett, Zechiedrich et al. 1992). Moreover, topoisomerase II can perform cleavage with only the G-DNA bound suggesting the T-DNA isn't necessary for this step in catalysis. However, complete activation of the ATP hydrolysis activity of topoisomerase II requires both DNA helices bound, as both DNA binding sites signal to the ATPase domains of topoisomerase II (Mueller-Planitz and Herschlag 2006).

As a mechanism to differentiate between DNA substrates and products, eukaryotic type II topoisomerases preferentially bind supercoiled DNA over relaxed DNA (Osheroff 1986). Moreover, topoisomerase II can recognise secondary structures which are unique to negatively supercoiled DNA. For example, left-handed Z-DNA, can be generated during transcription as a result of the negative supercoiling which arises (Lee, Kim et al. 2010). Such torsional strain is sufficient to induce a B- to Z-DNA structural change (Jaworski, Higgins et al. 1991, Wittig, Wölfl et al. 1992, Wang 1996). Thus, to maintain the conventional right-handed B-DNA structure, topoisomerases have a preference for binding and cleaving Z-DNA over B-DNA (Glikin, Jovin et al. 1991, Arndt-Jovin, Udvardy et al. 1993). In addition, cleavage of DNA hairpins by topoisomerase II is also influenced by the secondary structure as well as the DNA

sequence (Froelich-Ammon, Gale et al. 1994). Similarly, human TOP2B binds and cleaves a four-way DNA junction with higher affinity than a linear DNA substrate, and TOP2B bound to a four-way junction complex was significantly more salt stable than the complex with linear DNA (Rose, Thomas et al. 1990, West and Austin 1999). Hence, the secondary structure of the DNA substrate may influence topoisomerase II binding to a greater extent than the base sequence.

1.5.2 DNA Cleavage

After the DNA substrate has bound to topoisomerase II, cleavage of the DNA duplex occurs. Type II topoisomerases make sequential, staggered cuts in the DNA phosphodiester backbone on opposite strands of the double helix, evidenced by the presence of nicked DNA as an intermediate in the reaction (Zechiedrich, Christiansen et al. 1989). Cleavage requires the presence of a divalent cation and involves two successive transesterification reactions on opposite DNA strands (Liu, Rowe et al. 1983). Magnesium (Mg^{2+}) is the physiological cation utilised by type II topoisomerase enzymes, although DNA cleavage can occur in the presence of (calcium) Ca^{2+} or (manganese) Mn^{2+} ions *in vitro* (Osheroff and Zechiedrich 1987, Gilroy and Austin 2011). The DNA intermediate that occurs after DNA cleavage but before strand passage is known as the cleavable complex and is in equilibrium between the cleaved and ligated states.

The first step in DNA cleavage requires the enzyme tyrosyl groups from each monomer to cut an internucleotide phosphate group in the non-covalently bound G-DNA segment. A covalent DNA-protein bond at the 5’ end of the transiently broken DNA strand is formed, leaving an exposed 3’ hydroxyl group at the opposite end of the cleaved strand. The scissile bonds of the two double helix strands are staggered producing a four base 5’ overhang and are located across the major groove from one another. This covalent protein–DNA linkage is essential to prevent the cleaved G-DNA from dissociating away from the enzyme, which could otherwise result in DNA translocations, and conserves the bond energy of the DNA backbone (Berger, Gamblin et al. 1996, Wang 1996, Wang 1998, Schoeffler and Berger 2005).

The DNA cleavage reaction by type II topoisomerases utilises a general acid-base mechanism. The acidic residues within the TOPRIM domain and the catalytic Mg^{2+} ion associate with the active site tyrosine residues in the WHD domain so that they are in

proximity for catalysis. Cleavage is then initiated when a basic residue deprotonates the active site tyrosine hydroxyl group. Then the oxyanion can attack the scissile phosphate (Deweese and Osheroff 2009). After which, a conserved arginine residue adjacent to the active site tyrosine positions the scissile phosphate so that the transition state is stabilised (Berger, Fass et al. 1998).

For cleavage, topoisomerase II requires a DNA substrate with a length of 16 base pairs minimum in order for all necessary regions of the protein to be contacted. There is some DNA sequence preference for cleavage, although the stringency of sequence recognition is low (Spitzner and Muller 1988, Burden and Osheroff 1999, Mueller-Planitz and Herschlag 2007) and the two human type II topoisomerases cleave with similar base preferences (Strumberg, Nitiss et al. 1999). This is required as topoisomerase II cannot be restricted to specific sites in the genome in order to complete its function of relieving torsional strain on a global scale (Lund, Andersen et al. 1990). Moreover, protein-DNA interactions in addition to DNA bending have an important function in determining the cleavage efficiency (Vélez-Cruz, Riggins et al. 2005, Deweese and Osheroff 2010, Lee, Dong et al. 2013, Jang, Son et al. 2019).

1.5.3 Strand Passage

For type II topoisomerase enzymes, strand passage reactions cause the linking number of DNA to change by +2 or -2. To facilitate this reaction, topoisomerase enzymes have a protein structure containing a large central cavity that can capture the DNA strands. Strand passage is coordinated by the ATPase domains of topoisomerase II, which dimerise in the presence of ATP to capture the T-DNA. The ATPase domains also stimulate G-DNA cleavage and use the energy from ATP hydrolysis to coordinate the successive opening and closing of the gates (Schmidt, Osheroff et al. 2012). Topoisomerases can perform distributive relaxation reactions where the T-DNA is passed through the break once or alternatively the enzyme can initiate another round of catalysis with the same T-DNA being passed through the break multiple times before re-ligating the G-DNA (Roca and Wang 1994, Roca, Berger et al. 1996, Chen, Huang et al. 2018).

1.5.4 DNA Ligation

Following strand passage, topoisomerase II reseals the DNA break which is vital to maintain chromosomal integrity during catalysis (Robinson and Osheroff 1991). If

ligation activity is impaired, cellular levels of topoisomerase II associated DNA breaks would increase which would ultimately have lethal consequences for the cell (Baguley and Ferguson 1998, Fortune and Osheroff 2000). The DNA ligation reaction is less well characterised than the cleavage reaction although, essentially it is the reverse of the transesterification reaction used to cleave the DNA and restores the phosphodiester bond. As is the case with DNA cleavage, the DNA ligation reaction of G-DNA is not concerted with ligation of the top strand occurring at a threefold faster rate than the bottom strand (Bromberg, Hendricks et al. 2002). Ligation of G-DNA occurs without a high energy co-factor as the energy of the phosphodiester bond is maintained within the covalent phosphotyrosine enzyme bond. However, the presence of a divalent cation is necessary for DNA religation, with Mg^{2+} and Ca^{2+} ions able to perform this function (Deweese and Osheroff 2010).

To ensure the correct 5' ends are religated back together, the enzyme is covalently bound to the two DNA strands. In addition, a secondary mechanism is employed where complementary base pairing occurs between both strands (Lindsey, Bromberg et al. 2004). The ligation step is independent of DNA cleavage and is determined by chemical reactions rather than the binding affinity of topoisomerase II for its DNA substrate (Bromberg, Hendricks et al. 2002). The active site tyrosine residues are predominantly uninvolved in ligation, apart from providing a leaving group. Similarly, the adjacent arginine residue (Arg804 in TOP2A and Arg820 in TOP2B) that is crucial for positioning DNA during cleavage, has only a minimal function in ligation (Lindsey, Bromberg et al. 2004). Once ligation is complete, topoisomerase II is released from the DNA (Deweese and Osheroff 2010).

Failure to successfully complete ligation causes DNA DSBs that are covalently attached to the active site tyrosine of topoisomerase II through a 5′-phosphotyrosine bond (5′-Y) (Burden and Osheroff 1998). This results in a specific DNA lesion known as a topoisomerase II DNA–protein crosslink (TOP2-DPC). Many drugs that target topoisomerase II such as etoposide or doxorubicin (discussed further in Section 1.16) increase the levels of topoisomerase II associated DNA breaks by inhibiting the DNA ligation step. As a result, TOP2-DPCs accumulate which can eventually result in apoptotic cell death (Pommier 2013). Therefore, a robust DNA damage response (DDR) to identify and repair TOP2-DPCs is necessary to maintain genome integrity.

1.5.5 ATP Hydrolysis and Enzyme Turnover

ATP hydrolysis is required for topoisomerase II enzyme turnover, although DNA cleavage can occur in its absence. Two sequential ATP hydrolysis reactions happen during catalysis of type II topoisomerases (Figure 1-2). The first ATP hydrolysis event is necessary for ATPase domain dimerisation, T-DNA capture and G-DNA cleavage. After strand passage the first ADP molecule is then released (Baird, Harkins et al. 1999). Whilst the second ATP hydrolysis reaction facilitates the release of T-DNA and is required to reset the enzyme back to its original conformation to permit another round of catalysis (Bjergbaek, Kingma et al. 2000, Mueller-Planitz and Herschlag 2006).

Yeast TOP2 (Lindsley and Wang 1993) and human TOP2A (Campbell and Maxwell 2002) kinetic studies have demonstrated that each protein dimer binds two ATP molecules in a cooperative manner. The first ATP molecule binds to topoisomerase II and induces a conformational change in the enzyme, which causes the enzyme to have a higher affinity for ATP so that the second nucleotide binds more rapidly. The first ATP molecule is hydrolysed quickly, whilst hydrolysis of the second ATP molecule is rate limited by the release of P_i or ADP. ATP hydrolysis is essential for enzyme turnover with topoisomerase II enzymes bound to the non-hydrolysable ATP analogue, AMPPNP only able to catalyse one round of strand passage (Osheroff 1986). The number of ATP molecules hydrolysed per reaction varies according to the number of ATP molecules available. When ATP is at a sub-saturating concentration each monomer hydrolyses one ATP molecule during the catalytic cycle, however when ATP is saturating multiple hydrolysis events occur even in the absence of strand passage (Lindsley and Wang 1993). Moreover, DNA binding can stimulate the ATPase activity of type II topoisomerases (Hammonds and Maxwell 1997, Gardiner, Roper et al. 1998, West, Turnbull et al. 2002).

1.6 *In Vitro* Analysis

The catalytic activity of type II topoisomerases can be studied *in vitro* using relaxation, decatenation, cleavage, and ATP hydrolysis assays. Relaxation and decatenation assays assess strand passage activity such that a functional ATPase domain and breakage reunion core are necessary (Papapietro, Chandra et al. 2020), while DNA cleavage and ATP hydrolysis assays measure one individual step in the catalytic cycle.

DNA cleavage assays measure the cleavage-ligation equilibrium of topoisomerase II via its ability to cleave a linear oligonucleotide or a plasmid DNA substrate, whereas ATP hydrolysis assays measure the ability of the ATPase domain of topoisomerase II to hydrolyse ATP, releasing ADP and inorganic phosphate (P_i).

1.7 *In Vivo* Analysis

Yeast has been used extensively as a model organism to study topoisomerases, for reasons such as having an efficient DNA transformation system, rapid eukaryotic growth, and a well-defined genetic system. Specifically, *S. cerevisiae* strains are most commonly used due to the presence of a stable haploid and diploid state (Sherman 2002). Yeast cells differ from higher eukaryotes as they only contain one type II topoisomerase enzyme and two type I topoisomerases, although the latter aren't essential for cell viability (Reid, Benedetti et al. 1998). Therefore, yeast strains bearing a deletion in topoisomerase I genes have been created to aid purification of topoisomerase II enzymes.

Yeast strains are available that contain a temperature-sensitive (*ts*) mutation in the topoisomerase II gene, *top2-4.* Consequently, growth of such cells at the non-permissive temperature, 35 °C or above, causes cell death unless transformed with a plasmid encoding a functional topoisomerase II. Growth at the semi-permissive temperature of 30 °C results in some topoisomerase II activity so that cell viability is maintained but growth is less than at 25 °C where yeast topoisomerase II is not affected. The *top2-4* mutation provides an *in vivo* system for complementation analysis where plasmid borne topoisomerase II enzymes can be studied. Both human isoforms of topoisomerase II can complement the yeast strain JN394 at the non-permissive temperature (Wasserman, Austin et al. 1993, Meczes, Marsh et al. 1997).

1.8 Human Type II DNA Topoisomerases

Human cells encode six different topoisomerases; TOP1, TOP1mt, TOP2A, TOP2B, TOP3A and TOP3B, two of which are type II topoisomerases (TOP2A and TOP2B) (Cowell, Willmore et al. 1998). The cDNAs for both type II human isoforms have been cloned (Tsai-Pflugfelder, Liu et al. 1988, Chung, Drake et al. 1989, Austin and Fisher 1990, Austin, Sng et al. 1993, Davies, Jenkins et al. 1993), and the proteins

have been expressed recombinantly in yeast (Wasserman, Austin et al. 1993, Austin, Marsh et al. 1995). *In vitro* cleavage experiments have shown both enzymes can promote drug-induced DNA cleavage although the two isoforms have different DNA cleavage specificities (Drake, Hofmann et al. 1989, Austin, Marsh et al. 1995). In addition, both TOP2A and TOP2B have been implicated in drug resistance (Dereuddre, Frey et al. 1995, Harker, Slade et al. 1995).

The two human type II isoforms are regulated independently with different temporal and spatial expression. TOP2A protein levels rise in late S phase, peak in G2M, and decrease as cells complete mitosis (Heck, Hittelman et al. 1988, Woessner, Chung et al. 1990, Woessner, Mattern et al. 1991, Prosperi, Negri et al. 1994). Tissues containing many proliferating cells such as the thymus, spleen, bone marrow, intestine and testis show the greatest expression of TOP2A as demonstrated by Northern and Western analysis. Moreover, there is a positive correlation between the cellular concentration of TOP2A and the rate of proliferation, consistent with its role in mitotic processes (Drake, Hofmann et al. 1989). Protein expression of TOP2A is regulated in part post-transcriptionally by changing mRNA stability and increasing the rate of protein degradation during the transition from M to G1 phase (Goswami, Roti Roti et al. 1996). In contrast, expression of TOP2B is more widespread, with TOP2B mRNA detectable in all tissue types including fully differentiated tissues (Capranico, Tinelli et al. 1992, Holden, Rolfson et al. 1992, Juenke and Holden 1993, Watanabe, Tsutsui et al. 1994). The TOP2B isoform is present throughout the cell cycle and has a critical role during development (Prosperi, Negri et al. 1994, Meyer, Kjeldsen et al. 1997). The half-life of TOP2B is more than 40 hours and is stable during the transition from M to G1 phase unlike TOP2A (Kroll and Rowe 1991, Kimura, Nozaki et al. 1996). Only the TOP2B isoform is present in post-mitotic cells such as neurons and cardiomyocytes.

TOP2A and TOP2B cannot functionally compensate for each other *in vivo*. Deletion of murine *TOP2B* results in defective brain development in embryos and perinatal death upon birth and cultured neurons derived from TOP2B knockout mice display reduced neurite outgrowth (Nur, Meiners et al. 2007). Moreover, gene expression is altered in TOP2B knockout cells (Lyu, Lin et al. 2006, Tiwari, Burger et al. 2012, Madabhushi, Gao et al. 2015, Khazeem, Cowell et al. 2020, Khazeem, Casement et al. 2022) and many of the genes whose expression changes are involved in neuronal functions, supporting the hypothesis that TOP2B is necessary for activating and

repressing specific developmental genes. In contrast, inactivating *TOP2A* caused defects in nuclear division and early embryonic lethality, as TOP2A is the isoform that decatenates sister chromatids during mitosis (Akimitsu, Adachi et al. 2003, Lyu and Wang 2003, Thakurela, Garding et al. 2013).

1.9 Structural Properties of DNA Topoisomerases

Despite the different functions *in vivo*, human TOP2A and TOP2B protein sequences share a large amount of homology (Figure 1-3). Overall, the amino acid sequences are 68% identical between TOP2A and TOP2B. However, this homology is not equally distributed throughout the protein. The C-terminal regions have the least similarity with only 34% identity, whereas the N-terminal region is the most conserved region displaying 82% sequence identity (Austin, Sng et al. 1993).

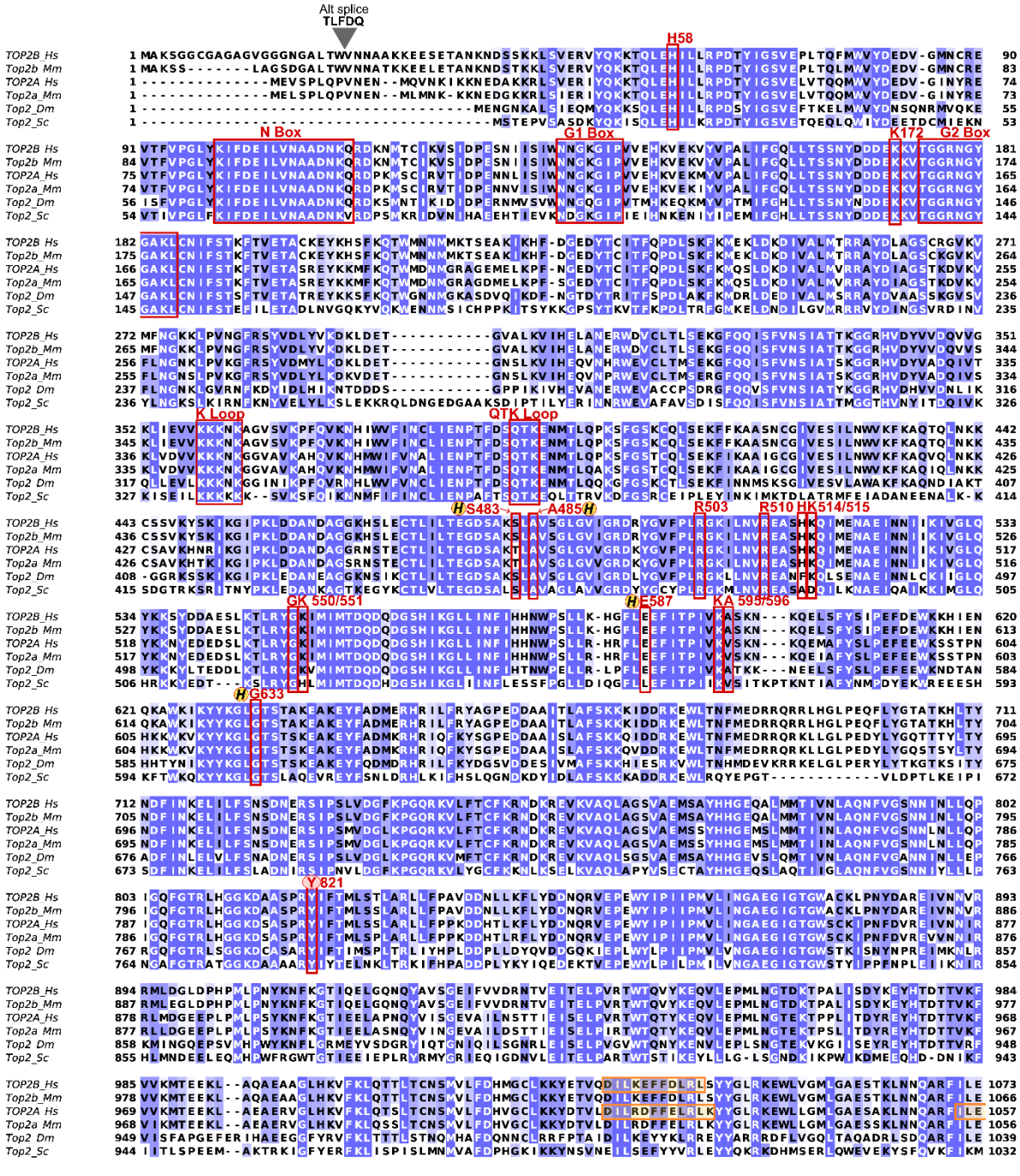
Alt splice
TLFDQ
H58
N Box
G1 Box
K172
G2 Box
K Loop
QTK Loop
S483
A485
R503
R510
HK514/515
GK 550/551
E587
KA 595/596
G633
Y821

Figure 1-3 Alignment of various eukaryotic type II topoisomerase enzymes

Clustal alignment of human TOP2B, mouse TOP2B, human TOP2A, mouse TOP2A, *Drosophila* TOP2 and *S. cerevisiae* TOP2. Amino acid numbering is shown, and residues mutated throughout this study are highlighted. The N, G1, and G2 boxes indicated in red as well as the K loop and the QTK loop in the ATPase domain. The nuclear localisation signal (NLS) and nuclear export signal (NES) in the C-terminal domain highlighted in green and yellow respectively.

Prior to protein crystallography, information about the structure of topoisomerases was deduced by limited proteolysis studies. SV8 protease cleaves human TOP2A, human TOP2B and yeast TOP2 enzymes at three proteolytic sites A, B, and C (Figure 1-4A), breaking the enzyme into four discrete domains ATPase, B′ domain, the A′ domain and the C-terminal domain (CTD) (Figure 1-4B). The N-terminal domain contains the ATP binding and hydrolysis region, the B′ and A′ domains comprise the breakage reunion catalytic centre, and the C-terminal domain contains the nuclear location signals (Brown and Cozzarelli 1979, Reece and Maxwell 1989, Lindsley and Wang 1991, Berger, Gamblin et al. 1996). In contrast, the prokaryotic enzymes are tetrameric, composed of A and B subunits. The amino acid sequence of the N-terminal region of the eukaryotic enzyme is homologous to the bacterial Gyrase B subunit (GyrB) containing the ATP-binding domain (Ali, Jackson et al. 1993). Whilst the A subunit of Gyrase (GyrA) is related to the C-terminal half of eukaryotic topoisomerase II and contains the active site tyrosine residue for DNA cleavage (Reece and Maxwell 1989). The C-terminal domains of type II topoisomerase enzymes share little homology, even with enzymes from closely related species. Moreover, the function of the C-terminal domain is not well understood, though in prokaryotes it is believed that the C-terminal domain assists in DNA binding (Reece and Maxwell 1991). In eukaryotes the C-terminal domain possesses the nuclear localisation signals and many phosphorylation sites (Gasser, Walter et al. 1992, Crenshaw and Hsieh 1993, Caron, Watt et al. 1994, Wells and Hickson 1995).

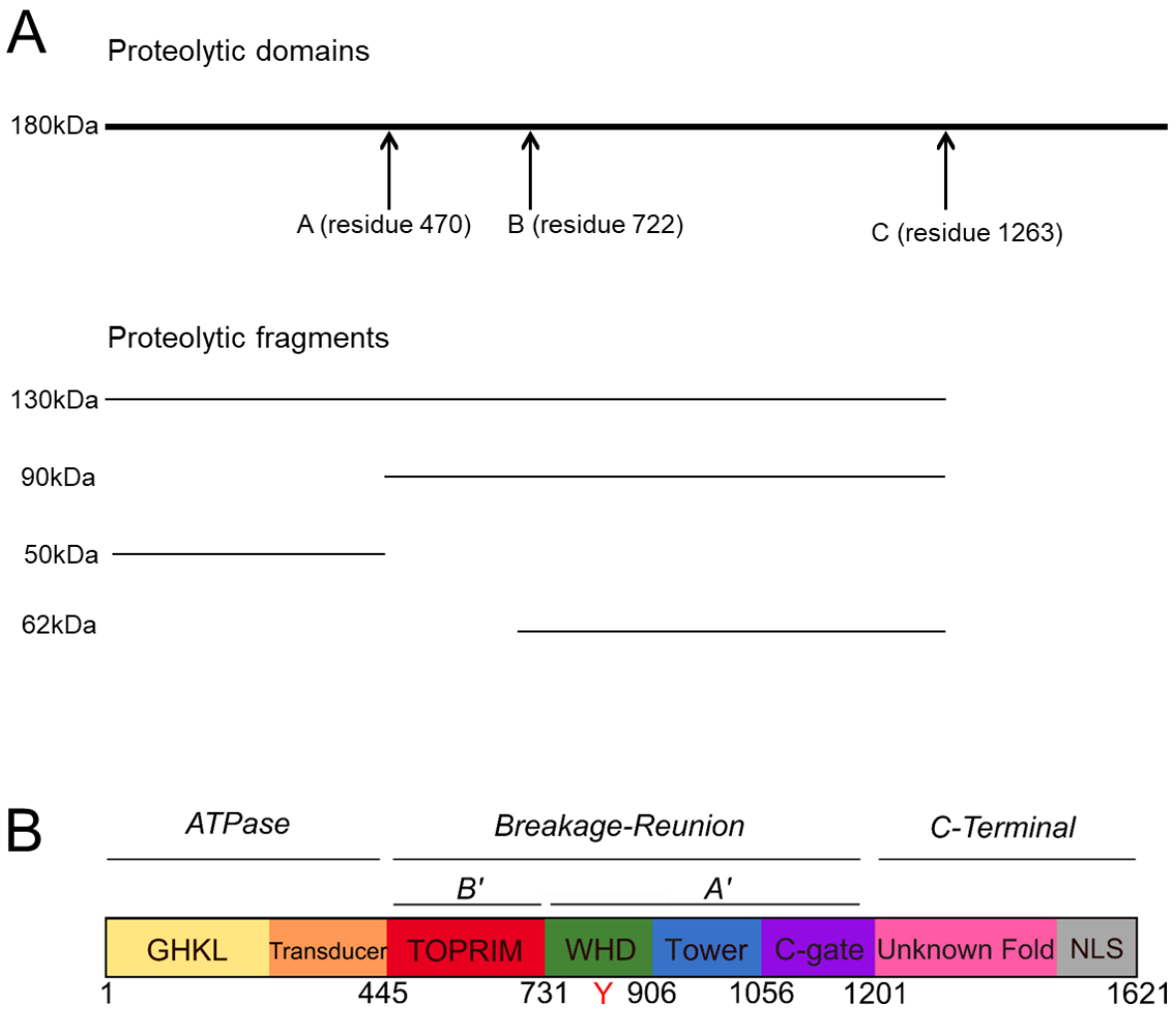

Figure 1-4: Schematic representation of the domain arrangement of human TOP2B and the proteolytic domains

(**A**) The proteolytic domains reported by Austin et al (Austin, Marsh et al. 1995) are indicated in a line diagram with their corresponding residue numbers and the size of the proteolytic fragments shown below. (**B**) Human topoisomerase II consists of four domains: N-terminal ATPase, B', A', and the C-terminal domain (CTD). The B' and A' domains comprise the breakage reunion domain, with the B' domain containing a TOPRIM domain (red), and the A' domain containing winged helix domain (WHD) (green), Tower (blue), and C-gate domain (purple). The catalytic tyrosine is found within the WHD domain, indicated by a red Y. Within the ATPase domain is a GHKL domain at the N-terminus (yellow) and a transducer domain forming the N-gate adjacent to this (orange). The CTD contains an unknown fold (pink) and a nuclear localisation signal (NLS) at the C-terminus (grey). Amino acid numbering is shown below.

1.10 N-terminal ATPase Domain

The N-terminal ATPase domain is highly conserved in all type II topoisomerases and has the highest sequence conservation of the whole enzyme (Figure 1-3). The ATPase domain is essential and sufficient for ATP hydrolysis, demonstrated by the ATPase hydrolysis activity of isolated N-terminal fragments of human TOP2A, *S. cerevisiae* TOP2, and GyrB (Classen, Olland et al. 2003). The ATPase domain is split into two subdomains; GHKL subdomain and the transducer subdomain (Figure 1-4B) (Oestergaard, Giangiacomo et al. 2004).

1.10.1 GHKL Subdomain

All type II topoisomerases contain an N-terminal strap that forms the beginning of the ATP binding site, located at the N-terminus of the protein. The ATP-binding fold within this region is known as the Bergerat fold which is common to the GHKL-type ATPases. Other members belonging to this superfamily include **G**yrase (Corbett and Berger 2003), the molecular chaperone **H**sp90, Histidine **K**inase, and the DNA mismatch repair protein Mut**L** (Ban and Yang 1998), which gives rise to the GHKL domain acronym. The ATP lid of the Bergerat fold is unique to the GHKL superfamily and varies in amino acid sequence between enzymes (Bergerat, de Massy et al. 1997, Dutta and Inouye 2000, Corbett and Berger 2004). Even though the superfamily members have little sequence homology (~15%) the structural fold can superpose between different enzymes (Dutta and Inouye 2000). Indeed, inhibitors designed to target the ATP-binding pocket of Hsp90 such as radicicol are effective against other GHKL family members, such as archaeal topo VI and human TOP2A (Gadelle, Bocs et al. 2005).

1.10.2 Transducer Subdomain

The C-terminal region of the ATPase domain forms the transducer subdomain, which connects the ATPase domain to the enzyme core. The transducer subdomain relays the signals of ATP binding and hydrolysis between the ATPase domain and the breakage reunion core via conformational changes in the enzyme. The transducer domain contains a ‘switch lysine’ residue (K378 in TOP2A and K394 in TOP2B) that is absolutely conserved in all type II topoisomerases (Wei, Ruthenburg et al. 2005). The switch lysine is located within the conserved QTK loop (Figure 1-3) and points into the ATP binding pocket to form a salt-bridge with the γ-phosphate of ATP. This salt-bridge is believed to stabilise the transition state of the hydrolysis reaction (Smith and Maxwell 1998). The switch lysine residue moves considerably upon ATP binding to allow the

correct positioning of the lysine which helps transduce signals to allosteric sites within the enzyme (Wigley, Davies et al. 1991, Lamour, Hoermann et al. 2002, Classen, Olland et al. 2003, Oestergaard, Giangiacomo et al. 2004, Wei, Ruthenburg et al. 2005).

Characterisation of a mutated TOP2A protein where two amino acids (valine and proline) were inserted after residue 351, abolished the enzyme's ability to catalyse DNA strand passage. However, the mutated protein could hydrolyse ATP and cleave DNA suggesting it could perform each of the catalytic reactions individually (Oestergaard, Giangiacomo et al. 2004). Therefore, despite the two catalytic reactions of the mutated enzyme being functional, communication between the two domains was impaired as shown by the absence of strand passage activity. This provided evidence that the transducer domain is essential to coordinate ATP binding and hydrolysis to DNA cleavage in order to perform efficient topoisomerase II catalysed reactions.

1.11 Breakage Reunion Domain (Core)

The breakage reunion domain is composed of two domains: B' and A' (Figure 1-5A) that assemble to form a heart shaped dimer with a large central cavity where DNA binds (Figure 1-5B). The B' domain is located at the N-terminus of the breakage reunion domain and consists of a divalent metal ion binding region termed the TOPRIM domain. Whilst the A' domain provides the site of covalent attachment to the DNA substrate via the catalytic tyrosine residue (Berger, Gamblin et al. 1996), formed by two winged-helix domains (WHDs), a tower domain and a C-gate domain. The active site tyrosine is located within the WHD domain as part of a common structural scaffold motif found in many DNA binding proteins. The motif is comparable to the *E. coli* catabolite activator protein (CAP-like domain), histone H5 and members of the helix–turn–helix (HTH) family (Osheroff 1987, Schultz, Shields et al. 1991, Aravind, Leipe et al. 1998, Noble and Maxwell 2002, Dong and Berger 2007, Schmidt, Burgin et al. 2010). Specifically, the TOPRIM and WHD domains function together in catalysis to cleave the G-DNA. Whilst the tower domain participates in binding DNA (Dong and Berger 2007), and is adjacent to the C-gate which provides the dimerisation interface where the T-DNA exits the enzyme (Berger, Gamblin et al. 1996, Nitiss 2009).

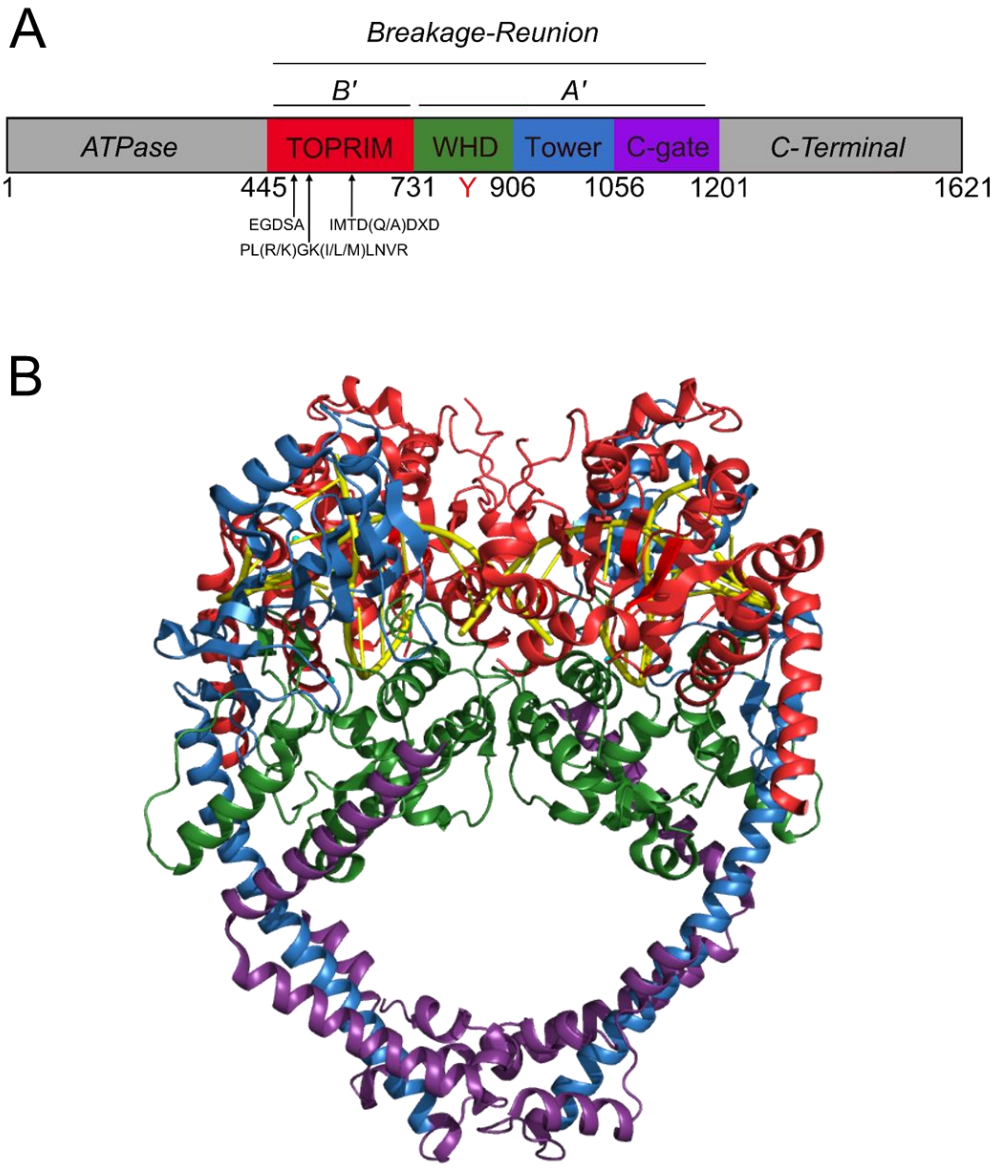

Figure 1-5: Domain and crystal structure for the breakage reunion domain of human TOP2B

(**A**) The breakage reunion domain comprises four subdomains: TOPRIM, WHD, tower, and the C-gate, coloured according to Figure 1-4B. The TOPRIM domain contains multiple evolutionary conserved amino acid motifs which include the acidic triad within IMTD(Q/A)DXD required for metal ion binding, EGDSA, and PL(R/K)GK(I/L/M)LNVR. The winged helix domain (WHD) possesses the conserved catalytic tyrosine (red Y). The TOPRIM domain is coloured in red, WHD domain in green, tower domain in blue, and the C-gate in purple. (**B**) The crystal structure of the breakage reunion domain of human TOP2B (residues 445–1201, PDB code 5ZRF) in complex with DNA (yellow). The different domains are coloured according to **A**.

1.11.1 B' Domain

The B' domain consists of a metal binding TOPRIM domain that contains three evolutionary conserved amino acid motifs that are necessary for DNA cleavage and religation. The motifs are conserved in prokaryotic and eukaryotic type II topoisomerases and are required for Mg^{2+} ion coordination during catalysis (Osheroff 1987, Aravind, Leipe et al. 1998, West, Meczes et al. 2000, Noble and Maxwell 2002, Schmidt, Burgin et al. 2010). Their sequences are EGDSA (residues 447-481 in human TOP2B), PL(R/K)GK(I/L/M)LNVR (residues 501-510 in human TOP2B), and IMTD(Q/A)DXD (residues 554-561 in human TOP2B). Indeed, mutagenesis of E447 in the EGDSA motif to a glutamine (Q) and K505 in the PLRGKILNVR motif to a glutamate (E) residue altered the magnesium dependence of TOP2B during strand passage (West, Meczes et al. 2000). The three motifs are located within different loops of the enzyme with hydrogen bonds occurring between the motifs to ensure correct secondary structure folding (Berger, Gamblin et al. 1996, Aravind, Leipe et al. 1998, Berger, Fass et al. 1998). The acidic residues found within the conserved motifs are located within 4–8 Å of each other and form an E/D-X-E/D-X-E/D pattern in order to coordinate the catalytic Mg^{2+} ions (Berger, Fass et al. 1998).

The central region of the B' domain contains a four stranded, parallel β-sheet located between two pairs of α-helices to give a βαβαβαβα fold. This secondary structure resembles the "Rossmann fold" which is commonly found in DNA-binding proteins (Vella 1992). Contacts also occur between each B' protomer to give rise to the dimeric structure of the enzyme. The surface of B'-B' dimerisation contains a small hydrophobic patch comprising residues I540, L551, L557 of one monomer and Y602 of the second monomer in human TOP2B. During catalysis, a conformational change occurs in the B' subfragment whereby it undergoes a large rotation in respect to the A′ fragments. This correctly positions the acidic residues towards the active site tyrosine, forming a functional cleavage complex (Dong and Berger 2007).

1.11.2 A' Domain

The A' domain is composed of three subdomains: winged helix domain (WHD), tower, and C-gate. Located within the WHD (CAP-like domain) is a semi-circular groove that has many positively charged residues to enhance DNA binding. The WHD domain contains three α-helices with three or four-β stranded sheets organised between the helices in the same order as CAP: αβααββ (Nelson 1995). Further downstream of the

groove is an extended loop where the active site tyrosine is located, Y805 in human TOP2A and Y821 in human TOP2B (Clark, Halay et al. 1993). In the absence of DNA, the A' domains are in an open conformation until DNA binds and a conformational change within the protein brings the A' domains together to position the active site tyrosine's for catalysis. After cleavage, the A' domains open via a swivel mechanism, coordinated by the WHDs, which separates the cleaved G-DNA to create a physical gap for the passage of the T-DNA through the break. Once the T-DNA has entered the central cavity, the A' domains come back together to allow religation of the cleaved G-DNA. This movement constricts the central cavity forcing the C-gate to open and provides an exit for the T-DNA to leave the enzyme (Berger, Gamblin et al. 1996).

1.12 C-Terminal Domain

The C-terminal domain of type II topoisomerase enzymes has the least homology and shows high sequence diversity between isoforms (Figure 1-3). Although, one feature that is common among species is that the C-terminal domain always incorporates many charged amino acids. These charged residues are proposed to interact with the basic regions of DNA or proteins. Thus, the C-terminal domain is involved in protein-protein interactions (Caron, Watt et al. 1994) and undergoes extensive posttranslational modifications (Cowell, Willmore et al. 1998). Moreover, the C-terminal domain is believed to be responsible for conferring biochemical and pharmacological differences between the two human isoforms. Therefore, the C-terminal domain is implicated in the regulation of topoisomerase functions within the cell and is dispensable for catalytic activity *in vitro* (Adachi, Miyaike et al. 1997).

In contrast, the CTD is vital for topoisomerase II functions *in vivo.* Without the CTD, topoisomerase II is unable to localise to the nucleus, where it performs the majority of its functions. This is due to the presence of a nuclear localisation signal (NLS) within the CTD (Figure 1-3) (Crenshaw and Hsieh 1993, Adachi, Miyaike et al. 1997, Mirski, Gerlach et al. 1999). In human TOP2A a NLS sequence has been identified in the region 1454-1497 (Wessel, Jensen et al. 1997) and a second NLS sequence has been identified in TOP2A at residues 1259–1296 (Mirski, Gerlach et al. 1999). Human TOP2B has two strong NLS sequences in the region homologous to TOP2A at 1522-1548 and 1538-1573 (Turner, Engel et al. 2004) and a third weaker NLS sequence at positions 1294–1332 (Cowell, Willmore et al. 1998, Mirski, Gerlach et al. 1999).

Nuclear export sequences (NES) are also present within the CTD of type II topoisomerase enzymes to control the export of the enzyme out of the nucleus. In human TOP2A the NES is present between residues 1017–1028 and 1054–1066, the latter being the stronger sequence (Turner, Engel et al. 2004). Whilst in TOP2B a single NES has been identified between residues 1034–1044 (Mirski, Bielawski et al. 2003).

Studies with chimeric 'tail swap' proteins, where the CTD of one isoform is joined to the ATPase and breakage-reunion domain of the alternative isoform, has provided useful insight into the function of the CTD. A chimera of murine TOP2 consisting of the core of TOP2A and the CTD of TOP2B showed that this protein could support growth in a temperature-sensitive *S. cerevisiae* strain (Adachi, Miyaike et al. 1997). Chimeric 'tail swap' proteins between the human isoforms led to interesting results. The presence of the TOP2B CTD on the TOP2A isoform core resulted in a decrease in strand passage activity *in vitro* compared to wild type TOP2A. Whereas the presence of the TOP2A CTD on the TOP2B core had the opposite effect and resulted in an increase in strand passage activity compared to wild type TOP2B. However, when the CTD was deleted for each isoform, there was no difference in *in vitro* activity. Thus, it is likely that the CTD acts as a regulator for strand passage. Furthermore, the TOP2A core with the TOP2B CTD was unable to support growth *in vivo*, in yeast, however, the TOP2B core with the TOP2A CTD could support low levels of growth. Thus, the CTD of the human topoisomerase II enzymes are necessary for the *in vivo* function of the enzyme, but not necessarily for *in vitro* catalytic activity (Meczes, Gilroy et al. 2008).

Casein kinase II phosphorylates residues within the C-terminal domain of a variety of eukaryotic type II topoisomerases, and some of these modifications are cell cycle dependent (Cardenas, Dang et al. 1992). Various studies have identified the phosphorylation status of human TOP2A at specific stages in mitosis, with phosphorylation of residue S1212 only occurring during mitosis (Ishida, Takashima et al. 2001). Moreover, it has been suggested that phosphorylation can activate TOP2A for chromatid segregation during anaphase (Heck, Hittelman et al. 1989), and casein kinase II mediated phosphorylation at residue S1469 in TOP2A is associated with chromatin condensation during prophase (Escargueil, Plisov et al. 2000). Likewise, phosphorylation of TOP2A of Ser1337 and Ser1524 at specific stages of the cell cycle increases TOP2 activity and perturbation of phosphorylation at these residues decreases TOP2A decatenation activity (Li, Wang et al. 2008).

1.13 Tertiary Structure of Type II DNA Topoisomerases

The solving of topoisomerase II structures by X-ray crystallography has provided a detailed understanding of the key aspects of the molecular mechanism utilised by type II topoisomerases. Structures determined by protein crystallography provide information at the atomic level that allows specific interactions between the enzyme and ligands to be determined. To date, the ATPase and core domain of human TOP2A have been solved as well as the core domain of TOP2B. The ATPase domain of *S. cerevisiae* is available, as well as the *S. cerevisiae* core domain. Furthermore, the full catalytic *S. cerevisiae* enzyme comprising both the ATPase and core domain has been solved (Appendix 1).

From solving the structures of the *S. cerevisiae* breakage reunion core in different conformations (T2O (Berger, Gamblin et al. 1996) and T2M (Fass, Bogden et al. 1999)), and bound to a G-DNA segment (Dong and Berger 2007) it has been established that eukaryotic topoisomerase II monomers assemble to form a heart-shaped dimer with a large central cavity where DNA binds. During catalysis *S. cerevisiae* TOP2 bends the G-DNA by ~75° as the G-DNA enters the catalytic interior. This bent conformation is stabilised by the positively charged amino acids located near the WHD domain, and directs the DNA backbone towards the active site for catalysis (Dong and Berger 2007).

Generally, the human TOP2A and TOP2B breakage reunion core structures are in agreement with the *S. cerevisiae* structures with the enzymes displaying many common features. Like *S. cerevisiae,* the human isoforms in complex with DNA adopt a dimeric structure. Although the TOP2A and TOP2B cores have a slightly more open quaternary structure compared to bacterial and yeast type II topoisomerases (Laponogov, Pan et al. 2010, Wu, Li et al. 2011). Like *S. cerevisiae,* the TOP2A and TOP2B isozymes distort the DNA substrate and maintain a closed DNA gate. However, additional structural features are observed in the human type II breakage reunion cores that are absent in the *S. cerevisiae* core. For example, human TOP2A and TOP2B contain an extended helix between the TOPRIM and WHD domain as well as an additional helix near the C-gate (Wendorff, Schmidt et al. 2012). Moreover, the human TOP2B breakage reunion core was crystallised with G-DNA in an open conformation which provided further insight into how the T-DNA physically passes through the break. The individual monomers of the DNA gate undergo a conformational change from a

closed to open state that requires movement along the helical axis of the G-DNA. This reveals a funnel shaped trough that is wide enough to allow the passage of T-DNA through the break. To prevent electrostatic interactions occurring between the T-DNA and the enzyme that would slow T-DNA passage and delay completion of the catalytic cycle, this region of the protein is predominately comprised of basic residues (Chen, Huang et al. 2018). Although this was the first report of a crystal structure with the G-DNA in an open conformation, the structures confirmed earlier biophysical FRET analysis of DNA gate opening (Smiley, Collins et al. 2007, Huang, Lee et al. 2017).

Determining the structure of isolated topoisomerase II domains in complex with drugs has given mechanistic insights into their mode of action. For example, the breakage reunion core of TOP2B has been solved in complex with the topoisomerase II poison etoposide. From the crystal structure, the etoposide binding site could be identified which results from a global conformational change of TOP2B upon drug binding. The WHDs change position which causes the DNA to become deformed, which in turn pushes the TOPRIM domain away so that the distance between the active site tyrosine and the catalytic Mg^{2+} ions is increased. Consequently, the cleavage complex is stabilised as the cleaved DNA cannot be religated (Wu, Li et al. 2011).

The etoposide drug bound crystals were then used to generate drug soaked crystals with the drugs mAMSA, mitoxantrone, and ametantrone. Structural analysis of the breakage reunion core of TOP2B in the presence of these clinically active anticancer drugs provided a structural basis of their inhibition and enabled a rationalised prediction of drug-resistant mutations to these compounds (Wu, Li et al. 2013). Furthermore, by solving the *S. cerevisiae* ATPase domain in complex with ICRF187 there was structural evidence that the drug does not compete with ATP for binding to the ATP site. Instead ICRF187 binds in a region at the dimer interface between two topoisomerase II protomers locking the ATPase domain into a closed-clamp conformation. Consequently, ICRF187 inhibits topoisomerase II in a non-competitive manner (Classen, Olland et al. 2003).

When the structure of the ATPase domain of human TOP2A was determined bound to two different nucleotides; AMPPNP (a non-hydrolysable ATP analogue) and ADP (the ATP hydrolysis product) (Wei, Ruthenburg et al. 2005) insight into how ATP binding and hydrolysis result in gate opening and closing was revealed. The two discrete structural domains were observed in TOP2A, as were previously observed in the *S.*

cerevisiae ATPase domain structure (Classen, Olland et al. 2003): the N-terminal GHKL domain and the C-terminal transducer domain. The active site of TOP2A was very similar in the two different nucleotide bound states with the catalytic Mg^{2+} ion, nucleotide, and most of the active site residues in the same conformation. However, in the post ATP hydrolysis structure (ADP bound), a 10° movement of the transducer domain was observed. This increased the diameter of the cavity at the narrowest point from 6 Å in the AMPPNP bound state to 17 Å in the ADP bound complex (Classen, Olland et al. 2003, Wei, Ruthenburg et al. 2005).

However, it is difficult to definitively understand how ATP hydrolysis is conformationally transduced to the breakage reunion core from the individual domain structures of the human enzymes. Albeit information from the *S. cerevisiae* full catalytic structure, comprising the ATPase domain and breakage reunion core can be applied to the human enzymes due to their similarity in catalytic mechanisms. From the fully functional *S. cerevisiae* structure (residues 1-1177), it became evident that there was a direct connection between the K loop in the ATPase transducer domain and the bound G-DNA. Site directed mutagenesis of the conserved lysines in this loop reduced strand passage in both relaxation and decatenation assays whereas DNA cleavage was not impacted. In addition, the K loop mutated proteins failed to stimulate topoisomerase II ATP hydrolysis activity in the presence of nucleic acid. Moreover, the length of the G-DNA had an effect on whether the ATPase activity would be stimulated with wild type protein. The G-DNA had to be long enough in order to make contacts with the K loop for ATP hydrolysis to occur. Indeed, it is only when the G-DNA is religated that it makes contacts with the K loop which stimulates the second ATP hydrolysis event to reset the enzyme for another round of catalysis. Overall, this work indicated the transducer domain, specifically the K loop, has a direct function in coupling DNA binding to ATP hydrolysis and strand passage activity (Schmidt, Osheroff et al. 2012).

1.14 Mutated Type II Topoisomerases

Mutated proteins can provide valuable insight into an enzyme's structure and function. Naturally occurring temperature-sensitive topoisomerase II mutations in yeast have been very powerful tools in the field. When the location of the mutations was determined it also related structure with function. More recently a range of patient

mutations have provided important insights into the functions of type II topoisomerases in humans. Similarly, site directed mutagenesis enabled the roles of specific amino acids to be determined. Whilst forced molecular evolution has been used to generate mutated topoisomerase II proteins that were drug-resistant.

1.14.1 Yeast Temperature Sensitive Mutations

Mutations in yeast topoisomerase II have been discovered that cause a temperature sensitive phenotype. The mutated proteins are functional at the permissive temperature, however exposure to the non-permissive temperature causes the enzyme to become inactive. Temperature-sensitive (*ts*) mutations have provided an *in vivo* system to study plasmid-borne mutated topoisomerase enzymes. Currently, 14 heat sensitive and 4 cold sensitive mutations in *S. cerevisiae* TOP2 have been identified that are predominantly located within the conserved regions of the WHD domain (Holm, Goto et al. 1985, Lavoie, Tuffo et al. 2000). It is believed that the heat sensitive mutations function by disrupting the protein secondary or tertiary structure at the increased temperature. Whereas cold sensitive mutations allow additional interactions to occur between the type II topoisomerase dimer interface so that opening the C-gate requires more energy. Therefore, at lower temperatures the C-gate remains closed so that T-DNA cannot exit the enzyme causing the protein to be inactive (Thomas, Spell et al. 1991). The *ts* mutation in the JN394 *top2-4* strain that is utilised during complementation analysis involves a proline to glutamine amino acid change at position 821 (P821Q) (Nitiss, Liu et al. 1992). Whilst mutations R884P, R886I and M887I within the *top2-5* allele confer sensitivity to temperature and resistance to the topoisomerase II poisons etoposide and mAMSA.

1.14.2 Patient Mutations in TOP2B

Human mutations in TOP2B have been identified with patients exhibiting a wide range of phenotypes from B cell immunodeficiency to neurological defects such as autism.

1.14.2.1 Hoffman Syndrome

Patients present with autosomal dominant B cell immunodeficiency in addition to facial and limb abnormalities. Hoffman syndrome is a monogenic syndrome caused by heterozygous *de novo* mutations in TOP2B that were identified in multiple independent families. Patients possess normal T cell responses to antigens (Hoffman, Bastian et al. 2001, Hügle, Hoffman et al. 2011, Kallish, McDonald-McGinn et al. 2011, Broderick,

Yost et al. 2019, Papapietro, Chandra et al. 2020), but lack mature B cells and have altered NK cells (Broderick, Yost et al. 2019, Broderick, Clay et al. 2022). The TOP2B mutations (S483L, A485P, EE587E and G633S) are causative for Hoffman syndrome and define a novel class of B cell immunodeficiency. Murine models were generated to study the mechanism of this immunodeficiency and revealed the expression of key transcription factors such as Pax5 for B cell development were significantly reduced whilst expression of Rag1, a transcription factor required for both B and T cell development was comparable to wild type (Nutt, Heavey et al. 1999, Fuxa and Busslinger 2007, Schebesta, McManus et al. 2007, Broderick, Yost et al. 2019). There was a profound loss in the number of B cells at multiple stages of B cell development and the few numbers of mature B cells that were produced were not properly activated in response to antigen stimulation consistent with the patient phenotype (Broderick, Yost et al. 2019, Papapietro, Chandra et al. 2020). Further research is needed to determine how these heterozygous TOP2B mutations alter the transcriptional programmes to produce the observed phenotype.

1.14.2.2 Other Patient Mutations

Other mutations in TOP2B have been identified in patients that do not present with Hoffman syndrome and less is known about their etiology.

TOP2B is important for the expression of neural and developmentally regulated genes and defects in TOP2B may cause various neurodevelopmental disorders, such as autism spectrum disorder or schizophrenia (Harkin, Gerrelli et al. 2016). A *de novo* heterozygous missense mutation in TOP2B (H58Y) has been identified in two patients with developmental delay, intellectual disability, and autistic features (Lam, Yeung et al. 2017, Xia, Hu et al. 2019, Hiraide, Watanabe et al. 2020).

A heterozygous missense mutation in TOP2B at position 1613, D1613H, is hypothesised to be involved in the development of the auditory system as the patient with this mutation is deaf (Xia, Hu et al. 2019). Residue 1613 is conserved among many species, and the TOP2B D1613H mutation is believed to disrupt protein function and cause autosomal-dominant nonsyndromic hearing loss through inhibition of the PI3K-Akt signalling pathway. Indeed, when TOP2B was knocked down in zebrafish inner ear development was disrupted.

One patient with severe disabilities has a compound heterozygous biallelic mutation causative for disease in TOP2B. These mutations affect highly conserved amino acids in the TOPRIM domain of TOP2B: R503S and R510Q, within the conserved PL**R**GKILNV**R** motif that is in close proximity to the DNA helix. Both mutations were inherited from the parents, one from each parent, although the parents do not present with a phenotype.

Two further heterozygous mutations in TOP2B (K172R and L1146V) have been reported on the Genematcher database from two patients with unknown phenotypes. TOP2B K172R is in the GHKL nucleotide binding region of the ATPase domain of TOP2B. K172 is located towards the surface of the protein, thus it is possible that K172 is involved in contacting and capturing the transported DNA (T-DNA) for passage through the cleaved G-DNA. Whereas TOP2B L1146V is located within the C-gate of the protein, a region of the enzyme that constitutes the primary dimer interface that holds the topoisomerase II subunits together until ATP is hydrolysed and it undergoes a conformational change to allow the T-DNA to exit the enzyme after G-DNA cleavage and religation. As such, L1146 is unlikely to be involved in binding or catalysing G-DNA cleavage, rather it is likely to have a more structural function.

1.14.3 Site Directed Mutagenesis of TOP2B

Clustal analyses of primary sequences revealed motifs absolutely conserved between all type II topoisomerases, three of these lie in the TOPRIM region within the B' domain of TOP2B. To investigate the functions of these highly conserved motifs, EGDSA, PL(R/K)GK(I/L/M)LNVR, and IMTD(Q/A)DXD, West *et al* used site directed mutagenesis (West, Meczes et al. 2000, West, Turnbull et al. 2002). When the conserved aspartic acid residues within the IMTD(Q/A)DXD motif (D557 and D561) were mutated the proteins could not be successfully purified as the proteins degraded rapidly during the purification process, suggesting the conserved aspartic acid residues are essential for protein stability. Of the mutations that could be produced, TOP2B activity was significantly impacted, and two mutations altered the magnesium optima of the enzyme indicating the highly conserved residues are important for catalysis.

S165R is a mutation in human TOP2B that was introduced during construction of the original expression construct. The mutated protein had reduced strand passage activity and reduced ATP hydrolysis activity. However, the DNA binding properties of S165R

were not affected suggesting this specific region of the GHKL domain is not essential for binding the DNA substrate (West, Turnbull et al. 2002).

1.14.4 Drug-Resistant Mutations

Drug-resistant mutations have been identified throughout the entire topoisomerase II protein demonstrating resistance to topoisomerase II targeting drugs is complex and mutations do not solely occur at the drug binding site (Chen and Liu 1994). To illustrate the power of these mutations in determining function some of the reported drug mutations are summarised below.

Four TOP2A GHKL domain mutations have been reported that are resistant to bisdioxopiprazines. TOP2A Y50F, was identified in CHO cell lines resistant to ICRF193 but sensitive to the topoisomerase II poisons mAMSA and etoposide (Sehested, Wessel et al. 1998, Wessel, Jensen et al. 1999). TOP2A mutations R162Q, Y165S and L169F in the GHKL domain were selected for resistance to the bisdioxopiprazine, ICRF187 (Walker, Saraste et al. 1982, Wessel, Jensen et al. 1999). Using site directed mutagenesis this mutation was reconstituted in the yeast TOP2 enzyme and caused hypersensitivity to mAMSA and etoposide but resistance to ICRF187 and ICRF193. The homologous residue in GyrB (L115) is believed to hydrogen bond with the γ-phosphate of the ATP and therefore R162 could have a similar function. However, R162Q can overcome resistance to ICRF187 at saturating levels of ATP (Wessel, Jensen et al. 1999). Whilst R162Q was resistant to ICRF187 only at sub saturating ATP concentrations, Y50F was resistant to ICRF193 at any ATP concentration. These results suggested that residue Y50 is located within the drug binding site, whereas R162 is a residue situated in the ATP binding site. Indeed, the *S. cerevisiae* ATPase domain structure in complex with ICRF187 confirmed this hypothesis (Classen, Olland et al. 2003). The TOP2A mutated protein, Y165S, had reduced affinity for ATP and could not perform DNA cleavage in the presence of ICRF187. From the *S. cerevisiae* (Classen, Olland et al. 2003) and human TOP2A (Wei, Ruthenburg et al. 2005) ATPase domain structures it was deduced that residue Y165 is directly involved in forming the ICRF187 binding site. Consequently mutating Y165 to a serine residue could cause a change in the drug binding site (Jensen, Renodon-Corniere et al. 2002). The TOP2A mutation, L169F, showed an increased requirement for ATP during catalysis, however the mutated protein was not cross resistant to other topoisomerase II poisons (Jensen, Wessel et al. 2000).

ICRF187 resistance mutations in the B' domain of TOP2A have been reported, D465N, G551S and P592L. *In vitro* analysis showed the mutated protein D465N had reduced strand passage activity. Residue D465 is located within the linker region between the B' and A' subfragments of the breakage reunion core which appear to have an important function during topoisomerase II catalysis. By contrast, the G551S and P592L mutations are thought to destabilise the B-B' clamp between TOP2A monomers rather than reducing the catalytic activity of TOP2A (Jensen, Wessel et al. 2000).

A number of mutations have been selected for resistance to acridines such as mAMSA. For example, TOP2A R486K located in the breakage reunion domain within the conserved PLRGK motif conferred resistance to mAMSA (Hinds, Deisseroth et al. 1991) and the same residue (R486) was also mutated in an independent study (Lee, Wang et al. 1992). Additionally, the mutation has been identified in patients with small cell lung cancer that were treated with etoposide in addition to the point mutation E484G (Kubo, Yoshikawa et al. 1996). Interestingly, mutation of the equivalent yeast residue, R476K, did not confer resistance to mAMSA, suggesting there are species-specific differences in this region of the protein for drug action (Wasserman and Wang 1994, Patel, Keller et al. 2000).

Another study identified functional drug-resistant mutations in TOP2B by forced molecular evolution. To ensure the mutations were functional, selection to four acridine compounds, mAMSA, mAMCA, AMCA and DACA was performed in yeast at the non-permissive temperature. Nine mutations were identified by this method that conferred resistance to the chosen acridines and seven of the mutations were located in the B' domain. All mutated proteins identified during this study have been characterised *in vitro* apart from H514Y and A596T (Leontiou, Watters et al. 2007). TOP2B P732L was selected for resistance to mAMSA but was cross resistant to etoposide, ellipticine, mAMCA, AMCA and doxorubicin. The mutated protein P732L had unique DNA cleavage activity whereby the protein could not support cleavage in the presence of calcium ions and displayed hyper-cleavage activity in the presence of magnesium ions (Leontiou, Lakey et al. 2006).

Mutations causing resistance to quinolones have been identified in the A' domain often clustering within the WHD subfragment (CAP-like domain). Bacterial GyrA is commonly mutated in the CAP-like domain causing resistance to quinolones. Mutations within this region (residues 67-106 of GyrA) are prevalent in clinical isolates

and confer drug resistance by reducing quinolone binding in the ternary complex (Cullen, Wyke et al. 1989, Hallett and Maxwell 1991). Residues S83 and D87 in GyrA are commonly mutated to a leucine/tryptophan or asparagine/valine respectively and mutagenesis studies revealed these residues directly bind to the quinolone compounds (Willmott and Maxwell 1993, Barnard and Maxwell 2001). Moreover, when the homologous GyrA S83 residue was mutated to a trytophan in *S. cerevisiae* (S740W) resistance to quinolones was also conferred but the protein became hypersensitive to the topoisomerase II poison etoposide. Thus, suggesting this residue has an important function in interacting with drug and DNA (Strumberg, Nitiss et al. 1999).

Drug-resistant mutations in human TOP2A have provided further evidence for the CAP-like domain interacting with drugs. Two TOP2A mutations, K798L and K798P, confer 8-fold resistance to etoposide and cross resistance to doxorubicin and mAMSA. Characterisation of the mutated proteins determined the mechanism of drug resistance was due to altered drug interaction (Okada, Ito et al. 2000, Okada, Tosaka et al. 2001). TOP2A P803S also conferred resistance to etoposide, doxorubicin, mAMSA and mitoxantrone. However, resistance was only observed in the absence of ATP. Residue P803 is in the vicinity of the catalytic tyrosine and therefore may perturb DNA cleavage by changing the conformation of the enzyme (Mao, Yu et al. 1999). Indeed, further mutagenesis studies around the active site tyrosine of human TOP2A (Y805) were performed to characterise this region of the enzyme (Okada, Tosaka et al. 2001). The catalytic tyrosine was essential, and no mutations were tolerated at this position. Although, conserved amino acid changes were accepted at residues L794, D797, A801 and R804.

Several drug-resistant cell lines have identified mutations within the CTD that perturb the nuclear localisation signal (NLS) (Mirski, Evans et al. 1993, Wasserman and Wang 1994, Mirski, Sparks et al. 2000). For example, a human small cell lung cancer cell line that was selected for resistance to etoposide had a C-terminal deletion of basic residues 1490-1492 that function as the strong NLS. Accordingly, nuclear localisation was abolished and the protein was mainly cytosolic (Wessel, Jensen et al. 1997).

1.15 Posttranslational Modifications

Type II topoisomerase enzymes can be modified post translationally to regulate catalytic activity, protein stability, protein-protein interactions, and subcellular localisation. Posttranslational modifications (PTMs) of the human type II topoisomerase isoforms include phosphorylation, SUMOylation and ubiquitination (Ackerman, Glover et al. 1985, Chikamori, Grabowski et al. 2003, Bedez, Lotz et al. 2018).

There is evidence for phosphorylation of topoisomerase II *in vivo* in a wide range of organisms including *Drosophila,* chicken, mouse, yeast and human (Ackerman, Glover et al. 1988, Heck, Hittelman et al. 1989, Saijo, Enomoto et al. 1990, Kroll and Rowe 1991, Cardenas, Dang et al. 1992). Phosphorylation of the human topoisomerase II isoforms is cell cycle dependent (Saijo, Enomoto et al. 1990, Burden and Sullivan 1994, Wells, Fry et al. 1995). Several kinases have been shown to phosphorylate topoisomerase II *in vitro* including casein kinase II, protein kinase C, Ca^{2+}/calmodulin-dependent kinase and $p34^{cdc2}$ kinase (Ackerman, Glover et al. 1985, Cardenas, Dang et al. 1992, Bedez, Lotz et al. 2018). The majority of these sites are residues located within the C-terminal domain (Wells, Addison et al. 1994, Wells and Hickson 1995, Ishida, Iwai et al. 1996). Some phosphorylation sites have been reported to alter the effectiveness of topoisomerase II targeting drugs (Takano, Kohno et al. 1991, Ritke, Murray et al. 1995, Ganapathi, Constantinou et al. 1996, Aoyama, Grabowski et al. 1998, Qi, Hou et al. 2011, Sigrist, de Castro et al. 2012, Nakazawa, Arakawa et al. 2019, Lotz, Lamour et al. 2020).

Topoisomerase enzymes can become specifically modified by ubiquitin. Ubiquitin (Ub) is a small regulatory protein comprised of 76 amino acids (8.5 kDa) that can be attached to substrate proteins post translationally either as a monomer or as polyubiquitin chains that vary in length and linkage type (Dikic and Dötsch 2009). The addition of Ub to target proteins requires the action of three enzymes: an E1 activating enzyme, an E2 conjugating enzyme and an E3 ubiquitin ligase. The type of Ub modification on a substrate determines the downstream response. For example, monoUb, regulates DNA repair, whilst lysine 48-linked polyUb chains target proteins for proteasomal degradation (Dikic and Dötsch 2009, Ikeda and Dikic 2008). In addition, ubiquitin modifications can alter the cellular localisation, catalytic activity, and molecular interactions of the protein substrate (Gilberto and Peter 2017). As such,

ubiquitination of target proteins must be tightly controlled by balancing the E1/E2/E3 ligase activity and the deubiquitylases (DUBs) activity that remove Ub modifications (Clague, Barsukov et al. 2013, Fielding, Concannon et al. 2018).

SUMOylation is a posttranslational modification where SUMO proteins are conjugated to substrates by a similar activation pathway to ubiquitin but use different E1 and E2 enzymes. SUMO proteins are 'small ubiquitin-related proteins' and mammals possess four different SUMO isoforms (SUMO-1, SUMO-2, SUMO-3 and SUMO-4). It has been shown that topoisomerases can be modified by the first three SUMO isoforms (1-3) (Hochstrasser 2000, Mao, Desai et al. 2000, Isik, Sano et al. 2003). Evidence obtained in yeast and Xenopus model organisms indicates that conjugation of SUMO to topoisomerase II is required for its mitotic functions and if SUMOylation of topoisomerase II is disrupted during this period, sister chromatid disjunction can be delayed or inhibited which can cause pre-anaphase checkpoint arrest or chromosome segregation errors (Azuma, Arnaoutov et al. 2005, Agostinho, Santos et al. 2008). A consensus sequence for SUMOylation has been identified: (I/V/L)KX(E/D), where SUMO is attached to the lysine residue (Lee and Bachant 2009, Hendriks, D'Souza et al. 2014, Yoshida and Azuma 2016).

1.16 Type II Topoisomerase Targeting Drugs

DNA topoisomerases are important targets for anticancer and antibacterial drugs (McClendon and Osheroff 2007, Deweese and Osheroff 2009, Ketron and Osheroff 2014). For example, bacterial type II topoisomerases (Gyrase and topo IV) are the targets of quinolones and aminocoumarin antibiotics (Pommier, Leo et al. 2010).

1.16.1 Topoisomerase II Poisons

Topoisomerase II poisons function by increasing DNA cleavage within the cell (Robinson and Osheroff 1990, Robinson and Osheroff 1991, Sørensen, Sinding et al. 1992, Corbett and Osheroff 1993, Constantinou, Mehta et al. 1995). By increasing the concentration of cleavable complexes within the cell, topoisomerase II poisons cannot act on free enzyme only the covalently bound topoisomerase II DNA complex (TOP2-DPC). This converts topoisomerase II into a physiological toxin that can create permanent double strand breaks (Tewey, Rowe et al. 1984, Pommier, Capranico et al. 1991). Due to the mechanism of action of topoisomerase II poisons, the sensitivity of

cells to these drugs is related to the amount of topoisomerase II protein in the nucleus. Specifically, cells containing high levels of topoisomerase II such as proliferating cells are significantly more sensitive to topoisomerase II poisons. Thus, immunohistochemical assessment of cancer cells prior to treatment can determine whether the cancer type would be a prime target for topoisomerase II poisons (Wu, Li et al. 2011).

Although, topoisomerase II poisons comprise some of the most commonly prescribed anticancer drugs, they are associated with serious side effects such as myelosupression, cardiotoxicity and therapy related leukaemia (Pendleton, Lindsey et al. 2014). These off-target effects arise because of the difficulty in specifically targeting cancer cells as every cell within the body expresses at least one of the type II topoisomerase isoforms. For example, it has been estimated that 2–3% breast cancer of patients develop secondary therapy related leukaemia's after treatment with topoisomerase II targeting drugs.

1.16.2 Catalytic Inhibitors

Catalytic inhibitors are the other class of topoisomerase II targeting drugs and comprise a group of structurally and mechanistically diverse compounds. Catalytic inhibitors act by blocking a specific stage in the topoisomerase II catalytic cycle so that cells are deprived of the essential type II topoisomerase functions. As catalytic inhibitors function independently of DNA break formation, they can act as antagonists to topoisomerase II poisons. Indeed, many catalytic inhibitors reduce the number of cleavage complexes formed by topoisomerase II poisons *in vitro* and *in vivo* (Ishida, Miki et al. 1991, Jensen, Sørensen et al. 1994, Sehested and Jensen 1996). Consequently, the cytotoxicity of topoisomerase II poisons can be decreased in the presence of catalytic inhibitors. Specifically, ICRF187 is used therapeutically for the treatment of anthracycline extravasations and provides protection against anthracycline induced cardiotoxicity (Conde-Estévez, Saumell et al. 2010, Geisberg and Sawyer 2010, Bansal, Joshi et al. 2021). ICRF187 exerts its cardioprotective effect by inhibiting or depleting human TOP2B, the predominant isoform in cardiac cells. Indeed, a conditional knockout of TOP2B in mice protected against the toxic effects of anthracycline therapy (Zhang, Liu et al. 2012). Whereas for decades it was believed that the cardioprotective effect of ICRF187 was due to Fe^{3+} ion chelation that reduced

the production of oxygen radicals which would otherwise cause cellular damage (Doroshow 1983, Buss and Hasinoff 1993, Myers 1998).

1.17 Aims

Overall, the work presented in this thesis aims to further advance the understanding of the mechanism of human TOP2B through structural determination and biochemical characterisation of individual domains and mutated proteins.

Specifically, the major aims of the current study were as follows:

- To investigate the ATP hydrolysis activity of a range of human TOP2B ATPase domain constructs (Chapter 3)
- To determine the tertiary structure of the ATPase domain of human TOP2B and identify the conformational changes that occur within the protein during ATP hydrolysis (Chapter 4)
- To investigate the impact of drug-resistant mutations on human TOP2B function *in vivo* (Chapter 5)
- To investigate the impact of patient mutations on human TOP2B function *in vivo* (Chapter 6)
- To biochemically characterise a subset of patient mutations on enzymatic function *in vitro* (Chapter 7)

Chapter 2 Materials and Methods

2.1 Chemicals and Reagents

Chemicals were purchased from Sigma-Aldrich (Dorset, U.K.) or Melford (Ipswich, U.K.) unless otherwise stated. Restriction endonucleases and polymerases were from New England Biolabs (Ipswich, U.S.). Yeast nitrogen base was from Formedium (Norfolk, U.K.); yeast extract, bactopeptone, and tryptone were from Melford. Agar was from Fisher Scientific (Hampton, U.S.). Deionised water (dH_2O) was used for all solutions unless otherwise stated.

2.2 Buffers and Reagents for Purification of the ATPase Domain of TOP2B

All purification buffers were made up with MilliQ water and vacuum filtered before use to degas and remove particulates.

His Trap Buffer A: 50 mM Tris HCl pH 8, 150 mM NaCl.

His Trap Buffer B: 50 mM Tris HCl pH 8, 150 mM NaCl, 500 mM Imidazole.

Heparin Buffer A: 50 mM Tris HCl pH 8, 150 mM NaCl.

Heparin Buffer B: 50 mM Tris HCl pH 8, 500 mM NaCl.

2nd His Trap Buffer A: 50 mM Tris HCl pH 8, 150 mM NaCl, 30 mM Imidazole.

2nd His Trap Buffer B: 50 mM Tris HCl pH 8, 150 mM NaCl, 500 mM Imidazole.

Superdex 75 Buffer A: 25 mM Tris HCl pH 8, 150 mM NaCl.

2.3 Buffers and Reagents for Purification of Full-Length TOP2B (residues 46-1621)

All purification buffers were made up with MilliQ water and vacuum filtered before use to degas and remove particulates.

Protease Inhibitors: 1 mM Benzamidine, 1 mM Phenylmethanesulponyl Fluroride (PMSF), 2 µg/mL Leupeptin and 2 µg/mL Pepstatin were present during cell lysis.

His Trap Buffer A: 50 mM Tris HCl pH 8.5, 320 mM KCl, 1% (v/v) Glycerol.

His Trap Buffer B: 50 mM Tris HCl pH 8.5, 320 mM KCl, 500 mM Imidazole, 1% (v/v) Glycerol.

Heparin Buffer A: 50 mM Tris HCl pH 8.5, 320 mM KCl, 1% (v/v) Glycerol.

Heparin Buffer B: 50 mM Tris HCl pH 8.5, 1 M KCl, 1% (v/v) Glycerol.

Q Buffer A: 50 mM Tris HCl pH 8.5, 320 mM KCl, 1% (v/v) Glycerol.

Q Buffer B: 50 mM Tris HCl pH 8.5, 1 M KCl, 1% (v/v) Glycerol.

Dilution Buffer: 50 mM Tris HCl pH 8.5, 1% (v/v) Glycerol.

Dialysis Buffer: 50 mM Tris HCl pH 8.5, 200 mM KCl, 20% (v/v) Glycerol.

2.4 Buffers and Reagents for *In Vitro* Assays of Topoisomerase II

Relaxation Buffer: 50 mM Tris HCl pH 7.4, 10 mM $MgCl_2$, 0.5 mM EDTA, 30 µg/mL Bovine Serum Albumin (BSA), 1 mM DTT, 100 mM KCl.

GR Buffer: 50 mM Tris HCl pH 7.5, 50 mM KCl, 1% (v/v) Triton X100, 30 µg/mL BSA, 0.5 mM EDTA, 1 mM DTT and 5% (v/v) Glycerol.

Oligonucleotides: Oligonucleotides were ordered from IDT (San Diego, U.S.). Annealed oligonucleotides (4 µg) were 5' end labelled with fluorescence (fluorochrome was IRDye700).

Plasmids: pBR322 and pUC19 were purchased from New England Biolabs. pTCS1 was propagated in *E. coli* XL1 blue cells (Section 2.7). Plasmid DNA was extracted using the alkaline lysis method and purified by caesium chloride-ethidium bromide gradients by C. Austin as described by Sambrook *et al* (Sambrook 1989).

Proteinase K: 10 mg/mL stock solution stored at -20 °C.

ATP: Adenosine 5'-triphosphate, disodium salt. 50 mM stock in 80 mM NaOH stored at -80 °C.

2.5 Buffers for Electrophoresis:

TAE: 40 mM Tris, 20 mM Acetic Acid, 1 mM EDTA.

SDS-PAGE Loading Buffer: 10% (v/v) Glycerol, 2% (v/v) SDS, Trace Bromophenol Blue, 5% (v/v) β-Mercapthoethanol.

SDS-PAGE Running Buffer: 192 mM Glycine, 25 mM Tris, 0.1% (v/v) SDS.

Formamide Loading Buffer: 900 µL Formamide, 22.2 µL 500 mM EDTA, 26.5 µL 7.5% (w/v) Orange-G, 51.3 µL dH_2O.

Agarose Gel Loading Buffer: 0.5% (v/v) SDS, 25% (v/v) Glycerol, 0.1% Bromophenol Blue.

Western Blot Transfer Buffer: 25 mM Tris, 192 mM Glycine, 20% (v/v) Methanol.

2.6 Media

Media was made up with deionised water and autoclaved at 121 °C for 2 hours.

2.6.1 Media for Bacterial Culture

LB (Luria Bertani) Media per litre: 10 g Tryptone, 5 g Yeast Extract, 10 g NaCl.

LB Agar Plates per litre: As LB media with 15 g Agar.

NYZ+ Broth per litre: 10 g NZ Amine, 5 g Yeast Extract, 5 g NaCl, pH to 7.5 with NaOH, 12.5 mM $MgCl_2$, 12.5 mM $MgSO_4$.

Terrific Broth per litre: 20 g Tryptone, 24 g Yeast Extract, 4 mL Glycerol, 0.017 M KH_2PO_4, 0.072 M K_2HPO_4.

2X YT per litre: 16 g Tryptone, 10 g Yeast Extract, 5 g NaCl, pH 7.0 with NaOH.

Autoinduction media per litre: 45.85 g 2xYT Autoinduction Media (Formedium) supplemented with 0.3% (v/v) Glycerol.

2.6.2 Media for Yeast Culture

50% Lactic Acid: Solid NaOH pellets were added to 294 mL of 85% (v/v) Lactic Acid until the pH was between 5-6. The volume was then made up to 500 mL with dH_2O.

UGLA per litre: 0.72 g Ura- Dropout (Formedium), 2.8 g Yeast Nitrogen Base without amino acids and ammonium sulphate, 5 g Ammonium Sulphate, 3% (v/v) Glycerol, 40 mL 50% Lactic Acid.

GUGLA per litre: 900 mL UGLA media supplemented with 100 mL 20% (w/v) Glucose.

Ura- Agar Plates: 1 g Ura- Dropout (Formedium), 7 g Yeast Nitrogen Base without amino acids, 25 g Agar.

YPDA Media per litre: 10 g Yeast Extract, 20 g Bactopeptone, 20 g Glucose, 17 g Agar, 2 mL Adenine Sulphate (stock 2 mg/mL).

YPDA Agar Plates: As for YPDA media, but with 20 g Agar per litre.

LiOAc/TE: 100 mM Lithium Acetate, 10 mM Tris HCl pH 8, 1 mM EDTA.

PEG/LiOAc/TE: 400 g PEG4000 in LiOAc/TE.

2.7 Bacterial Strains

XL1 Blue Competent Cells: Bacterial host for amplification of plasmid vectors. *RecA1 endA1 gyrA96 thi-1 hsdR17 supE44 relA1 lac* [F' *proAB lacI^q ZΔM15* Tn*10* (Tet^r)].

XL10 Gold Ultracompetent Cells: Bacterial host for the transformation of large plasmids and ligation of DNA. Tet^R *Δ (mcrA)183 Δ (mcrCB-hsdSMR-mrr)173 endA1 supE44 thi-1 relA1 gyrA96 recA1 lac* Hte [F' *proAB lacI^q ZΔM15* Tn*10* (Tet^r) Amy Cam^R].

BL21 (DE3) pLysS Competent Cells: Bacterial host for high efficiency protein expression of a gene under the control of a T7 promoter. T7 expression strains are lysogens of bacteriophage DE3. These hosts carry a chromosomal copy of the T7

RNA polymerase gene under the control of a lacUV5 promoter. pLysS, carries the gene encoding T7 lysozyme which reduces non-specific expression of target genes under the control of the T7 promoter until the inducer is added. F^- *ompT hsdS*$_B$ (r_B^- m_B^-) *gal dcm* (DE3) pLysS (Cam^R).

Rosetta 2 (DE3) pLysS Competent Cells: BL21 derivatives that enhance the expression of eukaryotic proteins containing the codons rarely used in *E. coli*. These strains supply tRNAs for 7 rare eukaryotic codons. F^- *ompT hsdS*$_B$ (r_B^- m_B^-) *gal dcm* (DE3) pLysS pRARE (Cam^R).

Rosetta-Gami 2 (DE3) Competent Cells: The above features of Rosetta 2 cells combined with Origami 2 strains that enhance disulphide bond formation in the cytoplasm during recombinant protein expression in *E. coli.* Δ(*ara-leu*) *7697* Δ*lacX74* Δ*phoA* *Pvu*II *phoR* *araD139* *ahpC* *galE* *galK* *rpsL* (DE3) F′ [*lac*$^+$ *lacI*^{q} *pro*] *gor522*::Tn*10* *trxB* pRARE2 (Cam^R, Str^R, Tet^R).

Arctic Express (DE3) Competent Cells: BL21 derivatives that possess cold-adapted chaperonins; Cpn60 and Cpn10 to facilitate proper protein folding at low temperatures. *E. coli* B F^- *ompT hsd*S (rB^- mB^-) *dcm*$^+$ Tet^R *gal* λ (DE3) *endA* Hte [*cpn10 cpn60* $Gent^R$].

2.8 Bacterial Expression Vectors

1B: 6xHis tagged vector with a cleavable TEV site. Addgene number 29653. *E. coli* T7. Kan^R (Figure 2-1A).

1C: 6xHis tagged maltose binding protein (MBP) vector with a cleavable TEV site. Addgene number 29654. *E. coli* T7. Kan^R (Figure 2-1B).

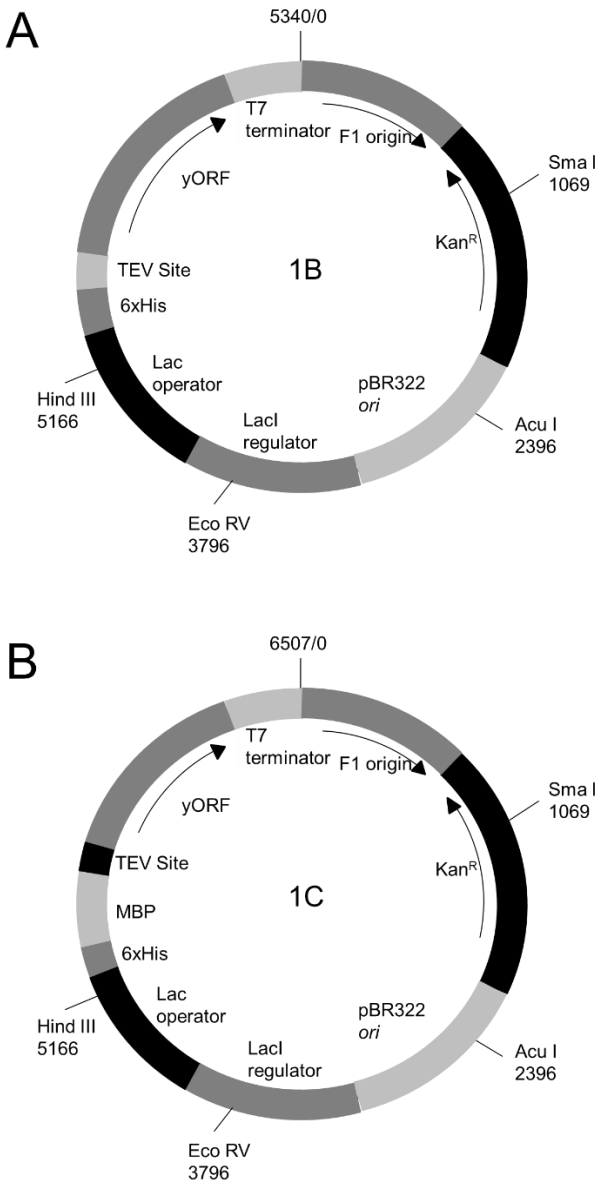

*Figure 2-1: Maps of bacterial expression vectors 1B (**A**) and 1C (**B**)*

2.9 Bacterial Expression Plasmids

M1 1B: Codons 1-444 of human TOP2B in the 1B vector.

S45 1B: Codons 45-444 of human TOP2B in the 1B vector.

TOP2A 1B: Codons 29-428 of human TOP2A in the 1B vector.

M1 1C: Codons 1-444 of human TOP2B in the 1C vector.

S45 1C: Codons 45-444 of human TOP2B in the 1C vector.

TOP2A 1C: Codons 29-428 of human TOP2A in the 1C vector.

M1 Splice: Codons 1-449 of human TOP2B in the 1C vector where an additional five amino acids are inserted after V23 to give rise to the alternative splice variant.

M1 E103A: Codons 1-444 of human TOP2B in the 1C vector containing a point mutation at position 103 (E103A).

M1 V23S: Codons 1-444 of human TOP2B in the 1C vector containing a point mutation at position 23 (V23S).

S45 K172R: Codons 45-444 of human TOP2B in the 1C vector containing a point mutation at position 172 (K172R).

S45 E103A: Codons 45-444 of human TOP2B in the 1C vector containing a point mutation at position 103 (E103A).

PGEX BATG-A: Codons 1-1621 of the human *TOP2B* gene.

2.10 Yeast Strains

Jel1 *Δtop1*: A protease deficient *S. cerevisiae* strain for the expression of topoisomerase II with a deletion in the topoisomerase I gene: *α leu2 trp1 ura3-52 prb1-1122 pep4-3 Δhis3::PGAL 10-GAL4.*

JN394 *t2-4*: A yeast strain with a temperature-sensitive mutation in the yeast *top2* gene that enables yeast to be viable at 25 °C but non-viable at 35 °C: α *ISE2 ura3-52 top2-4 rad52::LEU2.*

2.11 Yeast Expression Plasmids

12UraB TOP2B: The first 7 codons of the *S. cerevisiae TOP2* gene fused to codons 46-1621 of the human *TOP2B* gene in a 6xHis tagged vector with a cleavable TEV site. Galactose inducible expression in *S. cerevisiae* (Figure 2-2A).

YEpTOP2-PG1T2: *S. cerevisiae TOP2* gene under the control of a GAL1 promoter.

YEphTOP2βKLM: The first 7 codons of the *S. cerevisiae TOP2* gene fused to codons 46-1621 of the human *TOP2B* gene under the control of a GAL1 promoter (Figure 2-2B).

YEpWOB6: First 7 codons of the *S. cerevisiae TOP2* gene fused to codons 30-1531 of the human *TOP2A* gene under the control of a GAL1 promoter (Figure 2-2C).

YCp50: A control plasmid lacking the topoisomerase II codon sequence.

YCpDEDWOB10: *S. cerevisiae TOP2* gene under the control of the constitutive yeast DED1 gene promoter.

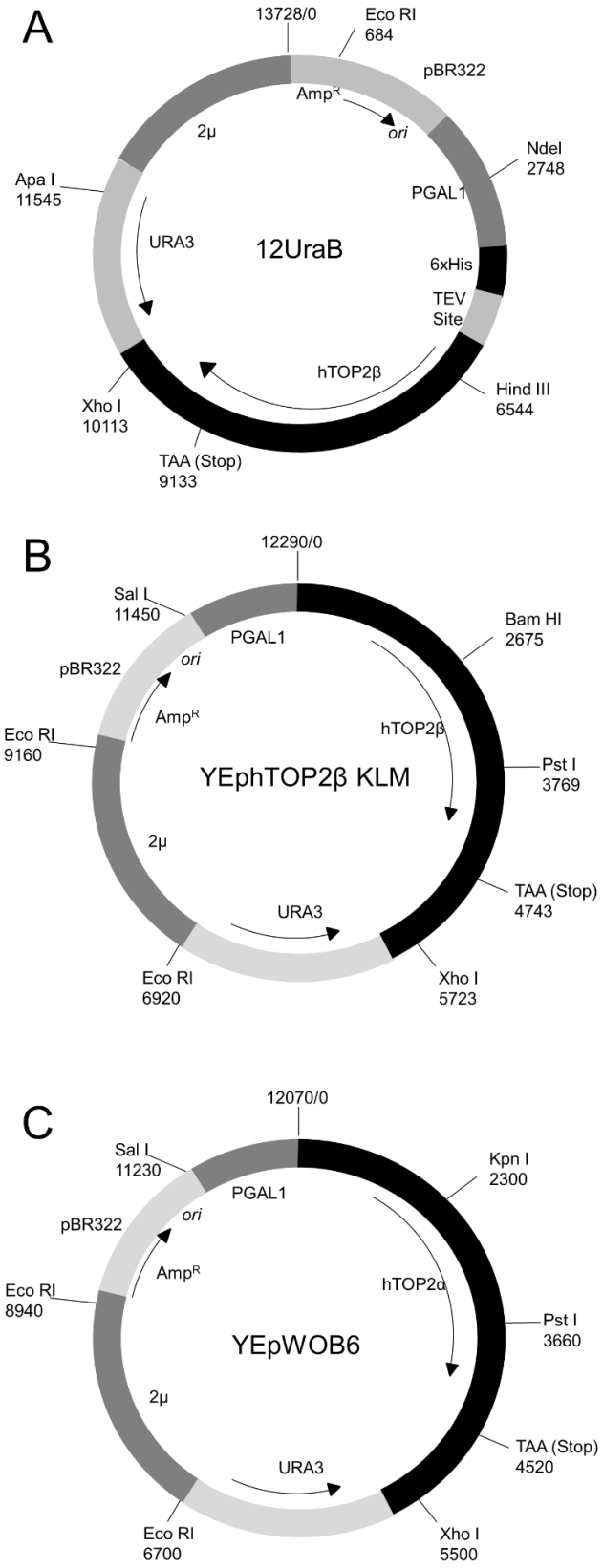

Figure 2-2: Maps of yeast expression plasmids

Plasmids constructed for the expression of human TOP2B in the 12UraB vector (**A**), human TOP2B in the YEphTOP2β construct (**B**) and TOP2A in the YEpWOB6 construct (**C**).

2.12 Antibiotics

Ampicillin: Working concentration 100 µg/mL, dissolved in dH_2O and filter sterilised.

Kanamycin: Working concentration 50 µg/mL, dissolved in dH_2O filter sterilised.

Chloramphenicol: Working concentration 25 µg/mL, dissolved in ethanol.

2.13 Drugs

All drugs were purchased from Sigma-Aldrich (Dorset, UK) and dissolved in DMSO.

Topoisomerase II Poisons: mAMSA, mAMCA, AMCA, DACA, Doxorubicin, Etoposide, Mitoxantrone.

Topoisomerase II Catalytic Inhibitors: ICRF187, ICRF193.

2.14 Cloning of the ATPase Domain of Human TOP2B

2.14.1 Primer Design

The region of the ATPase domain that was initially cloned into the 1B and 1C vectors was between amino acid 1 (M1) or amino acid 45 (S45) to amino acid 444 of human TOP2B. This is the homologous region of human TOP2A that was previously expressed and crystallised (Wei, Ruthenburg et al. 2005).

Forward and reverse primers were designed to contain the LIC sequences: TACTTCCAATCCAATGCA and TTATCCACTTCCAATGTTATTA respectively (Table 2-1).

Forward Primers	
Region	**Sequence**
M1 TOP2B	5'-TACTTCCAATCCAATGCAATGGCCAAGTCGGGTGGCTGC-3'
S45 TOP2B	5'-TACTTCCAATCCAATGCATCTGTTGAGAGAGTGTATCAGAAG-3'
L28 TOP2A	5'-TACTTCCAATCCAATGCATCTGTTGAAAGAATCTATCAAAAGAAAAC-3'

Reverse Primers	
Region	**Sequence**
S444 TOP2B	5'-TTATTCACTTCCAATGTTATTATGAACACTTCTTATTCAGCTGAGTCTG-3'
S428 TOP2A	5'-TTATCCACTTCCAATGTTATTAAGCTGAACACTTCTTGTTTAACTGGAC-3'

Table 2-1: Ligation independent cloning primers

2.14.2 Ligation Independent Cloning (LIC)

The ATPase domain was cloned into the 1B and 1C vectors via ligation-independent cloning (LIC). PCR was performed with 10 µM primers, 2 mM dNTP's, Q5 high fidelity DNA polymerase, 10 ng template DNA (YEphTOP2βKLM or PGEX BATG-A), and Q5 reaction buffer for 25-35 cycles with an annealing temperature of 55 °C. The products were run on an agarose gel and gel purified with QIAquick Gel Extraction Kit as per manufacturer's instructions. The LIC reaction was then performed with 10 µL gel purified insert, 2.5 mM dCTP, NEB 2.1 Buffer, 5 mM DTT, T4 DNA polymerase and incubated at 22 °C for 30 minutes then 75 °C for 20 minutes.

Plasmid vector 1B or 1C (500 ng) was digested with *SspI* restriction enzyme and gel purified. The LIC reaction was performed with 25 µL gel purified vector, 2.5 mM dGTP, NEB 2.1 Buffer, 5 mM DTT, T4 DNA polymerase and incubated at 22 °C for 30 minutes then 75 °C for 20 minutes.

LICed vector (2 µL) was then combined with 2 µL LICed insert and incubated at room temperature for 5 minutes prior to transformation.

2.14.3 Transformation of E. coli with Plasmid DNA

Products of LIC reactions were transformed into commercially supplied competent XL1 Blue *E. coli* cells by the heat shock method. 40 µL cells were aliquoted per transformation reaction and treated with 2 µL β-mercaptoethanol on ice for 10 minutes. Cells were transformed with 10 µL of the LIC reaction or 1 µL of intact plasmid DNA and incubated on ice for a further 30 minutes. Heat shock was carried out for 30 seconds at 42 °C followed by rapid cooling of the cells on ice for 2 minutes. 0.5 mL NYZ+ broth was added, and the cells were incubated at 37 °C for 1 hour with gentle agitation, prior to plating on LB antibiotic agar plates. Agar plates were then incubated at 37 °C overnight.

2.14.4 Small Scale Preparation of Plasmid DNA

LB (5 mL) with the appropriate antibiotic was inoculated with a single transformed colony and grown overnight at 37 °C. DNA extraction was performed by QIAprep spin miniprep kit or QIAprep midiprep kit as per manufacturer's instructions.

2.14.5 DNA Sequencing

To ensure cloning had been successful, plasmid DNA was sequenced by Lightrun (Eurofins). 80-100 ng/µL of plasmid DNA was sent with 5 pmol/µL of the appropriate primer (Table 2-2).

Forward Primers	
Position on Human TOP2B	**Sequence**
337-354	5'-CAGAGGGATAAGACCATG-3'

Reverse Primers	
Position on Human TOP2B	**Sequence**
390-370	5'-GTTAGATTCAGGATCAATAG-3'

Table 2-2: Primers used to sequence the human TOP2B ATPase domain plasmids

2.14.6 Site Directed Mutagenesis of the ATPase Domain of Human TOP2B

Mutations in the human TOP2B cDNA were created via site directed mutagenesis with Agilent's QuikChange II XL site directed mutagenesis kit as per manufacturer's instructions. 10 ng of template plasmid (M1 or S45) was used in the PCR with 125 ng of the forward primer and 125 ng of the reverse primer (Table 2-3). PCR cycling parameters were used as per manufacturer's instructions with an 8-minute incubation at 68 °C. The non-mutated template plasmid was digested by *DPN* I restriction enzyme as per instructions.

Forward and reverse primers were designed to contain the desired mutations with the Tm of the primer ≥78 °C (Table 2-3). The primers were synthesised by IDT and purified by PAGE.

Mutation	Primer	Sequence
K172R	Forward	5'-GATGATGATGAGAGAAAAGTTACAGGTGGTCGTAATGG-3'
	Reverse	5'-CCATTACGACCACCTGTAACTTTTCTCTCATCATCATC-3'
E103A	Forward	5'-CCAGGTTTATACAAGATCTTTGATGCAATTTTGGTTAATGCTGC-3'
	Reverse	5'-GCAGCATTAACCAAAATTGCATCAAAGATCTTGTATAAACCTGG-3'
Alternative Splice	Forward	5'-GGGCACTGACCTGGGTGACTCTTTTTGATCAGAACAATGCTGC-3'
	Reverse	5'-GCAGCATTGTTCTGATCAAAAAGAGTCACCCAGGTCAGTGCCC-3'

Table 2-3: Primers used to insert the desired mutations into ATPase domain of Human TOP2B

2.15 Expression and Purification of TOP2B ATPase Domain

2.15.1 Preparation of Competent Bacterial Cells

For transformation of intact plasmid DNA for protein expression, “homemade” competent bacterial cells were used. Bacterial cells were made competent by the $CaCl_2$ method. LB media (50 mL) was inoculated with a single colony of the desired bacterial cells and grown at 37 °C until the OD_{600} was between 0.4-0.5. Cells were cooled on ice for 10 minutes and harvested by centrifugation at 2058 g for 10 minutes at 4 °C. The pellet was resuspended in 0.1 mM $CaCl_2$ (10 mL) and the cells were recovered by centrifugation at 2058 g for 10 minutes at 4 °C. The pellet was resuspended in 0.1 mM $CaCl_2$ (2 mL) and flash frozen on dry ice. Stocks of competent bacterial cells were stored at -80 °C until required.

2.15.2 Small Scale Test Inductions

LB (50 mL) with the appropriate antibiotic was inoculated with a single colony of the transformed bacterial strain and grown at 37 °C until the OD_{600} reached 0.6-0.8. Recombinant protein expression was induced by adding IPTG (50 µM – 1 mM) and cells were grown at a range of different temperatures (16 °C – 30 °C) overnight. The culture was harvested by centrifuging at 2058 g for 15 minutes and the supernatant discarded. The pellet was resuspended in His Trap Buffer A (50 mM Tris HCl pH 8, 150 mM NaCl) and lysed by sonication. Samples were centrifuged at 19,721 g for 20 minutes, the supernatant taken as the soluble sample and the pellet as the insoluble sample. SDS loading buffer was added and samples run on a 10% SDS polyacrylamide gel (PAGE) that was subsequently stained with Expedeon Instant Blue dye.

2.15.3 Large Scale Expression

Once optimum conditions were established for the expression of the ATPase domain of human TOP2B, expression was scaled up. 2xYT media (50 mL) containing kanamycin and chloramphenicol was inoculated with a single colony of transformed Rosetta 2 (DE3) cells and grown at 37 °C overnight. The following morning, overnight culture (5 mL) was used to inoculate autoinduction media (1 L) containing kanamycin and chloramphenicol. The flasks were incubated at 37 °C for 4 hours then the temperature was reduced to 20 °C until the following morning. Cultures were then

centrifuged at 2824 g for 15 minutes at 4 °C and the supernatant discarded. Cell pellets were stored at -20 °C until the proteins were required. Typically, 6 L of culture was used per preparation.

2.15.4 Cell Lysis

Cell pellets were thawed on ice prior to resuspension in His Trap Buffer A (50 mM Tris HCl pH 8 and 150 mM NaCl). Cells were lysed via sonication (Misonix Sonicator 3000) at 30 kHz for a total of 15 minutes with 10 seconds pulses followed by 10 second intervals. The sample was kept on ice throughout the sonication protocol. Centrifugation was performed at 75397 g for 30 minutes at 4 °C to separate the broken cell debris from the soluble proteins.

2.15.5 Purification

Purification was performed at room temperature, but all buffers, samples and fractions kept on ice. 30 µL samples taken after each column for analysis by SDS PAGE.

2.15.5.1 His Trap

35 mL His Trap column (Cytiva) was equilibrated in His Trap Buffer A (50 mM Tris HCl pH 8, 150 mM NaCl) prior to sample loading. The sample was loaded at 5 mL/min and flow through collected. The column was washed with His Trap Buffer A and 50 mM imidazole to remove any non-specifically bound proteins to the column. The protein was then eluted with His Trap Buffer B (50 mM Tris HCl pH 8, 150 mM NaCl, 500 mM Imidazole) as a step and collected in 50 mL Falcon tubes.

2.15.5.2 TEV

TEV cleavage was required to remove the 6xHis-MBP tag from the target protein. TEV protease expressed from the pRK793 plasmid was added at a 1:20 ratio (protease:substrate). Cleavage was performed at room temperature for a minimum of 4 hours.

2.15.5.3 Heparin

5 mL Hi Trap Heparin column (Cytiva) was equilibrated in Heparin Buffer A (50 mM Tris HCl pH 8, 150 mM NaCl). TEV cleaved sample was loaded onto the column at 5 mL/min and flow through collected. The column was washed with a 5 column volume

(CV) gradient to 40% B (50 mM Tris HCl pH 8, 500 mM NaCl). Once the UV plateaued, topoisomerase was eluted off the column with a 5 CV gradient to 100% B. 5 mL fractions were collected and the fractions around the UV peak were pooled for the next column.

2.15.5.4 2nd His Trap

5 mL His Trap column (Cytiva) was equilibrated in 2nd His Trap Buffer A (50 mM Tris HCl pH 8, 150 mM NaCl, 30 mM Imidazole). 30 mM imidazole (final concentration) was added to the pooled heparin fractions prior to column loading. The sample was loaded at 5 mL/min and the flow through collected. Due to the lack of the 6xHis-MBP tag the target protein did not bind to the column and eluted in the flow through. Once the UV plateaued a step elution to 100% B (50 mM Tris HCl pH 8, 150 mM NaCl, 500 mM Imidazole) was performed to remove bound contaminants, collected as 5 mL fractions.

2.15.5.5 Superdex 75

Superdex 75 gel filtration column (Cytiva) was equilibrated in Superdex 75 Buffer A (25 mM Tris HCl pH 8, 150 mM NaCl) before use. The 2nd His Trap flow through was concentrated to 5 mL or less with an Amicon Ultra Centrifugal Filter [30 kDa molecular weight cut off (MWCO)] prior to injection onto the Superdex 75 column. 2 mL fractions were collected from 45-65 mL and a sample was taken from fractions around the UV peak for SDS PAGE analysis.

2.15.6 Storage

The fractions which contained TOP2B were pooled and concentrated to either 16 mg/mL for use in crystallography immediately or 3.5 mg/mL for biochemistry experiments. 50% (v/v) glycerol was added to protein fractions for biochemistry analysis and material was flash frozen in liquid nitrogen then stored at -80 °C until required.

2.15.7 Protein Crystallography

Initially, MRC 96 well sitting drop vapour diffusion plates were used for crystallography screening. Five different crystallisation screens were used: JSCG Plus, PACT Premier, Structure and Morpheus II (Molecular Dimensions) and the Hampton screen

Index. Details of all the conditions are listed in Appendix 2. 80 µL of each crystal solution was pipetted into the reservoir well of the MRC 96 well plate. The Mosquito crystallization robot (TTP Labtech) was used to pipette 100 nL protein:100 nL reservoir in the top drop and 100 nL protein:200 nL reservoir in the bottom drop. The plates were sealed with a layer of film to make each well airtight, required for vapour diffusion and plates were incubated at 20 °C for several days before checking under the microscope (Leica). Conditions which gave protein crystals are detailed in Table 2-4. The size of the drop was increased during optimisation by 3-fold: 300 nL protein:300 nL reservoir and 300 nL protein:600 nL reservoir. Crystals were harvested in crystallisation solution supplemented with 20% (v/v) PEG400 for cyro-protection and flash cooled in liquid nitrogen.

Condition	Salt	Buffer	pH	Precipitant	Ligand
C4 PACT	N/A	0.1 M PCTP	7.0	25% (v/v) PEG 1500	5 mM $MgCl_2$ 1 mM AMPPNP
C5 PACT	N/A	0.1 M PCTP	8.0	25% (v/v) PEG 1500	5 mM $MgCl_2$ 1 mM AMPPNP
B4 JCSG Plus	N/A	0.1 M Sodium Cacodylate	6.5	5% (v/v) PEG 8000	5 mM $MgCl_2$ 1 mM AMPPNP
H7 JCSG Plus	0.2 M Ammonium Sulphate	0.1 M Bis Tris	5.5	25% (v/v) PEG 3350	5 mM $MgCl_2$ 5 mM ADP
H7 JCSG Plus	0.2 M Ammonium Sulphate	0.1 M Bis Tris	5.5	25% (v/v) PEG 3350	5 mM $MgCl_2$ 5 mM ADP 0.1 mg ICRF193

Table 2-4: Conditions of the screens that gave rise to protein crystals

2.15.8 Data Collection and Processing

To determine whether the crystals were protein crystals or salt crystals, diffraction patterns were obtained at Diamond Beamline I03 with unattended data collection. The native data collection strategy https://www.diamond.ac.uk/Instruments/Mx/I03/I03-Manual/Unattended-Data-Collections/Experiment-Types.html was used. Data were processed at Diamond with the automated pipeline Xia2 (Winter, Lobley et al. 2013) with Dials (Winter, Waterman et al. 2018). The data were scaled with Aimless (Evans and Murshudov 2013) and the space groups were confirmed with Pointless (Evans and Murshudov 2013). 5% of the data were randomly selected for Rfree calculations.

2.15.9 Solving the Phases and Model Building

The phases were solved for the human TOP2B ATPase AMPPNP structure on CCP4 cloud Newcastle (Potterton, Agirre et al. 2018) by molecular replacement using Molrep or Phaser (Vagin and Teplyakov 1997, McCoy, Grosse-Kunstleve et al. 2007). The human TOP2A ATPase domain (Wei, Ruthenburg et al. 2005) (pdb code 1ZXM) was used as a search model for the AMPPNP-bound structure. In turn the AMPPNP model (pdb code 7QFO) was used to solve the ADP-bound structures. The models were improved by iterative cycles of manual model building in COOT (Emsley, Lohkamp et al. 2010) and refined using Refmac (Murshudov, Skubák et al. 2011). The models were validated using COOT (Emsley, Lohkamp et al. 2010) validation tools and Molprobity (Williams, Headd et al. 2018). Metal type, co-ordination and bond distances were validated using Check My Metal (Zheng, Cooper et al. 2017). Structural figures were generated using Pymol (The Pymol Molecular Graphics System, Version 2.0 Schrödinger, LLC). Structures were superposed with the Secondary Structure Matching or Least Squares Fitting tool in COOT. Other software used were from the CCP4 suite (Potterton, Agirre et al. 2018).

2.16 Mutagenesis of Full-Length TOP2B (residues 46-1621)

Mutations in the full-length human TOP2B cDNA were created via site directed mutagenesis with Agilent's QuikChange II XL site directed mutagenesis kit using 10 ng of template plasmid (12UraB TOP2B).

2.16.1 Primer Design

Forward and reverse primers were designed to contain the desired mutations with the Tm of the primer ≥78 °C (Table 2-5). The primers were synthesised by IDT and PAGE purified.

Mutation	Primer	Sequence
K172R	Forward	5'-GATGATGATGAGAGAAAAGTTACAGGTGGTCGTAATGG-3'
	Reverse	5'-CCATTACGACCACCTGTAACTTTTCTCTCATCATCATC-3'
A485P	Forward	5'-GGAGACTCTGCCAAATCACTGCCTGTGTCTGGATTAGG-3'
	Reverse	5'-CCTAATCCAGACACAGGCAGTGATTTGGCAGAGTCTCC-3'
S483L	Forward	5'-CAGAGGGAGACTCTGCCAAATTACTGGCTGTGTCTGGATTAGG-3'
	Reverse	5'-CCTAATCCAGACACAGCCAGTAATTTGGCAGAGTCTCCCTCTG-3'
R503S	Forward	5'-GGAGTTTTTCCACTCAGCGGCAAAATTCTTAATGTACGG-3'
	Reverse	5'-CCGTACATTAAGAATTTTGCCGCTGAGTGGAAAAACTCC-3'
R503K	Forward	5'-GGAGTTTTTCCACTCAAGGGCAAAATTCTTAATGTACGG-3'
	Reverse	5'-CCGTACATTAAGAATTTTGCCCTTGAGTGGAAAAACTCC-3'
R503A	Forward	5'-GGAGTTTTTCCACTCGCGGGCAAAATTCTTAATGTACGG-3'
	Reverse	5'-CCGTACATTAAGAATTTTGCCCGCGAGTGGAAAAACTCC-3'
K515A	Forward	5'-GTACGGGAAGCTTCTCATGCACAGATCATGGAAAATGCTG-3'
	Reverse	5'-CAGCATTTTCCATGATCTGTGCATGAGAAGCTTCCCGTAC-3'
K551A	Forward	5'-CCTTACGCTATGGAGCGATTATGATTATGACCGATCAGG-3'
	Reverse	5'-CCTGATCGGTCATAATCATAATCGCTCCATAGCGTAAGG-3'
EE587E	Forward	5'-CATCACTTTTGAAGCATGGTTTTCTTGAGTTCATTACTCCTATTGTAAAGGC-3'
	Reverse	5'-GCCTTTACAATAGGAGTAATGAACTCAAGAAAACCATGCTTCAAAAGTGATG-3'
K595A	Forward	5'-CTCCTATTGTAGCGGCAAGCAAAAATAAGCAGGAACTTTCC-3'
	Reverse	5'-GGAAAGTTCCTGCTTATTTTTGCTTGCCGCTACAATAGGAG-3'
G633S	Forward	5'-GGAAAATAAAGTACTATAAAGGATTGAGTACTAGTACAGCTAAAGAAGC-3'
	Reverse	5'-ACTTCTTTAGCTGTACTAGTACTCAATCCTTTATAGTACTTTATTTTCC-3'
Y821F	Forward	5'-GATGCTGCAAGCCCTCGTTTTATTTTCACAATGTTAAGC-3'
	Reverse	5'-GCTTAACATTGTGAAAATAAAACGAGGGCTTGCAGCATC-3'
L1146V	Forward	5'-GGCCCAGATTTTAATTATATTTTAAATATGTCTGTGTGGTCTCTTAC-3'
	Reverse	5'-GTAAGAGACCACACAGACATATTTAAAATATAATTAAAATCTGGGCC-3'

Table 2-5: Primers used to insert the desired mutations into the full-length TOP2B plasmid

2.16.2 DNA Sequencing

To ensure mutagenesis had been successful, plasmid DNA was sequenced by Lightrun (Eurofins). 80-100 ng/µL of plasmid DNA was sent with 5 pmol/µL of the appropriate primer (Table 2-6).

Forward Primers	
Position on Human TOP2B	**Sequence**
337-354	5’-CAGAGGGATAAGACCATG-3’
834-852	5’-GCCTGTAAATGGATTTCGC-3’
1276-1293	5’-ATGATCCTGAACTGGGTG-3’
1674-1692	5’-GGATCAAGATGGTTCTCAC-3’
2059-2075	5’-GACCGGAGACAGCGTAG-3’
2551-2568	5’-CGTGTAGAGCCTGAGTGG-3’
3058-3075	5’-GATCATATGGGATGTCTG-3’
3301-3318	5’-GACCCAGTGAAAGCCTGG-3’
3544-3562	5’-GAGGATTTAGCGGCATTTG-3’
4031-4049	5’-CAGAACCTGTGGTTATTCC-3’
4537-4554	5’-GAGGCTGTAAACTCTGAC-3’

Reverse Primers	
Position on Human TOP2B	**Sequence**
390-370	5'-GTTAGATTCAGGATCAATAG-3'
1277-1293	5'-CACCCAGTTCAGGATACT-3'

Table 2-6: The primers used to sequence the full-length human TOP2B plasmids

2.17 Expression and Purification of TOP2B (Residues 46-1621)

2.17.1 Transformation of Yeast with Plasmid DNA

Plasmid DNA was transformed into *S. cerevisiae* via the lithium acetate method. YPDA media (50 mL) was inoculated with a single colony of yeast and grown at 25 °C (JN394) or 30 °C (Jel1*Δtop1)* until OD_{600} 1-5. The cells were harvested by centrifuging at 896 g for 5 minutes and the pellet was washed with 0.1 M LiOAc/TE (10 mL). Cells were harvested by a second centrifugation step at 896 g for 5 minutes and resuspended in 100 µL 0.1 M LiOAc/TE per transformation. 0.05 µg carrier DNA and 1 µg sample DNA was added to the cells with PEG/LiOAc/TE (1.2 mL) and incubated at 25 °C with gentle agitation for 30 minutes. Heat shock was performed at 42 °C for 15 minutes and the transformation reaction was plated on Ura- plates which were incubated for 3-5 days at the appropriate temperature.

2.17.2 Small Scale Test Inductions

2 mL GUGLA media was inoculated with a single JEL1Δ*top1* transformed colony and grown at 30 °C for 24 hours. Cultures were then diluted with UGLA media (8 mL) and incubated overnight at 30 °C until reaching OD_{600} 0.4-1.0. Recombinant protein expression was induced by adding filter sterilised galactose to a final concentration of 2% (v/v) and induction performed for a minimum of 3 hours.

Cultures were pelleted by centrifuging at 896 g for 5 minutes and then resuspended in 500 µL sterile dH_2O and transferred to a microfuge tube. Cells were pelleted for 2 minutes at 14,000 g and resuspended in 250 µL Heparin Buffer B (50 mM Tris HCl pH 8.5, 1 M KCl, 1% Glycerol) containing protease inhibitors (1 mM PMSF, 1 mM Benzamidine, 50 µM Leupeptin and 50 µM Pepstatin). An equal volume of glass beads were added (425-600 µm), and the yeast lysed at 4 °C by 15 cycles of vortexing for 30 seconds followed by 30 seconds on ice. The samples were centrifuged at 14,000 g for 2 minutes, and the supernatant kept for analysis on a 5% SDS polyacrylamide gel which was subsequently stained with Expedeon Instant Blue dye.

2.17.3 Large Scale expression

GUGLA media (50 mL) was inoculated with a single colony of transformed yeast and grown at 30 °C for several days until the OD_{600} was ~1.0. GUGLA media aids yeast growth hence it is used in the first step of expression, but the presence of glucose

inhibits expression of the recombinant proteins from the GAL1 promoter. As such, the culture was then transferred to UGLA media (1 L) which lacks glucose. ~15 mL GUGLA culture was used to inoculate 1 L UGLA, and typically, 9-12 L of UGLA was inoculated per preparation. The flasks were incubated at 30 °C for several days until the OD_{600} for each culture was between 0.4-0.8. Then a non-induced sample was taken (10 mL), centrifuged at 2824 g and the pellet stored at -80 °C. Protein expression was induced by adding 20 g galactose per 1 L culture for a minimum of 3 hours. After induction, the yeast cells were pelleted by centrifugation and cell pellets stored at -80 °C until required

2.17.4 Cell lysis

Frozen yeast pellets were thawed on ice and resuspended in Heparin Buffer B (50 mM Tris HCl pH 8.5, 1 M KCl, 1% Glycerol). Protease inhibitors were added to the final concentrations: 1 mM PMSF, 1 mM Benzamidine, 50 µM Leupeptin and 50 µM Pepstatin. The cells were lysed by mechanical disruption, at 37 kPSI using the Constant Systems CF1 Cell Disrupter. After which, centrifugation was performed at 27143 g for 20 minutes at 4 °C to separate the broken cell debris from the soluble proteins.

2.17.5 Purification

Purification was performed at room temperature, but all buffers, samples and fractions kept on ice. 30 µL samples taken after each column for analysis by SDS PAGE.

2.17.5.1 His Trap

2x 5 mL His Trap columns (Cytiva) were equilibrated in His Trap Buffer A (50mM Tris HCl pH 8.5, 320 mM KCl, 1% (v/v) Glycerol) prior to sample loading. The sample was loaded at 5 mL/min and flow through collected. The column was washed with buffer A and 20 mM imidazole to remove any non-specifically bound proteins to the column. The protein was then eluted with His Trap Buffer B (50 mM Tris HCl pH 8.5, 320 mM KCl, 500 mM Imidazole, 1% (v/v) Glycerol) as a step and collected in 50 mL Falcon tubes.

2.17.5.2 Heparin

5 mL Hi Trap Heparin column (Cytiva) was equilibrated in Heparin Buffer A (50 mM Tris HCl pH 8.5, 320 mM KCl, 1% (v/v) Glycerol). His Trap eluate was loaded onto the column at 5 mL/min and flow through collected. The column was washed with Heparin

Buffer A until the UV absorbance plateaued. Elution was achieved with Heparin Buffer B (50 mM Tris HCl pH 8.5, 1 M KCl, 1% (v/v) Glycerol) during which a 5 CV salt gradient was performed increasing the salt concentration from 320 mM KCl (Buffer A) to 1 M KCl (Buffer B). 2 mL fractions were collected and the fractions around the UV absorbance peak were pooled for the final purification column.

2.17.5.3 Anion Exchange (Q)

5 mL Hi Trap Q column (Cytiva) was equilibrated in Q Buffer A (50 mM Tris HCl pH 8.5, 320 mM KCl, 1% (v/v) Glycerol). Prior to loading the sample onto the Q column, the salt concentration had to be diluted by 70% with buffer containing no salt (50 mM Tris HCl pH 8.5, 1% (v/v) Glycerol) to ensure the ionic strength of the sample was low enough to allow binding to the column. Once the sample was loaded the column was washed with Buffer A to remove contaminants, prior to a 100% B step elution (50 mM Tris HCl pH 8.5, 1 M KCl, 1% (v/v) Glycerol). 2 mL fractions were collected, and a sample was taken from the fractions around the UV peak for SDS PAGE analysis. Fractions which contained TOP2B underwent dialysis before storage at -80 °C.

2.17.6 Dialysis

Dialysis was performed with slide-a-lyzer cassettes with a 7 kDa molecular weight cut off (MWCO) (ThermoFisher). Dialysis of protein samples into the required buffer (50 mM Tris HCl pH 8.5, 200 mM KCl, 20% (v/v) Glycerol) was carried out at 4 °C whilst stirring for 2 hours. Protein concentrations were determined using 1 µL protein sample on the A280 Nanodrop setting. Final protein concentration was calculated using the theoretical molar extinction coefficient [167540 for human TOP2B (residues 46-1621)].

2.17.7 Storage

After dialysis, protein was stored at -80 °C in small aliquots (50 µL) and large aliquots (0.5-1 mL) until required for *in vitro* analysis. Prior to storage at -80 °C, protein was flash frozen with dry ice.

2.18 SDS Polyacrylamide Gel Electrophoresis

Bio-Rad (mini-PROTEAN II) SDS polyacrylamide mini gel apparatuses were used. Gels were poured and run according to the manufacturer's instructions. Separating gel mix contained 5% or 10% acrylamide (19:1 acrylamide:bisacrylamide) and 0.1% (v/v)

SDS in 375 mM Tris HCl pH 8.8. Polymerisation was induced with 10% (w/v) ammonium persulphate (APS) and TEMED before pouring. Water-saturated butanol was added to the top of the separating gel to prevent bubble formation, and then poured off once the gel was set. The stacking gel mix contained 5% acrylamide and 0.1% (v/v) SDS in 125 mM Tris HCl pH 6.8. Polymerisation was induced with 10% (w/v) APS and TEMED.

Samples were mixed with SDS loading buffer and heated at 95 °C for 10 minutes before loading. Each gel contained protein markers (Novex Sharp pre-stained protein standard). Gels were electrophoresed at 120 V until the bromophenol blue dye reached the bottom of the gel, and then the gels were stained with Expedeon Instant Blue dye for 1 hour.

2.19 Agarose Gel Electrophoresis

1% TAE agarose gel electrophoresed at 50 V then stained with 0.2 µg/mL ethidium bromide for 30 minutes.

2.20 Western Blotting

For immunological detection, proteins were transferred to a nitro-cellulose membrane using a mini trans-blot electrophoretic transfer cell (Bio-Rad). Transfer was carried out at 100 V for 1 hour.

Prior to antibody probing, the membrane was blocked with 3% (w/v) blotto (dry milk powder) in Tris Buffered Saline (TBS; 20 mM Tris HCl pH 7.4, 150 mM NaCl) overnight at 4 °C with gentle agitation. The membrane was washed 3 times with TBST (TBS containing 0.05% (v/v) Tween 20) for a duration of 5 minutes per wash. The blot was incubated with the primary antibody for 1 hour at room temperature. The membrane was washed as previously and then the secondary antibody was added for 1 hour at room temperature. The membrane was washed again before ECL detection.

2.21 *In Vivo* Complementation Analysis

The viability of temperature-sensitive yeast strains (JN394*t2-4*) transformed with various plasmids encoding TOP2B cDNA were tested by growth at 25 °C, 30 °C, and 35 °C. This was performed semi quantitatively. Transformed yeast strains were grown in selective (Ura-) media at 25 °C then diluted to an OD_{600} of 1. The cultures were then serially diluted in sterile micro-titre plates. These cultures were then transferred to the Ura- and YPDA plates using a replicator containing an array of cylindrically shaped prongs.

2.22 *In Vitro T*opoisomerase II Activity Assays

2.22.1 ATP Hydrolysis Activity

ATPase activity was assayed by measuring the release of inorganic phosphate (P_i) during ATP hydrolysis. Release of P_i was detected using the reagent BioMOL green (Enzo) (Rule, Patrick et al. 2016). Reactions contained 50 mM Tris HCl pH 7.5, 50 mM KCl, 10 mM $MgCl_2$, and 0.1 mM ATP (unless otherwise stated). TOP2B ATPase domain proteins were then added to start the reaction and incubated at 37 °C for 30 minutes. The concentrations of TOP2B were varied as detailed in figure legends. For DNA stimulation experiments, 4 µg pBR322 DNA was added prior to protein addition. 50 µL of the reaction was then transferred to a microtitre plate containing BioMOL green (100 µL) to terminate the experiment. After 20 minutes the absorbance was measured at 655 nm. Reactions containing no enzyme were performed to generate a background reading of inorganic phosphate and were subtracted from the experimental results. The inorganic phosphate released was then calculated based on the absorbance standard curve established by phosphate standards. The kinetic parameters Km and Vmax were calculated from the Lineweaver-Burk plots using GraFit (version 7). All experiments were repeated at least three times.

2.22.2 Relaxation of Supercoiled Plasmid DNA

Purified TOP2B was incubated with 1 µg of supercoiled plasmid DNA (pTCS1) in the presence of 1 mM ATP and 20 µL relaxation buffer at 37 °C for 30 minutes. Reactions were stopped by the addition of 5 µL agarose gel loading buffer, and then analysed by electrophoresis on a 1% TAE agarose gel (Figure 2-3). Gels were stained with 0.2

µg/mL ethidium bromide for 30 minutes and destained with deionised water. Gels were imaged under UV transillumination with a Bio-Rad gel doc 1000 imager.

Quantification of the relaxation activity of the mutated proteins was performed by assaying relaxation activity with increasing protein concentrations. ImageQuant software was used to measure the total amount of relaxed products and the total amount of supercoiled DNA. At each protein concentration the relaxation products were divided by the amount of supercoiled DNA and expressed as a percentage. Quantification was performed for three replicate experiments to allow statistical analysis to be performed. The means of relaxation activity were then plotted against protein concentration and error bars representing one standard deviation from the mean included.

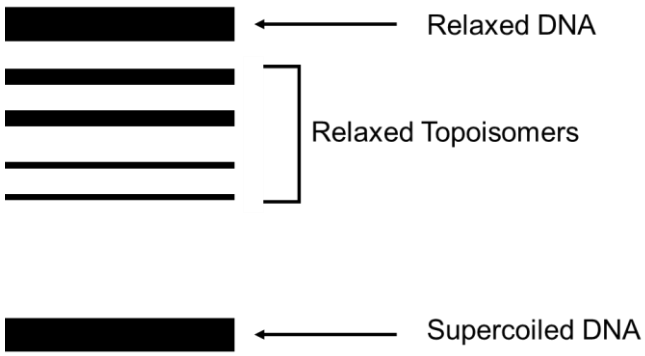

Figure 2-3: Relaxation of Supercoiled DNA by topoisomerase II

Relaxation products display a more open conformation causing them to migrate through the gel more slowly than the supercoiled DNA substrate that contains a compact structure.

2.22.3 Decatenation of Kinetoplast DNA

Decatenation assays were performed in the same way as relaxation assays, except 0.2 µg kinetoplast DNA (kDNA, Inspiralis) was used as a substrate instead of supercoiled plasmid DNA (Figure 2-4). kDNA is comprised of many interlinked minicircles that form a large network with a high molecular weight that is too large to enter the agarose gel. However, upon incubation with a type II topoisomerase, individual minicircles are released and migrate into the gel due to their smaller size.

Quantification of the decatenation activity of the mutated proteins was performed by assaying decatenation with increasing protein concentrations. ImageQuant software was used to measure the total amount of released minicircles (decatenation products) and the total amount of kDNA. At each protein concentration the decatenation products were divided by the amount of kDNA and expressed as a percentage. Quantification was performed for three replicate experiments to allow statistical analysis to be performed. The means of decatenation activity were then plotted against protein concentration and error bars representing one standard deviation from the mean included.

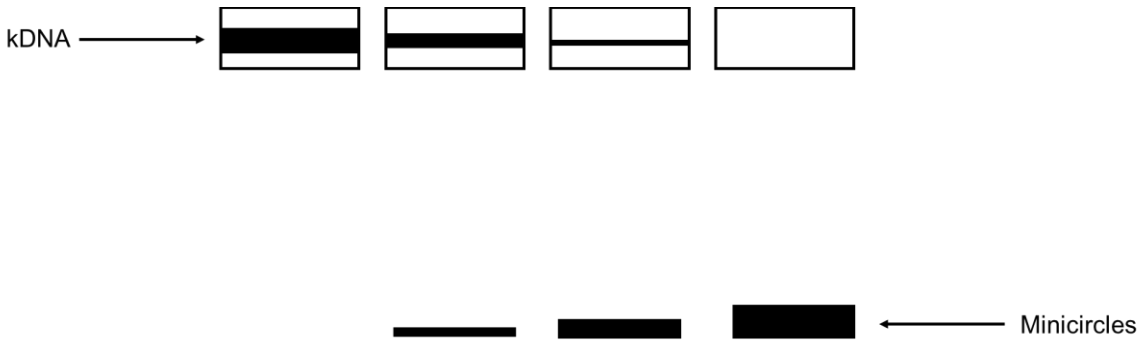

Figure 2-4: Decatenation of kDNA by topoisomerase II

Decatenation produces individual minicircles released from a large network of interlinked minicircles known as kDNA. Minicircles are visualised on an agarose gel, whereas kDNA is too large to enter the gel and therefore is concentrated at the top of the gel.

2.22.4 End Labelled Linear DNA cleavage

Double stranded oligonucleotides labelled at the 5' end with the fluorophore IRDye700 were incubated with 1.2 µg of TOP2B in the presence of 10 mM Ca^{2+} or 10 mM Mg^{2+} unless otherwise stated in figure legends. Drugs were added where specified to the concentration stated in figure legends. Cleavage reactions were carried out in 5x GR buffer, 1 mM ATP, and 1 µM oligonucleotide per reaction. Reactions were incubated at 37 °C for 30 minutes, then the covalent complexes were irreversibly trapped by adding 0.1% (v/v) SDS, followed by 25 mM EDTA, and proteinase K (0.5 mg/mL) to digest TOP2B, and incubation continued for 1 hour. Samples were ethanol precipitated (2x vol.), 0.1x vol. 3 M sodium acetate pH 5.2 and 5 µL glycogen at -20 °C overnight. DNA was pelleted by centrifugation at 19,721 g for 15 minutes and the supernatant was discarded. Precipitated DNA was re-suspended in 10 µL of dH_2O and 40 µL of formamide loading buffer. Samples were heated at 95 °C for 2 minutes and resolved by electrophoresis at 200 V in a 40% Tris/Bis (29:1) urea acrylamide gel made with 1x TBE. Gels were pre-run for 30 minutes at 200 V in 1x TBE buffer prior to sample loading. Cleavage products were visualised using Licor Odyssey imager (Figure 2-5) and quantified as a percentage of total DNA using ImageQuant software.

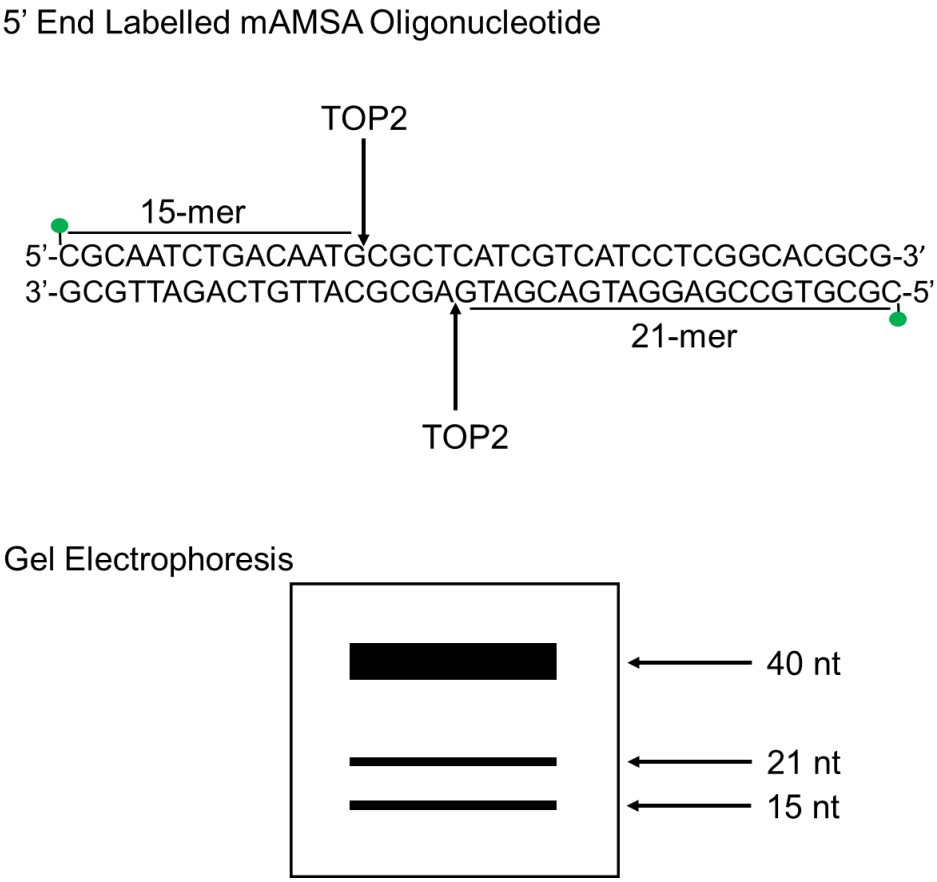

Figure 2-5: End labelled linear DNA cleavage by topoisomerase II

40 nucleotide mAMSA oligonucleotide is 5’ end labelled with IRDye700 (green circles). The cleavage site is asymmetrically positioned in the oligonucleotide. Consequently, cleavage of the oligonucleotide results in two products of different sizes; 21 and 15 nucleotides that migrate at different positions on an acrylamide gel. Thus, both cleavage products can be identified and quantified. The oligonucleotide was selected because there is a strong cleavage site for mAMSA. Arrows represent the site of enzyme cleavage. Only the 15-mer and 21-mer products are visualised by electrophoresis because a fluorescent tag is required for identification.

2.22.5 Statistical Analyses

Statistical analysis involving means, standard deviations and standard errors were calculated using GraphPad Prism (version 7). Statistical significance between different proteins and conditions was calculated using GraphPad Prism with a one or two way ANOVA and Tukey's Multiple Comparison Test or Bonferroni post-test respectively. A P value of 0.05 or less was considered significant.

Chapter 3 Cloning, Expression and Purification of TOP2B ATPase Domain and Biochemical analysis of ATP Hydrolysis Activity

3.1 Introduction

Type II topoisomerase enzymes are comprised of discrete structural domains that are evolutionarily conserved sharing sequence similarity and containing highly conserved functional motifs (Figure 1-4B and Figure 3-1A). The initial N-terminal half of the ATPase domain contains the ATP binding site and is directly involved in clamp closure, undergoing dimerisation upon ATP binding. The ATP-binding fold within this region is known as the Bergerat fold which is common to the GHKL-type ATPases (Dutta and Inouye 2000, Corbett and Berger 2004). The C-terminal half of the ATPase domain forms the transducer domain, which connects the ATPase domain to the enzyme core (Oestergaard, Giangiacomo et al. 2004). The transducer domain relays the signals of ATP binding and hydrolysis between the ATPase domain and the breakage-rejoining core via conformational changes in the enzyme (Classen, Olland et al. 2003, Schmidt, Osheroff et al. 2012, Vanden Broeck, Lotz et al. 2021). Human TOP2B possesses an alternative splice variant in the ATPase domain where an additional five amino acids (T-L-F-D-Q) encoded by 15 nucleotides are inserted into the mRNA via differential splicing after valine 23 (Davies, Jenkins et al. 1993) (Figure 3-1B). Both TOP2B isoforms are expressed in human tissues as detailed from RNA-seq data on the genotype-tissue expression (GTEx) portal (Consortium 2020).

The ATPase reaction of human TOP2B has been studied previously using the full-length enzyme, which showed it is a DNA-dependent ATPase (West, Turnbull et al. 2002). Although, the construct used in these studies lacked the initial N-terminal amino acids with the recombinant protein starting at residue 46. Similarly, when the isolated ATPase domain of TOP2A (residues 29-425) was utilised results showed that the intrinsic ATPase activity can be stimulated with nucleic acid (Gardiner, Roper et al. 1998, Campbell and Maxwell 2002). Using site-directed mutagenesis the catalytic residue for ATP hydrolysis of human TOP2A was identified as Glu86. As the amino acid sequences of type II topoisomerases are highly conserved within this region of the protein, it was possible to predict that the catalytic base in human TOP2B is Glu103. Thus, to investigate the ATPase activity of TOP2B further, and confirm the catalytic residue for ATP hydrolysis, the isolated ATPase domain was cloned, expressed and purified for biochemical analysis. A range of human TOP2B proteins

were generated: an N-terminal truncated protein (45-444) equivalent to the region of TOP2A that has been studied (Gardiner, Roper et al. 1998), the patient mutation K172R, the hypothesised catalytic inactive protein E103A, the full-length ATPase domain (1-444), the alternative splice variant (1-449) and a point mutation V23S. This chapter details the ability of these TOP2B proteins to carry out ATP hydrolysis by measuring the release of free phosphate (P_i).

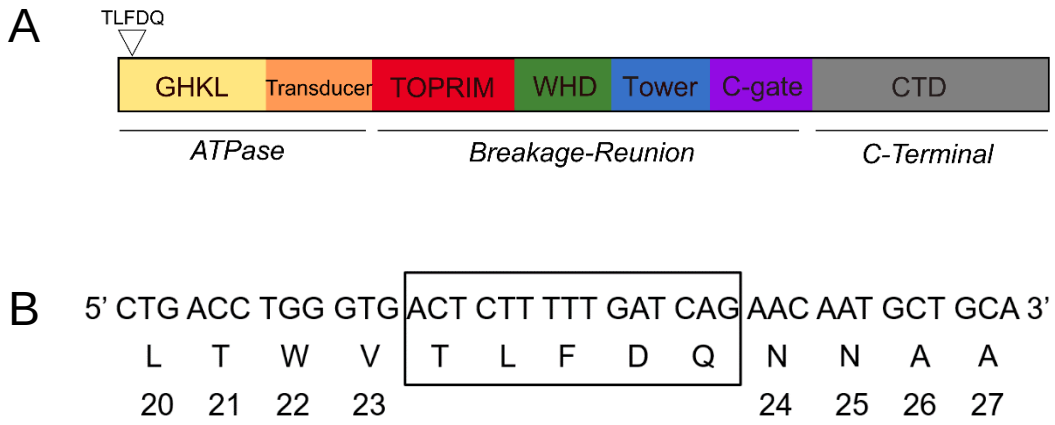

Figure 3-1: Domain arrangement and alternative splice variant of human TOP2B

(**A**) Schematic representation of the domain arrangement of type II topoisomerases with the alternative exon (TLFDQ) for human TOP2B indicated. (**B**) The exon sequence is arranged in coding triplets with the corresponding amino acid underneath in the one letter code. The numbering of amino acids shown below the one letter code corresponds to the constitutive spliced TOP2B protein. The 15 base pairs specific for the alternatively spliced TOP2B mRNA are within a box. Both TOP2B mRNAs are widely expressed in human cells and tissues.

3.2 Cloning

The ATPase domain of human TOP2A has previously been expressed and crystallised using a 6xHis-MBP tagged T7 expression vector with a tobacco etch virus (TEV) protease cleavage site (Wei, Ruthenburg et al. 2005). Therefore, owing to the high degree of similarity (82%) between the ATPase domains of TOP2A and TOP2B, the methodology used to express the ATPase domain of TOP2A could be applicable to TOP2B. The region homologous to TOP2A that was expressed and crystallized (28-428) corresponds to amino acids 45-444 of TOP2B (referred to as S45, for serine position 45). S45 was cloned into the bacterial expression vectors 1B (addgene #29653) and 1C (addgene #29654) by ligation independent cloning (LIC) described previously in Chapter 2, Section 2.14.2. The expression vector 1B contains a TEV cleavable N-terminal 6xHis tag and the vector 1C contains a TEV cleavable N-terminal 6xHis-MBP tag. The full-length ATPase domain starting at amino acid 1 (referred to as M1, for methionine position 1) of TOP2B was also cloned into the vectors to gain an understanding of the effect of the initial N-terminal region (1-44) on the ATPase activity. The ATPase domain of human TOP2A that has been previously crystallised (Wei, Ruthenburg et al. 2005) was also cloned for use as a positive control. Forward and reverse primers containing LIC sequences compatible with the expression vectors were used (Table 2-1). PCR products were run on an agarose gel to confirm the presence of a DNA fragment of the correct size (~1.2 Kb) and gel extracted via Qiagen gel extraction kit.

Both vectors, 1B and 1C, were then linearized with the restriction enzyme *SSP1* and the LIC reaction was performed. Combined LIC vector and LIC insert were transformed into XL1 Blue competent cells for plasmid DNA amplification. To confirm cloning had been successful plasmid DNA was sent for DNA sequencing with primers described in Table 2-2. M1, S45 and TOP2A (28-428) had been cloned into the 1B vector, whilst only M1 was successfully cloned in the 1C vector. Protein expression was initiated with the constructs in 1B and M1 in 1C, whilst cloning of S45 and TOP2A (28-428) into 1C continued.

3.3 Protein Expression

Due to the availability of the three target proteins as a 6xHis construct in the 1B vector, recombinant protein expression was first initiated with these constructs. Proteins

expressed with just a 6xHis tag have the advantage of not necessarily needing to undergo cleavage of the tag after purification. Whereas proteins expressed with an MBP tag require removal of the tag at some stage during purification because the tag is much larger in comparison to a 6xHis tag and may interfere with protein folding and/or the proteins *in vitro* activity. Thus, if successful expression with smaller tags like a 6xHis tag can save considerable time during the purification process.

Recombinant protein expression was under the control of an IPTG inducible promoter as continuous expression of topoisomerase II is deleterious to bacteria. Protein expression was first attempted under the same conditions that were used to obtain the ATPase domain of TOP2A. The 1B constructs were transformed into the Rosetta 2 (DE3) strain and induction was initiated with 1 mM IPTG at 30 °C (Wei, Ruthenburg et al. 2005). Unfortunately, these conditions did not yield soluble protein (Figure 3-2). The recombinant proteins were present in the pellet after cell lysis indicating their existence in insoluble inclusion bodies, whereas proteins present in the supernatant after cell lysis indicate proteins soluble in nature. The 1B vector gave rise to 6xHis tagged proteins with the corresponding sizes: M1 51.7 kDa, S45 47.6 kDa, and TOP2A (28-428) 47.3 kDa.

Several other conditions were trialled in an attempt to achieve soluble protein using *E. coli* cells. Such conditions included trying different strains containing mutations or additional plasmids that affect the cytoplasmic environment, and the type of tRNAs or chaperones available (Bessette, Aslund et al. 1999, Mogk, Mayer et al. 2002) (Table 3-1). Secondly, different induction conditions were trialled that can increase the amount of soluble protein by reducing the rate of protein expression allowing more time for protein folding to occur. For example, reducing the temperature and concentration of induction agent can slow protein synthesis allowing sufficient time for the target protein to fold which can aid solubility (Schein 1989). Furthermore, different media compositions can affect protein solubility as different medias contain different amounts of trace elements and vitamins (Sørensen and Mortensen 2005). As such, a range of expression conditions and bacterial strains shown in Table 3-2 were trialed on a small scale (50 mL) in order to produce soluble protein. Samples were taken four hours after induction and the following morning, however, unfortunately none of these conditions produced soluble recombinant protein.

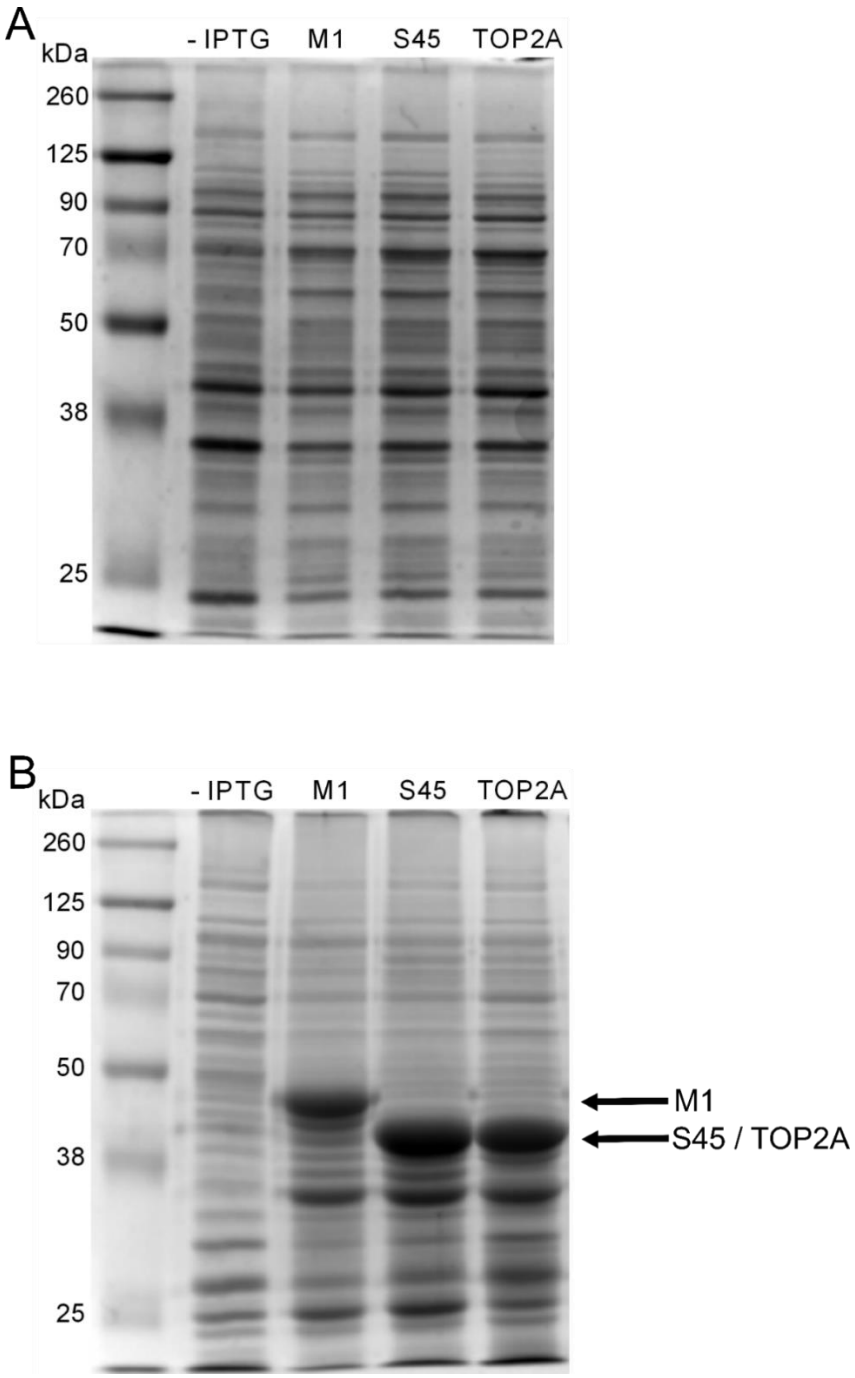

*Figure 3-2: Soluble (**A**) and insoluble (**B**) proteins expressed during induction of Rosetta 2 (DE3) cells transformed with the ATPase domain constructs*

12% SDS polyacrylamide gel of test inductions carried out in Rosetta 2 (DE3) cells transformed with M1 (1-444, lane 3), S45 (45-444, lane 4) or TOP2A (28-428, lane 5) in the 1B expression vector. Induction was performed with 1 mM IPTG at 30 °C. The molecular weights of protein markers are shown in lane 1. Lane 2 is the negative control containing transformed Rosetta 2 (DE3) cells grown without IPTG induction. Samples were lysed by sonicating for 2 minutes and centrifuged at 75397 g for 10 minutes at 4 °C. The supernatant was collected and loading buffer added prior to

heating at 95 °C for 10 minutes. The proteins from this soluble fraction are shown in gel A. Whilst the cell pellet was resuspended in equal amounts of lysis buffer (50 mM Tris HCl pH 8, 150 mM NaCl) and loading buffer before heating at 95 °C for 10 minutes. Gel B shows the insoluble proteins present in the cell pellet after lysis. Arrows indicate recombinant protein expression.

Bacterial Strain	Properties
BL21 (DE3)	Typical *E. coli* protein expression strain. BL21 cells contain the lambda DE3 prophage that carries the gene for T7 RNA polymerase under the control of a lacUV5 promoter. Therefore, expression of the T7 RNA polymerase is induced with IPTG.
Rosetta 2 (DE3)	BL21 derivative designed to enhance the expression of eukaryotic proteins. Supplies tRNAs for the seven codons specific to eukaryotic protein expression. Also, the strain used to obtain soluble protein expression of the ATPase domain of human TOP2A.
Rosetta – Gami 2 (DE3)	Rosetta - Gami 2 cells combine the features of Rosetta 2, to reduce codon bias with Origami 2 strains which allow disulfide bonds to form in the cytoplasm of *E. coli.*
Arctic Express (DE3)	BL21 derivative that allows protein expression to be performed at low temperatures (≤10 °C) to slow protein production with the aim of increasing protein solubility. Arctic Express cells contain cold adapted chaperones to ensure protein folding is not negatively impacted by the low temperatures.

Table 3-1: Different bacterial strains used in an attempt to express soluble ATPase domain protein

Rosetta 2 cells are a BL21 derivative and were trialed first as this was the strain used for expression of the TOP2A ATPase domain in soluble form (Wei, Ruthenburg et al. 2005). However, as Rosetta 2 cells did not produce soluble TOP2B ATPase domain expression, Rosetta-Gami 2 cells were trialed next. Rosetta-Gami 2 also possess the tRNAs for rare eukaryotic codons as well as mutations in glutaredoxin and thioredoxin reductases to allow disulphide bond formation. Incorrect or lack of disulphide bonds can lead to insoluble protein production; however, this strain did not give target protein expression. Following Rosetta-Gami 2, Arctic Express cells were trialed. Arctic Express cells slow protein expression by growth at low temperatures allowing sufficient time for protein folding. The cells feature the cold-adapted chaperonins; Cpn60 and Cpn10 to ensure proper protein folding occurs even at low temperatures. However, the proteins were not expressed in Arctic Express cells.

Bacterial Strain	Temperature (°C)	IPTG Concentration	Media	Target Protein Expressed	Solubility
Rosetta 2 (DE3)	25	1 mM	LB	Y	Insoluble
	16	0.5 mM	2xYT	Y	Insoluble
	20	0.5 mM	2xYT	Y	Insoluble
	20	50 µM	2xYT	Y	Insoluble
	16	10 µM	TB	N	N/A
	18	0	2xYT	N	N/A
	18	N/A	Autoinduction	Y	Insoluble
	18	0.5 mM	2xYT	Y	Insoluble
Rosetta-Gami (DE3)	20	0.1 mM	2xYT	N	N/A
	25	0.1 mM	LB	N	N/A
	16	0.5 mM	2xYT	N	N/A
Arctic Express (DE3)	10	0.5 mM	2xYT	N	N/A
	10	0.5 mM	LB	N	N/A

Table 3-2: All conditions trialled in order to try to achieve soluble ATPase domain protein expressed in bacterial cells

In the meantime, cloning of the target proteins into the 1C vector continued. Once it had been confirmed by DNA sequencing that all three proteins had been cloned into the 1C vector, expression trials with the 6xHis-MBP constructs were carried out. It was believed that soluble protein could be obtained in bacterial cells because the ATPase domain of human TOP2A had been produced in this manner, which is highly homologous to human TOP2B, and theoretical predictions of solubility from the online site Protein-Sol, gave high solubility values for the ATPase domain of TOP2B being produced in bacterial cells. From the amino acid sequence, the solubility predication values obtained for M1 and S45 were 0.451 (Hebditch, Carballo-Amador et al. 2017). The population average of the experimental solubility dataset is 0.45, thus a protein with a predicted solubility value greater than 0.45 is expected to have higher solubility than the average soluble *E. coli* protein and a protein with a lower solubility value is predicted to be less soluble (Niwa, Ying et al. 2009).

The 1C vector gives rise to 6xHis-MBP tagged proteins, thus target proteins in 1C have a much larger molecular weight than the constructs in 1B. M1 has a molecular weight of 94.6 kDa, S45 is 90.3 kDa and TOP2A (28-428) is 90.3 kDa. Insoluble target protein was achieved when induction was performed as per previously reported for crystallisation of TOP2A (Wei, Ruthenburg et al. 2005), with LB media and 0.5 mM IPTG overnight at 20 °C. However, when autoinduction media was used soluble protein was obtained for all three proteins (Figure 3-3), although there was a much lower quantity of the full-length ATPase domain of TOP2B M1 compared to TOP2B S45 and TOP2A (28-428).

To achieve soluble protein, 50 mL 2xYT, with appropriate antibiotics, was inoculated with a single colony of transformed Rosetta 2 (DE3) cells and grown overnight at 37 °C. The following morning 1 L of autoinduction media, supplemented with 0.3% glycerol and appropriate antibiotics was inoculated with 0.5% overnight culture. Inoculated flasks were incubated at 37 °C and shaken at 200 RPM for 4 hours before reducing the temperature to 20 °C and allowing induction to take place overnight. Cultures were then centrifuged at 2824 g for 15 minutes at 4 °C and the supernatant discarded. Cell pellets were stored at -20 °C until the proteins were required.

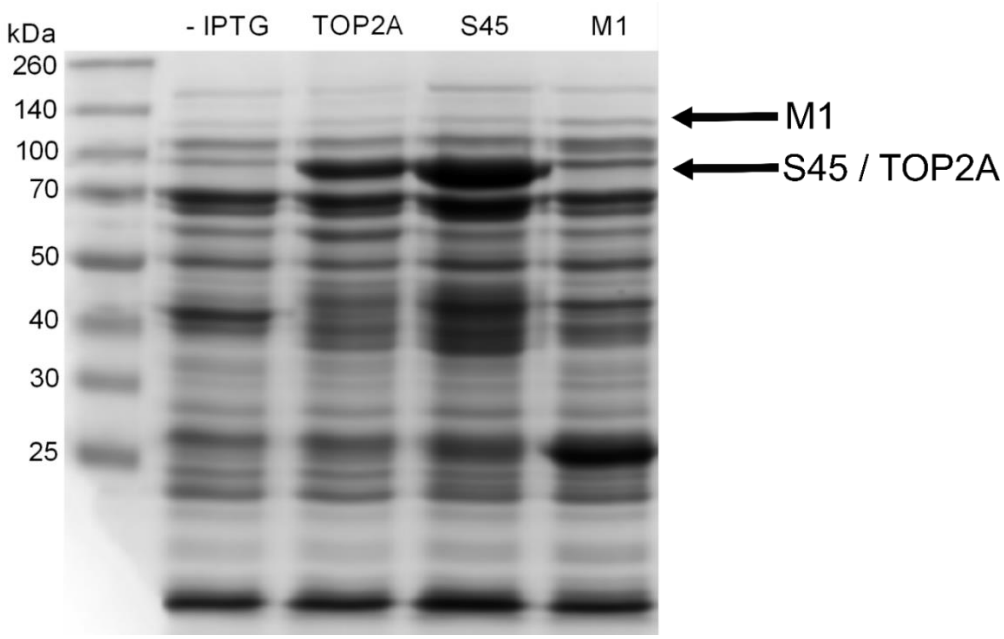

Figure 3-3: Soluble protein expression of the ATPase domain of human topoisomerase II fused to a 6xHis-MBP tag

10% SDS polyacrylamide gel of test inductions carried out on Rosetta 2 (DE3) cells transformed with the ATPase domain constructs in the 1C expression plasmid. Induction was performed with autoinduction media at 20 °C overnight. Samples were lysed by sonicating for 2 minutes and centrifuged at 75397 g for 10 minutes at 4 °C. 10 µL supernatant was mixed with 10 µL loading buffer before heating at 95 °C for 10 minutes for identification of proteins soluble in nature. The molecular weights of protein markers are shown in lane 1. Lane 2 is the negative control, Rosetta 2 (DE3) cells transformed with the 1C empty vector, lanes 3-5 are the overexpressed soluble target proteins in 1C vector (TOP2A, S45 and M1 respectively). Arrows indicate recombinant proteins.

3.4 Buffer Optimisation

To determine the optimum buffer conditions for purification of the ATPase domain proteins, three different buffers were trialed to find the pH which gives maximal protein binding to an affinity column. 1 L bacterial cell culture was used for each condition and the bacteria were lysed via sonication prior to loading on a nickel affinity column. The buffers ranged from pH 7 - pH 9 and contained 150 mM NaCl. The buffers used were 50 mM HEPES pH 7, 50 mM Tris pH 8 and 50 mM CHES pH 9. As observed in Figure 3-4, Tris pH 8 gave the best binding of target protein to the column with minimal loss of target protein in the flow through or wash stages, suggesting tight binding to the column. Whereas with HEPES pH 7, target protein was observed in all fractions including the flow through. This resulted in large losses of the target protein, indicating its unsuitability. CHES pH 9 gave a better elution profile compared to HEPES pH 7 however, there was still some target protein being lost in the flow through and the target protein was spread across multiple elution fractions. Whereas with Tris pH 8, the target protein was very concentrated in the second fraction and was therefore selected as the buffer to use during purification of the TOP2B ATPase domain.

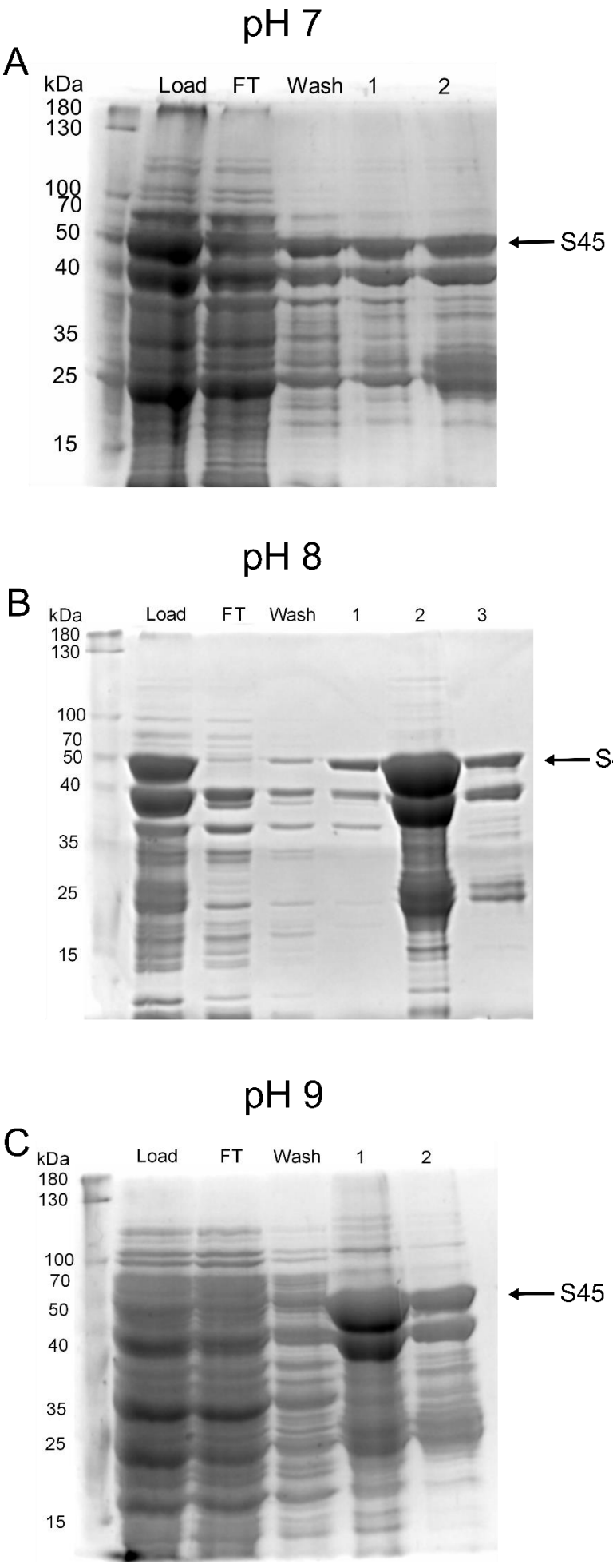
pH 7
A
kDa
Load
FT
Wash
1
2
180
130
100
70
50
40
35
25
15
S45
pH 8
B
kDa
Load
FT
Wash
1
2
3
180
130
100
70
50
40
35
25
15
S45
pH 9
C
kDa
Load
FT
Wash
1
2
180
130
100
70
50
40
35
25
15
S45

Figure 3-4: Purification of the S45 ATPase domain TOP2B 45-444 with a range of different buffers: HEPES pH 7, Tris pH 8 and CHES pH 9 (previous page)

To determine a suitable pH for purification of the ATPase domain, three different buffers with different pH's were trialled: 50 mM HEPES pH 7 (**A**), 50 mM Tris pH 8 (**B**) and 50 mM CHES pH 9 (**C**). All buffers also contained 150 mM NaCl. Bacterial pellets were resuspended in one of the above three buffers and lysed via sonication. Samples were centrifuged at 75397 g for 15 minutes at 4 °C to separate the cell debris from the soluble proteins. The target protein was then purified with a nickel affinity column (His Trap) and samples run on a 10% SDS polyacrylamide gel. Each lane contains 15µL of sample and 5µL SDS loading buffer. Lane 1 are the molecular markers, lane 2 lysed whole cell extract, lane 3 His trap flow through, lane 4 His trap wash, lane 5 His trap fractions 1-2 (for **A** and **C**) or fractions 1-3 (for **B**). Arrows indicate target protein.

3.5 Protein Purification

S45 was expressed on a large scale and 6 L of culture was used during each protein purification. 6 L of bacteria grown in autoinduction media overnight generally yielded ~80 g of cell pellet. The pellets were resuspended in 50 mM Tris HCl pH 8 and 150 mM NaCl prior to cell lysis via sonication. Centrifugation was performed at 75397 g for 15 minutes at 4 °C to separate the broken cell debris from the soluble proteins. Protein purification was performed as per Table 3-3. Employing the presence of a 6xHis tag, the proteins were first purified using nickel affinity chromatography (His Trap column). A 50 mM imidazole wash was included to remove any non-specifically bound proteins from the nickel column. The protein was then eluted from the nickel column with a 500 mM imidazole step. At this stage the protein was substantially purer (Figure 3-5A lane 4) so the 6xHis-MBP tag could be removed before the next purification steps.

The construct was designed to contain a TEV cleavage site between the 6xHis-MBP tag and the target protein for easy removal of the tag. TEV cleavage was initially trialed at 4 °C overnight and room temperature for 3-4 hours. When cleavage was performed at 4 °C, a large amount of uncleaved protein remained due to the TEV enzyme being less efficient at lower temperatures (Raran-Kurussi, Tözsér et al. 2013). Therefore, TEV cleavage at room temperature was routinely used. The TEV protease used during cleavage was expressed from the pRK793 plasmid as a 6xHis fusion protein (Kapust, Tözsér et al. 2001), permitting TEV to be easily removed during the purification process at a later stage.

As TOP2B is a DNA-binding protein, a heparin column was used next in the purification process (Figure 3-5A-B). Heparin acts as an affinity ligand for DNA binding proteins as it mimics the polyanionic structure of nucleic acids, as well as acting as a cation exchanger. Indeed, TOP2B bound to the column whilst other proteins, including the 6xHis-MBP tag, eluted either in the flow through or wash (Figure 3-5A lanes 6-7). Once the UV plateaued; TOP2B was eluted off the column with a 5 CV gradient to 100% buffer B, 50 mM Tris HCl pH 8, 500 mM NaCl (Figure 3-5B lanes 4-9). Notably, because the heparin column also acts as a cation exchanger, at pH 8 the TEV protease also bound to the column and eluted with TOP2B. Consequently, a 2nd nickel affinity column was required to remove TEV. Theoretically, TEV and any remaining 6xHis-MBP tag or uncleaved TOP2B protein should bind to the nickel column whilst the cleaved, untagged protein should no longer bind and instead appear in the flow through.

However, during the initial attempt the untagged protein bound to the column with all the other protein contaminants. This was due to the TOP2B ATPase having a low intrinsic affinity to the nickel column even in the absence of a 6xHis tag. Adding a small amount of imidazole (30 mM) to the sample prior to column loading prevented TOP2B from binding to the column (Figure 3-5C lane 3) whilst still allowing TEV to bind (Figure 3-5C lanes 4-8).

Finally, size exclusion chromatography was used as a polishing step. A Superdex 75 column was selected because the molecular weight (MW) of the untagged target protein is ~45 kDa which falls within the Superdex 75 range (3-70 kDa). The main UV peak was observed at 60 mL with typical UV absorbance of 300 mAU. The fractions within this peak were pooled (Figure 3-5D lanes 6-10) and concentrated to either 16 mg/mL for use in crystallography immediately (Chapter 4) or 3.5 mg/mL for biochemistry experiments. 50% glycerol was added to protein fractions used for biochemistry analysis and flash frozen in liquid nitrogen then stored at -80 °C for use within two months.

During the purification it became apparent that there were two recombinant protein bands, one at 90 kDa which is the theoretical size of the target protein and a smaller band at 80 kDa (Figure 3-5). Both protein bands were detected as the recombinant protein during an anti-His western blot. Therefore, it is likely that the smaller band was a C-terminal truncated version of the target protein. Protease inhibitors (1 mM Benzamidine, 1 mM PMSF, 50 µM Leupeptin and 50 µM Pepstatin) were included initially in case the target protein was being degraded during purification, however this did not reduce the presence of the smaller band and therefore protease inhibitors were not included during subsequent purifications.

Step	Column or Protease	Conditions
1	His Trap (35 mL)	Buffer A: 50 mM Tris HCl pH 8, 150 mM NaCl Buffer B: 50 mM Tris HCl pH 8, 150 mM NaCl, 500 mM Imidazole Load at 5 mL/min 10% B Step to remove non-specifically bound proteins Step elution to 100% B
2	TEV Cleavage	TEV added at a 1:20 ratio (protease:substrate) Cleavage performed at room temperature for 4 hours Gentle mixing
3	Heparin (5 mL)	Buffer A: 50 mM Tris HCl pH 8, 150 mM NaCl Buffer B: 50 mM Tris HCl pH 8, 500 mM NaCl Load at 5 mL/min 25 mL gradient to 40% B to remove non-target proteins 25 mL gradient to 100% B to elute target protein
4	His Trap (5 mL)	Buffer A: 50 mM Tris HCl pH 8, 150 mM NaCl, 30 mM Imidazole Buffer B: 50 mM Tris HCl pH 8, 150 mM NaCl, 500 mM Imidazole Prior to loading, 30 mM (final concentration) Imidazole was included in sample Load at 5 mL/min Flow through collected Step elution to 100% to remove bound TEV
5	Superdex 75 (120 mL)	Buffer A: 25 mM Tris HCl pH 8, 150 mM NaCl Flow through from the previous column concentrated to less than 5 mL using amicon ultra centrifugal filter (30 kDa MWCO) Sample eluted at ~60 mL

Table 3-3: Protocol for the purification of the ATPase domain of human TOP2B expressed from the 1C vector

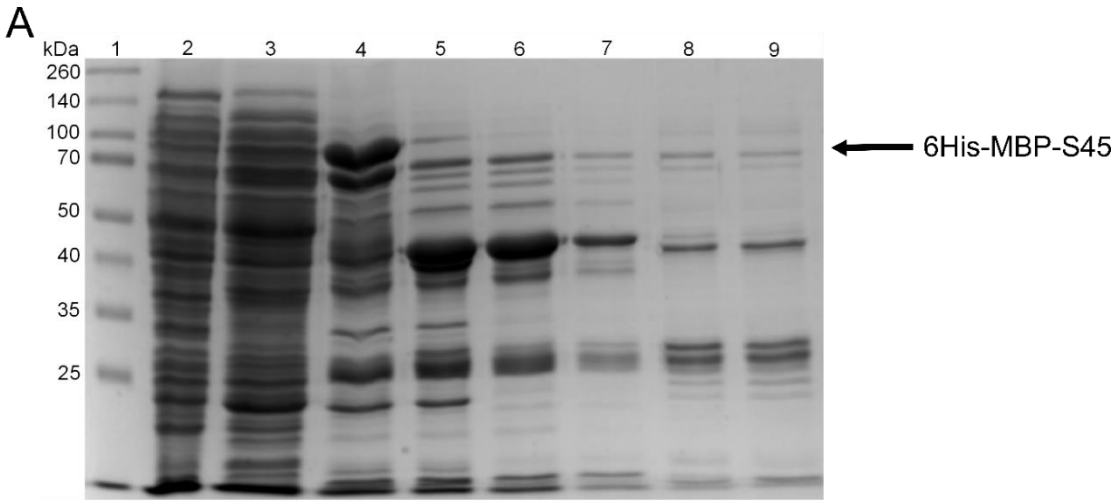
A
kDa
1
2
3
4
5
6
7
8
9
260
140
100
70
50
40
35
25
6His-MBP-S45

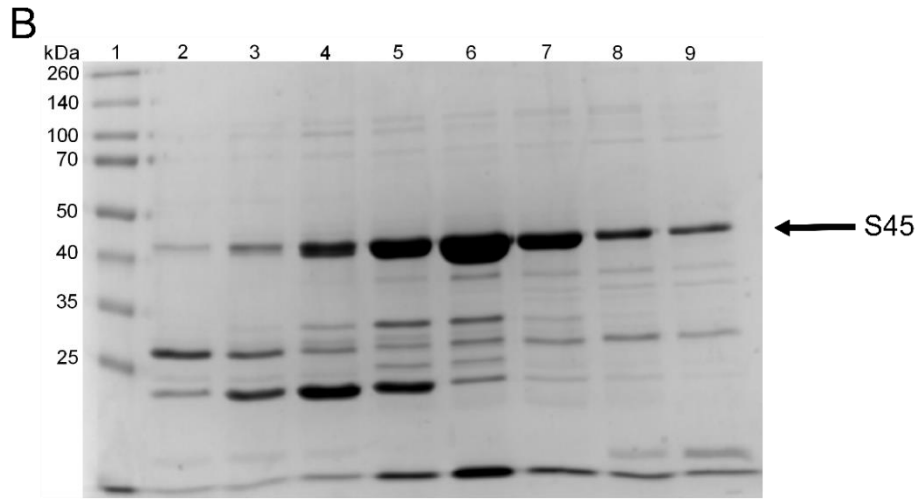
B
kDa
1
2
3
4
5
6
7
8
9
260
140
100
70
50
40
35
25
S45

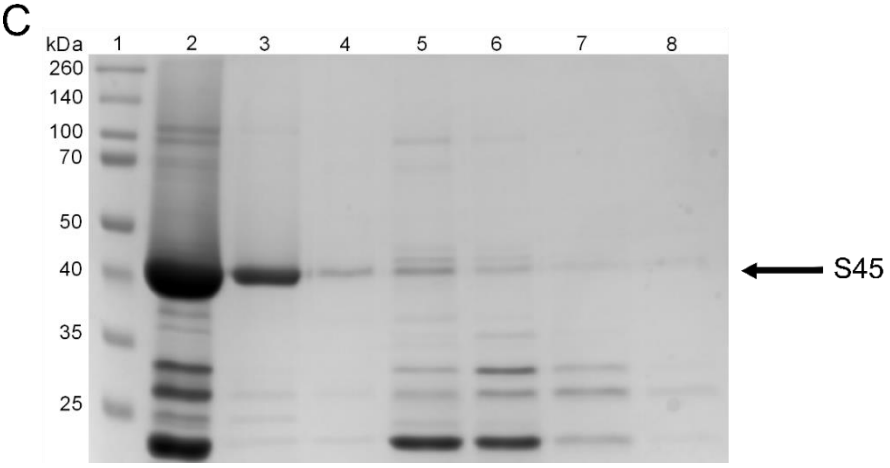
C
kDa
1
2
3
4
5
6
7
8
260
140
100
70
50
40
35
25
S45

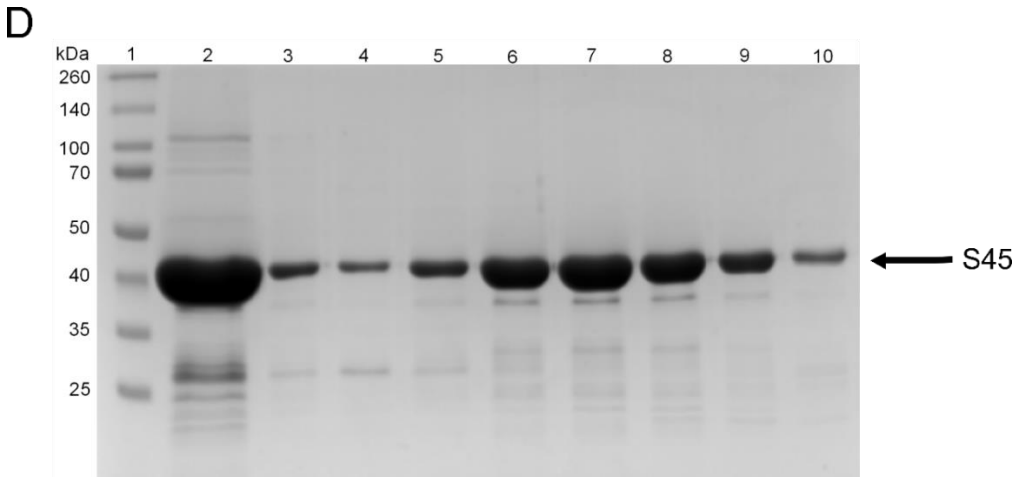

Figure 3-5: Purification of the ATPase domain of human TOP2B and cleavage of the N-terminal 6xHis-MBP tag (current page and previous page)

Each lane contains 15 µL of sample and 5 µL SDS loading buffer. Arrows indicate recombinant proteins. (**A**) 10% SDS polyacrylamide gel of samples from the first and second purification step, His trap and heparin. Lane 1 molecular markers, lane 2 lysed whole cell extract, lane 3 His trap flow through, lane 4 His trap elution, lane 5 heparin load, lane 6 heparin flow through, lane 7 heparin wash, lanes 8-9 heparin fractions 3 and 5. (**B**) 10% SDS polyacrylamide gel of the remaining heparin fractions. Lane 1 molecular markers, lanes 2-9 heparin fractions 11-18. (**C**) 10% SDS polyacrylamide gel of samples from the third purification step, 2nd His trap column. Lane 1 molecular markers, lane 2 2nd His trap load, lane 3 2nd His trap flow through, lanes 4-8 fractions 1-5. (**D**) 10% SDS polyacrylamide gel of samples from the final purification step, Superdex 75. Lane 1 molecular markers, lane 2 S75 load, lanes 3-4 S75 fractions 3-4, lanes 5-10 S75 fractions 6-11. In this purification, fractions 6-10 were pooled for use in either biochemistry or crystallography experiments.

3.6 Cloning of Mutated Proteins

Due to the success of expressing and purifying the wild type N-terminal truncated ATPase domain of human TOP2B (S45) a range of ATPase domain mutated proteins were generated. These included the patient mutation K172R, and the mutated protein E103A, to verify whether residue 103 is the catalytic base. Both K172R and E103A were generated via site directed mutagenesis of the TOP2B 45-444 S45 construct (S45 E103A). A forward and reverse oligonucleotide primer containing the desired mutation (Chapter 2, Section 2.14.6) were annealed onto the template plasmid. PCR was performed to amplify the mutation into the template followed by *DPNI* digestion to remove the original non-mutagenised plasmid. The mutated plasmid was transformed and replicated in *E. coli* prior to plasmid isolation by a Qiagen mini prep. Plasmid DNA was sent for sequencing using primers described in Chapter 2, Section 2.14.5 to determine whether the mutagenesis had been successful.

As soluble protein was achieved for the full-length TOP2B ATPase domain, M1 (1-444), albeit to a lower extent, a point mutation at residue 23 was studied (M1 V23S) as well as the catalytically inactive mutation E103A in the full-length TOP2B ATPase domain protein (M1 E103A). Moreover, the alternative splice variant of human TOP2B was also generated, which contains an additional five amino acids after V23, TOP2B 1-449 (M1 Splice). The site directed mutagenesis kit can efficiently insert 15 bps, therefore the additional five amino acids in the splice variant were inserted into the M1 construct by this method.

3.7 Purification of Mutated Proteins

The optimised protocol for purifying wild type N-terminal truncated human TOP2B ATPase domain (S45, 45-444) was also used to purify the other ATPase domain proteins from constructs described above: K172R (45-444), M1 (1-444), M1 V23S (1-444), M1 Splice (1-449), TOP2A (28-428), and the two predicted catalytically inactive proteins E103A in the S45 vector (S45 E103A, 45-444) and E103A in the M1 vector (M1 E103A, 1-444). As the mutated proteins are highly homologous to S45 it was hypothesised that the same purification protocol as per Table 3-3 would be efficient for purifying the mutated proteins.

Generally, the purification protocol worked well, however, the full-length M1 proteins (1-444 or 1-449) were less stable at low salt concentrations (150 mM NaCl). Therefore, the purification protocol was modified so that all buffers contained 500 mM NaCl, apart from buffer A during the heparin column (Table 3-4). As the heparin column acts as both an affinity and ion exchange column, the sample needs to be at low salt for maximum sample binding. Therefore, the heparin buffers were kept the same as previously (Table 3-3). However, immediately prior to loading the sample onto the heparin column, the sample was diluted 1:3 whilst being mixed with a buffer containing no salt (50 mM Tris HCl pH 8). All proteins for biochemistry experiments were purified following this modified protocol to allow comparisons between proteins to be made.

After purification, all proteins were concentrated to 3.5 mg/mL and 50% glycerol was added to enable long term storage of the proteins. The proteins were flash frozen with liquid nitrogen and stored at -80 °C until required for the ATPase assay. All eight TOP2B ATPase domain proteins were purified successfully (Figure 3-6).

Step	Column or Protease	Conditions
1	His Trap (35 mL)	Buffer A: 50 mM Tris HCl pH 8, 500 mM NaCl Buffer B: 50 mM Tris HCl pH 8, 500 mM NaCl, 500 mM Imidazole Load at 5 mL/min 10% B Step to remove non-specifically bound proteins Step elution to 100% B
2	TEV Cleavage	TEV added at a 1:20 ratio (protease:substrate) Cleavage performed at room temperature for 4 hours Gentle mixing
3	Heparin (5 mL)	Buffer A: 50 mM Tris HCl pH 8, 150 mM NaCl Buffer B: 50 mM Tris HCl pH 8, 500 mM NaCl Sample diluted 1:3 with 50 mM Tris HCl pH 8 before loading onto the heparin column Load at 5 mL/min 25 mL gradient to 40% B to remove non-target proteins 25 mL gradient to 100% B to elute target protein
4	His Trap (5 mL)	Buffer A: 50 mM Tris HCl pH 8, 500 mM NaCl, 30 mM Imidazole Buffer B: 50 mM Tris HCl pH 8, 500 mM NaCl, 500 mM Imidazole Prior to loading, 30 mM (final concentration) Imidazole was included in sample Load at 5 mL/min Flow through collected Step elution to 100% to remove bound TEV
5	Superdex 75 (120 mL)	Buffer A: 50 mM Tris HCl pH 8, 500 mM NaCl Flow through from the previous column concentrated to less than 5 mL using amicon ultra centrifugal filter (30 kDa MWCO) Sample eluted at ~60 mL

Table 3-4: Protocol for the purification of the mutated ATPase domain proteins of human TOP2B expressed from the 1C vector

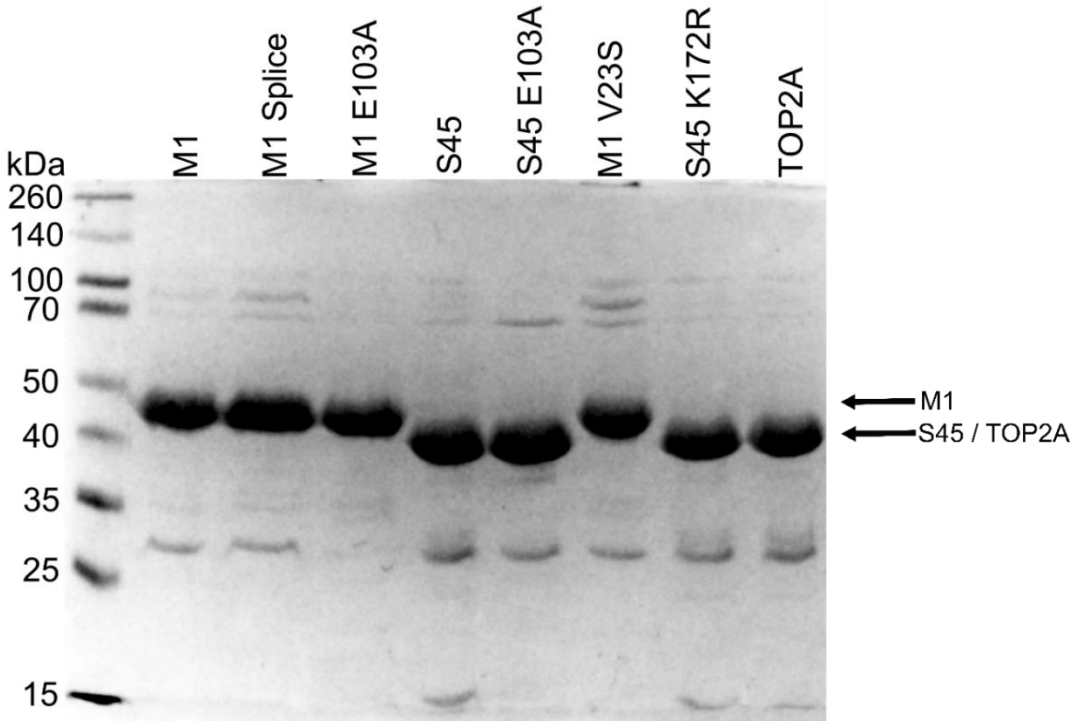

Figure 3-6: Purified human TOP2 ATPase domain proteins

10% SDS polyacrylamide gel with all the different TOP2 ATPase domain proteins. Each lane contains 15 µL of sample and 5 µL SDS loading buffer. Lane 1 molecular markers, lane 2 M1, lane 3 M1 Spice, lane 4 M1 E103A, lane 5 S45, lane 6 S45 E103A, lane 7 M1 V23S, lane 8, K172R, lane 9 TOP2A.

3.8 ATP Hydrolysis Activity

The intrinsic catalytic activity of the ATPase domain variants was tested via an ATPase assay. In the presence of ATP, a functional human topoisomerase II protein will hydrolyse ATP to ADP and release free phosphate ions (P_i). The phosphate ions can be detected by a colour change and thus an increase in absorbance occurs at 655 nm in the presence of the BioMOL green reagent. Using a phosphate standard curve, the amount of free phosphate released can be calculated to give a measure of the ATPase activity of the proteins. Method development and optimisation of the assay was performed with the S45 protein, where the optimal protein concentration was identified as 0.25 µM. The assays were performed in a reaction mixture containing 50 mM Tris HCl pH 7.5, 50 mM KCl, 10 mM $MgCl_2$, and 0.1 mM ATP unless otherwise stated. Protein was then added to start the reaction and incubated at 37 °C for 30 minutes before adding the BioMOL green reagent to terminate the reaction. The mutated proteins, TOP2A (28-428), S45 (45-444), M1 (1-444), M1 Splice (1-449), K172R (45-444), S45 E103A (45-444) and M1 E103A (1-444) were then assayed for ATPase activity at a range of protein and ATP concentrations, as well as in the presence of DNA. The ATPase activity for the M1V23S protein was kindly generated by Will Berry and included in the analysis. Statistical analysis was performed by a two-way ANOVA and Bonferroni post-test.

3.8.1 Activity of the Mutated Proteins

Initially, the ATPase activity of the mutated proteins was measured with a range of different protein concentrations in the presence of 0.1 mM ATP. Generally, increasing the amount of topoisomerase II protein increased the amount of phosphate released, except for the E103A mutations (Figure 3-7A). As hypothesized, neither of the E103A proteins, S45 E103A (TOP2B 45-444) nor M1 E103A (TOP2B 1-444) had appreciable ATPase activity under any of the conditions tested. Even at the highest protein concentration studied (2 µM), no ATPase activity was observed when Glu103 was mutated to an alanine, supporting the proposed role of Glu103 as the catalytic base for ATP hydrolysis by TOP2B. Thus, any ATPase activity observed for the other ATPase domain proteins is a result of a functional type II topoisomerase enzyme.

The ATPase domain of TOP2A was the most active out of all the proteins studied, followed by the equivalent TOP2B protein S45. These ATPase domain proteins lacked the N-terminal amino acids, TOP2A started at amino acid 29, whilst TOP2B S45 started

at amino acid 45. Indeed, it appeared that the initial N-terminal amino acids were inhibitory to ATP hydrolysis as the full-length ATPase domain proteins (M1, M1 V23S, and M1 Splice) had significantly reduced ATPase activity compared to S45 ($P < 0.001$) as shown in Figure 3-7. In fact, their activity could not be measured at protein concentrations below 0.50 µM, whereas TOP2A (28-428), TOP2B S45 (45-444) and the patient mutation TOP2B K172R (45-444) all had appreciable ATPase activity at a protein concentration of 0.10 µM. It is possible that the additional 44 or 49 amino acids at the N-terminus block ATP from binding or being hydrolysed.

When the ATPase activity for S45 (45-444) at a protein concentration of 1 µM was set to 100%, M1 (1-444) had just 36% activity, followed by the M1 Splice variant (1-449) with 45% activity and the point mutation V23S (1-444) was marginally more active with 49% activity compared to S45 (Figure 3-7B). However, there was no significant difference in activity between the three full-length proteins at all protein concentrations trialed ($P > 0.05$), Figure 3-7. The reported patient mutation, K172R in the S45 vector (45-444) had significantly higher activity than the full-length ATPase domain proteins ($P < 0.001$) but significantly lower activity compared to wild type S45 ($P < 0.001$). For example, at 1 µM, K172R had 86% activity compared to S45. As such, the K172R mutation reduced the activity of the S45 protein indicating this residue could be important for ATP hydrolysis.

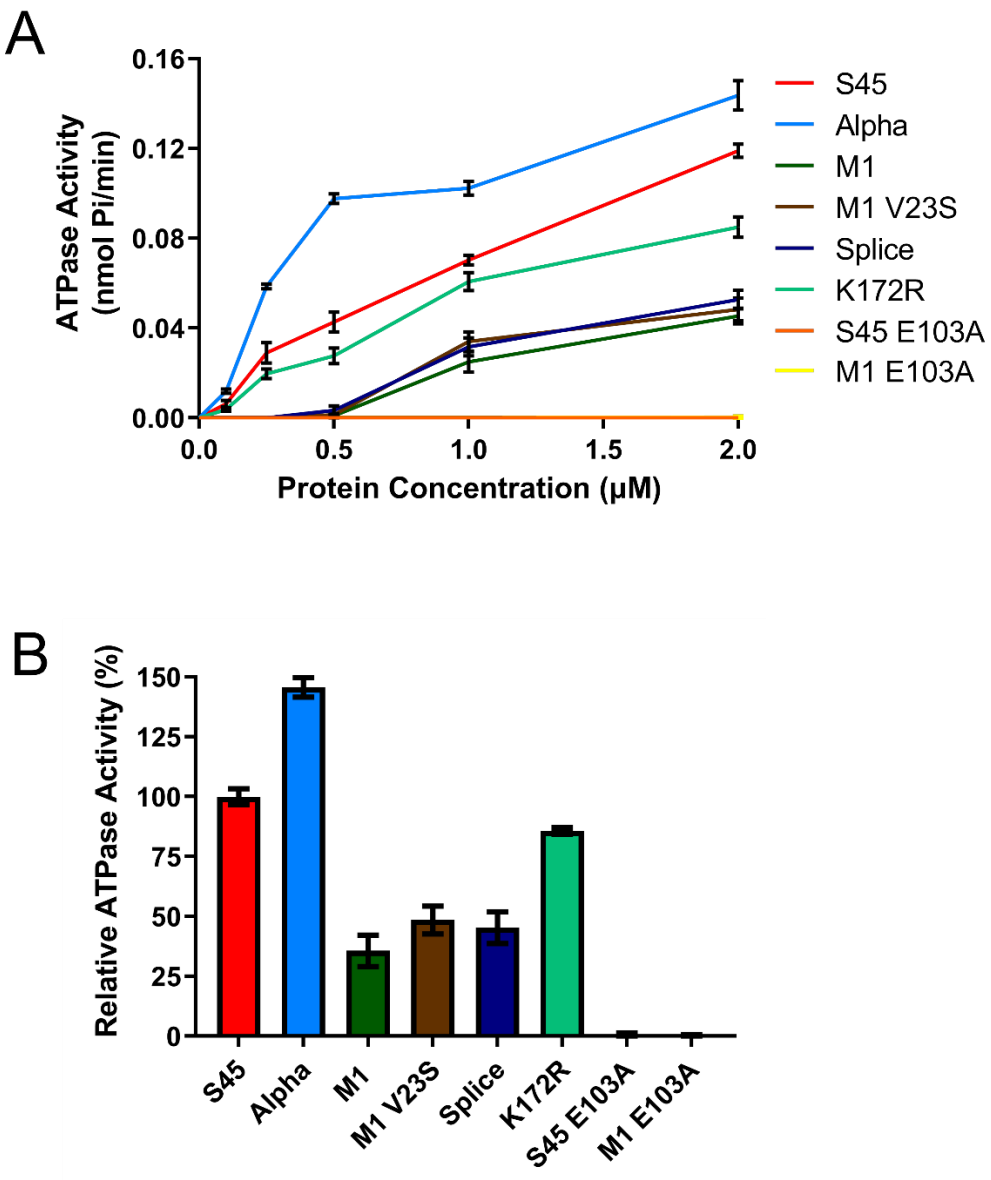

Figure 3-7: ATP hydrolysis by TOP2 ATPase domain proteins

(**A**) ATPase activity indicated by the amount of free phosphate released per minute for each of the ATPase domain proteins at a range of protein concentrations. The average of three experiments is plotted for each protein and the standard deviation is represented by black error bars. Red is S45, light blue is TOP2A, dark green is M1, brown is M1 V23S, dark blue is M1 Splice, light green is K172R, orange is S45 E103A and yellow is M1 E103A. (**B**) Comparison of relative ATP hydrolysis activities of the ATPase domain proteins. The mean for S45 was set to 100%. The different proteins were assayed for activity at a single concentration of 1 μM and the means of three replicates are shown. Error bars represent one standard deviation from the mean. Same colour scheme used as in part **A**.

3.8.2 ATPase Activity with a Range of ATP Concentrations

Next, the ATPase activity was studied with a range of different ATP concentrations. The lowest ATP concentration used was 0.05 mM and the highest was 0.4 mM. ATP concentrations above 0.5 mM gave too high a background signal during the assay and therefore this was the highest concentration that could be measured. To ensure the ATPase activity was being measured in the linear range, different concentrations of protein were used for different mutations. 0.25 µM protein was used for TOP2A (28-428), TOP2B S45 (45-444) and TOP2B K172R (45-444) (Figure 3-8A), whilst the amount of protein was increased to 1 µM for TOP2B M1 (1-444), the TOP2B alternative splice variant (1-449) and the M1 point mutation V23S (1-444) (Figure 3-8B). S45 (45-444) was also assayed at 1 µM protein for comparison.

It took four times as much protein for the full-length ATPase domains to reach similar levels of free phosphate release when compared to the N-terminal truncated ATPase domain proteins. For all proteins studied the same trend was observed, where increasing the amount of substrate increased the amount of product produced (P_i). Therefore, it is unlikely that the full-length ATPase domain proteins have reduced ATPase activity due to a reduced affinity for ATP.

For the N-terminal truncated proteins, TOP2A (28-428) was significantly more active at all ATP concentrations studied and TOP2B K172R (45-444) was significantly less active compared to TOP2A and wild type N-terminal truncated TOP2B S45 (45-444), when varying protein concentration (Figure 3-8A). Likewise, for the full-length TOP2B ATPase domain proteins M1 (1-444) and M1 Splice (1-449) there was no significant difference in activity at ATP concentrations 0.05 - 0.2 mM, but at 0.3 mM ATP the ATPase activity differed significantly between M1 and M1 Splice ($P < 0.05$), and at the highest ATP concentration studied (0.4 mM) both M1 and M1 Splice, and M1 and M1 V23S were significantly different ($P < 0.01$). Whilst the difference in ATPase activity between M1 Splice and M1 V23S at all ATP concentrations studied were not significant (Figure 3-8B).

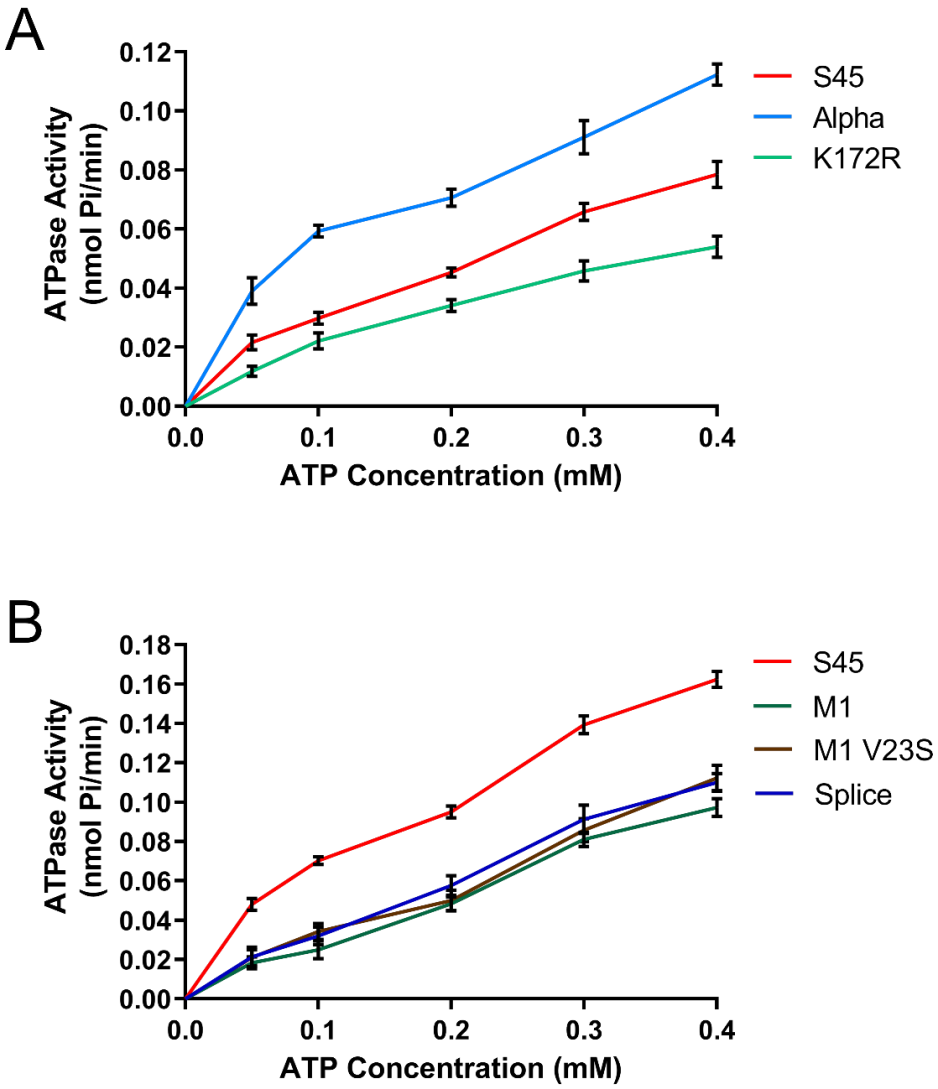

Figure 3-8: ATP hydrolysis by TOP2 ATPase domain proteins at a range of ATP concentrations

ATPase activity indicated by the amount of free phosphate released per minute for each of the ATPase domain proteins at a range of ATP concentrations (0.05, 0.1, 0.2, 0.3 and 0.4 mM ATP). The different proteins were assayed for activity at a concentration of 0.25 μM (**A**) or 1 μM (**B**) and the means of three replicates are shown. Error bars represent one standard deviation from the mean. Same colour scheme used as in Figure 3-7.

3.8.3 Effect of Nucleic Acids on ATPase Activity

DNA is known to stimulate the ATPase activity of type II topoisomerase proteins (Hammonds and Maxwell 1997, West, Turnbull et al. 2002). Therefore, to determine whether the isolated ATPase domain of human TOP2B could be stimulated in the presence of nucleic acids the ATPase activity of the full-length TOP2B ATPase domains (M1 1-445 and M1 Splice 1-449) and N-terminal truncated ATPase domains (45-444) was measured at a range of protein concentrations in the presence and absence of 4 µg pBR322 plasmid (Figure 3-9A-E). The analysis was only performed at one protein concentration (1 µM) in the presence of 4 µg DNA for the ATPase domain protein M1 V23S (Figure 3-9F).

Upon addition of supercoiled pBR322 all proteins studied had a significant increase in ATP hydrolysis activity ($P < 0.001$) despite lacking the core domain of the topoisomerase II protein. Generally, the same trends were observed as in the previous section, with TOP2A being the most active N-terminal truncated ATPase domain protein, and TOP2B K172R being the least active. However, at the highest protein concentration (2 µM) and in the presence of DNA, TOP2B S45 (45-444) had a comparable activity to TOP2A (28-428). The full-length TOP2B ATPase domain proteins M1 (1-444) and M1 Splice (1-449) were not significantly different to each other even in the presence of DNA ($P > 0.05$).

Interestingly, the full-length ATPase domain proteins (1-444 or 1-449) had the greatest stimulation in activity in the presence of nucleic acid. With 1 µM of protein, the activity of M1 was increased by 71%, followed by the alternative splice variant (M1 Splice) with a 62% increase and a 51% increase for the point mutation V23S in the M1 construct (Figure 3-9F). This resulted in detectable ATPase activity at much lower protein concentrations. For example, in the presence of 4 µg DNA, the ATPase activity of the full-length ATPase domain proteins could now be observed at a protein concentration as low as 0.1 µM. Whilst with 1 µM of protein, the N-terminal truncated proteins TOP2B S45 (45-444), TOP2A (42-428) and TOP2B K172R (45-444) were stimulated to a lower degree with a 30%, 40% and 37% increase in activity respectively. However, despite the full-length ATPase domain proteins having a greater stimulation in activity, they were still significantly less active than the N-terminal truncated proteins ($P < 0.001$).

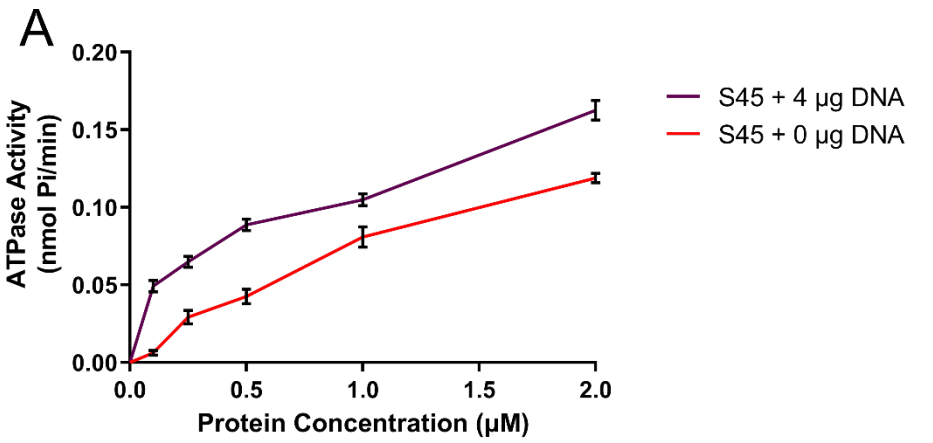
A
ATPase Activity (nmol Pi/min)
0.20
0.15
0.10
0.05
0.00
0.0
0.5
1.0
1.5
2.0
Protein Concentration (μM)
S45 + 4 μg DNA
S45 + 0 μg DNA

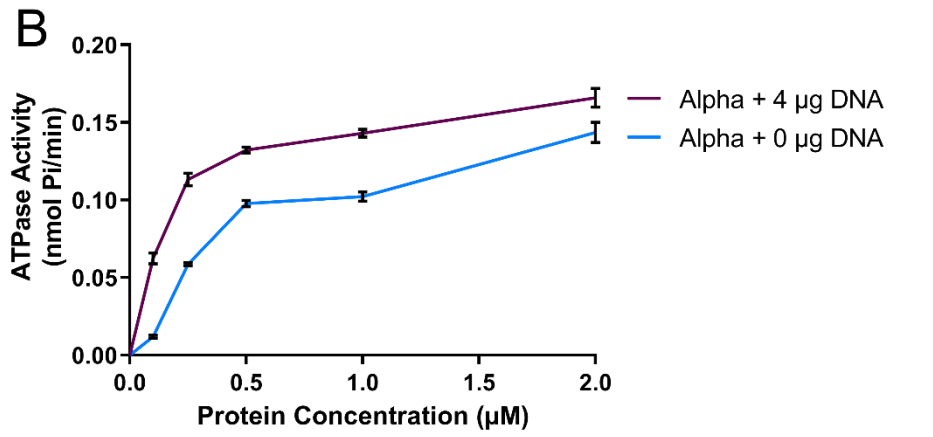
B
ATPase Activity (nmol Pi/min)
0.20
0.15
0.10
0.05
0.00
0.0
0.5
1.0
1.5
2.0
Protein Concentration (μM)
Alpha + 4 μg DNA
Alpha + 0 μg DNA

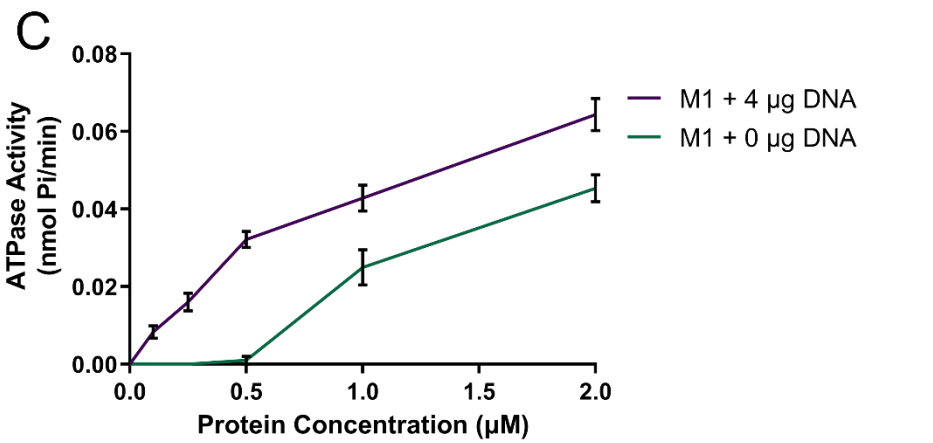
C
ATPase Activity (nmol Pi/min)
0.08
0.06
0.04
0.02
0.00
0.0
0.5
1.0
1.5
2.0
Protein Concentration (μM)
M1 + 4 μg DNA
M1 + 0 μg DNA

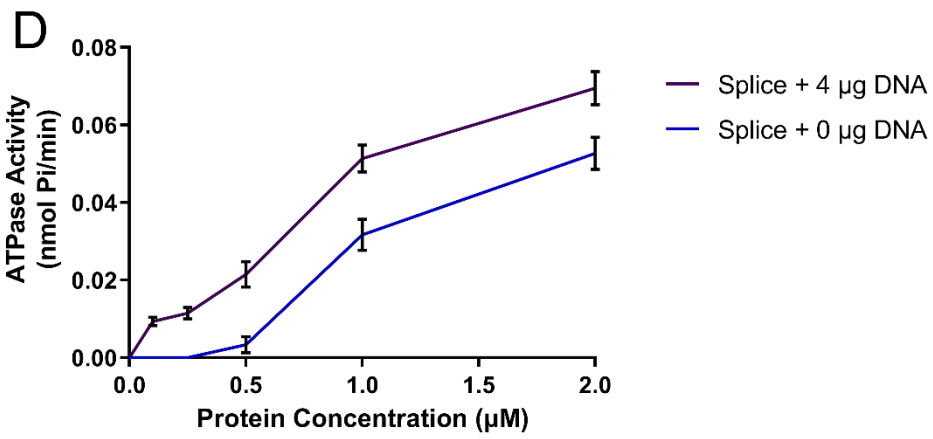
D
ATPase Activity (nmol Pi/min)
0.08
0.06
0.04
0.02
0.00
0.0
0.5
1.0
1.5
2.0
Protein Concentration (μM)
Splice + 4 μg DNA
Splice + 0 μg DNA

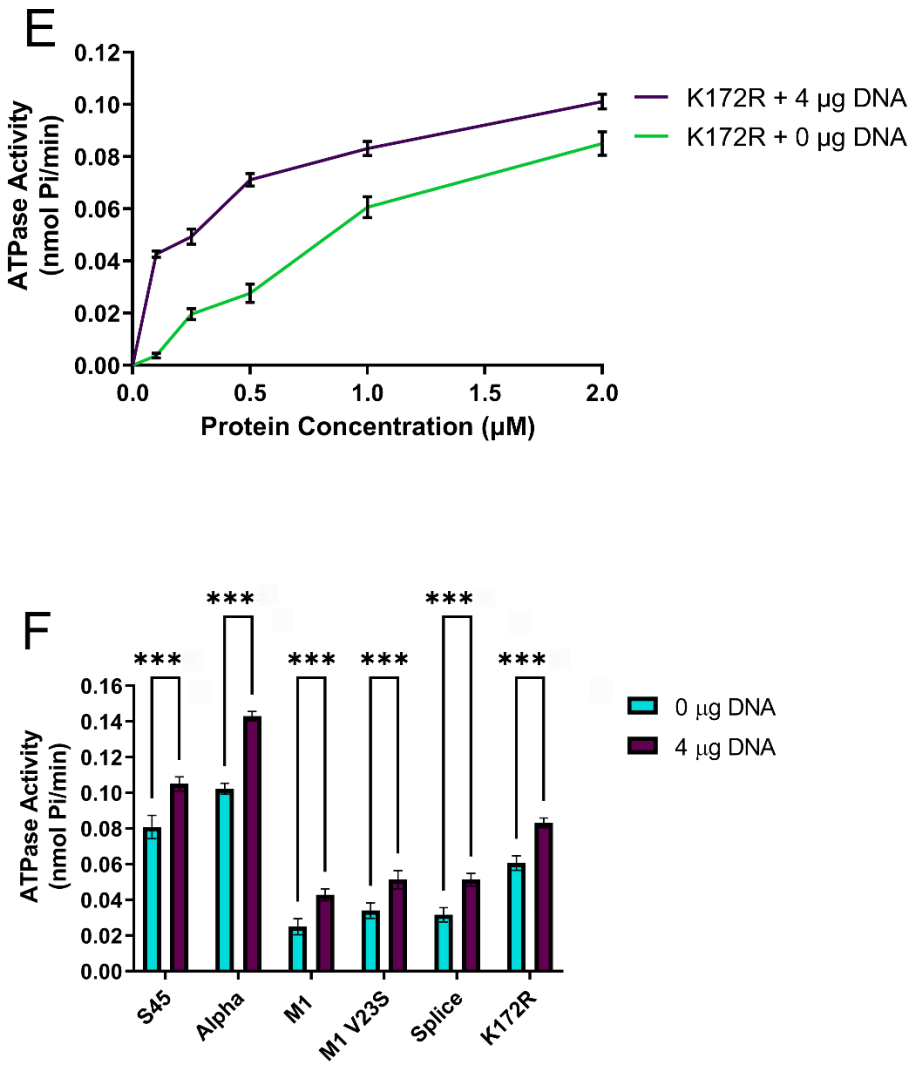

Figure 3-9: ATP hydrolysis by TOP2 ATPase domain proteins in the presence and absence of nucleic acid at a range of protein concentrations (current page and previous page)

ATPase activity indicated by the amount of free phosphate released per minute for each of the ATPase domain proteins in the presence and absence of 4 µg nucleic acid (pBR322). S45 (**A**), TOP2A 42-428 (**B**), M1 (**C**), M1 Splice (**D**), K172R (**E**). The means of three replicates are shown and error bars represent one standard deviation from the mean. Same colour scheme used as in part **A** for activity in the absence of nucleic acid, activity in the presence of 4 µg nucleic acid shown in purple. (**F**) Shows the mean ATPase activity at 1 µM for all the proteins studied in the presence and absence of 4 µg pBR32. Absence of nucleic acid is in cyan, and 4 µg shown in purple. Statistical analysis was performed by a two-way ANOVA and Bonferroni post-tests. *** indicates $P < 0.001$.

3.8.4 Km and Vmax

The ATPase activity of the TOP2B proteins was assayed over time at a range of ATP concentrations and the data were fitted to the Michaelis–Menten equation, as illustrated by the best fit curve in Figure 3-10A and B.

The Km values were lowest for TOP2A (28-428) and TOP2B S45 (45-444), suggesting these two proteins have the highest affinity for ATP and the values were not significantly different (Figure 3-10C). Whereas their Vmax values differed significantly with TOP2A having the highest Vmax because it had the quickest rate of reaction. TOP2B K172R (45-444) had the lowest Vmax out of the N-terminal truncated proteins suggesting a lower rate of reaction but it was still higher than the full-length ATPase domain proteins (1-444 or 1-449). Whereas the Km value for K172R was similar to both full-length ATPase domains (M1 and M1 Splice) suggesting a similar affinity for ATP. The Vmax value was the lowest for the full-length ATPase domain proteins and was the same for both M1 and M1 Splice (Figure 3-10C).

A

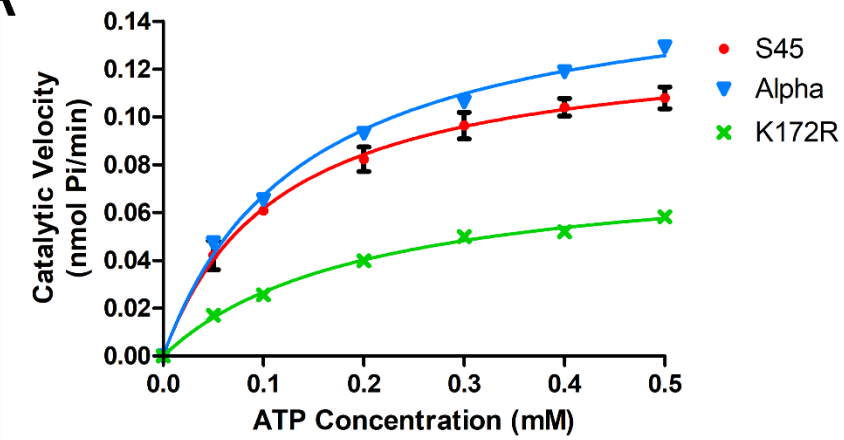

B

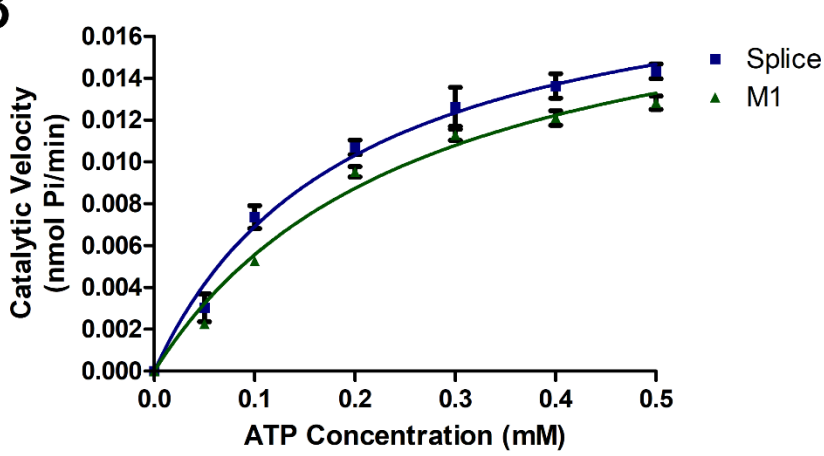

C

Protein	Km Value (mM)	Vmax Value (nmol Pi/min)
S45	0.1153 +/- 0.0067	0.1328 +/- 0.0025
Alpha	0.1390 +/- 0.0168	0.1605 +/- 0.0068
M1	0.2670 +/- 0.0697	0.0204 +/- 0.0025
Splice	0.1957 +/- 0.0397	0.0204 +/- 0.0017
K172R	0.2037 +/- 0.0238	0.0811 +/- 0.0039

+/- Standard error

Figure 3-10: Michaelis-Menten graphs for the TOP2 ATPase domain proteins

Rate of ATP hydrolysis plotted against ATP concentration with 0.25 µM S45, TOP2A 28-428 and K172R (**A**) and 0.25 µM M1 and M1 Splice (**B**). Note different scales in **A** and **B**. The means of three replicates are shown for S45, M1 and M1 Splice with error bars representing one standard deviation from the mean. (**C**) Table with Km and Vmax values +/- standard error for S45, TOP2A 28-428, M1, M1 Splice and K172R.

3.9 Discussion

A range of human topoisomerase II ATPase domain proteins were expressed and purified for *in vitro* biochemical analysis. One of which, S45 (45-444), was also purified for crystallographic studies (Chapter 4). The ability of the TOP2 ATPase domain proteins to carry out ATP hydrolysis was assayed spectrophotometrically by measuring the release of free phosphate (P_i) via a colour change. Previous reports have analysed the ATPase activity of N-terminal truncated human type II topoisomerases (Hammonds and Maxwell 1997, West, Turnbull et al. 2002), starting at amino acid 45 for TOP2B or amino acid 28 for TOP2A. Whereas the ATPase activity of the full-length human TOP2B proteins has not been reported. The N-terminal region of type II topoisomerases contains the N-terminal strap which forms part of the ATP binding site. Therefore, to gain a more in depth understanding of the function of the N-terminal strap, the full-length human TOP2B ATPase domain (1-444) M1, the alternative splice variant (1-449) M1 Splice and the mutated protein V23S (1-444) were expressed, purified and assayed.

All of the full-length proteins studied (1-444 or 1-449) had drastically reduced ATPase activity compared to the N-terminal truncated protein S45 (45-444). This data suggests that the first 44 or 49 amino acids can negatively regulate the ATPase activity, which could provide a mechanism to regulate TOP2B activity. The TOP2B mutation K172R in the N-terminal truncated protein (45-444) was more active than the full-length proteins but less active than the wild type truncated sequence, S45. TOP2A (28-428) was the most active ATPase domain protein studied under all conditions.

The lower ATPase activity of the M1 (1-444) and M1 Splice (1-449) could arise in several ways. One explanation could be that the additional amino acids in the N-terminal strap sequester ADP and P_i and prevent them from leaving the enzyme as easily. As such, it would take longer to reset the enzyme for another round of catalysis resulting in a slower ATP hydrolysis rate, or the active site could be blocked due to the additional amino acids so that ATP binds less efficiently. Alternatively, dimerisation between the two ATPase monomers could be hindered which would reduce ATPase activity because protein dimerisation is required for ATP hydrolysis.

The amino acids in the N-terminal strap are not conserved between isoforms or species (Figure 1-3) and have different phosphorylation sites. *S. cerevisiae* has the shortest N-terminal strap, followed by human TOP2A and then human TOP2B. Moreover, human

TOP2B has the greatest number of phosphorylation sites within this region which include S4, T21, S37, S45, and S46. By contrast, human TOP2A is only phosphorylated at S4 and S29 (Hornbeck, Zhang et al. 2015). In addition, TOP2B can be SUMOylated at K28 and K29 and ubiquitinated at K37 in the N-terminal strap (Hendriks, D'Souza et al. 2014). Thus, the N-terminal strap could provide a mechanism of enzyme regulation.

Indeed, *in vivo* it has been demonstrated that the N-terminal strap is necessary for interacting with PKC in *S. cerevisiae* (Mouchel and Jenkins 2006) and the phosphorylation status of the strap can modulate activity in human TOP2A (Wells and Hickson 1995). It has previously been proposed that the phosphorylation status of a different region of topoisomerase II, the C-terminal domain, can alter the conformation of the protein, enabling interactions with other molecules or proteins (Cardenas and Gasser 1993). Hence, a similar event could occur with the N-terminal strap whereby phosphorylation could promote or inhibit interactions with ATP which could account for the difference in activity between the full-length (1-444 and 1-449) and the N-terminal truncated proteins (45-444).

It was known from previous studies that the ATPase activity of human TOP2B (45-1621) is stimulated by DNA (West, Turnbull et al. 2002). Consistent with this, the work in this chapter shows that the ATPase activity of the isolated ATPase domain of human TOP2B is stimulated by DNA. Similar results have been reported for the TOP2A ATPase domain, yeast ATPase domain and Gyrase B ATPase domain (Hammonds and Maxwell 1997, Campbell and Maxwell 2002, Schmidt, Osheroff et al. 2012). The DNA stimulation of the ATPase activity was presumed to be due to binding of the T-DNA, however in addition to the T-DNA the K loop in the transducer region of the ATPase domain also contacts the G-DNA and mutagenesis of the K loop in yeast TOP2 and human TOP2A confirmed this region of the ATPase domain is responsible for DNA stimulation of ATP hydrolysis (Schmidt, Osheroff et al. 2012). Once the G-DNA has been religated it contacts the K loop to stimulate the second ATP hydrolysis event to reset the enzyme for another round of catalysis. One of the lysine residues in the K loop of *S. cerevisiae* was previously implicated in binding DNA via protein footprinting (Li and Wang 1997). Also, lysine residues in the K loop of TOP2B have been found to be acetylated, adding a further potential layer of regulation (Schmidt, Osheroff et al. 2012). As the K loop resides within the transducer region of the ATPase

domain, the transducer has been implicated as an essential element for this allosteric movement (Vanden Broeck, Lotz et al. 2021). By coupling DNA binding to ATPase stimulation, the enzyme has a regulatory mechanism which prevents ATP from being hydrolysed unnecessarily when there is no DNA substrate in proximity.

Chapter 4 Structural Analysis of the ATPase Domain of Human TOP2B

4.1 Introduction

As DNA topoisomerase II is a large protein of ~180 kDa, structural studies have utilised individual domains. Solving the structure of domains of type II topoisomerases from a wide range of species has provided a detailed understanding of the key aspects of the molecular mechanisms employed by these enzymes and remains the most definitive method of elucidating protein-ligand contacts. The structural domains are evolutionarily conserved sharing sequence similarity and contain highly conserved functional motifs (Figure 4-1). However, there are important differences in the ATPase domain of type II topoisomerases, such as a longer N-terminal strap in the human enzymes, with TOP2B being fourteen residues longer than TOP2A. In addition, TOP2B has a greater number of posttranslational modifications in the ATPase domain compared to TOP2A (Hornbeck, Zhang et al. 2015), and nucleotide 28 (residue 10) of TOP2B is an evolutionarily positively selected site (Moreira, Arenas et al. 2022). Moreover, the alternative splice variant of TOP2B contains an additional five amino acids in the ATPase domain (Davies, Jenkins et al. 1993).

The core domain of yeast TOP2 (Berger, Gamblin et al. 1996, Schmidt, Burgin et al. 2010) has been crystallised and its structure solved as well as the ATPase domain of yeast TOP2 in the presence and absence of the bisdioxopiperazine ICRF187 (Classen, Olland et al. 2003). A fully functional tailless structure comprising the ATPase and the core domain of yeast TOP2 (Schmidt, Osheroff et al. 2012) has been solved and revealed a new control mechanism for ATPase activity that links the transducer region of the ATPase domain and the G-DNA. For the human enzymes, the core domain of TOP2A (Wendorff, Schmidt et al. 2012) and the ATPase domain of TOP2A (Wei, Ruthenburg et al. 2005) have been solved. In addition, a CryoEM structure of full-length TOP2A has recently been published (Vanden Broeck, Lotz et al. 2019), allowing the allosteric interactions between the ATPase domain and the TOPRIM domain to be analysed.

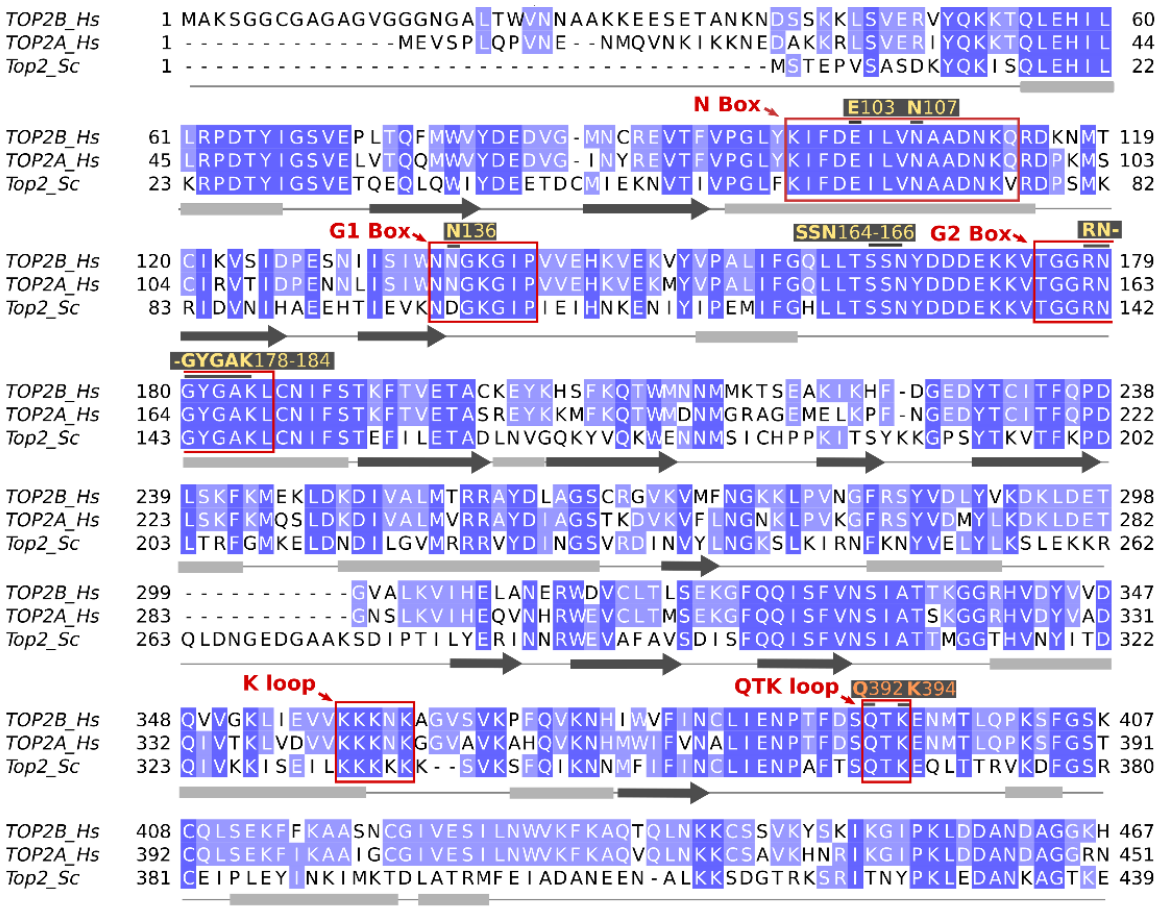

Figure 4-1: Clustal alignment of type II topoisomerase ATPase domain

Clustal alignment of human TOP2B, human TOP2A and *S. cerevisiae* ATPase domain. The N, G1, and G2 boxes indicated as well as the K loop and the QTK loop. The secondary structure for TOP2B is shown, grey boxes for alpha helices and black arrows for beta sheets.

For human TOP2B, the structure of the core domain has been reported (Wu, Li et al. 2011), but to date the ATPase domain has not been published (Figure 4-2). The ATPase domain of human TOP2B is the clinical target of the bisdioxopiperazine catalytic inhibitors, as TOP2B is the only topoisomerase II isoform present in postmitotic cardiac cells (Capranico, Tinelli et al. 1992, Atwal, Swan et al. 2019). Moreover, bisdioxopiperazines have been reported to inhibit the catalytic activity of human TOP2A and TOP2B differentially (Shapiro and Austin 2014) with the TOP2A isoform more sensitive to ICRF187 than TOP2B *in vitro* (Lee, Wendorff et al. 2017).

Bisdioxopiperazines inhibit topoisomerase II by binding to the N-terminal ATPase domain and trapping the enzyme in a closed clamp form in the presence of ATP (Roca, Ishida et al. 1994). Therefore, despite the TOP2A and TOP2B ATPase domains sharing significant homology there are distinct differences between the two isoforms providing the rationale for solving the structure of human TOP2B ATPase domain. Furthermore, *S. cerevisiae* TOP2 is less sensitive to ICRF187 than the human isoforms. ICRF187 is the drug used therapeutically for the prevention of anthracycline induced cardiotoxicity (Lee, Wendorff et al. 2017). Yet, the only published topoisomerase II ATPase domain structure in the presence of drug is the *S. cerevisiae* structure in the presence of AMPPNP and dexrazoxane (ICRF187) (Classen, Olland et al. 2003). As such, there are important insights that can be elucidated from solving the structure of the human TOP2B ATPase domain in the presence and absence of drug. Consequently, the overall aim of this chapter was to obtain protein crystals and determine the structure of the TOP2B ATPase domain bound to different nucleotides and drug.

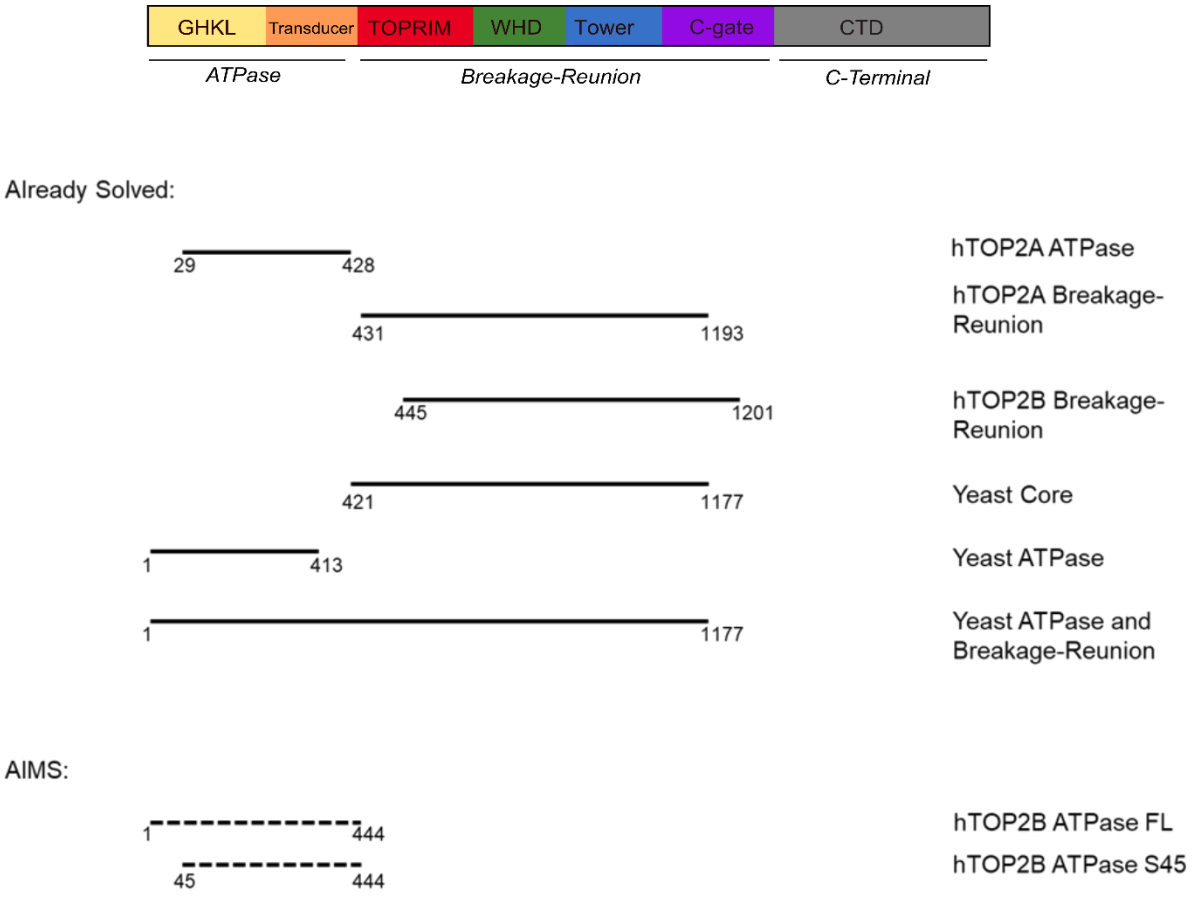

Figure 4-2: Schematic representation of which domains have been crystallised and which ones will be attempted to be crystallised during this chapter

The crystal structure of the ATPase domain starting at amino acid 29 has been solved for TOP2A (Wei, Ruthenburg et al. 2005), as well as the breakage-reunion domain for TOP2A (Wendorff, Schmidt et al. 2012) (residues 431-1193). However, only the breakage-reunion domain has been solved for TOP2B (Wu, Li et al. 2011) (residues 445-1201). As such, one of the aims of the project was to crystallise and solve the structure of the ATPase domain of TOP2B. The full-length (M1, 1-444) ATPase domain was expressed as well as the ATPase domain starting at amino acid 45 (S45) which corresponds to the start of the structure of TOP2A, which starts at amino acid 29.

4.2 Principles of Protein Crystallography

X-ray crystallography is based upon the principles of crystallisation and X-ray diffraction, and remains one of the most popular techniques for the elucidation of three-dimensional macromolecular structures (Johnson 1949, McPherson and Gavira 2014).

In crystallography molecules such as proteins are encouraged to form crystals, a regular, three-dimensional array of atoms, ions, or molecules within a lattice. The crystal comprises millions of sample molecules orientated together uniformly, which gives a strong amplification of the diffraction pattern to a level that can be detected during data collection. As biological macromolecules are composed of thousands of different atoms, bound together with multiple degrees of freedom, crystallisation of macromolecules is an extremely complex task, with many variables influencing the success rate (McPherson 1990). For a crystal to form it is vital that the solution is as homogeneous as possible to increase the chance that identical molecules will come together to form the lattice. For this reason, it is important that the sample has a high concentration of pure, uniform molecules as it helps in reaching the supersaturation point (D'Arcy 1994, Dale, Oefner et al. 2003). Additionally, stability and solubility of the sample are important variables that contribute to the success of crystallisation. Samples should contain biologically active molecules lacking aggregates, oligomers, precipitation or contaminants (Dessau and Modis 2011).

Crystallisation of macromolecules is a multistep process involving three main steps: nucleation, growth, and cessation of growth (Dessau and Modis 2011, McPherson and Gavira 2014). Numerous methods exist for crystallising molecules, all with the purpose of bringing the sample to a supersaturated state. Once supersaturation is reached, molecules are forced into the solid state, giving rise to crystals. The two most commonly used screening methods for crystallisation of macromolecules are sitting drop vapour or hanging drop vapour diffusion methods (Gernert, Smith et al. 1988). During vapour diffusion, the sample is mixed with the reagent containing buffer, crystallisation agent and additives, and is placed in vapour equilibration with a liquid reservoir of reagent. Generally, the reagent concentration is higher in the reservoir than in the droplet. As such, equilibration is achieved when volatile species (water or organic solvent) diffuse from the drop into the reservoir, causing the sample and the reagent concentration within the drop to increase. Equilibrium has been reached when the reagent concentration in the drop is approximately the same as that in the reservoir.

At this point, homonucleation of the sample begins and an array starts to form, resulting in a crystal lattice (Luft, Arakali et al. 1994).

Once the crystal lattice has grown large enough to form a crystal of reasonable size (50 x 50 x 50 µm) the crystal is exposed to electromagnetic (EM) radiation. EM radiation in the X-ray wavelength range is necessary to visualise molecular structures at atomic or near atomic resolution because it possesses a much shorter wavelength than visible light. For example, one wavelength that is used in protein crystallography is 1.542 Å, the approximate length of a carbon-carbon bond (Johnson 1949). Interactions between the EM waves, and electrons within the sample causes the X-rays to diffract into many specific directions, known as scattering. The angles and intensities of the diffracted beams are then measured to determine information about the crystal packing symmetry and the size of the repeating unit that forms the crystal. From the diffraction spots, a map of the electron density can be calculated producing a three-dimensional image, as well as the mean positions of the atoms and chemical bonds within the crystal (Berman 1977, Rupp 2010).

4.3 Analytical Gel Filtration

To understand how the human TOP2B ATPase domain protein behaves in the presence or absence of different compounds, analytical gel filtration was performed prior to crystallography studies. Protein dimerisation can be identified during analytical gel filtration, as it is a type of size exclusion chromatography. When a protein dimerises and remains as a dimer throughout the chromatography it will have approximately double the size compared to the individual monomers. Consequently, the dimer and monomer will elute from the gel filtration column at different times relative to their size.

In the presence of the non-hydrolysable ATP analogue, AMPPNP, S45 (45-444) dimerises and a shift in the elution time is observed. In the absence of AMPPNP, the protein elutes at a point indicative of a Mw 47.5 kDa. Whereas, on addition of AMPPNP, the protein predominantly elutes at a point indicative of a Mw 77.8 kDa (Figure 4-3), consistent with a stable protein dimer in the presence of AMPPNP. As such, AMPPNP was included in the initial crystallography trials. Similarly, TOP2A (28-428) and TOP2B K172R (45-444) also had a shift in elution profile in the presence or absence of AMPPNP. Moreover, TOP2B E103A in the 45-444 vector behaved the same as wild

type (S45) suggesting the protein is functional in binding ATP, despite ATP hydrolysis being perturbed.

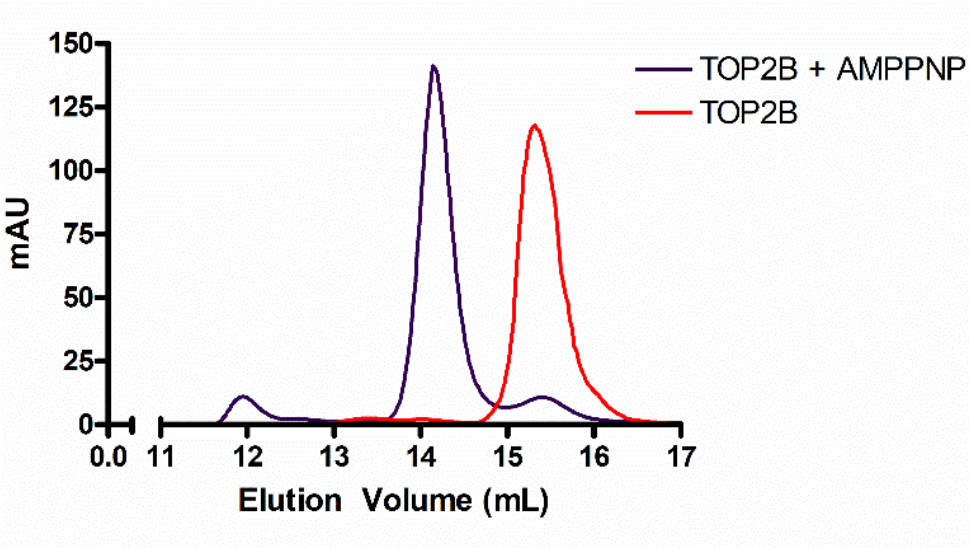

Figure 4-3: Analytical gel filtration of S45 (45-444) in the absence (red) and presence (purple) of AMPPNP

TOP2B S45 (45-444) protein injected onto a Superdex 200 Increase 10/300 GL column with 20 mM Tris HCl pH 8.0, 150 mM NaCl. Red line indicates UV absorbance in the absence of AMPPNP and purple line indicated UV absorbance in the presence of AMPPNP. In the absence of AMPPNP, S45 elutes at ~15.3 mL corresponding to an apparent Mw of 47 kDa, equivalent to the theoretical size (45 kDa), whereas upon addition of AMPPNP, the protein elutes earlier at ~14.1 mL, corresponding to an apparent Mw of 78 kDa. Chromatogram representative of all N-terminal truncated proteins: TOP2A (28-428), TOP2B K172R (45-444), TOP2B E103A (45-444).

4.4 Preparation and Screening of Protein for Crystallography

4.4.1 Protein screens with the non-hydrolysable ATP analogue, AMPPNP

Protein crystallography requires that samples are as concentrated as possible to increase the chance of supersaturation occurring. Using the 'ProtParam' tool (available online at www.ExPASy.org) the theoretical extinction coefficient of the protein can be calculated from the amino acid sequence. The extinction coefficient is required to determine the molar concentration from the absorbance of a protein sample. The Nanodrop was used to measure the absorbance, the value of which was then divided by 1.155, the extinction coefficient of TOP2B S45 (45-444) (Wilkins, Gasteiger et al. 1999). Samples were concentrated with a molecular weight cut off (MWCO) 30 kDa device (Millipore) to the desired protein concentration.

Once concentrated, crystallisation trays were set up. Initially, MRC 96 well sitting drop plates were used for crystallography screening with the top drop containing 100 nL protein:100 nL reservoir and the bottom drop containing 100 nL protein:200 nL reservoir. At first, the protein was concentrated to 10 mg/mL and five different crystallisation screens were used: JSCG Plus, Index, PACT Premier, Structure and Morpheus II (Appendix 2) at 20 °C. 1 mM AMPPNP was included in the initial crystallisation screen because from the previous gel filtration experiment (Figure 4-3) it was known that AMPPNP induced dimerisation of TOP2B S45 (45-444). The plates were sealed with a layer of film to make each well airtight to allow vapour diffusion to occur. Trays were then incubated for several days before checking under the microscope. However, during this trial most of the drops remained clear even after multiple weeks. Therefore, in the next screen the protein concentration was increased to 20 mg/mL and 5 mM $MgCl_2$ was included as this is the physiological ion that is required during catalysis. At 20 mg/mL a lot of protein precipitation was observed, and it was concluded that 20 mg/mL was too high a protein concentration.

All further screens were performed with 16 mg/mL protein in addition to the two ligands: 1mM AMPPNP and 5mM $MgCl_2$. During these trials many small protein crystals were observed in condition C4 (0.1 M PCTP pH 7.0, 25% w/v PEG 1500), and C5 of PACT (0.1 M PCTP pH 8.0, 25% w/v PEG 1500), (Figure 4-4A and B respectively). The crystals had the same octahedron shape in both conditions and were ~ 10 µm in size. The crystals appeared in the bottom drop (100 nL protein:200 nL reservoir) and took

~3 days to appear. However, these crystals were too small to harvest and send for X-ray diffraction, therefore optimisation was necessary.

Moreover, a couple of protein crystals were observed in condition B4 of JCSG Plus (0.1 M sodium cacodylate pH 6.5, 40% MPD, 5% PEG 8000) (Figure 4-4C). The crystals had the same octahedron shape as was observed with the PACT condition, though they were slightly bigger (~20 µm). The crystals appeared in the bottom drop (100 nL protein:200 nL reservoir) and took ~3 days to appear. However, like the PACT crystals, these crystals were too small to harvest and due to there being a smaller number of crystals present, efforts were focused on optimising the crystals obtained during the PACT screen.

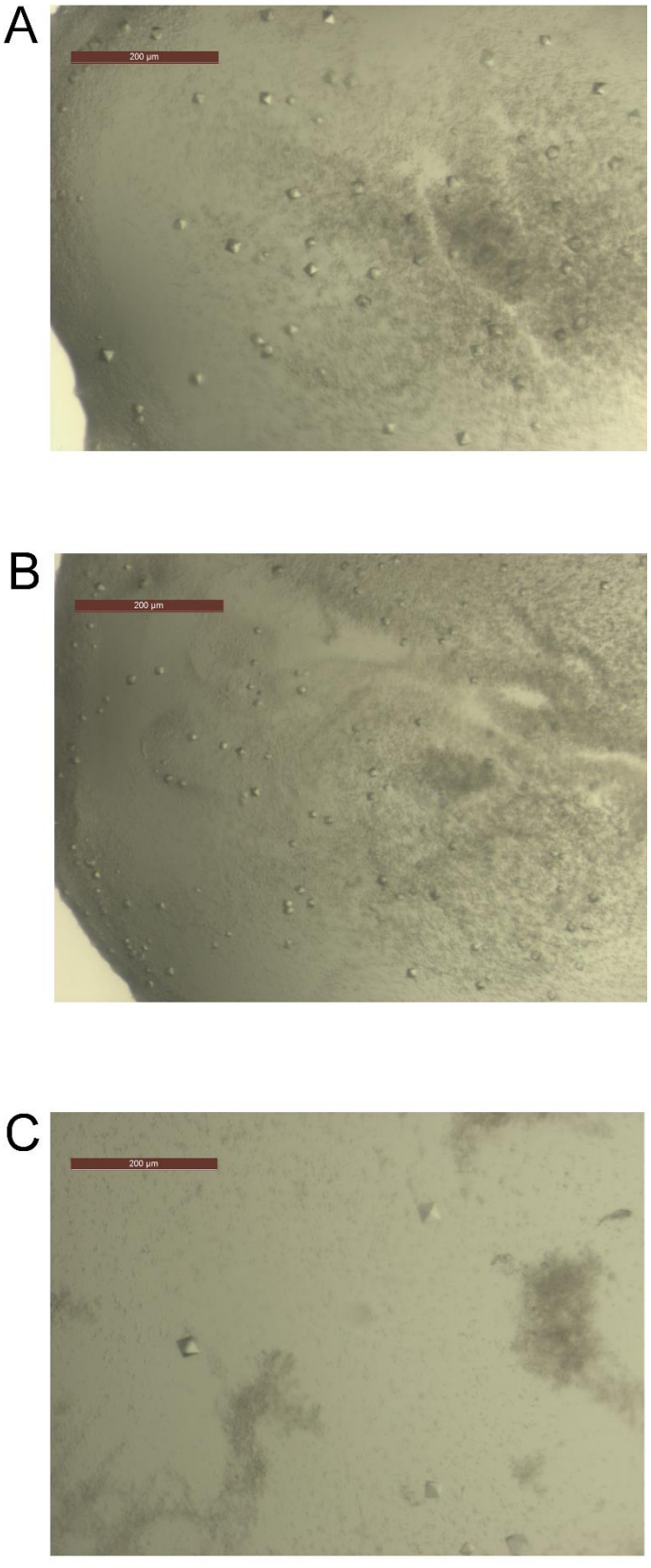

Figure 4-4: Images of crystals found in the initial S45 trials with 1 mM AMPPNP and 5 mM $MgCl_2$

(**A**) Condition C4 of PACT, (**B**) Condition C5 of PACT, (**C**) Condition B4 of JCSG Plus. Scale bar represents 200 µm.

Optimisation was performed in both sitting drop trays and hanging drop trays. The size of the drop was increased in the sitting drop trays by 3-fold: 300 nL protein:300 nL reservoir and 300 nL protein:600 nL reservoir. In addition, the reservoir stock solution was reduced by 5% increments with the aim of finding a condition that gave rise to optimal crystals. Hanging drop trays were also included as much larger drops (1 µL) can be made. The concentration of PEG and the pH of the buffer was also screened in the hanging drop trays. The 0.1 M PCTP buffer pH varied from pH 6.5, pH 7, pH 7.5 and pH 8, and the concentration of PEG 1500 varied from 19%, 21%, 23%, 25%, 27% and 29%. For both sitting and hanging drop experiments, fresh protein was made and concentrated to 16 mg/mL. 5 mM $MgCl_2$ and 1 mM AMPPNP was included as per the previous crystallography trial.

Unfortunately, there were no crystals in the hanging drop trays, only protein precipitation was observed. This can often be the case when scaling up crystallisation trials as the surface area to volume ratio differs for a small drop compared to a larger drop. Hence, the diffusion processes and reservoir equilibration rate will change which can impact the entire crystallisation process. Although, there were larger crystals in the sitting drop tray with the initial reservoir solution at 100-80% dilutions. For C4 PACT the largest crystals were obtained at a 90% reservoir dilution (Figure 4-5A) whilst 95% of reservoir gave the optimum crystals for C5 PACT (Figure 4-5B). There was very little difference in the crystals between the C4 and C5 PACT condition, in both cases they were ~100 x 50 x 20 µm in size. Consequently, a mixture of the largest crystals from both conditions were harvested with a MiTeGen crystal loop and cryoprotected with 100% PEG 800 to prevent damage to the crystals on storage in liquid nitrogen until they were sent to Diamond Beamline I03

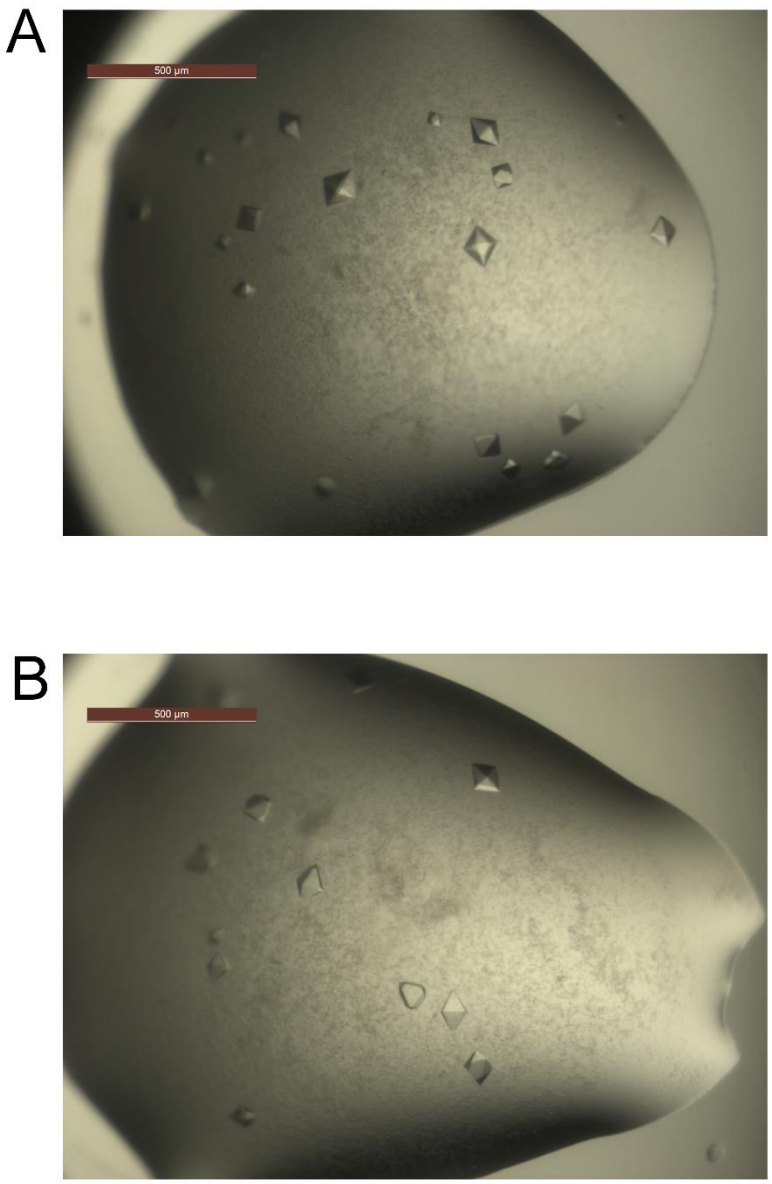

Figure 4-5: Images of crystals found in the larger scale S45 trials with 1 mM AMPPNP and 5 mM $MgCl_2$

(**A**) Condition C4 of PACT, (**B**) Condition C5 of PACT. Scale bar represents 500 µm.

4.4.1.1 Data Collection and Processing

During the process of collecting the diffraction data the crystal was mounted into a stream of liquid nitrogen to maintain a temperature of 100 K to ensure the crystal remains intact for as long as possible. The crystals were then exposed to X-rays and a diffraction pattern collected on the detector. The crystals were then rotated, and a series of diffraction images collected from which a three-dimensional image could be built.

Diffraction data for the AMPPNP crystals were collected at Diamond Beamline I03 with unattended data collection using the native data collection strategy https://www.diamond.ac.uk/Instruments/Mx/I03/I03-Manual/Unattended-Data-Collections/Experiment-Types.html. Data were processed at Diamond with the automated pipeline Xia2 with Dials. The data were scaled with Aimless, and the space groups were confirmed with Pointless. 5% of the data were randomly selected for R_{free} calculations. The processing statistics are presented in Table 4-1.

Data statistics*	
	AMPPNP
Beamline	I03
Date	06/05/21
Wavelength (Å)	0.980
Resolution (Å)	59.41- 1.90 (1.94 – 1.90)
Space group	$P4_12_12$
Unit-cell parameters	
a (Å)	84.02
b (Å)	84.02
c (Å)	127.09
α = β = γ (°)	90.00
Unit-cell volume (Å^3)	897205
Solvent content (%)	50
No. of measured reflections	1759478 (117137)
No. of independent reflections	36646 (2300)
Completeness (%)	100.0 (99.9)
Redundancy	48.0 (50.9)
$CC_{1/2}$ (%)	1.000 (0.568)
<I>/<σ(I)>	23.3 (1.2)
Refinement Statistics*	
R_{work} (%)	19.30
R_{free} (%)	23.20
No. of non-H atoms	
No. of protein, atoms	3044
No. of solvent atoms	99
No. of ligand atoms	32
R.m.s. deviation from ideal values	
Bond angle (°)	1.73
Bond length (Å)	0.01
Average B factor (Å^2)	
Protein	44
Solvent	41
Ligand	32
Ramachandran plot$^+$, residues in	
Most favoured regions (%)	96.8
Allowed regions (%)	3.2
Disallowed regions (%)	0.0

Table 4-1: Data statistics and refinement details for human TOP2B ATPase domain in the presence of AMPPNP

*(Values in parenthesis are for the highest resolution shell).
[#]5% of the randomly selected reflections excluded from refinement.
[+]*Calculated using MOLPROBITY.*

4.4.1.2 Solving the Phases and Model Building

The phases were solved for the human TOP2B ATPase AMPPNP structure on CCP4 cloud Newcastle (Potterton, Agirre et al. 2018) by molecular replacement using Molrep or Phaser (Vagin and Teplyakov 1997, McCoy, Grosse-Kunstleve et al. 2007). The human TOP2A ATPase domain structure (83% sequence identity to human TOP2B) was used as a search model (pdb code 1ZXM). The model was improved by iterative cycles of manual model building in COOT (Emsley, Lohkamp et al. 2010) and refined using Refmac (Murshudov, Skubák et al. 2011). The model was validated using COOT (Emsley, Lohkamp et al. 2010) validation tools and Molprobity (Williams, Headd et al. 2018). Metal type, co-ordination and bond distances were validated using Check My Metal (Zheng, Cooper et al. 2017).

4.4.1.3 Structure of the ATPase Domain of Human TOP2B bound to AMPPNP

The present study aimed to gain insights into the tertiary structure of the ATPase domain of human TOP2B and to determine whether ATP hydrolysis results in conformational changes within the enzyme. To this end, the TOP2B ATPase domain (45-444) was crystallised in the presence of the non-hydrolysable ATP analogue, AMPPNP. The ATPase domain of TOP2B in complex with AMPPNP was solved to 1.9 Å resolution, pdb code 7QFO (Figure 4-6A) by molecular replacement using the human TOP2A ATPase domain structure as a search model (Wei, Ruthenburg et al. 2005). The final TOP2B:AMPPNP model contains residues 46-429 and was refined to a R_{work} factor of 19.3% and an R_{free} of 23.2% (Table 4-1). The asymmetric unit contains one copy of the protein, and the biological dimer was generated by applying crystallographic symmetry. Furthermore, the analytical gel filtration experiment shown in Figure 4-3 confirmed the presence of a dimer, as well as interactions between monomers determined by PISA (Krissinel and Henrick 2007). The interface area of the dimer represents ~13% of the total monomer surface indicating significant interactions which include 24 hydrogen bonds and 18 salt-bridges between the two monomers. The electron density corresponding to the final 15 residues at the C-terminus of this domain was too weak to model, hence residues 430-444 were not modelled in the final structure.

The TOP2B ATPase domain dimerises in the presence of AMPPNP, giving rise to the ATP restrained state (Figure 4-6A) previously described for bacterial DNA Gyrase. A heart shape dimer is formed with a central cavity that is 31 Å high and 23 Å wide, the

dimensions of which cannot easily accommodate a DNA duplex. Each TOP2B ATPase protomer folds into two discrete structural modules: the N-terminal GHKL domain and the C-terminal transducer domain (coloured yellow and orange respectively in Figure 4-6A). The GHKL domain of TOP2B (residues 46-279) comprises an eight-stranded antiparallel β-sheet floor and four α-helical walls, giving rise to the Bergerat fold. The Bergerat fold typically consists of four conserved motifs: the N box, G1 box, G2 box and G3 boxFigure 4-1. The N box of TOP2B is located between residues 99-113 and contains a conserved asparagine, N107, that coordinates the catalytic Mg^{2+} ion and contains a conserved glutamate, E103 that acts as a general base to promote nucleophilic attack on the γ-phosphate of ATP using a water molecule (Figure 4-6B-D). The G1 box is located between residues 136-142 and houses a conserved asparagine, N136, that hydrogen bonds with the adenine ring of AMPPNP. Residues 175-185 comprise the G2 box, previously described as a Walker A motif. Moreover, the conserved lysine residue K168 in human TOP2A (K184 in TOP2B) located in the G2 box has been shown to undergo acetylation which can regulate ATP hydrolysis (Bedez, Lotz et al. 2018). The G3 box is absent from the linear sequence and tertiary structure of the eukaryotic type II topoisomerases. The transducer domain (residues 280-429) consists of a four-stranded mixed β-sheet backed by three α-helices and contains the 'switch lysine' (K394 in TOP2B) that is absolutely conserved in all type II topoisomerases. The switch lysine is part of a highly conserved QTK loop, residues 392-394 that extends into the ATP binding pocket. Towards the C-terminal end of the structure is the K loop, residues 358-362 (KKKNK) in TOP2B,that couples DNA binding to ATP hydrolysis and strand passage activity (Schmidt, Osheroff et al. 2012).

As anticipated from prior ATP-restrained structures (Classen, Olland et al. 2003, Wei, Ruthenburg et al. 2005, Stanger, Dehio et al. 2014), the active site of the TOP2B ATPase domain in the presence of AMPPNP is sequestered from solvent and poised for ATP hydrolysis. Side chains of residues in the conserved N box, SSN motif, G2 box and the QTK loop involved in AMPPNP binding are represented as green lines in Figure 4-6B or sticks in Figure 4-6C-D. Residues that contribute binding to AMPPNP via main chain bonding are located in the conserved G2 box and are represented as blue lines in Figure 4-6B or spheres in Figure 4-6C-D. The AMPPNP binding site is predominantly composed of residues from the GHKL domain, with only two transducer domain residues (Q392 and K394 from the QTK loop) making direct contacts with AMPPNP. To complete the binding site, the N-terminal strap motif from one monomer

reaches across the dimer interface to form the ATP lid of the partner monomer. However, the complete extent of nucleotide sequestering is not observed in this structure as the initial 44 amino acids are absent. The adenine ring of AMPPNP is held in place through direct hydrogen bonding with the carbonyl of N136, and stabilisation of the ribose sugar is achieved via hydrogen bonding to the hydroxyl group of S165. Hydrogen bonds are made to the α and β groups of AMPPNP by the side chains of residues N107 and K184, and S164 and N166 respectively. Moreover, the main chain of A183 contributes a hydrogen bond to the α-phosphate group (Figure 4-6B). The side chains of Q392 and K394 from the QTK loop of the transducer domain hold the γ-phosphate firmly in place, with the switch lysine, K394, forming a salt-bridge that is believed to stabilise the transition state of the hydrolysis reaction (Smith and Maxwell 1998). The γ-phosphate also forms an additional four hydrogen bonds with the main chain of residues R178, N179, Y181 and G182. The active site Mg^{2+} ion is coordinated by the conserved asparagine, N107, two water molecules and all three phosphates of AMPPNP to form a distorted octahedral metal ion coordination shell (Classen, Olland et al. 2003, Wei, Ruthenburg et al. 2005) (Figure 4-6B). The key catalytic residue in TOP2B, E103 forms a hydrogen bond to one of the two water molecules coordinated to Mg^{2+} which activates the water to allow nucleophilic attack on the γ-phosphate of ATP.

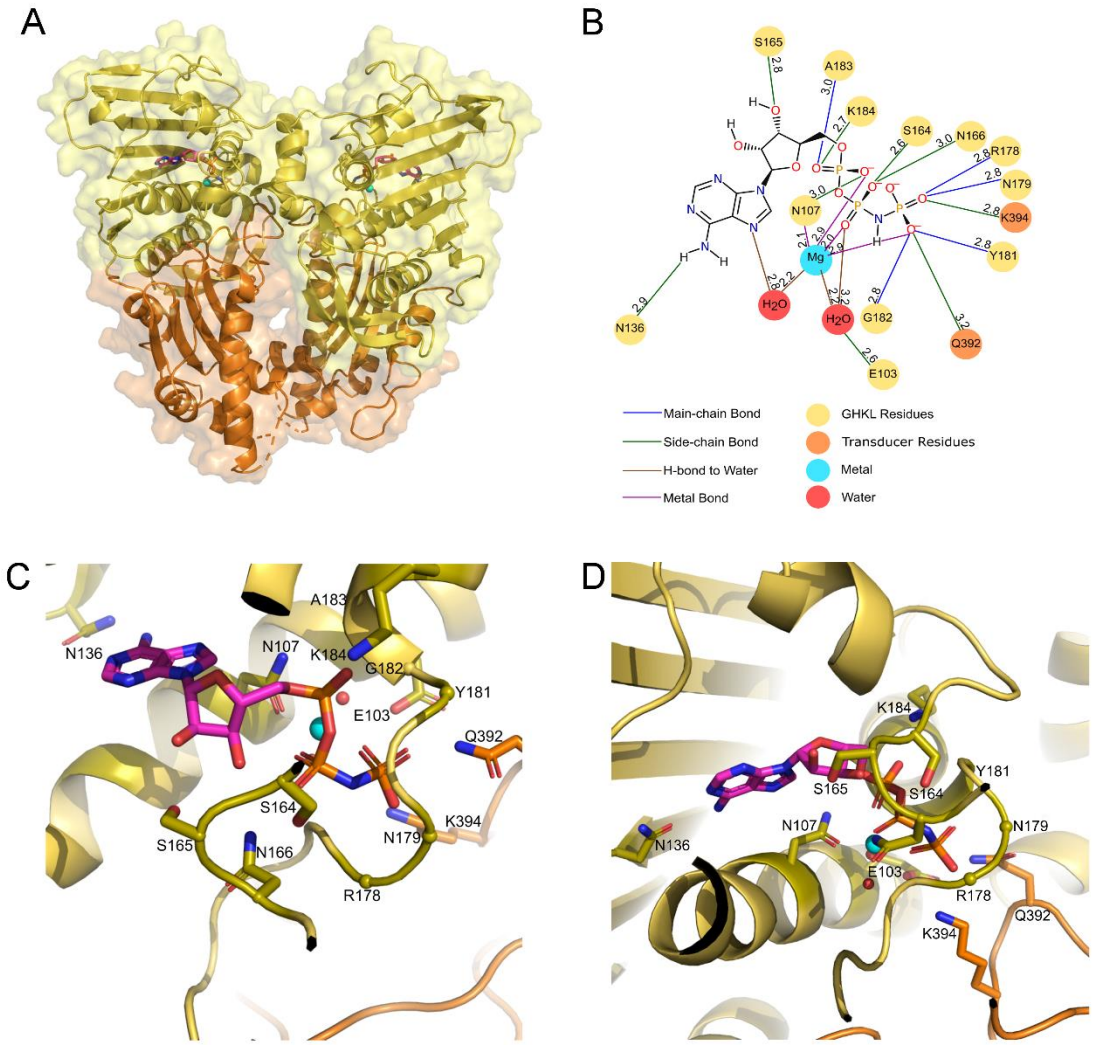

Figure 4-6: Overall structure and binding sites of the ATPase domain of human TOP2B bound to AMPPNP

(**A**) The GHKL and transducer domains of TOP2B are coloured yellow and orange respectively. Mg^{2+} ions coloured in cyan. AMPPNP coloured by atom – carbon pink, nitrogen blue, oxygen red and phosphate orange. The surface representation is also shown. (**B**) 2D diagram showing amino acid residues in TOP2B that interact with AMPPNP. Distances shown in Å. Blue lines represent a main chain hydrogen bond, green lines represent a side chain hydrogen bond, brown lines represent a hydrogen bond with water and a purple line indicates a hydrogen bond with a metal ion. (**C-D**) Two different views of the AMPPNP binding site of TOP2B coloured according to **A**. The side chains of residues involved in hydrogen bonding to the nucleotide are shown in stick representation and coloured by atom. Residues that bind nucleotide via main chain bonding are represented as spheres. Two water molecules are shown as red spheres and Mg^{2+} ions as cyan spheres.

Due to the success of obtaining crystals with S45 (45-444) crystallisation of the full-length ATPase domain of human TOP2B (M1, 1-444) was trialed. However, this was unsuccessful for several reasons. Firstly, the M1 protein is more unstable as demonstrated by the need for higher salt concentration in buffers during purification. The protein fragmented more, and the isolated polypeptide was not obtained in sufficiently pure form for crystallography. In addition, it is hypothesised that the extreme N-terminal amino acids of the TOP2B protein are highly flexible which makes it less than optimal for crystallography (Bedez, Lotz et al. 2018). Consequently, efforts were focused on the S45 (45-444) protein for crystallography trials.

4.4.2 Protein screens with the ATP hydrolysis product, ADP

To determine whether ATP hydrolysis results in conformational changes within the enzyme, crystallography trials were also performed with the ligand ADP. Any protein structures obtained with ADP would represent the structure of topoisomerase II after ATP hydrolysis whilst the structure bound to AMPPNP represents the conformation before ATP hydrolysis.

Firstly, crystallography trials were performed with TOP2B S45 (45-444) at 16 mg/mL, in the presence of 5 mM $MgCl_2$ and 5 mM ADP under the same condition that gave rise to the crystals with AMPPNP. However, unfortunately no crystals were observed. Therefore, the five different crystallisation screens were trialed: JSCG Plus, Index, PACT, Structure and Morpheus II. After 1 week, a small crystal was observed in condition H7 of JCSG Plus [0.2 M ammonium sulphate, 0.1 M bis tris (pH 5.5), 25% w/v PEG 3350], however, like the initial AMPPNP crystals, this crystal was too small to harvest (~10 µm) (Figure 4-7). As such, optimisation of the crystals was performed. The drop sizes were increased by three times to 300 nL protein:300 nL reservoir and 300 nL protein:600 nL reservoir, as well as diluting the reservoir stock solution by 5% increments. Crystals (~50 x 20 x 10 µm) were observed at a reservoir dilution of 95% and harvested with a MiTeGen crystal loop and cryoprotected with 100% PEG800. The crystals with ADP were a different morphology to those obtained with AMPPNP. Instead of being octahedron, the crystals were rhombohedron.

A

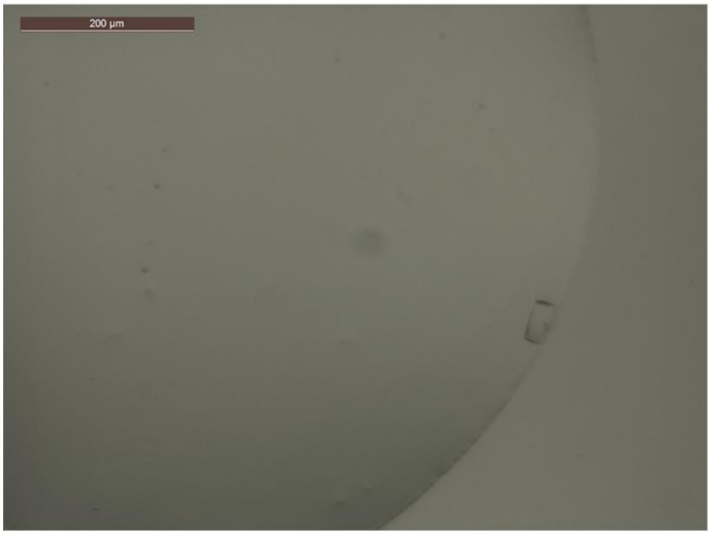

Figure 4-7: Image of the crystal found in the initial S45 trial with 5 mM ADP and 5 mM $MgCl_2$

(**A**) Condition H7 of JCSG Plus. Scale bar represents 200 µm.

4.4.2.1 Data Collection and Processing

Diffraction data for the ADP crystals was collected at Diamond Beamline I03 with unattended data collection using the native data collection strategy as per the AMPPNP bound structure (https://www.diamond.ac.uk/Instruments/Mx/I03/I03-Manual/Unattended-Data-Collections/Experiment-Types.html). Data were processed at Diamond with the automated pipeline Xia2 with Dials. The data were scaled with Aimless, and the space groups were confirmed with Pointless. 5% of the data were randomly selected for R_{free} calculations. The processing statistics are presented in Table 4-2.

Data Statistics*	
	ADP
Beamline	I03
Date	07/07/21
Wavelength (Å)	0.979
Resolution (Å)	89.22- 2.62 (2.74-2.62)
Space group	P 3 2 1
Unit-cell parameters	
a (Å)	103.02
b (Å)	103.02
c (Å)	66.69
α = β = γ (°)	90.00 = 90.00 = 120.00
Unit-cell volume ($Å^3$)	613005.13
Solvent content (%)	45.9
No. of measured reflections	256943 (32178)
No. of independent reflections	12596 (1513)
Completeness (%)	100.0 (100.0)
Redundancy	20.4 (21.3)
$CC_{1/2}$ (%)	0.997 (0.780)
<I>/<σ(I)>	9.0 (1.7)
Refinement Statistics*	
R_{work} (%)	20.70
R_{free} (%)	25.10
No. of non-H atoms	
No. of protein, atoms	2886
No. of solvent atoms	13
No. of ligand atoms	38
R.m.s. deviation from ideal values	
Bond angle (°)	1.66
Bond length (Å)	0.01
Average B factor ($Å^2$)	
Protein	60
Solvent	48
Ligand	50
Ramachandran plot$^+$, residues in	
Most favoured regions (%)	93.8
Allowed regions (%)	5.6
Disallowed regions (%)	0.6

Table 4-2: Data statistics and refinement details for human TOP2B ATPase domain in the presence of ADP

*(Values in parenthesis are for the highest resolution shell).
$^{\#}$5% of the randomly selected reflections excluded from refinement.
$^+$Calculated using MOLPROBITY.

4.4.2.2 Solving the Phases and Model Building

The phases were solved for the human TOP2B ATPase ADP bound structure on CCP4 cloud Newcastle (Potterton, Agirre et al. 2018) by molecular replacement using Molrep or Phaser (Vagin and Teplyakov 1997, McCoy, Grosse-Kunstleve et al. 2007). The AMPPNP model (pdb code 7QFO) was used to solve the ADP-bound structure. The model was improved by iterative cycles of manual model building in COOT (Emsley, Lohkamp et al. 2010) and refined using Refmac (Murshudov, Skubák et al. 2011). The model was validated using COOT (Emsley, Lohkamp et al. 2010) validation tools and Molprobity (Williams, Headd et al. 2018). Metal type, co-ordination and bond distances were validated using check my metal (Zheng, Cooper et al. 2017).

4.4.2.3 Structure of the ATPase Domain of Human TOP2B bound to ADP

To determine the difference in structure between pre- and post-ATP hydrolysis, I solved the structure of the TOP2B ATPase domain in complex with ADP, pdb code 7QFN (Figure 4-8). The structure was solved to 2.6 Å by molecular replacement using the AMPPNP structure as a search model. The final ADP model contains residues 47-422 with missing loops between residues 169-173 and 356-366, where the K-loop resides. The ADP model was refined to an R_{work} factor of 20.7% and an R_{free} of 25.1% (Table 4-2). For the ADP model, the statistics are in line with published models of similar resolution and were confirmed during validation. Similar to the AMPPNP model, the ADP structure has one copy of the protein per asymmetric unit and the biological dimer was confirmed by PISA (Krissinel and Henrick 2007). The interface area of the dimer represents ~11% of the total monomer surface indicating significant interactions which include 34 hydrogen bonds and 6 salt-bridges between the two monomers.

The ADP structure is composed of a virtually unchanged GHKL domain (Figure 4-8A) compared to the AMPPNP structure with the nucleotide and most of the active site residues in the same conformation, albeit a further distance from the ADP molecule (Figure 4-8B-D). In addition, the ligand binding site contains one bound ADP molecule per monomer. The adenine ring, ribose sugar, and α-phosphate of ADP make the same set of residue contacts as in the AMPPNP complex, despite the sugar pucker differing. Similarly, S164 and N166 which hydrogen bond with the β-phosphate of AMPPNP also bind with the β-phosphate of ADP, although the β-phosphate of ADP has an additional contact to G180 which does not occur in the AMPPNP structure. As the γ-phosphate is lost during ATP hydrolysis, R178 and N179 which were previously

bound to the γ-phosphate instead bind to the β-phosphate of ADP. Strikingly, the γ-phosphate binding site is now occupied by a sulphate ion present in the crystallisation condition (0.2 M ammonium sulphate). The sulphate ion is held in place by hydrogen bonds between Y181, G182 and N179 which previously bound the γ-phosphate. Thus, the ADP structure represents the post hydrolysis state with the sulphate group mimicking the ATP hydrolysis product, P_i.

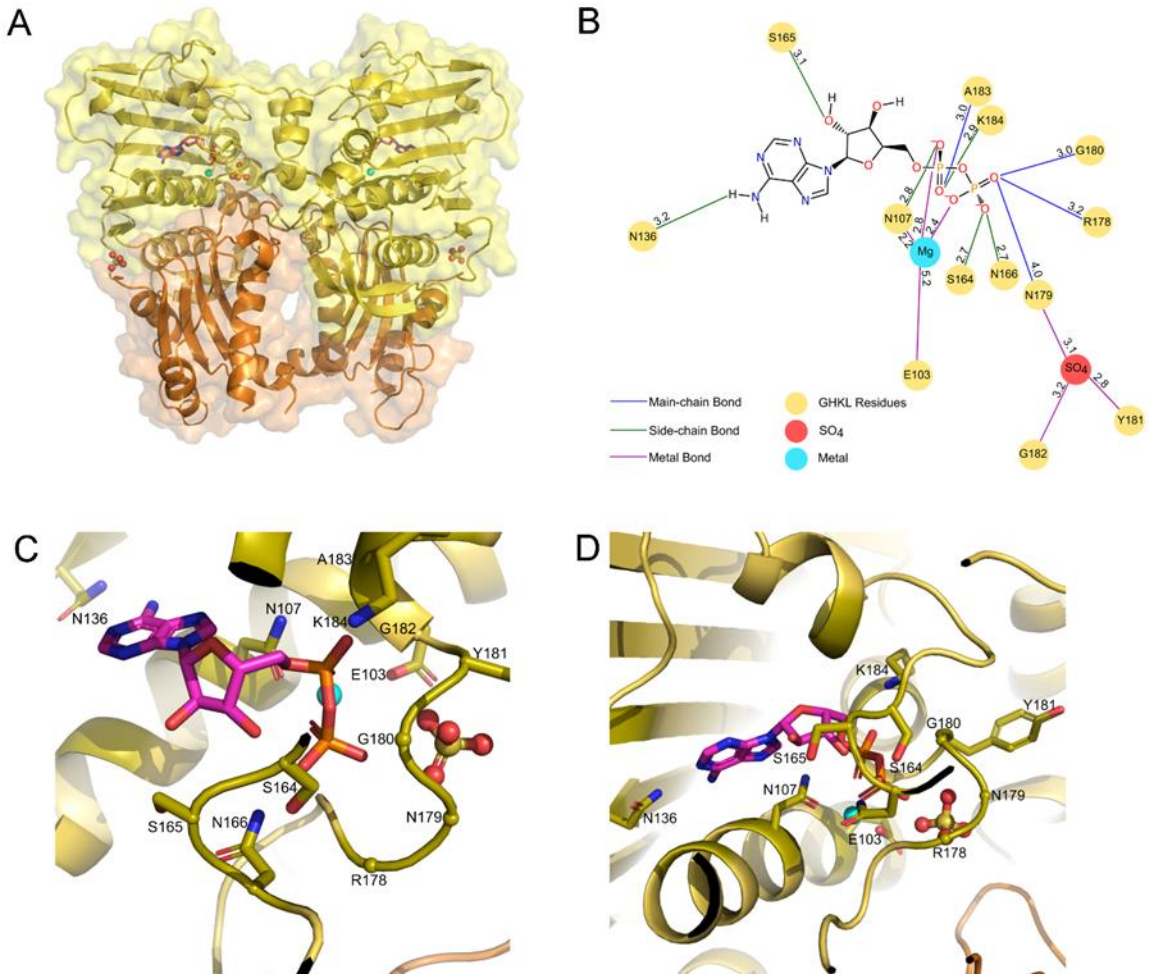

Figure 4-8: Overall structure and binding sites of the ATPase domain of human TOP2B bound to ADP

(**A**) The GHKL and transducer domains of TOP2B are coloured yellow and orange respectively. ADP coloured by atom – carbon pink, nitrogen blue, oxygen red and phosphate orange. The surface representation is also shown. Mg^{2+} ions coloured in cyan. Sulphate (SO_4) is represented by oxygen in red spheres and sulphur in yellow spheres. (**B**) 2D diagram showing amino acid residues in TOP2B that interact with ADP. Distances shown in Å. Blue lines represent a main chain hydrogen bond, green lines represent a side chain hydrogen bond, brown lines represent a hydrogen bond with water and a purple line indicates a hydrogen bond with a metal ion. (**C-D)** Two different views of the ADP binding site of TOP2B as per Figure 4-6.

4.4.2.4 Conformational change in the ADP structure to allow release of P_i

Although the GHKL domains of the two structures are virtually identical and the superposition of C-α atoms in this domain gives a root mean square deviation (RMSD) value of 0.47 Å, an important conformational change of the transducer domain occurs during ATP hydrolysis (Figure 4-9A-B). This is represented by an increase in the RMSD value (0.77 Å) when the C-α atoms in this domain are superposed. The transducer domain of the ADP monomer opens towards the C-terminus of the protein (represented by dashed box in Figure 4-9A) signifying the relaxed conformation. Moreover, during the reorganisation of the transducer domain, the QTK loop is shifted away from the ATP binding site (represented by dashed box in Figure 4-9B) preventing Q392 and K394 from making contacts with the nucleotide. Specifically, the side chain of Q392 moves by 3.8 Å and K394 moves by 2.5 Å. In turn, this opens the active site for the release of the ATP hydrolysis product P_i.

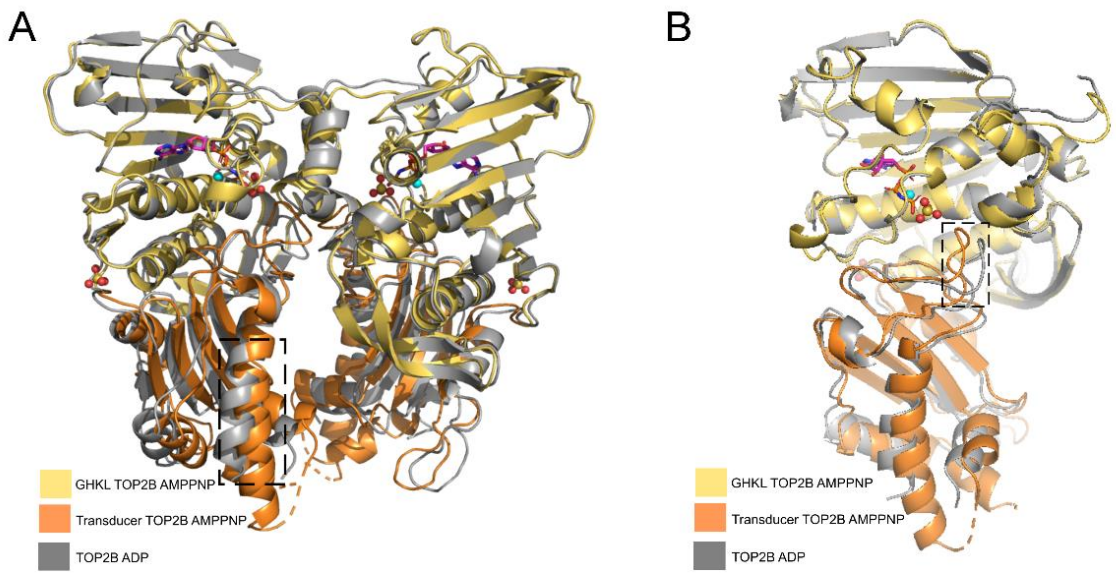

Figure 4-9: Two alternative views of the ATPase domain of human TOP2B bound to ADP superposed on the TOP2B AMPPNP bound structure

***(A-B)** The GHKL domain of the ADP (grey) structure superposed onto the AMPPNP structure coloured according to Figure 4-6 and Figure 4-8 using least squares superposition.*

4.4.3 Comparison of the TOP2B and TOP2A ATPase Domain Structures

To understand whether the two human enzymes have similar ATPase domain structures I compared my TOP2B structures to the previously published TOP2A structures (Wei, Ruthenburg et al. 2005). When bound to AMPPNP, the TOP2A structure is in the restrained conformation and is remarkably similar to TOP2B (Figure 4-10A). The individual domains possess nearly identical overall structures, with the C-α atoms of the GHKL domain of human TOP2A (28-264) superposing onto TOP2B with an RMSD value of 0.34 Å. Whilst the C-α atoms of the transducer domain of human TOP2A (265-428) superpose onto TOP2B with an RMSD value of 0.69 Å. The nucleotide binding sites of both structures exhibit a distorted octahedral geometry with the active site Mg^{2+} coordinated by the conserved asparagine of TOP2A N91 (N107 in TOP2B), all three phosphates of AMPPNP and two water molecules, one of which is activated by the catalytic base of TOP2A E87 (E103 in TOP2B).

Both human ADP structures are in an open conformation suggesting a conformational change is necessary after ATP hydrolysis to accommodate the free phosphate (represented as a sulphate in the structure). As shown in Figure 4-10B, the transducer domain of the TOP2B structure is in a more open conformation compared to TOP2A, the C-α atoms of this domain superpose onto TOP2B with an RMSD value of 0.76 Å. Moreover, the β sheets in one of the two GHKL domains do not completely align between human TOP2A and TOP2B (Figure 4-10B), though the C-α atoms of this domain superpose with an RMSD value of 0.38 Å. This could be due to differences in the internal flexibility of TOP2A and TOP2B or crystallisation effects. However, despite these minor differences overall, the ATPase domains of TOP2A and TOP2B are extremely similar.

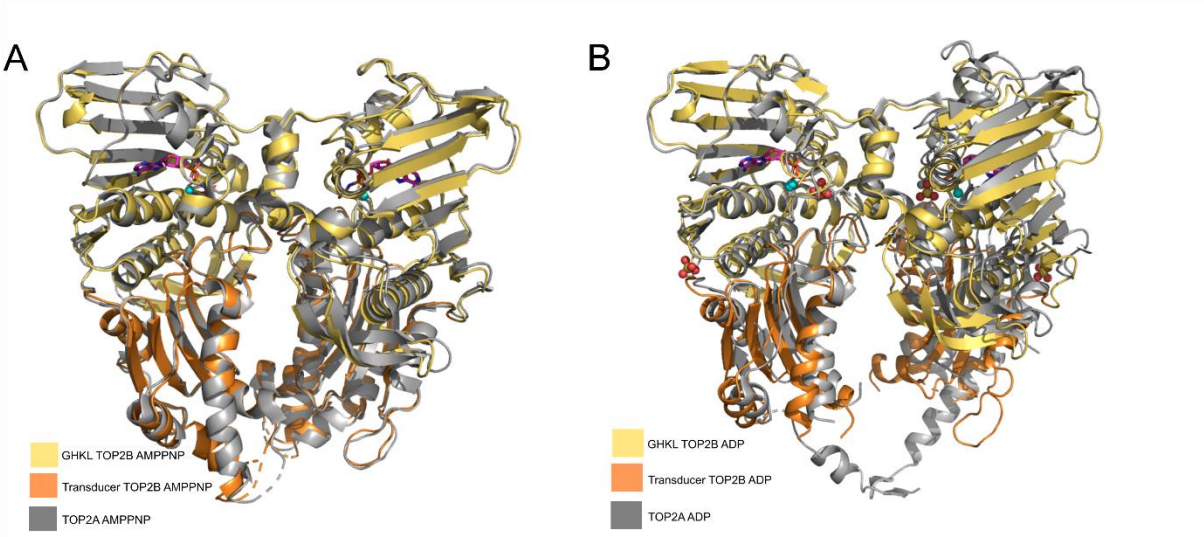

Figure 4-10: Superposition of the TOP2A and TOP2B ATPase domain structures

(A) The GHKL domain of human TOP2A (grey) in complex with AMPPNP superposed onto the TOP2B AMPPNP structure in Figure 4-6 using least squares superposition. **(B)** The GHKL domain of human TOP2A grey) in complex with ADP superposed onto the TOP2B ADP structure in Figure 4-8 using least squares superposition.

4.4.4 Protein screens with ICRF187

To date, the only topoisomerase II ATPase domain structure in the presence of a drug is the *S. cerevisiae* ATPase domain crystal structure in the presence of AMPPNP and dexrazoxane (ICRF187) (Classen, Olland et al. 2003). To understand how ICRF187 binds to the clinical target, I attempted co-crystallising the ATPase domain of TOP2B with ICRF187. 0.1 mg of ICRF187 was added to the protein solution and left to incubate for 1 hour at room temperature prior to addition of ADP and $MgCl_2$. Crystallisation was performed with the condition that gave crystals for ADP [0.2 M ammonium sulphate, 0.1 M bis tris (pH 5.5), 25% w/v PEG 3350] with 300 nL protein:300 nL reservoir and 300 nL protein:600 nL reservoir. Crystals with the same morphology as protein and ADP without drug were observed for ICRF187 (~50 x 20 x 10 µm in size) and harvested with a MiTeGen crystal loop and cryoprotected with 100% PEG 800.

4.4.4.1 Data Collection and Processing

Diffraction data for the ICRF187:ADP crystals was collected at Diamond Beamline I03 with unattended data collection using the native data collection strategy as per the AMPPNP and ADP bound structures. The crystal diffracted, however, there was insufficient electron density to support drug bound crystals.

4.4.4.2 Comparison of the Yeast ATPase domain in complex with ICRF187 reveals similarities in the drug binding site of TOP2B

As I was unsuccessful in obtaining an ICRF187 bound structure, I superposed the TOP2B ATPase domain structure and the TOP2A ATPase domain structure (Wei, Ruthenburg et al. 2005) onto the *S. cerevisiae* structure bound to ICRF187 (Classen, Olland et al. 2003) to identify the drug binding site (Figure 4-11A). Due to the conserved domain organisation between type II topoisomerases, the overall structure of the TOP2B ATPase domain is very similar to that of yeast with an RMSD of value 0.79 Å when using secondary structure matching of all C-α atoms in the protein. The side chains of residues within 3.5 Å of ICRF187 capable of hydrogen bonding are shown in Figure 4-11B. TOP2A was included in the analysis shown in Figure 4-11B to determine whether the drug binding site is comparable between TOP2A and TOP2B. As ICRF187 can inhibit all three enzymes, it was not surprising that the residues were highly conserved in the drug binding site and all three structures exhibited the same putative 12 residues, 6 per monomer (H58, T65, Y66, N179, Y181 and Q392 in human TOP2B)

involved in hydrogen bonding with ICRF187 (Figure 4-11B). The side chain with the greatest difference in conformation compared to yeast was the TOP2B residue H58, which is mutated to a tyrosine in two patients exhibiting developmental delay and intellectual impairment (Lam, Yeung et al. 2017). The equivalent TOP2A residue, H42, also varied in conformation compared to yeast. It is interesting to note that one of the residues found in the drug binding pocket is Q392, which is involved in binding the γ-phosphate of AMPPNP.

Of the six residues directly involved in binding ICRF187, two have been reported in human TOP2A to confer resistance to ICRF187 and ICRF193. Y165S in TOP2A (Y181 in TOP2B) has been described to be resistant to ICRF187 (Wessel, Jensen et al. 2002) and Y50F in TOP2A (Y66 in TOP2B) has been shown to confer resistance to ICRF193 (Sehested, Wessel et al. 1998). Both mutations likely act by disrupting hydrogen bonds between the enzyme and drug, hence reducing drug binding affinity. In rat TOP2B and human TOP2A, L178F and L169F respectively (L185 in human TOP2B) confer resistance to ICRF187 and ICRF193 (Patel, Jazrawi et al. 2000, Onoda, Hosoya et al. 2014). Although L185 in human TOP2B is not directly involved in hydrogen bonding ICRF187, it is near the drug binding residues N179 and Y181. Similarly, the human TOP2B residues D64N and R178Q that are equivalent to the human TOP2A residues D48N and R162Q that confer resistance to ICRF187 (Wessel, Jensen et al. 2002) don't appear to directly interact with the drug but mutating them could disrupt the drug binding pocket.

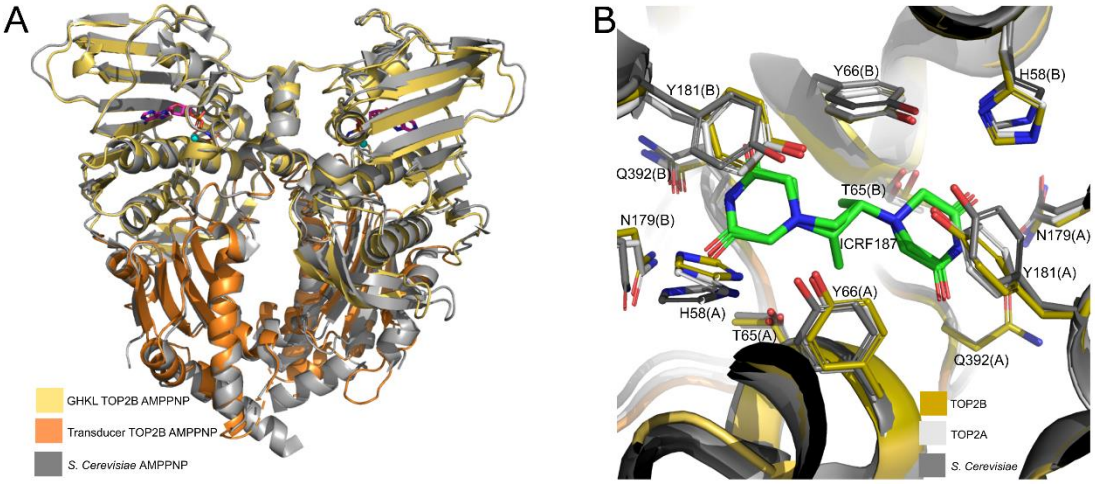

Figure 4-11: Superposition of the S. cerevisiae TOP2 ATPase domain structure onto TOP2B AMPPNP structure and ICRF187 drug binding site

(A) The *S. cerevisiae* ATPase domain (grey) in complex with AMPPNP and ICRF187 superposed onto the human TOP2B structure in complex with AMPPNP coloured according to Figure 4-6 using least squares superposition. ICRF187 is coloured by atom: carbons green, oxygens red and nitrogens blue. **(B)** The ICRF187 binding site of *S. cerevisiae* (dark grey) and TOP2A (silver) superposed onto the TOP2B ATPase structure coloured according to Figure 4-6. The side chains of residues within 3.5 Å of ICRF187 are shown in stick representation and coloured by atom. Residue labels according to human TOP2B (1-1621) numbering. (A)/(B) denotes the protein chain.

4.4.5 Protein screens with ICRF193

ICRF193 is a catalytic inhibitor of topoisomerase II that converts the nucleotide bound ATPase domain to an inactive, closed clamp intermediate around DNA akin to ICRF187's mechanism of action. ICRF193 is the most potent bisdioxopiperazine and shows the highest cardioprotective efficiency (Jirkovská, Karabanovich et al. 2021), but due to the low solubility of ICRF193 its use in the clinic has been limited. Due to the inability to obtain a TOP2B:ICRF187 structure, I attempted solving the structure bound to ICRF193. Crystallography trials were performed as per ICRF187 with 0.1 mg of ICRF193 added to the protein solution and left to incubate for 1 hour at room temperature prior to addition of ADP and $MgCl_2$. Crystallisation was performed as per the ADP condition (0.2 M ammonium sulphate, 0.1 M bis tris pH 5.5, 25% w/v PEG 3350) with 300 nL protein:300 nL reservoir and 300 nL protein:600 nL reservoir. Again, rhombohedron crystals were observed with ICRF193 and were ~50 x 20 x 10 µm in size. Crystals were harvested with a MiTeGen crystal loop and cryoprotected with 100% PEG 800.

4.4.5.1 Data Collection and Processing

Diffraction data for the ICRF193:ADP crystals was collected at Diamond Beamline I03 with unattended data collection using the native data collection strategy as per the AMPPNP and ADP bound structures (https://www.diamond.ac.uk/Instruments/Mx/I03/I03-Manual/Unattended-Data-Collections/Experiment-Types.html). Data were processed at Diamond with the automated pipeline Xia2 with Dials. The data were scaled with Aimless, and the space groups were confirmed with Pointless. 5% of the data were randomly selected for R_{free} calculations. The processing statistics are presented in Table 4-3.

Data Statistics*	
	ADP:ICRF193
Beamline	I03
Date	25/02/22
Wavelength (Å)	1.000
Resolution (Å)	53.66 - 2.30 (2.38-2.30)
Space group	P 3 2 1
Unit-cell parameters	
a (Å)	103.40
b (Å)	103.40
c (Å)	67.02
α = β = γ (°)	90.00 = 90.00 = 120.00
Unit-cell volume ($Å^3$)	620549.06
Solvent content (%)	45.8
No. of measured reflections	357987 (36121)
No. of independent reflections	18666 (1821)
Completeness (%)	99.8 (100)
Redundancy	19.2 (19.8)
$CC_{1/2}$ (%)	0.996 (0.565)
<I>/<σ(I)>	11.0 (1.5)
Refinement Statistics*	
R_{work} (%)	19.70
R_{free} (%)	25.93
No. of non-H atoms	
No. of protein, atoms	2944
No. of solvent atoms	50
No. of ligand atoms	41
R.m.s. deviation from ideal values	
Bond angle (°)	1.82
Bond length (Å)	0.01
Average B factor ($Å^2$)	
Protein	44
Solvent	36
Ligand	46
Ramachandran plot[+], residues in	
Most favoured regions (%)	97.2
Allowed regions (%)	2.2
Disallowed regions (%)	0.6

Table 4-3: Data statistics and refinement details for human TOP2B ATPase domain in the presence of ADP and ICRF193.

*(Values in parenthesis are for the highest resolution shell).
[#]5% of the randomly selected reflections excluded from refinement.
[+]Calculated using MOLPROBITY.

4.4.5.2 Solving the Phases and Model Building

The phases were solved for the human TOP2B ATPase ICRF193:ADP drug bound structure on CCP4 cloud Newcastle (Potterton, Agirre et al. 2018) by molecular replacement using Molrep or Phaser (Vagin and Teplyakov 1997, McCoy, Grosse-Kunstleve et al. 2007). The ADP model (pdb code 7QFN) was used to solve the ADP:ICRF193 bound structure. The model was improved by iterative cycles of manual model building in COOT (Emsley, Lohkamp et al. 2010) and refined using Refmac (Murshudov, Skubák et al. 2011). The model was validated using COOT (Emsley, Lohkamp et al. 2010) validation tools and Molprobity (Williams, Headd et al. 2018). Metal type, co-ordination and bond distances were validated using Check My Metal (Zheng, Cooper et al. 2017).

4.4.5.3 ICRF193 bound to the clinical target, human TOP2B ATPase domain, in complex with ADP

To define the interactions between the clinical target of the bisdioxopiperazines, I determined the structure of the ATPase domain of human TOP2B in complex with ADP and bound to ICRF193. This is the first report of a type II topoisomerase structure in complex with ICRF193 (PDB code 7ZBG). The structure was solved to 2.3 Å by molecular replacement using the ADP-bound structure as a search model. The final TOP2B:ADP:ICRF193 model contains residues 45-422 with a missing loop between residues 354-368. The TOP2B:ADP:ICRF193 model was refined to an R_{work} factor of 19.7% and an R_{free} of 25.9% (Table 4-3). Similar to the previous structures, the TOP2B:ICRF193:ADP-bound structure has one copy of the protein per asymmetric unit and the biological dimer was confirmed by PISA (Krissinel and Henrick 2007). The interface area of the dimer represents ~12% of the total monomer surface indicating significant interactions which include 36 hydrogen bonds and 12 salt-bridges between the two monomers.

The overall structure of the ADP:ICRF193 model is virtually unchanged compared to the ADP structure without drug (Figure 4-12A). The nucleotide binding sites are extremely similar in the presence and absence of ICRF193 and superpose with an RMSD value of 0.19 Å. Moreover, the transducer domains superpose with near identity and exhibit an RMSD value of 0.35 Å. A single drug molecule was observed bound in the previously reported ICRF187 binding site (Classen, Olland et al. 2003), bound in one of two possible conformations (Figure 4-12B). The same protein drug interactions

are observed in either binding mode due to the pseudo symmetry of ICRF193, which stabilises the nucleotide-bound transient dimer interface between the two ATPase protomers. The drug binding pocket consists of the same 12 amino acids (6 from each protomer) involved in hydrogen bonding ICRF187. The GHKL domain contributes the majority of residues (H58, T65, Y66, N179 and Y181), with only one transducer domain residue, Q392, binding to the drug. Y66 makes direct contact with ICRF193 accounting for the resistant phenotype when the equivalent residue in human TOP2A (Y50) is mutated to a phenylalanine (Sehested, Wessel et al. 1998). Similar to the ICRF187 *S. cerevisiae* binding site, superpositions of the drug free and ICRF193 bound structures show that the side chains of the 12 residues involved in drug binding do not change conformation and the drug binding site is a preformed feature of the nucleotide bound dimerised protein. However, the side chain of Q392 moves by ~4.5 Å in order to accommodate ICRF193 and prevent a steric clash. Whilst an alternative rotamer of T65 is observed to allow a hydrogen bond to form to the hydroxyl group of ICRF193 (Figure 4-12C). ICRF193 is similar in structure to ICRF187 but contains an additional methyl group on the ethanediyl linker, hence the bisdioxopiperazine binding site is large enough to accommodate either form of the drug. Though, the presence of one more methyl group allows ICRF193 to have an additional contact with Y66 which perhaps accounts for the increased potency of the drug.

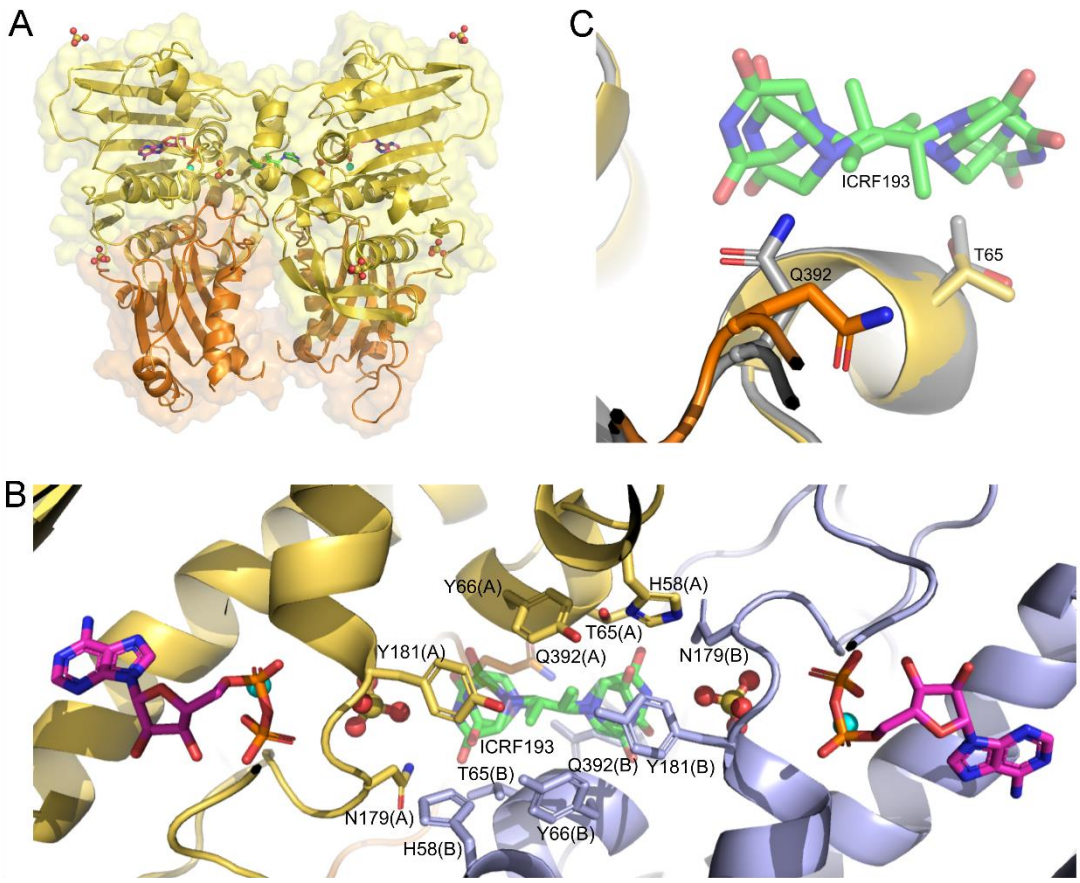

Figure 4-12: Overall structure and binding sites of the ATPase domain of human TOP2B bound to ADP and the bisdioxopiperazine ICRF193

(A) The GHKL and transducer domains of TOP2B are coloured in yellow and orange respectively. ADP coloured by atom - carbon pink, nitrogen blue, oxygen red and phosphate orange. The surface representation is also shown. Mg^{2+} ions coloured in cyan. Sulphate (SO_4) is represented by oxygen in red spheres and sulphur in yellow spheres. ICRF193 binds between the two TOP2B protomers and is coloured by atom – carbon green, nitrogen blue and oxygen red. **(B)** The side chains of residues involved in binding to ICRF193 are shown in stick representation. GHKL and transducer residues from one monomer are coloured in yellow and orange respectively, and the other monomer coloured in pale blue. (A)/(B) denotes protein chain. Both possible binding conformations of ICRF193 are shown. **(C)** The C-alpha atoms of the ADP complex in the absence of drug (grey) superposed onto the ADP:ICRF193 structure (yellow and orange) using least squares superposition. Q392 moves away from drug binding site in the ADP:ICRF193 structure to create space for the drug. Alternative conformer of T65 for formation of an extra hydrogen bond to ICRF193. Other side chains are not shown as they have the same conformation in the presence and absence of ICRF193 bound to ADP.

4.5 Discussion

The data generated in this Chapter shows that the ATPase domain of human TOP2B in complex with AMPPNP is in the restrained conformation with the nucleotide binding site sequestered from solvent (Figure 4-6). The cavity between the two monomers is not large enough to easily accommodate a DNA duplex. Upon T-DNA binding strain is induced within the ATPase dimer which is hypothesised to promote DNA cleavage of the G-DNA. By contrast, the ADP structure is in a more open, relaxed confirmation (Figure 4-8) with the QTK loop from the transducer domain undergoing a distinct movement away from the nucleotide binding site (Figure 4-9). This movement then accommodates a sulphate group, in place of the ATP hydrolysis product, P_i (Figure 4-8). Remarkably, the structures demonstrate that ATP hydrolysis results in a conformational change of the transducer domain, whilst the GHKL domain remains extremely similar between the two nucleotide-bound states (Figure 4-9). The catalytic Mg^{2+} ion is coordinated by a conserved asparagine residue (N107), all three phosphates of AMPPNP and two water molecules, one of which becomes activated by the catalytic glutamate residue (E103).

The bisdioxopiperazine dexrazoxane (ICRF187) is approved for use in the clinic to reduce the incidence of anthracycline-induced heart failure (van Dalen, Caron et al. 2011, Bansal, Joshi et al. 2021). The cardioprotective effect of ICRF187 acts via inhibiting TOP2B in cardiomyocytes. Although, I was unsuccessful in obtaining an ICRF187 TOP2B bound structure, I obtained a structure of the ATPase domain of human TOP2B bound to ADP:ICRF193, experimentally demonstrating that ICRF193 binds within the same binding site as was reported for *S. cerevisiae* TOP2 and ICRF187 (Figure 4-11 and Figure 4-12). Two main conformational changes occur in order to accommodate ICRF193 within the binding site. The side chain of Q392 from the QTK loop moves by ~4.5 Å to prevent a steric clash with the drug, and an alternative rotamer of T65 occurs to form an additional hydrogen bond to ICRF193. ICRF193 displays a higher potency against beta compared to ICRF187 (Hasinoff, Kuschak et al. 1995, Hasinoff, Patel et al. 2020, Jirkovská, Karabanovich et al. 2021), likely due to the extra methyl group in ICRF193 which forms an additional hydrogen bond to Y66. These crystal structures provide a valuable resource to study drug interactions with the ATPase domain and for analysis of drug-resistant mutations.

The TOP2B structures share an overall tertiary structure and transducer opening mechanism very similar with TOP2A (Figure 4-10). In both human structures and the *S. cerevisiae* structure, the beginning of the N-terminal strap is absent. Hence, there are no eukaryotic TOP2 ATPase domain structures containing the complete N-terminal strap, which is the most variable region of the ATPase domain. To gain further insight into what the N-terminal strap contributes to the structure I attempted crystallising the full-length ATPase domain (1-444) but was unable to obtain crystals. From Chapter 3 it is known that the N-terminal strap affects *in vitro* activity as the full-length TOP2B ATPase domain proteins (1-444 and 1-449) are less active than the N-terminally truncated proteins (45-444). It would be interesting to understand how the structure of the N-terminal strap results in a less active type II topoisomerase ATPase domain.

Chapter 5 *In Vivo* Analysis of Mutated Full-Length TOP2B Proteins (residues 46-1621)

5.1 Introduction

Type II topoisomerase enzymes form transient covalent complexes during catalysis. Topoisomerase II poisons stabilise these transient covalent complexes and this can lead to cytotoxic double strand DNA breaks. The efficacy of topoisomerase II poisons can be limited by drug resistance though. Classical multidrug resistance (MDR) involves increased expression of the transmembrane P-glycoprotein which pumps drug molecules out of the cell reducing the intracellular drug concentration. Overexpression of P-glycoprotein causes resistance to a broad range of drugs with varying structures and mechanisms of action (Nakagawa, Schneider et al. 1992).

A second method, atypical MDR (at-MDR) causes resistance to drugs with the same mechanism of action. For example, mutations in topoisomerase II have been described in patients and mammalian cell culture models that cause cross resistance to topoisomerase II targeting drugs, but they remain sensitive to compounds that target cancer cells via alternative mechanisms (e.g., inhibition of microtubule formation) (Odaimi, Andersson et al. 1986, Danks, Yalowich et al. 1987, Kubo, Kohno et al. 1995, Vassetzky, Alghisi et al. 1995, Kusumoto, Rodgers et al. 1996, Dereuddre, Delaporte et al. 1997, Herzog, Holmes et al. 1998). At-MDR does not involve reduced P-glycoprotein expression or decreased intracellular drug concentration but instead functions by reducing the ternary topoisomerase II drug complex (Pommier 1993). Mechanisms to achieve this include decreasing topoisomerase II protein expression (Eijdems, de Haas et al. 1995, Asano, Nakamura et al. 2005) or altering subcellular localisation of the enzyme (Fernandes, Danks et al. 1990, Feldhoff, Mirski et al. 1994), reducing the number of molecules of enzyme that can be targeted to generate cytotoxic DNA breaks. Generation of mutations within topoisomerase II that reduce DNA binding, drug affinity or reduce topoisomerase activity causing less efficient DNA cleavage can diminish the formation of drug induced cleavable complexes (Danks, Schmidt et al. 1988, Bugg, Danks et al. 1991). Furthermore, altering the posttranslational modifications of topoisomerase II can cause at-MDR. In particular, hyper or hypo-phosphorylation of topoisomerase II has been observed in drug-resistant cell lines and reduces cleavage complex formation (Larsen and Skladanowski

1998). By studying drug-resistant cell lines insight into drug resistance mechanisms has been revealed.

Focused mutagenesis studies have also provided powerful tractable model systems to identify key amino acid residues involved in the catalytic cycle of type II topoisomerases and residues that can confer resistance to topoisomerase II targeting drugs. Two main mutagenesis strategies have been utilised; site directed mutagenesis and random mutagenesis. Site directed mutagenesis targets and mutates a specific residue to analyse changes in protein activity and elucidate the function of the residue (West, Meczes et al. 2000). Whereas random mutagenesis followed by selection on drug plates has provided a valuable tool for identifying residues that can confer drug resistance (Leontiou, Watters et al. 2007).

The functional mutated proteins H514Y, G550R and A596T, were selected for drug resistance by C. Leontiou (Leontiou, Lakey et al. 2004) in a yeast temperature-sensitive system, using forced molecular evolution (Figure 5-1). Random mutations were introduced using hydroxylamine and libraries of mutated plasmids were generated and transformed into temperature-sensitive yeast and grown at the non-permissive temperature. Yeast that could survive on plates containing drugs were selected, thus only selecting functional proteins. All three of the proteins were selected for resistance to the topoisomerase II poison DACA, whilst G550R and A596T were also selected for resistance to the topoisomerase II poison AMCA. The mutated residues are located within the core catalytic domain (residues 400-1200) and reside within the TOPRIM domain of TOP2B. G550R has previously been expressed and purified and the *in vitro* activity characterised (Leontiou, Watters et al. 2007). G550R demonstrated an increase in relaxation activity by 50% but decreased decatenation activity by 50% when compared to wild type TOP2B.

Interestingly, three of the mutated residues in the drug-resistant proteins (H514Y, G550R, A596T) are immediately adjacent to lysine residues that can be ubiquitinated in humans, K515, K551 and K595 (https://ggbase.hms.harvard.edu/). This region of topoisomerase II is important for strand passage, yet the role of ubiquitination modifications on the catalytic activity of TOP2B is not understood. Alterations of other posttranslational modifications, such as phosphorylation (Takano, Kohno et al. 1991), can provide resistance to topoisomerase II poisons, so it may be possible that a ubiquitin modification can act in a similar manner. Moreover, a similar posttranslational

modification, SUMOylation, has been reported to alter the enzyme activity of topoisomerase II, and a SUMO modification site is present in the core of TOP2A on a residue directly involved in binding G-DNA (Wendorff, Schmidt et al. 2012). Similarly, K595 in human TOP2B has been shown to be SUMOylated, though the function of this modification is not yet understood (Hendriks, D'Souza et al. 2014). The mutations conferring drug resistance may prevent ubiquitin from being added onto the lysine residue. Therefore, to investigate this hypothesis, lysine to alanine mutations at the ubiquitination target sites; K515A, K551A and K595A were generated, as an alanine residue cannot be ubiquitinated.

In this chapter, the *in vivo* functionality of the K515A, K551A and the K595T mutated proteins was analysed in the yeast temperature-sensitive system (JN394t2-4) and compared to the original drug-resistant mutated proteins H514Y, G550R and A596T.

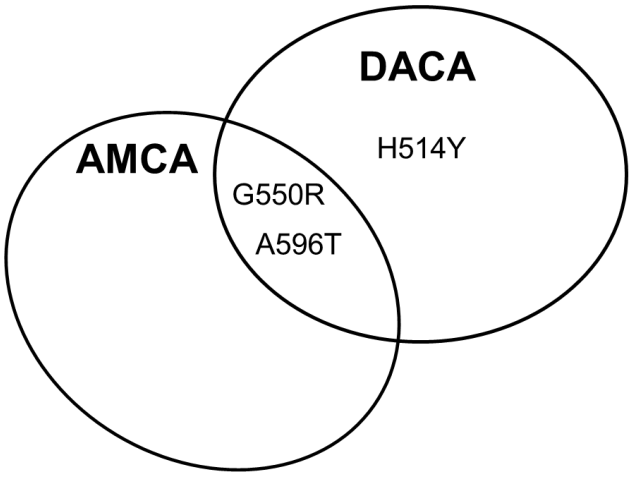

Figure 5-1:Venn diagram showing human TOP2B mutations that generate resistance to specific acridines adapted from C. Leontiou et al (Leontiou, Watters et al. 2007).

5.2 Introduction to *In Vivo* Complementation Analysis

To determine whether the mutations of K515A, K551A and K595A in human TOP2B are functional *in vivo*, complementation analysis was performed. Yeast is a powerful model organism for eukaryotic biology because many of the fundamental processes are similar and many human genes have a yeast homolog. Therefore, determining key processes in yeast cells can provide a basis for understanding higher eukaryotes. Furthermore, genetic manipulation of yeast cells is relatively easy and inexpensive. Plasmids containing mutated TOP2B were transformed into an *S. cerevisiae* strain (JN394t2-4) carrying a temperature-sensitive (*ts*) mutation in the *top2* gene, *top2-4,* to observe whether they could complement *in vivo.* The *ts* yeast strains are able to grow at the permissive temperature of 25 °C and exhibit some growth at the semi-permissive temperature of 30 °C albeit at a reduced rate. However, when the temperature is increased to 35 °C, the non-permissive temperature, the yeast strains are unable to grow due to lack of a functional yeast topoisomerase II. If yeast are transformed with a plasmid encoding a functional topoisomerase II, the *ts* phenotype can be rescued and cell viability restored at the non-permissive temperature, providing an *in vivo* system to study plasmid borne DNA topoisomerase II.

Studies in *S. cerevisiae* confirmed that topoisomerase II is the cellular target of many anticancer drugs. Although, initially yeast strains were not particularly sensitive to DNA topoisomerase targeting drugs, due to the impermeable cell wall. However, a strain was developed by Nitiss (Nitiss and Wang 1988), JN394, that contains multiple mutations to allow drug sensitivity of topoisomerases to be studied. For example, JN394 carries an *ise2* mutation that allows drug molecules to penetrate the yeast cells and the *rad52* gene is deleted which causes erroneous DNA repair. Both mutations increase the sensitivity of yeast cells to DNA damaging agents and topoisomerase II poisons which makes the strain particularly relevant for studying the effects of cytotoxic agents. When JN394 is transformed with a yeast TOP2 expression plasmid the level of topoisomerase II within the cell increases by tenfold, and increases the sensitivity of the cells to topoisomerase II targeting drugs like mAMSA and etoposide (Nitiss, Liu et al. 1992). These results indicate that topoisomerase II is a cellular target of mAMSA and etoposide, and that overexpressing topoisomerase II causes cells to become more sensitive to these drugs.

5.3 Creation of TOP2B Mutations for *In Vivo* Analysis

Before complementation could be performed, the mutations had to be generated in the human TOP2B plasmid, YEphTOP2βKLM. This plasmid has a galactose-inducible promoter (GAL1) upstream of the human TOP2B cDNA for controllable protein expression. The plasmid also contains the URA3 and *amp* genes and the replication origins of pBR322 and yeast 2 µm plasmid to allow growth and selection of the plasmid in both *E. coli* and yeast. The *amp* gene provides resistance to ampicillin in *E. coli* transformants and the URA3 gene acts as a selection marker to enable the growth of yeast transformants in media lacking uracil. The plasmids containing the cDNA encoding TOP2A (YEpWOB6) or TOP2B (YEphTOP2βKLM) lack the poorly conserved N-terminal strap (residues 1-28 in TOP2A and 1-44 in TOP2B). The first TOP2A residue in YEpWOB6 is serine 29 and the first TOP2B residue in YEphTOP2βKLM is serine 45, both of which align with serine 7 of yeast TOP2. YEpWOB6 and YEphTOP2βKLM were designed with the first 7 yeast residues fused to the human topoisomerase II coding sequence for optimal protein expression and to account for the N-end rule (Varshavsky 1997, Tasaki, Sriram et al. 2012).

Mutagenesis was performed using the site directed mutagenesis kit from Agilent to insert the mutations into YEphTOP2βKLM plasmid as previously described (Chapter 2 Section 2.16). Table 5-1 lists the mutations which were successfully generated and assayed via the *in vivo* complementation assay.

Mutation
H514Y
K515A
G550R
K551A
A596T
K595A

Table 5-1: Full-length TOP2B mutations in YEphTOP2BKLM analysed via complementation of S. cerevisiae

5.4 *In Vivo* Complementation Analysis

In this study, the six mutated human TOP2B proteins were analysed. All mutations were successfully transformed into the temperature-sensitive *S. cerevisiae* strain JN394t2-4. Prior to transformation, the strain JN394 cannot grow on media lacking uracil (Ura-) due to a mutation in the URA3 gene. However, the transformed plasmids contain a functional copy of this gene providing a selection mechanism for yeast transformed with TOP2B plasmids.

To determine whether the mutated proteins retained sufficient activity to carry out the essential roles of topoisomerase II *in vivo*, complementation was performed semi-quantitatively. Liquid cultures of transformed yeast are grown in selective Ura- media at 25 °C then diluted to an OD_{600} of 1.0 in sterile micro-titre plates. The cultures were then transferred to YPDA and Ura- plates using a replicator containing an array of cylindrically shaped prongs. The plates were then incubated at the permissive temperature (25 °C), the semi permissive temperature (30 °C) and the non-permissive temperature (35 °C). As the same number of yeast cells were transferred for each temperature, comparisons can be made between the different conditions. The level of expression of topoisomerase II proteins is influenced by the carbon source as they are under the control of a GAL1 promoter. Consequently, complementation was tested using three different carbon sources: glucose, raffinose and galactose.

In the presence of glucose, the GAL1 promoter is repressed such that only a low amount of topoisomerase II protein is produced. Whereas galactose activates the GAL1 promoter, inducing high levels of protein production. Raffinose on the other hand, produces intermediate effects as it neither represses nor induces expression from the GAL1 promoter. By contrast, yeast topoisomerase II expressed from the plasmid YEpDEDWOB10, is not under the control of the GAL1 promoter and is therefore not affected by the different carbon sources.

5.4.1 Complementation of Lysine to Alanine Mutations at Positions 515, 551 and 595

By identifying the lowest dilution at which the yeast could grow, an assessment of relative levels of growth were made. These results are shown in Figure 5-2 and Table 5-2. At 25 °C, all transformants grew on both YPDA and Ura- agar because at this temperature the endogenous yeast topoisomerase II enzyme is still functional. At 30 °C all transformants supported growth albeit to a reduced extent than the permissive temperature (25 °C). Whereas, at 35 °C the strain transformed with the control plasmid (YCp50) did not grow due to the absence of a functional plasmid-encoded topoisomerase II. At 25 °C transformed yeast grew well on complete media (YPDA) in the presence of all three types of sugars. Similarly, at 30 °C transformants grew well on glucose and raffinose. However, the presence of galactose at 30 °C reduced the amount of growth, which was further exaggerated at 35 °C. At these temperatures, galactose had a deleterious effect upon growth, because high levels of topoisomerase II expression is toxic to yeast cells. Whilst at 35 °C there was less growth in the presence of raffinose than glucose however this reduction in growth was far less than that observed with galactose. Yeast transformed with the *S. cerevisiae TOP2* gene (G1T2) under the control of a GAL1 promoter exhibited the greatest growth under all conditions tested. Complementation analysis carried out on selective Ura- media showed the same patterns of growth with the different carbon sources as observed with the complete media. However, generally the yeast transformants did not grow as well on Ura- media as on complete media because complementation on Ura- agar is more demanding due to the absence of uracil.

From the previous study (Leontiou, Watters et al. 2007) it was known that the drug-resistant mutations, H514Y, G550R, and A596T could complement *in vivo,* and the same result was observed in this study. The lysine residues adjacent to the drug-resistant mutations were mutated to an alanine residue to determine whether complementation was seen and whether these mutated proteins were drug-resistant. All the proteins where the lysine residue was mutated to alanine could complement and displayed a complementation profile better than wild type (Figure 5-2). Moreover, most mutations complemented similarly to the adjacent drug-resistant mutation. As a lysine residue has a positive charge and alanine is nonpolar, the fact that the mutations can complement suggests the charge on the lysine is not essential for function in yeast.

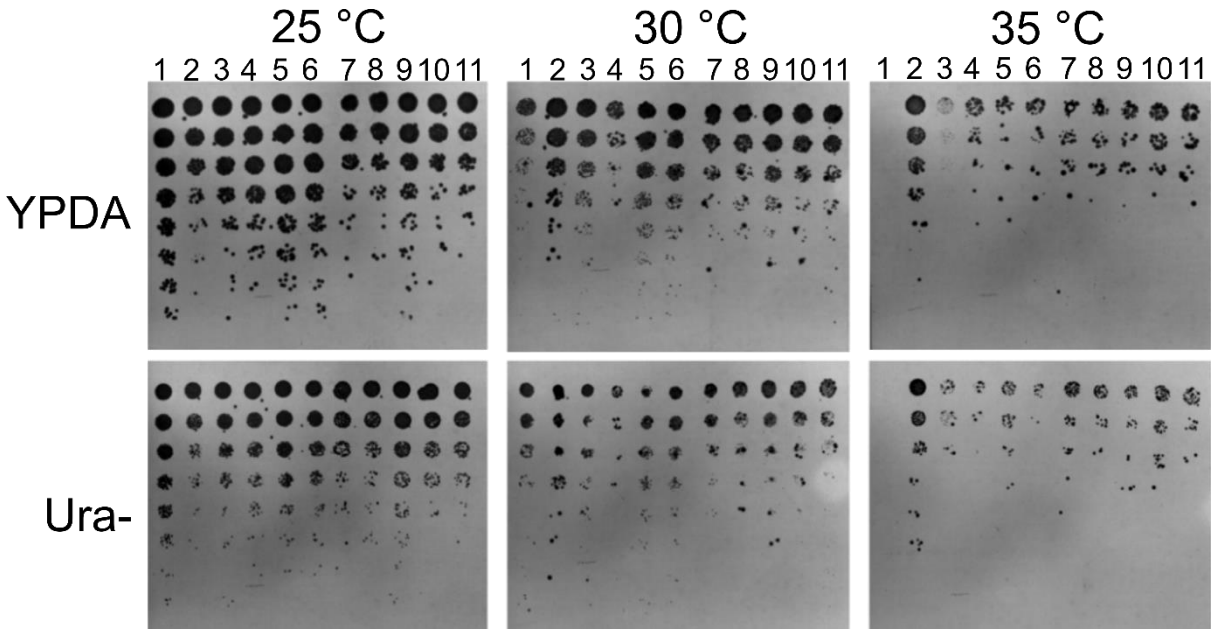

Figure 5-2: Complementation of S. cerevisiae TOP2 temperature-sensitive strain JN394t2-4 with plasmids bearing human TOP2B mutations on YPDA or Ura- media containing glucose

JN394t2-4 strain was transformed with (1) YCp50, (2) G1T2, (3) YCpDEDWOB10, (4) YEphTOP2βKLM, (5) YEpWOB6, (6-10) TOP2B mutations H514Y (6), K515A (7), G550R (8), K551A (9), A596T (10), K595A (11). The transformants were grown to an OD_{600} of 1.0 and serially diluted in a 96 well plate prior to transfer to either YPDA or Ura- agar with a replicator. Growth was tested at the permissive temperature (25 °C), semi-permissive temperature (30 °C) and the non-permissive temperature (35 °C). N = 1.

A

YPDA	25 °C			30 °C			35 °C		
Strain / Mutation	**Glu**	**Raf**	**Gal**	**Glu**	**Raf**	**Gal**	**Glu**	**Raf**	**Gal**
YCP50	++++++++	++++++++	++++++	++++	++	++	-	-	-
G1T2	+++++++	+++++	++++++	++++++	+++++++	+++	+++++	++++++	+
PDEDWOB10	++++++++	+++++++	++++++++	++++++	+++++	++++	++	+++	-
TOP2B	+++++++	+++++++	+++++	+++++	++++	+++	+++++	++	-
TOP2A	++++++++	++++++++	+++++++	++++++	++++++	++++	+++++	++++	
H514Y	++++++++	++++++++	++++++++	++++++	+++++	+++++	++++	++	-
K515A	+++++++	++++++	++++++	++++++	++++	++++	++++	++++	-
G550R	++++++	++++++	++++++++	+++++	++++	++++	++++	++++	-
K551A	++++++++	+++++++	++++++++	++++++	++++++	+++++	++++	+++	-
A596T	++++++	+++++	+++++	++++++	++++++	++++	++++	++++	-
K595A	+++++	+++++	++++++	+++++++	+++++	++++	++++	++++	-

B

Ura-	25 °C			30 °C			35 °C		
Strain / Mutation	**Glu**	**Raf**	**Gal**	**Glu**	**Raf**	**Gal**	**Glu**	**Raf**	**Gal**
YCP50	++++++++	++++++++	++++++++	++++	++++	+++++	-	-	-
G1T2	++++++	+++++	+++++	+++++++	++++++	+++	++++++	++++	+
PDEDWOB10	++++++	+++++	++++++++	+++++	+++++	+++++	+++	++	-
TOP2B	+++++++	++++++	+++++	++++	+++	+++	+++	++	-
TOP2A	+++++++	+++++++	++++++++	++++++	++++++	++++++	++++	+++	-
H514Y	+++++++	+++++++	++++++++	++++++	++++++	+++++	++	++	-
K515A	+++++	++++	++++++	+++++	++++	++++	+++++	++++	-
G550R	++++++	+++++	+++++	+++++	+++++	++++	+++	+++	-
K551A	++++++++	++++++	+++++++	++++++	++++	++++	++++	+++	-
A596T	+++++	++++++	++++++	+++++	++++	++++	++++	+++	-
K595A	++++++	++++	+++++	++++	++++	+++	+++	+++	-

*Table 5-2: Summary of the complementation analysis of temperature-sensitive S. cerevisiae strain by full-length human TOP2B mutations at 25 °C, 30 °C and 35 °C on YPDA (**A**) or Ura- media (**B**) (previous page)*

JN394t2-4 strain was transformed with Ycp50, G1T2, YCpDEDWOB10, YEphTOP2βKLM, YEpWOB6, TOP2B mutations H514Y, K515A, G550R, K551A, A596T, K595A. The transformants were grown to an OD_{600} of 1.0 and serially diluted in a 96 well plate prior to transfer to either YPDA (**A**) or Ura- (**B**) agar with a replicator. Growth was tested at the permissive temperature (25 °C), semi-permissive temperature (30 °C) and the non-permissive temperature (35 °C) on three different carbon sources: glucose, raffinose or galactose. Growth of transformants was scored by plus (+) or minus (-) symbols. No growth is indicated by a minus symbol and poor to very good growth is indicated by the number of plus symbols with ++++++++ being the maximal amount of growth.

5.4.2 Determination of Drug Sensitivity In Vivo

To test whether the human TOP2B lysine to alanine mutations were resistant to topoisomerase II targeting drugs *in vivo,* the yeast strain JN394t2-4 was used. The drug resistance properties of the mutated proteins to acridines and other topoisomerase II poisons including etoposide, ellipticine, and doxorubicin were tested and compared to wild type protein.

Sensitivity of the mutated proteins to the different drugs was assayed by performing complementation at 35 °C with continuous exposure to topoisomerase II poisons at a range of concentrations. At 35 °C, the plasmid-borne human TOP2B protein is the *in vivo* drug target because the endogenous yeast TOP2 is inactive at this temperature. Thus, the drug sensitivity of wild type and the mutated proteins can be compared. Transformed yeast were grown and diluted to an OD_{600} 1.0 and then transferred to YPDA agar containing the desired drug (mAMSA, mAMCA, AMCA, DACA, ellipticine, etoposide or doxorubicin). The concentration of solvent (DMSO) was kept constant at 1% for every drug concentration. Plates were incubated at 35 °C for 4 days and the levels of growth of different transformants was compared to the wild type enzyme for a direct comparison of sensitivities to cytotoxics. Transformed yeast were tested for drug resistance to a variety of topoisomerase II poisons to determine whether mutated proteins displayed cross-resistance. By utilising multiple different drugs, the potential mechanism of drug resistance can be elucidated. For example, if a residue involved in a conserved function of the enzyme is mutated, then the mutated protein will be cross resistant to a variety of drugs with distinct structures and mechanisms of action. Likewise, a mutation that causes the protein to be deficient in DNA cleavage would likely be cross resistant to most topoisomerase II poisons. Alternatively, if a mutation occurs in a specific drug binding site, the mutation would only cause resistance to the drug that binds within that region and would not provide resistance to drugs that bind at a distant site.

5.4.2.1 Effect of acridines on growth of yeast expressing wild type or mutated TOP2B proteins

The sensitivity of wild type human TOP2B to the acridines has been reported previously and the IC_{50} values are known (Turnbull, Meczes et al. 1999). IC_{50} is the concentration of drug necessary to inhibit the growth of a colony by 50% when compared to cells grown in the absence of drug. The lower the IC_{50} value, the more

potent a drug is. In terms of the acridines, mAMCA is the most potent against human TOP2B and DACA is the least potent acridine. Therefore, a higher concentration of drug was used for DACA (5 µg/mL – 100 µg/mL) whilst the concentration of the other acridines ranged between 1 µg/mL – 50 µg/mL.

5.4.2.1.1 mAMSA Resistance

JN394t2-4 cells transformed with the wild type and the mutated human TOP2B proteins were tested for growth on increasing concentrations of mAMSA at 35 °C (Table 5-3). JN394t2-4 transformed with the empty vector YCP50 was also included to provide a negative control. As expected, this strain did not grow since it does not express a functional topoisomerase II enzyme at the non-permissive temperature. Yeast cells transformed with wild type topoisomerase II were sensitive to 25 µg/mL mAMSA as demonstrated by the absence of growth. Similarly, H514Y which was previously selected for resistance to DACA was sensitive to mAMSA at 25 µg/mL and above. Interestingly, when the adjacent lysine residue was mutated to an alanine (K515A) resistance was observed at all concentrations of mAMSA tested up to 50 µg/mL. Likewise, the mutations A596T and K551A could also support growth of JN394 cells in the presence of 50 µg/mL mAMSA. Whereas the final lysine to alanine mutation (K595A) was sensitive to 25 µg/mL mAMSA. G550R which was previously selected for resistance to AMCA and DACA was more resistant to mAMSA compared to H514Y, as it could still complement at 25 µg/mL mAMSA.

5.4.2.1.2 AMCA Resistance

JN394t2-4 cells transformed with wild type and mutated human TOP2B proteins were tested for sensitivity on varying concentrations of AMCA at 35 °C (Table 5-3). Yeast cells transformed with wild type enzyme were sensitive to 25 µg/mL AMCA. Indeed, all mutations studied were also sensitive to 25 µg/mL AMCA despite G550R and A596T being previously selected for resistance to AMCA.

5.4.2.1.3 mAMCA resistance

JN394t2-4 cells transformed with wild type and mutated human TOP2B proteins were tested for growth on varying concentrations of mAMCA at 35 °C (Table 5-3). Yeast cells transformed with plasmid encoding wild type enzyme were sensitive to 10 µg/mL mAMCA and very little growth was observed at 5 µg/mL mAMCA. Similarly, all human TOP2B mutations studied could not support growth of JN394 cells in the presence of 10 µg/mL mAMCA. Although at 5 µg/mL mAMCA, K515A grew much better than the

other TOP2B plasmids. Perhaps if growth was tested in smaller increments of mAMCA concentrations between 5 and 10 µg/mL, K515A would display a stronger resistance profile compared to the other mutated human TOP2B proteins. mAMCA is the most potent acridine against human topoisomerase II so it is not surprising that all plasmids studied were sensitive to mAMCA at such low concentrations (10 µg/mL).

5.4.2.1.4 DACA Resistance

Lastly, JN394t2-4 cells transformed with wild type and mutated human TOP2B proteins were tested for growth with increasing concentrations of DACA at 35 °C (Table 5-3). However, the range of concentrations used (5-100 µg/mL) was not high enough to prevent growth of wild type and therefore the drug resistance phenotype could not be determined. Similarly, all TOP2B mutations studied were still able to grow in the presence of the highest concentration of DACA, 100 µg/mL. Therefore, none of the mutations caused hypersensitivity to this poison and the lysine to alanine mutations had no impact on the resistance profile to the acridine DACA.

	mAMSA Concentration (µg/mL)					AMCA Concentration (µg/mL)				mAMCA Concentration (µg/mL)				DACA Concentration (µg/mL)				
Strain / Mutation	**1**	**5**	**10**	**25**	**50**	**1**	**5**	**10**	**25**	**1**	**5**	**10**	**25**	**5**	**10**	**25**	**50**	**100**
YCp50	-	-	-	-	-	-	-	-	-	-	-	-	-	-	-	-	-	-
H514Y	+++	++	+	-	-	++	++	+	-	+++	+	-	-	+++	+++	+++	+++	++
K515A	+++	+++	+++	+++	++	++++	++++	+++	-	++++	++++	-	-	++++++	+++++	++++	+++	+++
G550R	++++	+++	+++	+	-	++++	+++	++	-	++	++	-	-	+++++	++++	++++	+++	+++
K551A	+++++	+++++	++++	++	+	++++	+++	+++	-	+++	++	-	-	++++	++++	++++	++++	++++
A596T	++++	+++	+++	+++	+	++++	++++	++++	-	+++	++	-	-	+++++	++++	++++	++++	++++
K595A	++++	+++	+++	-	-	++++	++++	+++	-	+++++	++	-	-	++++	+++	+++	+++	+++
TOP2B	++++	++++	+++	-	-	+++	+++	+++	-	++++	+	-	-	++++	+++	++++	++++	++++

Table 5-3: Summary of the drug sensitivity analysis of temperature-sensitive S. cerevisiae expressing full-length human TOP2B mutations in the presence of a range of acridines on YPDA media at 35 °C

JN394t2-4 strain was transformed with YCp50, TOP2B mutations H514Y, K515A, G550R, K551A, A596T, K595A, and wild type human TOP2B, YEphTOP2βKLM. Each of these transformants were tested for drug sensitivity to a range of acridines. The transformants were grown to an OD_{600} of 1.0 and serially diluted in a 96 well plate prior to transfer to YPDA agar. Growth was tested at the non-permissive temperature (35 °C) with glucose as the carbon source. Growth of transformants was scored by plus (+) or minus (-) symbols. No growth is indicated by a minus symbol and poor to very good growth is indicated by the number of plus symbols with +++++ being the maximal amount of growth. mAMSA was tested at the concentrations 1 µg/mL, 5 µg/mL, 10 µg/mL, 25 µg/mL and 50 µg/mL. AMCA 1 µg/mL, 5 µg/mL, 10 µg/mL and 25 µg/mL. mAMCA 1 µg/mL, 5 µg/mL, 10 µg/mL and 25 µg/mL. DACA 5 µg/mL, 10 µg/mL, 25 µg/mL, 50 µg/mL, 100 µg/mL. N = 1.

5.4.2.2 Effect of etoposide, ellipticine and doxorubicin on growth of yeast expressing wild type or mutated TOP2B proteins

Yeast transformed with wild type and mutated TOP2B plasmids were next tested for resistance to multiple different topoisomerase II poisons with diverse structures and mechanisms of action. Etoposide increases the amount of DNA cleavage within the cell by inhibiting the religation reaction of the enzyme (Huang, Hou et al. 1973, Singh and Gupta 1983, Fortune and Osheroff 2000, Montecucco, Zanetta et al. 2015). By contrast, ellipticine increases the forward rate of cleavage, without affecting the religation reaction (Froelich-Ammon, Patchan et al. 1995). Doxorubicin has a broad mechanism of action which involves poisoning topoisomerase II as well as DNA adduct formation, chromatin damage via histone eviction and oxidative stress (Tewey, Rowe et al. 1984, Davies and Doroshow 1986, Coldwell, Cutts et al. 2008, Forrest, Swift et al. 2012, Pang, Qiao et al. 2013).

5.4.2.2.1 Etoposide Resistance

JN394t2-4 cells transformed with wild type and mutated human TOP2B proteins were tested for growth in the presence of increasing concentrations of etoposide at 35 °C (Table 5-4). Yeast cells transformed with plasmid encoding wild type enzyme survived up to the highest concentration of etoposide used, 200 µg/mL. Additionally, all lysine to alanine mutations K515A, K551A, and K595A as well as A596T could support growth of JN394 cells in the presence of 200 µg/mL etoposide. Whereas the previously selected mutations H514Y and G550R were hypersensitive to etoposide with no growth observed at 100 µg/mL and 200 µg/mL etoposide respectively.

5.4.2.2.2 Ellipticine Resistance

JN394t2-4 cells transformed with wild type and mutated human TOP2B proteins were then tested for growth on varying concentrations of ellipticine at 35 °C (Table 5-4). However, the range of drug concentrations used (5-100 µg/mL) was not high enough to inhibit growth of the wild type enzyme. Therefore, the drug-resistant phenotype could not be determined. Similarly, all TOP2B mutations studied grew at the highest concentration of ellipticine tested (100 µg/mL). Although, H514Y, K551A, A596T and K595A grew to less of an extent than wild type.

5.4.2.2.3 Doxorubicin Resistance

Finally, drug sensitivity of the yeast transformants to doxorubicin was measured and is shown in Table 5-4. However, the range of concentrations used 5-50 µg/mL was not high enough to inhibit growth of the wild type enzyme. Similarly, all TOP2B mutations except H514Y grew at the highest concentration of doxorubicin, 50 µg/mL. Therefore, the lysine to alanine mutations did not cause hypersensitivity to this poison and had no impact on the resistance profile to doxorubicin.

	Etoposide Concentration (µg/mL)					Ellipticine Concentration (µg/mL)					Doxorubicin Concentration (µg/mL)			
Strain /Mutation	**10**	**25**	**50**	**100**	**200**	**5**	**10**	**25**	**50**	**100**	**5**	**10**	**25**	**50**
JN394 *t2-4*	-	-	-	-	-	-	-	-	-	-	-	-	-	-
H514Y	+++	+	+	-	-	++++	++	++	+	+	+++	+++	+	-
K515A	+++++	+++	+++	+	+	++++	++++	+++	+++	++	++++	+++	+++	+
G550R	+++	+++	++	+	-	++++	+++	+++	+++	++	+++++	+++++	++++	+
K551A	++++	+++	++	+	+	++++	++++	+++	+++	+	++++	++++	+++	+
A596T	++++	++++	++	++	++	++++	++++	++++	++++	+	++++	++++	++	++
K595A	+++	+++	++	+	+	+++++	++++	+++	+++	+	++++	++++	++	+
TOP2B	+++	++++	++	++	+	+++++	+++	+++	+++	++	++++	+++	++	+

Table 5-4: Summary of the drug sensitivity analysis of temperature-sensitive S. cerevisiae expressing full-length human TOP2B mutations in the presence of etoposide, ellipticine and doxorubicin on YPDA media at 35 °C

JN394t2-4 strain was transformed with YCp50, TOP2B mutations (H514Y, K515A, G550R, K551A, A596T, K595A), and wild type human TOP2B, YEphTOP2βKLM. Each of these transformants were tested for drug sensitivity to etoposide (10 µg/mL, 25 µg/mL, 50 µg/mL, 100 µg/mL, 200 µg/mL), ellipticine (5 µg/mL, 10 µg/mL, 25 µg/mL, 50 µg/mL, 100 µg/mL) and doxorubicin (5 µg/mL, 10 µg/mL, 25 µg/mL, 50 µg/mL). The transformants were grown to an OD_{600} of 1.0 and serially diluted in a 96 well plate prior to transfer to YPDA agar. Growth was tested at the non-permissive temperature (35 °C) with glucose as the carbon source. Growth of transformants was scored by plus (+) or minus (-) symbols. No growth is indicated by a minus symbol and poor to very good growth is indicated by the number of plus symbols with +++++ being the maximal amount of growth.

5.5 Discussion

Of the six human TOP2B mutations analysed, all were able to complement in a yeast TOP2 temperature-sensitive strain at the non-permissive temperature (35 °C). In fact, the lysine to alanine mutations at positions 515, 551 and 595 complemented to a greater extent than wild type TOP2B. Although, the experiments reported in this chapter are from only one replicate, three other experiments have been performed, one at 32 °C, one at 33 °C and one at 34 °C. While these temperatures are lower than the reported non-permissive temperature, growth of the JN395 strain transformed with YCp50 was still inhibited, whereas complementation of the mutated proteins was observed, thus complementation was seen a total of four times.

Despite possessing N-terminal truncations in the protein, where the first 44 amino acids are missing, the human TOP2B protein expressed from YEphTOP2βKLM is referred to here as wild type TOP2B. This region of the ATPase domain is also absent from the mutated proteins. The drug sensitivity of the mutated proteins was then tested by continuous exposure to topoisomerase II poisons at a range of concentrations.

5.5.1 K515A and H514Y

The mutation H514Y in TOP2B was selected for resistance to the acridine DACA and did not show cross resistance to any of the other topoisomerase II poisons studied (Leontiou, Watters et al. 2007). Immediately adjacent to position 514 is a lysine residue (K515) that can be frequently ubiquitinated. To understand whether posttranslational modification by ubiquitin is important for drug resistance, K515 was mutated to an alanine residue that cannot be modified with ubiquitin. Interestingly, the K515A mutation conferred resistance to mAMSA. Even at concentrations as high as 50 µg/mL growth of *S. cerevisiae* was observed. Whilst wild type TOP2B and H514Y became sensitive to mAMSA at 25 µg/mL. Consequently, the lysine to alanine mutation increased the drug resistance profile to mAMSA compared to H514Y. Likewise, yeast transformed with K515A grew to a much greater extent in the presence of 5 µg/mL of mAMCA when compared to H514Y and wild type TOP2B.

There is a crystal structure of human TOP2B bound to mAMSA available, that was obtained by soaking the mAMSA ligand into the original co-crystallised structure of the TOP2B core bound to etoposide (Wu, Li et al. 2013). From this structure, it is apparent that K515 is not within the drug binding site of mAMSA. Therefore, the K515A mutation

is unlikely to confer resistance by reducing direct interactions with mAMSA or by directly changing the drug binding site. However, soaking can sometimes be misleading because the ligand must bind within a pre-formed protein conformation. Whereas co-crystallisation with a ligand allows conformational changes in the protein to enable the ligand to bind within in native drug site.

In terms of the other drugs studied, there was no difference in the drug sensitivity of yeast transformed with K515A in the presence of AMCA, etoposide, ellipticine or doxorubicin when compared to wild type. However, there was slightly less growth of K515A in the presence of 100 µg/mL of DACA compared to wild type TOP2B.

5.5.2 K551A and G550R

G550R is a mutation in TOP2B that was selected with AMCA and DACA. When the adjacent lysine residue was mutated to an alanine (K551A), resistance to mAMSA was observed. Wild type TOP2B and G550R transformants became sensitive to mAMSA at 25 µg/mL and 50 µg/mL respectively whereas growth of yeast transformed with K551A was still observed at 50 µg/mL of mAMSA. Thus, the lysine to alanine mutation increased the drug resistance profile to mAMSA compared to G550R.

Like K515, K551 is not in the vicinity of the mAMSA drug binding site and instead is surface exposed pointing away from the bound DNA substrate (Wu, Li et al. 2013). Thus, K515A must confer resistance to mAMSA via a different mechanism. It is unlikely that the mutation K551A results in a topoisomerase II enzyme that is less active, as resistance to multiple different drugs would occur, which is not the case.

5.5.3 K595A and A596T

The TOP2B mutation A596T was selected with the acridines DACA and AMCA, but also displays cross resistance to mAMSA. However, mutating the adjacent lysine residue to an alanine (K595A) did not increase the resistance properties of the enzyme. In fact, the TOP2B K595A protein was sensitive to mAMSA at the same concentration as wild type TOP2B. Whereas yeast transformed with A596T were able to survive at the highest concentration of mAMSA studied, 50 µg/mL unlike K595A and wild type that couldn't grow at 25 µg/mL mAMSA. Additionally, yeast transformed with the mutated TOP2B plasmid K595A grew to a slighter lower extent than A596T in the presence of AMCA, etoposide and doxorubicin. Indeed, under no conditions was the growth of yeast transformed with K595A greater than A596T transformants. As such,

mutating position 595 appeared to have a negative impact on the drug-resistant properties of human TOP2B.

The residue K595 could not be observed in the TOP2B core structure because it is within a flexible region of the protein (Wu, Li et al. 2013). However, in contrast to the other lysine residues (K515 and K551), K595 is absolutely conserved in evolution, with the lysine residue being maintained even in prokaryotes, and position K595 can be SUMOlyated or ubiquitinated.

Chapter 6 *In Vivo* Analysis of Full-Length TOP2B (residues 46-1621) Containing Patient Mutations

6.1 Introduction

Patients have been identified with mutations in the human enzyme DNA TOP2B (Figure 6-1). Three of these mutations give rise to Hoffman syndrome which is an autosomal dominant B cell immunodeficiency where patients also have facial and limb abnormalities (Hoffman, Bastian et al. 2001, Hügle, Hoffman et al. 2011, Broderick, Yost et al. 2019). The first realisation that human TOP2B was involved in this human immunodeficiency syndrome came from whole genome sequencing. The patients all possessed a causative, heterozygous mutation in TOP2B (S483L, EE587E or G633S) (Broderick, Yost et al. 2019, Erdős, Lányi et al. 2021). Since this first report, another heterozygous mutation, A485P in TOP2B, has been identified that causes Hoffman syndrome in two independent families (Papapietro, Chandra et al. 2020). Three of the mutations are a *de novo* missense mutation (S483L, G633S, A485P) and the other mutation is a *de novo* in-frame deletion of TOP2B (EE587E). The novel TOP2B mutations cause reduced TOP2B function which underlies the syndromic B-cell immunodeficiency resulting in defects in B-cell development. These findings defined a new class of B cell immunodeficiency and were the first description of a monogenic syndrome due to mutations in human TOP2B. In addition, a biallelic causative, mutation in TOP2B (R503S and R510Q) has been identified in a patient with severe disabilities, though this patient does not appear to present with Hoffman syndrome. The patient cannot sit without support or hold their head upright and are fed exclusively through a G-tube. Both mutated copies of TOP2B were inherited from the parents; the parents are heterozygous for one mutation and appear unaffected. R503 is a conserved amino acid in the PLRGK motif in the TOPRIM domain of the enzyme (Figure 1-3).

Another two heterozygous mutations in TOP2B (K172R and L1146V) have been reported on the Genematcher database from two patients with unknown phenotypes (Sobreira, Schiettecatte et al. 2015). K172R and L1146V reside outside of the TOPRIM domain, K172R in the ATPase domain and L1146V in the C-gate of TOP2B respectively (Figure 6-1B). Currently, it is not understood how a mutation in TOP2B can give rise to the observed patient phenotypes, though it is likely that TOP2B's role

in transcriptional regulation may be part of the mechanism (Austin, Cowell et al. 2021, Khazeem, Casement et al. 2022).

The human TOP2B mutation R510Q, has been analysed *in vivo* and *in vitro* previously, the results of which showed R510Q retains catalytic activity (West, Meczes et al. 2000). Similarly, the mutation EE587E has been studied in a constitutive heterozygous knock-in murine model, where mice had a reduced number of mature B cells and were unable to produce antibodies in response to an antigen stimulus. In addition, the mutations EE587E, G633S and S483L were studied in a diploid *S. cerevisiae* model with the strain possessing one wild type and one mutated copy of topoisomerase II. A partial dominant negative phenotype was also observed, with nuclear extracts isolated from the heterozygous mutated strain decatenating kDNA less efficiently than the strain with only one wild type copy of topoisomerase II (Broderick, Yost et al. 2019). Although, other aspects of the catalytic cycle such as DNA cleavage or ATP hydrolysis have not been investigated. A485P has been expressed recombinantly from HEK293 cells and analysed *in vitro* where the DNA relaxation and decatenation activities were reduced more than 10-fold. Although its ability to complement an *S. cerevisiae* strain *in vivo* was not determined (Papapietro, Chandra et al. 2020). Patient mutations: K172R, R503S and L1146V have not been studied previously.

In this chapter, interest was primarily focused on how mutating these residues altered TOP2B function. The aim was to analyse the *in vivo* functionality of the mutated human TOP2B proteins using a yeast *TOP2 ts* complementation assay.

A

Human Topoisomerase II Beta Residue	Location of Mutation
K172R	GHKL (ATPase Domain)
S483L	TOPRIM (Breakage-Reunion Domain)
A485P	TOPRIM (Breakage-Reunion Domain)
R503S*	TOPRIM (Breakage-Reunion Domain)
R510Q*	TOPRIM (Breakage-Reunion Domain)
EE587E	TOPRIM (Breakage-Reunion Domain)
G633S	TOPRIM (Breakage-Reunion Domain)
L1146V	C-gate (Breakage-Reunion Domain)

B

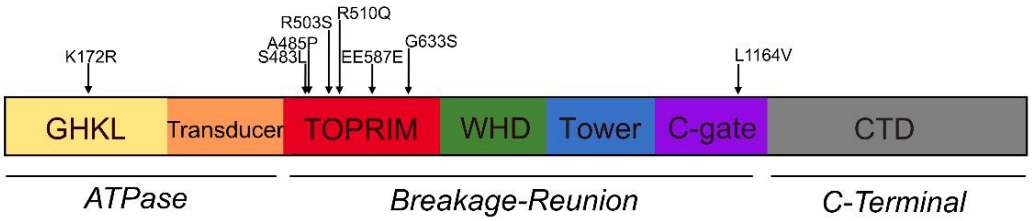

C

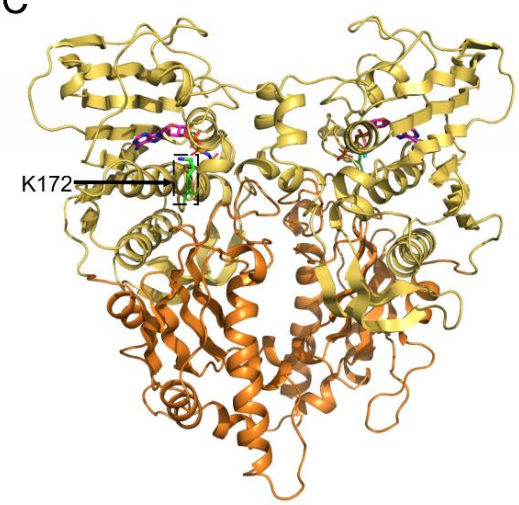

D

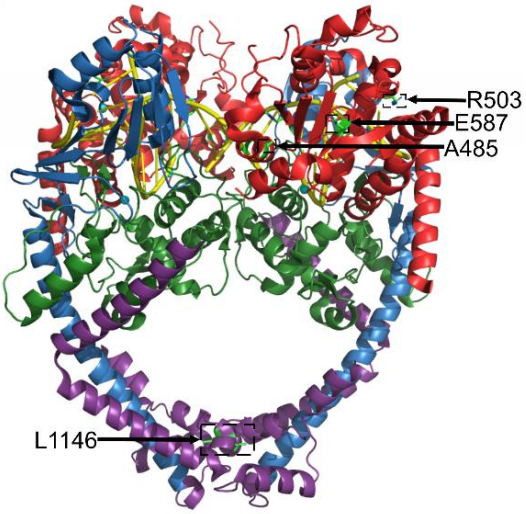

E

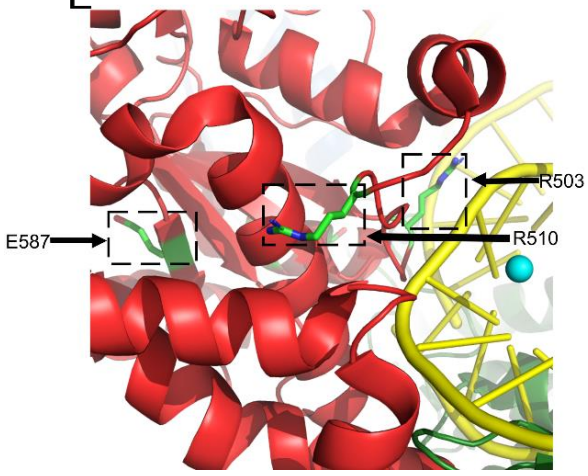

F

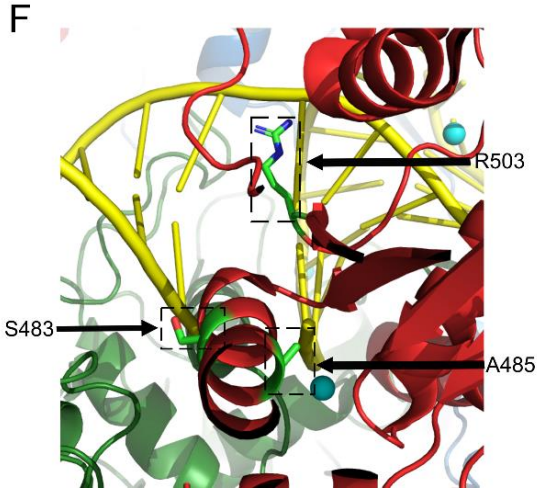

Figure 6-1: Location of reported patient mutations in TOP2B (previous page)

(**A**) Table listing the known patient mutations that result from either a *de novo* missense mutation or a *de novo* in-frame deletion mutation of TOP2B. Asterisk (*) indicates both these mutations are present in the same patient. (**B**) The reported patient mutations mapped onto a domain diagram of TOP2B. The majority of mutations affect highly conserved amino acids in the TOPRIM domain of the enzyme, although a mutation in the ATPase domain and a mutation in the C-gate of TOP2B have also been reported. (**C**) The location of the patient mutation, K172, highlighted on the solved crystal structure of the ATPase domain of human TOP2B (PDB code 7QFO, residues 46-429). GHKL domain coloured in yellow and transducer domain coloured in orange. AMPPNP coloured by atom, carbon pink, nitrogen blue, oxygen red. Side chain of K172 residue shown and coloured by atom, carbon green and nitrogen blue. (**D**) The locations of the patient mutations (A485, R503, EE587 and L1146) highlighted on the solved crystal structure of the breakage reunion domain of human TOP2B (PDB entry 5ZRF, residues 445–1201) coloured according to the line diagram in **A**. DNA in yellow and Mg^{2+} ions coloured cyan. Most of the mutations cluster around the G-DNA binding and cleavage site, although, the mutation L1146V is found at the C-gate where the T-DNA exits the enzyme. These positions in the enzyme are vital in catalysis and therefore the patient mutations are likely to impact topoisomerase function. Residue G633 could not be highlighted as this region of the protein is not defined in the crystal structure due to lack of electron density. (**E**) Side chains of residues R503, R510 and E587 are shown and coloured by atom, carbon green, nitrogen blue and oxygen red. DNA in yellow and Mg^{2+} ions coloured cyan. (**F**) Side chains of residues S483, A485 and R503 are shown and coloured by atom, carbon green, nitrogen blue and oxygen red. DNA in yellow and Mg^{2+} ions coloured cyan.

6.2 Introduction to *In Vivo* Complementation Analysis

To determine whether the mutated TOP2B proteins are functional *in vivo*, complementation analysis was performed as detailed in Chapter 5. The yeast strain JN394t2-4 exists in its haploid state, thus yeast transformed with the mutated topoisomerase II plasmids do not possess a wild type copy of human TOP2B, just a homodimer of the mutated TOP2B. In contrast, patients are heterozygous and possess one wild type *TOP2B* allele and one mutated *TOP2B* allele so can produce three forms of the enzyme: a heterodimeric enzyme (wild type and mutated), a homodimer of wild type and a homodimer of mutated TOP2B. Except for the patient that is heterozygous for R503S and R510Q. This is a limitation of using the haploid yeast model because only homodimers will be produced. Nevertheless, using a homozygous yeast model can be advantageous to gain a greater understanding of the function of the mutation without compensation occurring from a wild type copy.

6.3 Generation of mutated TOP2B plasmids for *In Vivo* Analysis

The mutations were introduced into the YEphTOP2BKLM plasmid containing the cDNA of human TOP2B. Mutagenesis was performed using the site directed mutagenesis kit from Agilent as per previously described (Chapter 2, Section 2.16). A forward and reverse oligonucleotide primer containing the desired mutation were annealed onto the template plasmid. PCR was performed to amplify the mutation into template followed by *DPNI* digestion to cleave the original non-mutagenised plasmid. The mutated plasmid was transformed and replicated in *E. coli* prior to plasmid isolation by a Qiagen mini prep. Plasmid DNA was sent for sequencing to determine whether the mutagenesis had been successful.

In order to study the site of the novel patient mutation R503S in more detail, the arginine residue was also mutated to an alanine (R503A), a lysine (R503K), and a glutamate (R503E) in addition to the serine (R503S). Table 6-1 lists the mutations which were successfully generated and assayed via the *in vivo* complementation assay.

Human TOP2B Mutation
K172R
S483L
A485P
R503S
R503A
R503E
R503K
R510Q
EE587E
G633S
L1146V

Table 6-1: Full-length human TOP2B mutations generated in YEphTOP2βKLM and analysed via complementation of S. cerevisiae

6.4 *In Vivo* Complementation Analysis

In this study, the eleven human TOP2B mutated proteins detailed in Table 6-1 were analysed. All mutations were successfully transformed into the *S. cerevisiae* strain JN394t2-4 to determine whether the mutated proteins retained sufficient activity to carry out the essential roles of topoisomerase II *in vivo*. It was expected that the patient mutations would complement because these patients survive despite having a compromised immune system and/or disabilities, indicating their TOP2B enzyme retains some catalytic activity.

6.4.1 Complementation of Mutated Proteins at Positions R503 and R510

The mutations R503S and R510Q complement at the non-permissive temperature on both YPDA and Ura- media with glucose or raffinose as the carbon source. R503S complemented to a similar extent to wild type whilst R510Q complemented extremely well and showed more growth at 35 °C than wild type (Figure 6-2). Similarly, R510Q was the only mutation that could grow on galactose at 35 °C (Table 6-2). Moreover, the lab-generated mutations R503A and R503K could complement whilst R503E could not. In R503E, the positively charged arginine has been replaced with a negatively charged glutamate, this change in amino acid properties could cause local repulsion in the protein structure, thus, it is not surprising that R503E could not complement as has previously been reported (West, Meczes et al. 2000). Whereas an arginine to lysine mutation maintains the positive charge and the branched methyl side chain, resulting in a topoisomerase that is still functional. In fact, R503K complements better than wild type. Although alanine doesn't maintain the positive charge, it doesn't provide a negative charge either because it is a non-polar amino acid. The lack of negative charge in the mutation R503A is presumably tolerated since R503A complemented albeit not as well as wild type. As expected, the plasmid encoding the yeast TOP2 (G1T2) complemented the greatest under all conditions.

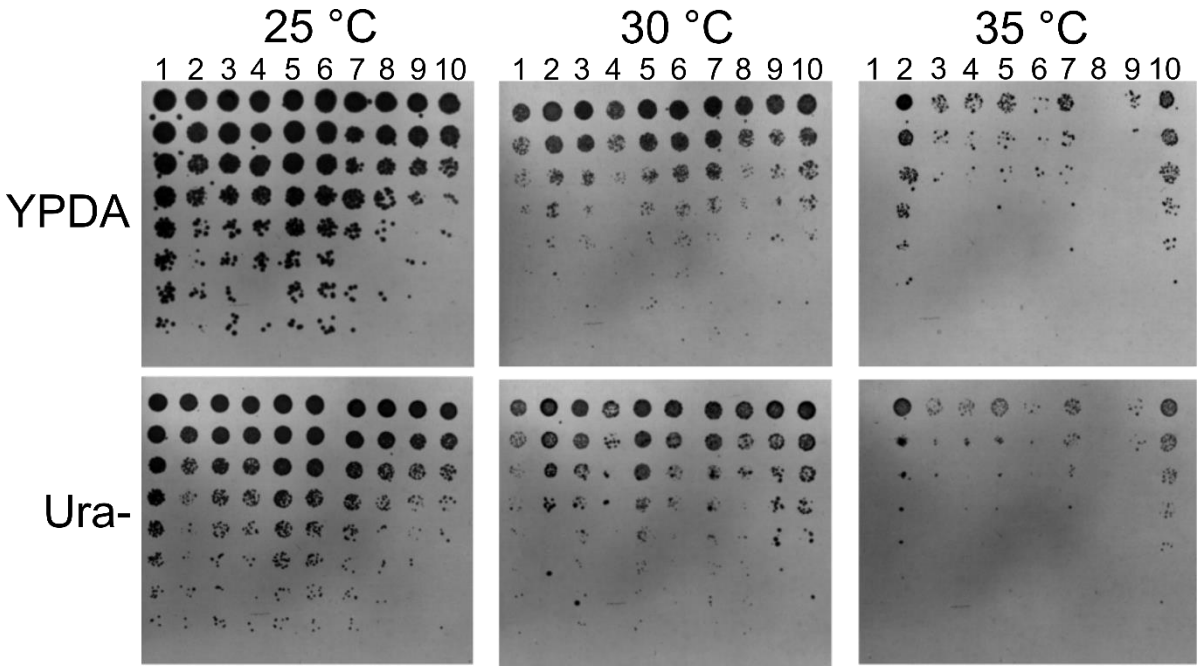

Figure 6-2: Complementation of S. cerevisiae TOP2 temperature-sensitive strain JN394t2-4 with plasmids bearing human TOP2B mutations on YPDA or Ura- media containing glucose

JN394t2-4 strain was transformed with (1) YCp50, (2) G1T2, (3) YCpDEDWOB10, (4) YEphTOP2βKLM, (5) YEpWOB6, (6-10) TOP2B mutations R503A (6), R503K (7), R503E (8), R503S (9), R510Q (10). The transformants were grown to an OD_{600} of 1.0 and serially diluted in a 96 well plate prior to transfer to either YPDA or Ura- agar with a replicator. Growth was tested at the permissive temperature (25 °C), semi-permissive temperature (30 °C) and the non-permissive temperature (35 °C). N = 1.

A.

YPDA	25 °C			30 °C			35 °C		
Strain / Mutation	Glu	Raf	Gal	Glu	Raf	Gal	Glu	Raf	Gal
YCP50	++++++++	+++++++	++++++	+++	++	+	-	-	-
G1T2	+++++++	+++++	++++	+++++	++++	++	++++++	++++	+
PDEDWOB10	++++++++	+++++	++++	++++	++++	++++	+++	+	-
TOP2B	++++++	++++++	+++++	+++	++	+	++	+	-
TOP2A	++++++++	+++++++	++++++	+++++	++++	+++	+++	+	-
R503A	++++++++	++++++++	+++++	++++	++++	+++	++	-	-
R503K	+++++	++++++	++++	++++	+++	+++	+++	++	-
R503E	+++++	++++	+++	+++	+++	++	-	-	-
R503S	++++	++++	++++	+++++	++	++	++	+	-
R510Q	++++	++++	+++	+++++	+++	++	++++++	+++	+

B.

Ura-	25 °C			30 °C			35 °C		
Strain / Mutation	Glu	Raf	Gal	Glu	Raf	Gal	Glu	Raf	Gal
YCP50	++++++++	++++++++	+++++++	++++	++++	++	-	-	-
G1T2	++++++++	+++++	+++++	++++	+++	+++++	++++++	++++	-
PDEDWOB10	++++++++	++++++	++++++	+++++	+++++	+++	+++	+	-
TOP2B	++++++	+++++	+++++	++++	++	++	++	++	-
TOP2A	++++++++	+++++++	+++++++	++++++	++++++	+++	++++	++	-
R503A	++++++++	++++++++	++++++++	++++	+++	+++	++	+	-
R503K	++++++++	+++++++	+++++++	+++++	+++++	++	++++	+++	-
R503E	+++++++	+++++	+++++	+++	+++	++	-	-	-
R503S	++++++	++++	++++	+++++	+++	+++	++	+	-
R510Q	+++++	+++++	++++	+++++	++++	+++	+++++	+++	-

*Table 6-2: Summary of the complementation analysis of temperature-sensitive S. cerevisiae strain by mutated full-length human TOP2B at 25 °C, 30 °C and 35 °C on YPDA (**A**) or Ura- media (**B**) (previous page)*

JN394 strain was transformed with YCp50, G1T2, YCpDEDWOB10, YEphTOP2βKLM, YEpWOB6, mutated TOP2B R503A, R503K, R503E, R503S, R510Q. The transformants were grown to an OD_{600} of 1.0 and serially diluted in a 96 well plate prior to transfer to either YPDA (**A**) or Ura- (**B**) agar with a replicator. Growth was tested at the permissive temperature (25 °C), semi-permissive temperature (30 °C) and the non-permissive temperature (35 °C) on three different carbon sources: glucose, raffinose or galactose. Growth of transformants was scored by plus (+) or minus (-) symbols. No growth is indicated by a minus symbol and poor to very good growth is indicated by the number of plus symbols with ++++++++ being the maximal amount of growth.

6.4.3 Complementation of Mutated Proteins That Cause Hoffman Syndrome

The ability of the Hoffman mutations to complement the temperature-sensitive JN394t2-4 strain was tested. Interestingly, there were differences in the complementation abilities of the four Hoffman mutations. A485P and EE587E could complement at the non-permissive temperature on both YPDA and Ura- media whilst S483L and G633S could not complement at all (Figure 6-3). A485P and EE587E could complement on the carbon sources glucose or raffinose, but like wild type TOP2B no growth was observed on galactose plates (Table 6-3). Even though all four mutations are in TOP2B and are causative for Hoffman syndrome, the different patients have varying phenotypes (Hügle, Hoffman et al. 2011). Thus, some mutations will be more detrimental to TOP2B function than others which could explain why some mutations can complement and others can't. In a previous study it was found that S483L, EE587E, and G633S could not complement at the non-permissive temperature (Broderick, Yost et al. 2019). Similarly in this study, S483L and G633S could not complement however, EE587E could weakly. One likely explanation for this difference is that complementation was tested at 35 °C here and at 37 °C in the previous study. At 35 °C, EE587E may retain enough activity to be functional whereas increasing the temperature by 2 °C could be enough to make the protein inactive. The mutation S483L will result in a different local charge as serine is a polar amino acid whilst leucine is nonpolar. As such, interactions between DNA and topoisomerase II could be disrupted, or aggregation could occur giving rise to an inactive topoisomerase enzyme. Likewise, the local environment at position G633 will be altered in the G633S mutated protein because glycine is non-polar, and serine is polar. The Hoffman mutation, A485P had not been studied previously *in vivo* but results from this study show that A485P could complement. The non-polar properties of alanine are maintained in the A485P mutation as proline is also non-polar, which could explain why A485P can complement *in vivo.*

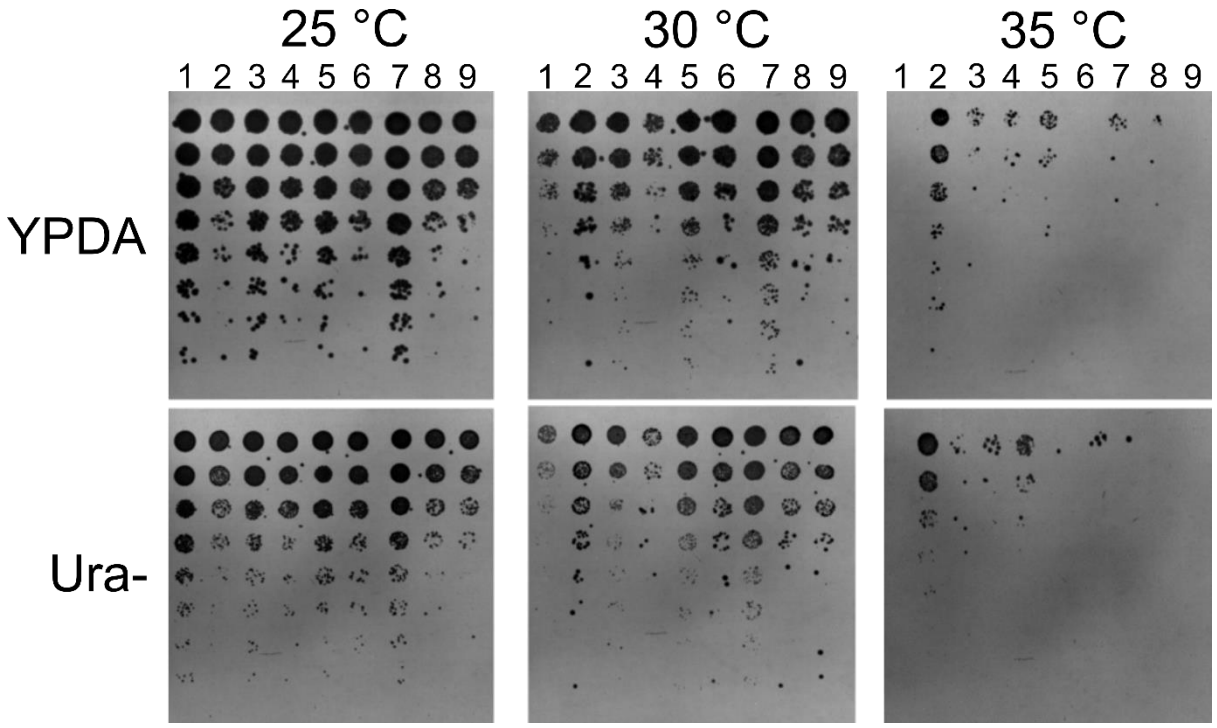

Figure 6-3: Complementation of S. cerevisiae TOP2 temperature-sensitive strain JN394t2-4 with plasmids bearing human TOP2B mutations on YPDA or Ura- media containing glucose

JN394t2-4 strain was transformed with (1) YCp50, (2) G1T2, (3) YCpDEDWOB10, (4) YEphTOP2βKLM, (5) YEpWOB6, (6-10) TOP2B mutations S483L (6), A485P (7), EE587E (8), G633S (9). The transformants were grown to an OD_{600} of 1.0 and serially diluted in a 96 well plate prior to transfer to either YPDA or Ura- agar with a replicator. Growth was tested at the permissive temperature (25 °C), semi-permissive temperature (30 °C) and the non-permissive temperature (35 °C). N = 1.

A.

YPDA	25 °C			30 °C			35 °C		
Strain / Mutation	Glu	Raf	Gal	Glu	Raf	Gal	Glu	Raf	Gal
YCP50	++++++++	++++++++	++++++++	+++	+++	++	-	-	-
G1T2	++++++++	++++++	+++++++	++++++	++++	++++	+++++++	+++++	+
PDEDWOB10	++++++++	++++++++	++++++++	+++++	+++++	++++	+++	++	-
TOP2B	+++++++	+++++++	++++++++	++++	+++	++	+++	++	-
TOP2A	++++++++	+++++++	++++++++	++++++++	+++++++	++++	+++	+++	-
S483L	++++++	+++++++	++++	++++++	++++	++++	-	-	-
A485P	++++++++	++++++++	++++++++	++++++++	++++++++	+++++	+++	++	-
EE587E	++++++	++++++	+++++	++++++	++++	++++	+++	+	-
G633S	+++++	+++++	+++++	+++++	++++	+++	-	-	-

B.

Ura-	25 °C			30 °C			35 °C		
Strain / Mutation	Glu	Raf	Gal	Glu	Raf	Gal	Glu	Raf	Gal
YCP50	++++++++	+++++++	+++++++	+++	+++	++	-	-	-
G1T2	+++++	++++	++++++	++++++	+++	+++++	++++	++++	+
PDEDWOB10	++++++++	++++++	++++++++	++++++	++++	+++	+++	+	-
TOP2B	++++++	+++++	++++++	++++	++	++	++	+	-
TOP2A	++++++	++++++	++++++	++++++	++++	+++	+++	+++	-
S483L	++++++	++++++	++++	+++++	++++	+++	-	-	-
A485P	++++++++	+++++++	++++++	++++++	+++++	+++	+	++	-
EE587E	++++	+++++	++++	+++++	+++	+++	+	-	-
G633S	++++	+++++	++++	++++	+++	+++	-	-	-

*Table 6-3: Summary of the complementation analysis of temperature-sensitive S. cerevisiae strain by full-length human TOP2B mutations at 25 °C, 30 °C and 35 °C on YPDA (**A**) or Ura- media (**B**) (previous page)*

JN394t2-4 strain was transformed with YCp50, G1T2, YCpDEDWOB10, YEphTOP2βKLM, YEpWOB6, TOP2B mutations S48L, A485P, EE587E, G633S. The transformants were grown to an OD_{600} of 1.0 and serially diluted in a 96 well plate prior to transfer to either YPDA (**A**) or Ura- (**B**) agar with a replicator. Growth was tested at the permissive temperature (25 °C), semi-permissive temperature (30 °C) and the non-permissive temperature (35 °C) on three different carbon sources: glucose, raffinose or galactose. Growth of transformants was scored by plus (+) or minus (-) symbols. No growth is indicated by a minus symbol and poor to very good growth is indicated by the number of plus symbols with ++++++++ being the maximal amount of growth.

6.4.4 Complementation of the Mutated Proteins at positions K172 and L1146

The patient mutations K172R and L1146V, reported on Genematcher that give rise to an unknown phenotype were tested for functional topoisomerase II activity *in vivo*. Both mutations could complement on both YPDA and Ura- media at the non-permissive temperature (Figure 6-4). No growth was observed on galactose-containing plates because high levels of topoisomerase II expression induced by galactose is toxic to the yeast cells (Table 6-4). Both K172R and L1146V mutations result in conservative differences in the amino acid side chains which could explain why the mutated TOP2B is still functional. Additionally, it is not yet known whether these mutations are causative for the observed patient phenotype, but from this study the mutations result in a functional topoisomerase II *in vivo.* Both the K172R and L1146V mutations complement better than the known causative mutation R503S but not as well as the other causative patient mutation R510Q.

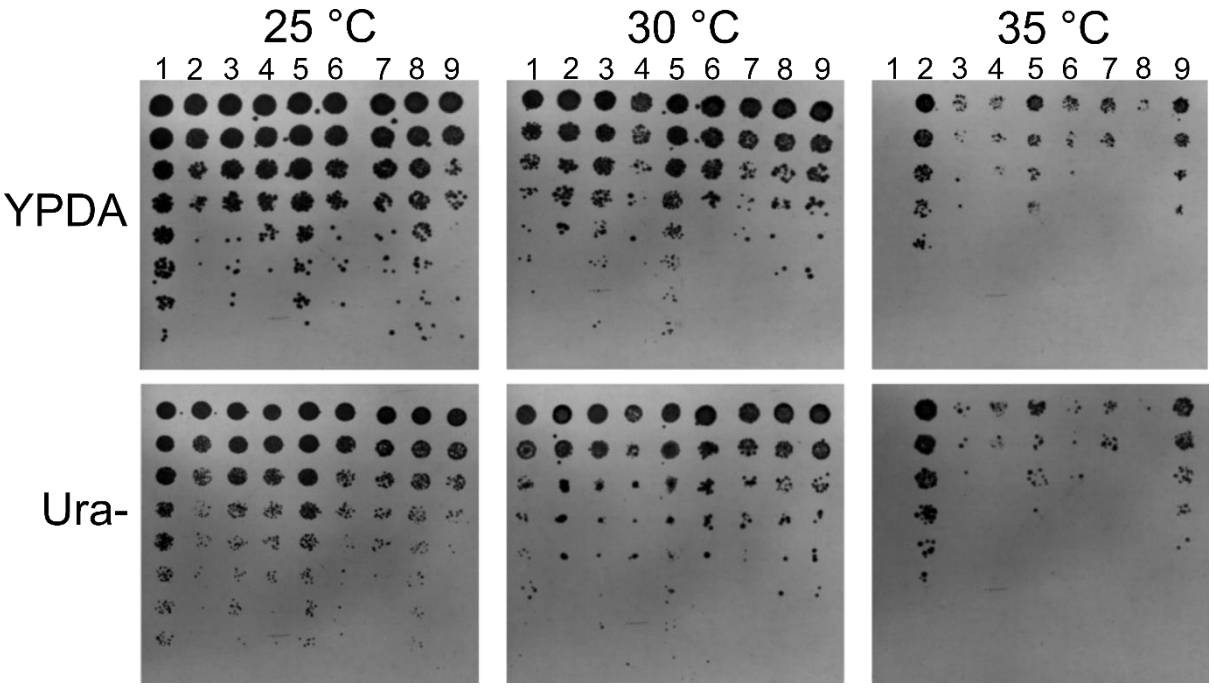

Figure 6-4: Complementation of S. cerevisiae TOP2 temperature-sensitive strain JN394t2-4 with plasmids bearing human TOP2B mutations on YPDA or Ura- media containing glucose

JN394t2-4 strain was transformed with (1) YCp50, (2) G1T2, (3) YCpDEDWOB10, (4) YEphTOP2βKLM, (5) YEpWOB6, (6-10) TOP2B mutations K172R (6), L1146V (7), R503S (8), R510Q (9). The transformants were grown to an OD_{600} of 1.0 and serially diluted in a 96 well plate prior to transfer to either YPDA or Ura- agar with a replicator. Growth was tested at the permissive temperature (25 °C), semi-permissive temperature (30 °C) and the non-permissive temperature (35 °C). N = 1.

A.

YPDA	25 °C			30 °C			35 °C		
Strain / Mutation	Glu	Raf	Gal	Glu	Raf	Gal	Glu	Raf	Gal
YCP50	++++++++	++++++++	+++++	++++++	++++	++++	-	-	-
G1T2	++++++	+++++	+++++	+++++	++++++	++++	+++++	++++++	+
PDEDWOB10	+++++++	++++++++	+++++++	++++++++	+++++	++++++	++++	++	-
TOP2B	++++++	+++++++	+++++	+++++	++++	++++	+++	++	-
TOP2A	++++++++	++++++++	+++++++	++++++++	++++++	++++++++	++++	+++	-
K172R	+++++++	+++++	+++	++++	++++++	++++++	+++	+++	-
L1146V	++++++++	++++++	++++++	+++++	+++++	+++++	++	++	-
R503S	++++++++	++++++++	++++++	++++++	++++	+++++	+	+	-
R510Q	++++	+++++	++++	++++++	++++	+++++	++++	+++++	-

B.

Ura-	25 °C			30 °C			35 °C		
Strain / Mutation	Glu	Raf	Gal	Glu	Raf	Gal	Glu	Raf	Gal
YCP50	++++++++	++++++++	++++++++	++++++	++++	++++	-	-	-
G1T2	+++++++	+++++	++++++	+++++	+++++++	+++	++++++	++++++	+
PDEDWOB10	+++++++	++++++++	+++++++	+++++	+++++	+++++++	+++	++	-
TOP2B	++++++	++++++	++++++	+++++	++++	+++	++	+++	-
TOP2A	++++++++	+++++++	++++++++	++++++	+++++	+++++	++++	+++	-
K172R	+++++	++++++	+++++	+++++	++++	+++	+++	++++	-
L1146V	+++++	++++	+++++	++++	++++	+++	++	+++	-
R503S	++++++++	++++++	+++++++	++++++	+++++	++	+	+	-
R510Q	++++	+++++	+++++	++++++	+++++	+++++	+++++	+++++	-

*Table 6-4: Summary of the complementation analysis of temperature-sensitive S. cerevisiae strain by full-length human TOP2B mutations at 25 °C, 30 °C and 35 °C on YPDA (**A**) or Ura- media (**B**) (previous page)*

JN394t2-4 strain was transformed with YCp50, G1T2, YCpDEDWOB10, YEphTOP2βKLM, YEpWOB6, mutated TOP2B K172R, L1146V, R503S, R510Q. The transformants were grown to an OD_{600} of 1.0 and serially diluted in a 96 well plate prior to transfer to either YPDA (**A**) or Ura- (**B**) agar with a replicator. Growth was tested at the permissive temperature (25 °C), semi-permissive temperature (30 °C) and the non-permissive temperature (35 °C) on three different carbon sources: glucose, raffinose or galactose. Growth of transformants was scored by plus (+) or minus (-) symbols. No growth is indicated by a minus symbol and poor to very good growth is indicated by the number of plus symbols with ++++++++ being the maximal amount of growth.

6.5 Discussion

Of the eleven mutated human TOP2B proteins analysed, eight were able to complement in a yeast *TOP2* temperature-sensitive strain at the non-permissive temperature (35 °C). They were: R503A, R503K, R503S, R510Q, A485P, EE587E, K172R, L1146V. Although, the experiments reported in this chapter were only from one replicate, one other experiment has been performed at 34 °C, thus complementation was seen a total of two times. While this temperature is lower than the reported non-permissive temperature, growth of the JN395 strain transformed with YCp50 was still inhibited, whereas complementation of the mutated proteins was observed.

6.5.1 R503 and R510

R503S and R510Q are biallelic mutations in human TOP2B found within a patient with severe disabilities. Both mutations are located within the conserved TOPRIM domain of human TOP2B which is necessary for divalent metal ion binding. In addition, the TOPRIM domain communicates signals between the ATPase domain and the rest of the protein which include conformational changes to correctly position the DNA breakage reunion core for catalysis (Vanden Broeck, Lotz et al. 2021). The TOP2B mutation R510Q has been studied previously (West, Meczes et al. 2000), where the results showed that mutating arginine at position 510 to a glutamine residue could rescue the growth of temperature-sensitive yeast strain (JN394t2-4). Whilst position R503 has been mutated to a glutamate residue and studied before (West, Meczes et al. 2000), R503E did not retain sufficient topoisomerase II activity to complement JN394t2-4 at the non-permissive temperature. Therefore, to understand the function of the patient mutation, R503S, on topoisomerase II activity *in vivo,* this mutation was generated in the YEphTOP2βKLM plasmid. Moreover, to study position 503 in greater detail, arginine was mutated to a lysine residue (R503K) and an alanine residue (R503A), then complementation was performed with the mutated plasmids at the non-permissive temperature.

The results above showed that the patient mutation R503S was able to complement at the non-permissive temperature, 35 °C, albeit to a reduced extent than wild type TOP2B (Figure 6-2). Serine is tolerated at position 503 which is located within the highly conserved PL**R**GK motif. Serine is a polar amino acid with an uncharged side

chain, whereas arginine has a positively charged side chain. Indeed, when R503 was mutated to a lysine residue (R503K) which is a more conservative amino acid substitution, complementation of JN394t2-4 was more robust. In fact, yeast transformed with the R503K mutated plasmid grew better than transformants with wild type TOP2B. The lysine side chain maintains the positive charge and interestingly a lysine residue naturally occurs at the equivalent position in *E. coli* GyrB and parE, demonstrating that a lysine at the position equivalent to 503 can perform the function of a type II topoisomerase in prokaryotes. By contrast, when arginine was mutated to a glutamic acid (R503E), growth of *S. cerevisiae* at the non-permissive temperature was not observed. Mutating an arginine residue to a glutamic acid is a dramatic amino acid substitution where a basic residue is replaced with an acidic residue. The opposite charge could disrupt this region of the protein and will likely interfere with hydrogen bonding explaining why R503E didn't complement in this study or the previous one (West, Meczes et al. 2000). Moreover, the fact that a mutation at position 503 can abolish topoisomerase activity suggests this residue is important for type II topoisomerase function and only conservative amino acid changes can be tolerated.

The second patient mutation, R510Q, was able to complement the JN394t2-4 strain at the non-permissive temperature extremely well. In fact, R510Q was the only TOP2B protein that could complement on galactose containing media at 35 °C. It was expected that the patient mutations would be functional and support growth in the *in vivo* complementation assay as the patient is alive. Whereas when TOP2B is inactivated in mice, perinatal death results due to diaphragm innervation defects (Yang, Li et al. 2000). Consequently, a functional TOP2B enzyme is essential for differentiation and neural function in higher organisms. However, a limitation of using *S. cerevisiae* to study mutations in the human TOP2B isoform is that *S. cerevisiae* only has one type II topoisomerase enzyme whereas human cells have two; TOP2A and TOP2B. Hence, the results described above cannot necessarily be extended to higher eukaryotes and studying these mutations in a mammalian system will be of value.

6.5.2 Hoffman Syndrome Mutations (S483L, A485P, EE587E, G633S)

Four mutations in human TOP2B have been identified that cause Hoffman syndrome. Patients have defects in B-cell development as well as facial and limb abnormalities. Three of the mutations result in a *de novo* missense mutation (S483L, A485P and G633S) and one causes a *de novo* in-frame deletion of residue E587 (EE587E). All patients are heterozygous so possess one wild type copy of TOP2B in addition to the mutated copy.

Two out of the four Hoffman mutations were able to complement the *S. cerevisiae* strain at the non-permissive temperature. They were A485P, which complemented to a similar extent to wild type TOP2B, and EE587E that complemented much less than wild type. An alanine to proline substitution is unique as proline has an unusual structure that is not comparable to alanine. Moreover, proline residues are generally associated with reverse turns whereas A485 is located within an alpha helix (Marcelino and Gierasch 2008, Wu, Li et al. 2011). However, alanine at position 485 is not entirely conserved in evolution, with the equivalent residue being a glycine in prokaryotes. Thus, it appears that residue A485 is not essential for topoisomerase II function in yeast and a proline substitution can be tolerated. Similarly, deletion of one of the glutamate residues at position 587 was able to support very low levels of growth at 35 °C, the non-permissive temperature. The in-frame deletion was not significantly dramatic to entirely abolish the activity of the topoisomerase II protein in *S. cerevisiae,* although there was a reduction in the complementation efficiency compared to wild type TOP2B. Glutamate residues are negatively charged and frequently form salt-bridges within proteins. Hence, deletion of a glutamate could destabilise the topoisomerase II protein. However, because human TOP2B contains two consecutive glutamate residues (E587 and E588), when E587 is deleted in the patient, a glutamate remains in the protein vicinity which could still provide a salt-bridge if necessary. Moreover, *S. cerevisiae* only contains one glutamate residue, at the equivalent position in yeast there is a leucine (Figure 1-3), suggesting one glutamate is sufficient for topoisomerase II activity in yeast. When the level of expression of A485P and EE587E was increased by induction of the GAL1 promoter, the growth of transformants decreased at the non-permissive temperature. This result has been reported previously for wild type TOP2B (West, Meczes et al. 2000) and is consistent with the concept that over expression of TOP2B is toxic in yeast cells. Moreover, it

suggests that the inability of some mutated proteins to complement may not result from there being a lower amount of topoisomerase II activity, as when the expressed protein levels were increased with galactose cell growth was still not observed.

It is interesting that the remaining two Hoffman mutations, S483L and G633S, could not complement on either YPDA or Ura- media. This suggests that as homodimers, these mutated proteins do not retain enough activity to support the growth of yeast cells and that positions 483 and 633 perform an important function for activity of the human TOP2B protein in yeast cells. Perhaps if the proteins were expressed as heterodimers with wild type TOP2B, as is the case in their physiological setting, they could rescue the temperature-sensitive phenotype due to the presence of one wild type copy of human TOP2B. Both mutations result in a dramatic change in amino acid properties, serine is a polar amino acid and S483 is in close proximity to the DNA substrate (Wu, Li et al. 2011), likely forming a hydrogen bond to the DNA via the hydroxyl group in its side chain. Whilst leucine is a non-polar amino acid that would be unable to hydrogen bond with DNA and could cause aggregation within the protein due to its hydrophobic side chain. Likewise, glycine residues are non-polar amino acids, therefore in the G633S mutation the residue changes from being non-polar to polar (serine). Moreover, the glycine residue at position 633 is absolutely conserved in evolution with prokaryotes possessing a glycine at the equivalent position. Thus, it is likely that this glycine performs an important function in type II topoisomerases and a G633S homodimer does not retain functional topoisomerase activity *in vivo.*

Altogether, the Hoffman mutations complemented to varying extents with some proteins completely inactive *in vivo.* Similarly, the patients exhibit varying phenotypes (Hoffman, Bastian et al. 2001, Hügle, Hoffman et al. 2011, Broderick, Yost et al. 2019). Thus, some TOP2B mutations are more detrimental than others, and may impact functions other than catalysis. For example, the mutations could alter protein-protein interactions with TOP2B and thus modify cellular processes such as transcription.

6.5.3 TOP2B Mutations Outside of the TOPRIM Domain

Another two heterozygous mutations in human TOP2B (K172R and L1146V) have been identified in two patients with unknown phenotypes. The mutations are listed on

the Genematcher database, though it is yet to be determined whether the TOP2B mutations are causative. Both mutations reside in a different region of the protein compared to the Hoffman syndrome and the R503/R510Q mutations. K172R is found within the ATPase domain of human TOP2B and L1146V is located in the C-gate of the DNA breakage reunion core.

The residue K172 is within the GHKL domain of the ATPase domain, which is responsible for nucleotide binding and hydrolysis. The patient mutation K172R was able to complement the yeast system to a similar extent to wild type TOP2B. This is not surprising since an arginine to lysine mutation is a conservative amino acid substitution. Both residues have a branched, positively charged side chain which does not significantly reduce topoisomerase activity *in vivo.* Indeed, the K172R mutation retained ATP hydrolysis activity as reported in Chapter 3, Section 3.8. Likewise, L1146V had comparable complementation activity compared to wild type TOP2B. The mutation L1146V is another conservative substitution, where the non-polar leucine residue is replaced with a slightly smaller, non-polar valine residue. The hydrophobic properties of a leucine residue are maintained within this change, though the side chain of valine is shorter, lacking a methyl group. Position 1146 is at the C-terminus of the breakage reunion core which constitutes the primary dimer interface that holds the individual topoisomerase II monomers together until T-DNA is ready to exit the enzyme. L1146 is not involved in the catalytic mechanism and instead performs a structural function that can be equally achieved with a valine residue.

As both mutations could rescue the temperature-sensitive phenotype in *S. cerevisiae* it suggests that these specific residues are not essential for topoisomerase II function in yeast and the mutated homodimer proteins retain enough catalytic activity to support the growth of yeast cells.

Chapter 7 *In Vitro* Analysis of Mutated Full-Length TOP2B Proteins (residues 46-1621)

7.1 Introduction

A subset of the human TOP2B mutated proteins analysed via the complementation assay (Chapter 6) were taken forward for expression and determination of their catalytic activity *in vitro.* The proteins which were expressed and purified for *in vitro* analysis included A485P, R503S, R510Q, and EE587E. A485P and EE587E are mutations identified in patients with Hoffman syndrome (Broderick, Yost et al. 2019), and retain *in vivo* activity by rescuing the temperature-sensitive phenotype of *S. cerevisiae,* JN394t2-4. Whilst the TOP2B mutations R503S and R510Q are biallelic, found within the same patient on different alleles, this patient does not possess a wild type copy of TOP2B. In this chapter, an additional mutated plasmid was generated that encodes TOP2B with both R503S and R510Q mutations within the same plasmid to understand the impact of both mutations together as would be the situation in the patient. This chapter details the expression and purification of the mutated proteins to elucidate whether the TOP2B protein containing these mutations are functional *in vitro*.

Strand passage activity of type II topoisomerases was studied using relaxation and decatenation assays. Relaxation and decatenation assays assess the full catalytic cycle of type II topoisomerases, requiring both functional ATP hydrolysis activity and cleavage-religation activity. In relaxation assays supercoiled plasmid DNA is the substrate, and in the presence of an active type II topoisomerase, supercoiled DNA is is converted to relaxed DNA products through a series of intermediates that have decreasing levels of supercoiling. The reaction is visualised on an agarose gel as supercoiled plasmid molecules migrate through the gel faster than relaxed products, due to their more compact structure. (Figure 7-1A). Whilst catenated kinetoplast DNA (kDNA) is the substrate used in decatenation assays and is purified from the mitochondria of trypanosomes (Figure 7-1B). kDNA consists of a network of minicircles (2.5 kb) and maxicircles (37 kb) that are catenated together to form a large, interlinked substrate. In the presence of a functional topoisomerase II, the minicircles are unlinked allowing them to migrate into the agarose gel due to their smaller size. Whereas the catenated kDNA substrate is too large to enter the gel and remains as a visible band in the wells. The DNA cleavage activity of the mutated proteins was then

investigated using an oligonucleotide substrate in the presence and absence of topoisomerase II poisons.

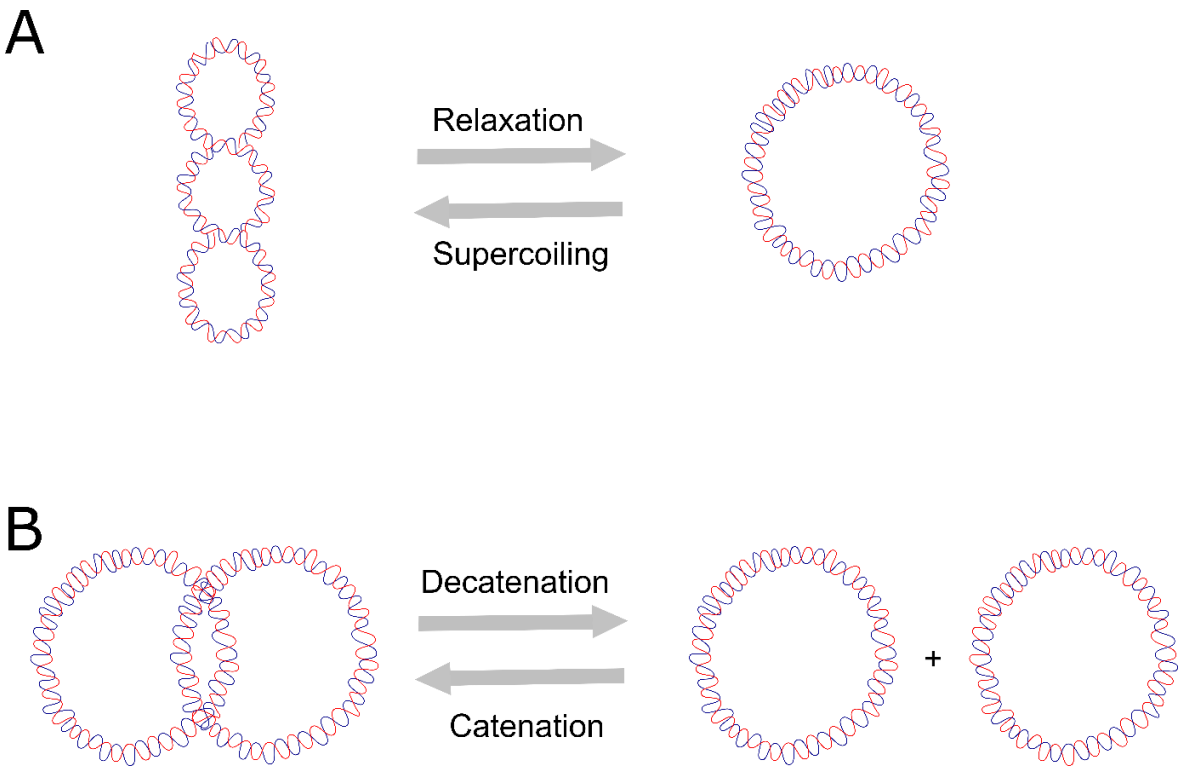

Figure 7-1: Relaxation and decatenation reactions performed by topoisomerase II

(**A**) During relaxation of supercoiled plasmid DNA, supercoils are removed which gives DNA a more open conformation. Type II topoisomerases can progressively relax the same DNA molecule multiple times resulting in a ladder of products relaxed to different extents. (**B**) The decatenation reaction releases interlinked DNA from a large network of kinetoplast DNA (kDNA). Whilst the reverse reaction joins individual DNA molecules together in a process called catenation. Topoisomerase II acts in a distributive manner during decatenation or catenation reactions because there are a limited number of interlinks that can be added or removed before the enzyme needs to find another substrate to continue catalysis. Therefore, the rate of DNA binding is an important factor during decatenation or catenation reactions.

7.2 Effects of Patient Mutations on TOP2B Structure

To investigate the possible structural effects of the patient mutations on TOP2B, the computer programme, Chimera, was used to visualise the mutations onto solved TOP2B structures (Figure 7-2). The mutations (A485P, R503S, R510Q and EE587E) are found within the TOPRIM domain of human TOP2B so are within the solved human TOP2B breakage reunion core (PDB 3QX3). It was hypothesised that the patient mutations would not have large disruptions on the overall structure, only local conformational changes because the mutated enzymes studied previously retained at least partial activity *in vivo.*

7.2.1 A485P

Alanine is one of the smaller amino acids with just one methyl group as the side chain, thus it is a non-polar hydrophobic amino acid. Due to its small size, it is capable of fitting into tight loops or chains and at position 485 it is towards the end of an alpha helix (Figure 7-2A-B). The A485P substitution could disrupt the shape of the alpha helix because generally a proline residue is associated with reverse turns in protein secondary structure. It is likely that a misfolded or unstable protein with a tendency to aggregate could result from this substitution.

7.2.2 EE587E

Glutamate (E) is a negatively charged, polar amino acid that is generally found on the surface of proteins exposed to an aqueous environment. However, if buried within the protein, as is the case with E587 and E588, glutamates are frequently involved in salt-bridges, where they pair with a positively charged amino acid to create stabilising hydrogen bonds. In TOP2B E587 forms a salt-bridge to R561 and E588 forms a salt-bridge to K566. Consequently, in the patient that possesses an in-frame deletion of the amino acid E587, protein stability will be reduced as the beta sheet where E587 and E588 are found will be destabilised (Figure 7-2C-D). However, because there are two consecutive glutamate residues it is unclear without a crystal structure of the mutated protein which salt-bridge will be impacted. Although, in either scenario it is likely that the temperature stability of the purified, mutated enzyme will be reduced compared to the wild type.

7.2.3 R503S

Arginine (R) is a positively charged, polar amino acid and because of its basic properties, it can form particularly favourable interactions with DNA bases. Arginine residues are also frequently involved in salt-bridges, where they pair with a negatively charged amino acid to create stabilising hydrogen bonds that can be important for protein stability. As shown in Figure 7-2E-F, R503 is solvent exposed in the TOP2B breakage reunion core and is in close proximity to the DNA helix. Consequently, it is likely that R503 forms hydrogen bonds to the G-DNA to help position the DNA in a conformation optimal for cleavage by topoisomerase II. Serine (S) is a much smaller amino acid compared to arginine and therefore, in the R503S mutation it is likely that contacts between the enzyme and DNA are abolished or reduced despite serine being able to form hydrogen bonds.

7.2.4 R510Q

Like R503, R510 is solvent exposed and near to the DNA helix (Figure 7-2G-H). However, the R510Q mutation is less severe compared to R503S because glutamine (Q) is more comparable in size to arginine and glutamine is a polar amino acid. Moreover, the side chain of glutamine now points towards the DNA, thus it could provide a hydrogen bond with the bound DNA. Although, if R510 forms a salt-bridge with an oppositely charged residue in the topoisomerase II structure, the salt-bridge will be disrupted in the mutated protein because glutamine is not charged. Accordingly, protein folding could be impacted which could make the mutated protein less stable.

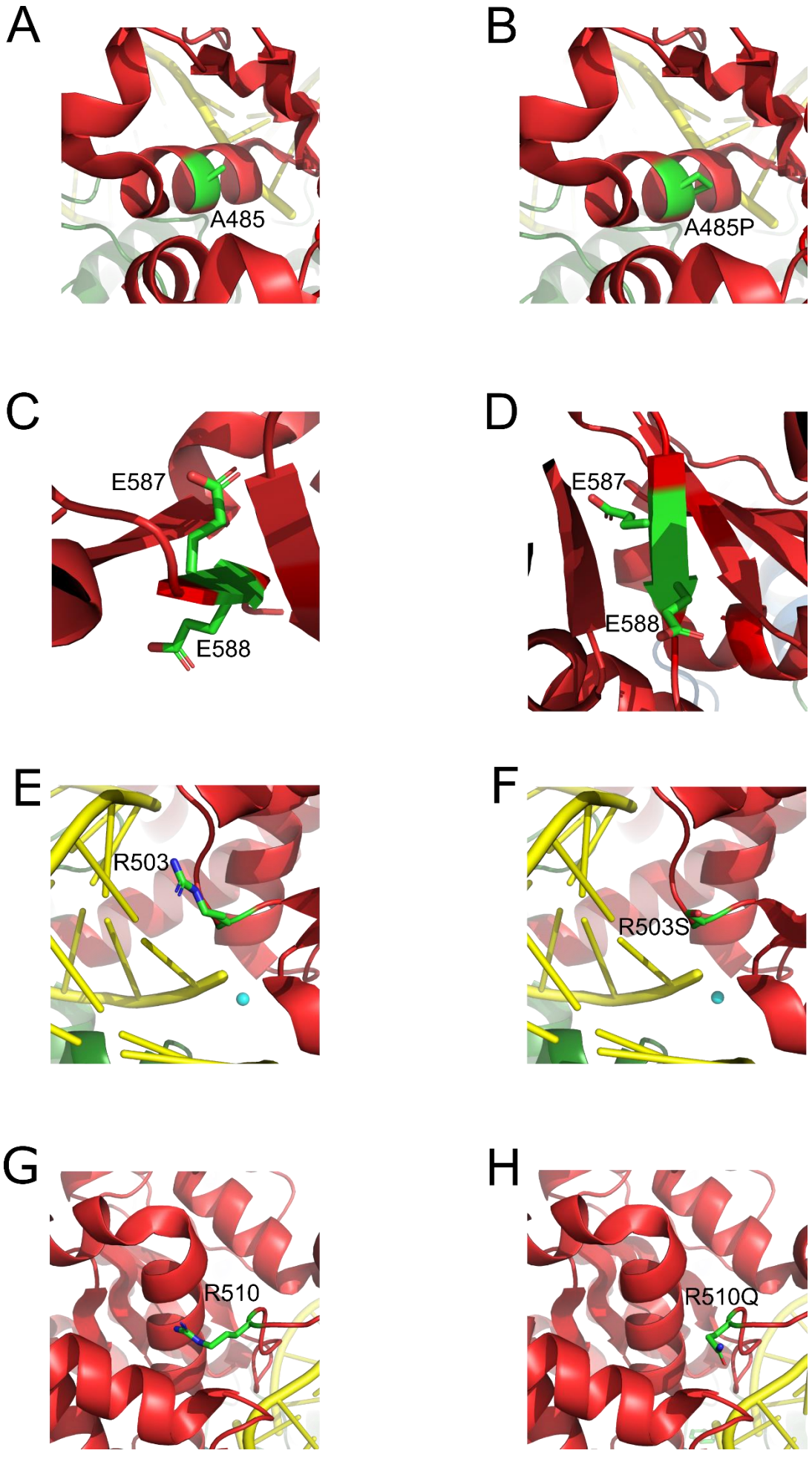
A
A485
B
A485P
C
E587
E588
D
E587
E588
E
R503
F
R503S
G
R510
H
R510Q

Figure 7-2: Effect of the patient mutations on the breakage reunion core structure of human TOP2B (PDB number 5ZRF) (previous page)

Position of mutation and side chain coloured in green, TOPRIM domain coloured in red, DNA in yellow and Mg^{2+} ion in cyan. Alanine 485 is part of an alpha helix, found within the TOPRIM domain of the breakage reunion core of TOP2B. Wild type A485 structure in (**A**) and the mutation A485P in (**B**). Two different views of the residues E587 and E588 in (**C**) and (**D**). The residues E587 and E588 are part of a beta-pleated sheet which is disrupted in the patient that possesses an in-frame deletion of one of the glutamic acid residues. R503 is part of the conserved PLRGKILNVR motif. Wild type TOP2B structure in (**E**) and the mutation R503S in (**F**). This residue is extremely close to the DNA and therefore the R503S mutation will likely have reduced contacts. R510 also located in the PLRGKILNVR motif. Wild type TOP2B structure in (**G**) and the mutation R510Q in (**H**). R510Q is a relatively conserved amino acid change, although the mutated R510Q residue now points towards the DNA and could offer an additional contact between the enzyme and DNA.

7.3 Yeast Expression Plasmids

To determine the impact of the amino acid change on the catalytic activity of human TOP2B, the recombinant proteins were expressed and purified. For ease of purification, a different yeast expression plasmid was used compared to the plasmid used in the previous complementation chapter. The multicopy yeast expression plasmid 12UraB TOP2B has been described previously (Blower, Bandak et al. 2019) to express human TOP2B encoding residues 46-1621 with an N-terminal 6xHis tag which facilitates protein purification. The plasmid contains a galactose inducible yeast gene GAL1 promoter, yeast TOP2 codons 1-7, the URA3 marker gene, the yeast 2 μm plasmid replication origin, and the β-lacatamase gene and replication origin of *E. coli* pBR322. The resulting constructs are chimeric proteins consisting of the first seven yeast TOP2 amino acids fused to amino acids 45-1621 of human TOP2B with an N-terminal tobacco etch virus (TEV) protease-cleavable 6xHis tag. Similar to the YEphTOP2βKLM plasmid used in complementation, the initial 44 amino acids of the human TOP2B coding sequence were not included in the plasmid to enhance protein expression. The desired patient mutations (Table 7-1) were generated in the 12UraB plasmid using site directed mutagenesis and confirmed via sequencing as per previously described (Chapter 2, Section 2.16). In addition, the mutated protein Y821F was also generated where the catalytic tyrosine is mutated to a phenylalanine which results in an inactive protein to provide a negative control.

Mutation
A485P
R503S
R510Q
R503S/R510Q
EE587E
Y821F

Table 7-1: Full-length human TOP2B mutations generated in 12UraB TOP2B and expressed and purified for in vitro analysis.

7.4 Protein Expression

The expression of human TOP2B in yeast has been described previously (Blower, Bandak et al. 2019). The expression plasmids were first transformed into a protease-deficient *Ura3* yeast strain, JEL1Δtop1 (Lindsley and Wang 1991). Topoisomerase I is knocked out in the expression strain to ensure that any strand passage activity is a result of topoisomerase II protein and not topoisomerase I contamination. Positive transformants were selected by their ability to grow on minimal agar lacking uracil, due to the expression plasmid containing the URA3 marker gene. As TOP2B cDNA are under the control of a GAL1 promoter, recombinant protein expression was induced by adding 2% galactose final w/v for a minimum of 3 hours. Approximately 9-12 L of yeast culture were grown and induced per preparation. After induction, the yeast cells were pelleted by centrifugation and stored at -80 °C until required. All six TOP2B mutated proteins were expressed by this method and Figure 7-3 shows a typical example of induction.

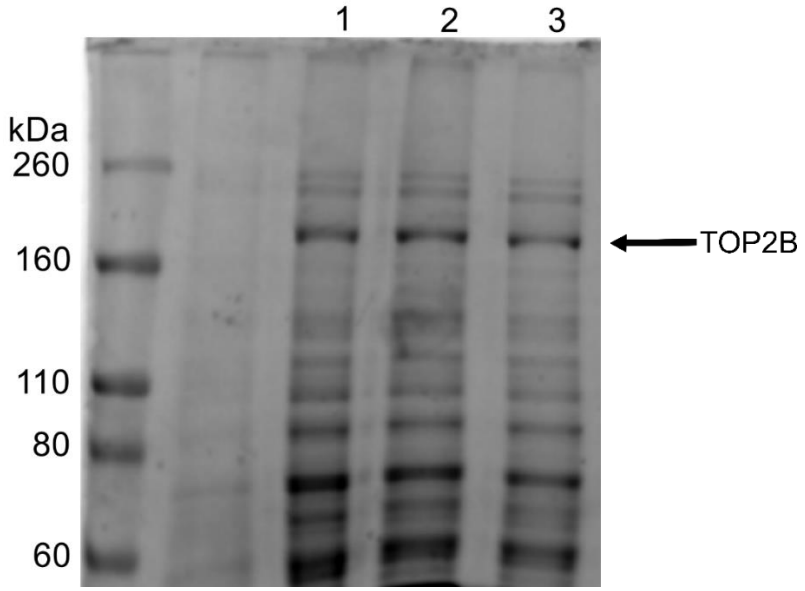

Figure 7-3: Expression of human TOP2B from the 12UraB plasmid

Whole cell extract of three different 1 L flasks checked for human TOP2B recombinant protein expression (180 kDa) were run on a 6% SDS polyacrylamide gel and proteins visualised by staining with Coomassie blue. Each lane contains 30 µL protein and 9 µL SDS-PAGE loading buffer. Lane 1 protein molecular markers, lanes 3-5 induced flasks 1-3.

7.5 Protein Purification

Frozen yeast pellets were slowly thawed on ice to prevent protein degradation and buffers were kept cool. The yeast cells were resuspended in 50 mM Tris HCl pH 8.5, 1 M KCl and 1% glycerol with the following protease inhibitors: 1 mM Benzamidine, 1 mM PMSF, 50 µM Leupeptin and 50 µM Pepstatin. The cells were lysed by mechanical disruption, at 37 kPSI followed by centrifugation at 27143 g for 20 minutes at 4 °C to separate the broken cell debris from the soluble proteins. Protein purification was performed as per Table 7-2. Due to the presence of a 6xHis tag, the proteins were first purified using nickel affinity chromatography using a His Trap column. The metal ion nickel binds strongly to a chain of histidine residues which separates the target protein from other endogenous proteins. A 20 mM imidazole wash was included to remove any non-specifically bound proteins from the nickel column. The protein was then eluted off the nickel column with a 500 mM imidazole step.

As TOP2B is a DNA-binding protein, a heparin column was used next in the purification process. TOP2B bound to the column whilst other proteins, were removed in the flow through. Once contaminants were removed, TOP2B was eluted from the heparin column with a 5 column volume (CV) salt gradient, during which the salt concentration increased from 320 mM KCl to 1 M KCl. The fractions around the UV peak were pooled for the final purification column. The TOP2B proteins typically eluted at a salt concentration of approximately 550 mM KCl.

The chimeric 6xHis-human TOP2B proteins have a theoretical isoelectric point of 8.15, thus at pH 8.5 the surface of the proteins are predominantly negatively charged. Therefore, an anion exchange column (Q) was selected for the final polishing step. Prior to loading the samples onto the column, the salt concentration was diluted by 70% with buffer containing no salt (50 mM Tris HCl pH 8.5, 1% glycerol) to ensure the ionic strength of the sample was low enough to allow binding to the Q column. Once the sample was loaded the column was washed with 320 mM KCl to remove any contaminants, prior to a step elution to 100% B (50 mM Tris HCl pH 8.5, 1 M KCl, 1% glycerol). By eluting with a step, the protein was much more concentrated than when a gradient was used which is preferable for biochemical analysis.

Finally, dialysis was performed on the purified human TOP2B fractions to ensure the proteins were in a buffer compatible for long term storage and *in vitro* experiments.

The samples were injected into dialysis cassettes and dialysis was performed at 4 °C for 2 hours with gentle stirring. The dialysis buffer contained 50 mM Tris HCl pH 8.5, 200 mM KCl, 20% glycerol and was used at 500 times the volume of the sample. Then the samples were flash frozen and stored at -80 °C until required.

The mutated proteins R503S, R510Q, R503S/R510Q, EE587E and Y821F were purified successfully to a purity greater than 90% (Figure 7-4) and had similar elution profiles. However, there was no visible protein band on the SDS-PAGE for the A485P mutated protein fractions despite the protein being visible when checked after cell lysis. The alanine to proline mutation is likely to destabilise the protein and it has been reported previously that A485P is rapidly degraded during protein purification (Papapietro, Chandra et al. 2020). Although, there was a UV peak during the Q elution which was ~1/4 of the typical absorbance so activity was still assayed for A485P in case there was any residual topoisomerase II protein.

Step	Column	Conditions
1	His Trap (10 mL)	Buffer A: 50 mM Tris HCl pH 8.5, 320 mM KCl, 1% Glycerol Buffer B: 50 mM Tris HCl pH 8, 320 mM KCl, 500 mM Imidazole, 1% Glycerol Load at 5 mL/min 4% B Step to remove non-specifically bound proteins Step elution to 100% B
2	Heparin (5 mL)	Buffer A: 50 mM Tris HCl pH 8.5, 320 mM KCl, 1% Glycerol Buffer B: 50 mM Tris HCl pH 8.5, 1 M KCl, 1% Glycerol Load at 5 mL/min 25 mL gradient to 100% B to elute target protein
3	Hi Trap Q (5 mL)	Buffer A: 50 mM Tris HCl pH 8.5, 320 mM KCl, 1% Glycerol Buffer B: 50 mM Tris HCl pH 8.5, 1 M KCl, 1% Glycerol Sample diluted by 70% with 50 mM Tris HCl pH 8.5, 1% Glycerol before loading onto the Q column Load at 5 mL/min Step elution to 100% B
4	Dialysis	Buffer: 50 mM Tris HCl pH 8.5, 200 mM KCl, 20% Glycerol Buffer at 500 times the volume of sample Performed at 4 °C for 2 hours with gentle mixing

Table 7-2: Protocol for the purification of the full-length mutated human TOP2B proteins expressed from the 12UraB vector

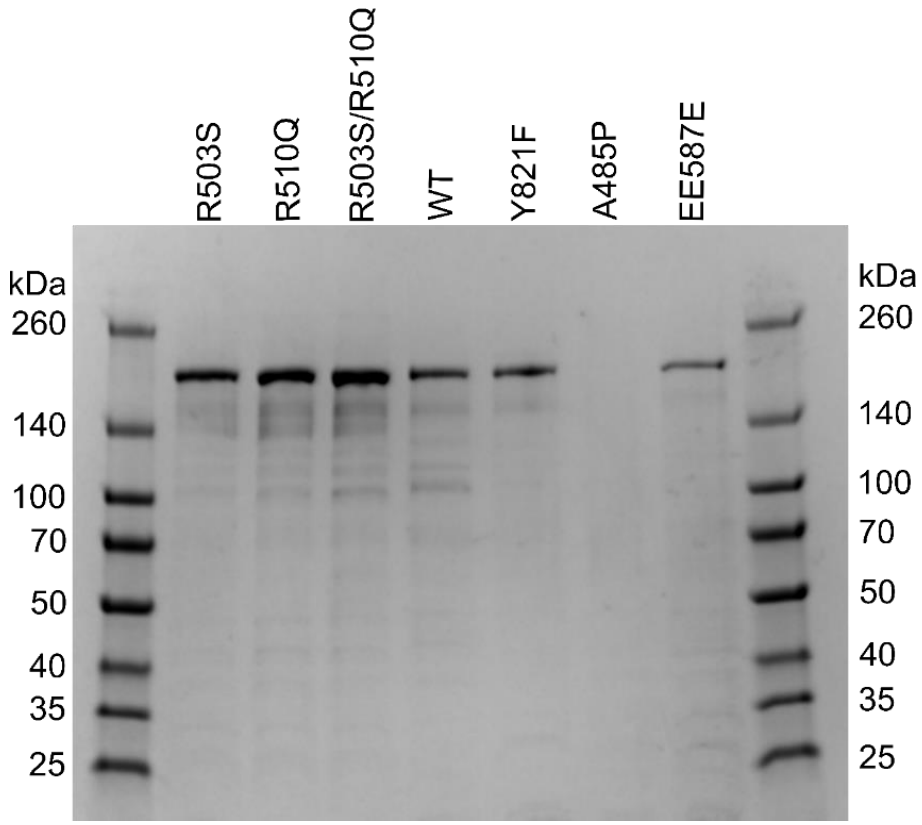

Figure 7-4: Purified full-length human TOP2B mutated proteins

4-20% precast SDS polyacrylamide gradient gel with the different TOP2B mutated proteins. Each lane contains 21 µL of sample and 7 µL SDS loading buffer. Lane 1 and 9 molecular markers, lane 2 R503S, lane 3 R510Q, lane 4 R503S/R510Q, lane 5 wild type TOP2B (WT), lane 6 Y821F, lane 7 A485P, lane 8 EE587E.

7.6 Strand Passage Activity on Wild Type and Mutated TOP2B Proteins

Once all the mutated proteins were purified, the strand passage activity was assayed using relaxation and decatenation assays. To quantify the relaxation activity of the mutated proteins, the amount of relaxed product and supercoiled DNA was quantified. Then the percentage of total DNA relaxed was calculated for each mutation for three replicate experiments (Chapter 2, Section 2.22.2). Whilst released minicircles were quantified as a percentage of total kDNA for three replicates to quantify the decatenation activity (Chapter 2, Section 2.22.3). Statistical analysis of the mutated proteins was performed by a two-way ANOVA and Bonferroni post-test (Chapter 2, Section 2.22.5).

7.6.1 DNA Relaxation of Supercoiled Plasmid DNA

The relaxation activities of the mutated proteins were investigated by incubating supercoiled plasmid DNA with increasing amounts of protein (Figure 7-5A-G) and the percentage relaxation activity was calculated (Figure 7-5H).

0-150 ng of protein was used for wild type TOP2B (WT), R510Q, R503S and the double mutation R503S/R510Q. Relaxed products began to appear with 40 ng of wild type TOP2B. However, interestingly activity was observed with the patient mutations R510Q, R503S and R503S/R510Q at lower protein concentrations. Indeed, all mutations were significantly more active than wild type TOP2B. For R510Q, the supercoiled DNA band disappeared at a protein concentration as low as 10 ng displaying significantly more relaxation activity ($P < 0.001$) than wild type TOP2B at protein concentrations 10-40 ng. The second mutation within the patient, R503S, was less active than R510Q but still had a significant increase in activity ($P < 0.05$) compared to wild type at 10 ng protein and $P < 0.001$ for 20-40 ng of protein compared to wild type TOP2B. The double mutation was less active than each individual mutation and displayed a relaxation profile more closely aligned to R503S than R510Q. In fact, there was no significant difference between the relaxation activity of R503S and R503S/R510Q at any of the protein concentrations studied. Whereas R503S/R510Q was significantly less active ($P < 0.001$) compared to R510Q at 10 and 20 ng of protein.

There was no relaxation activity observed for the Hoffman patient mutations EE587E or A485P even at high protein concentrations (1.5 µg). For A485P there was no detectable protein band when analysed via SDS-PAGE which likely explains the lack

of strand passage activity, however for EE587E there was a strong band corresponding to the molecular weight of TOP2B. Y821F was inactive in relaxing supercoiled DNA as expected because the catalytic tyrosine directly involved in the transesterification reaction is mutated to a phenylalanine. Consequently, Y821F provides a negative control and any strand passage activity observed with the mutated topoisomerase II proteins will be due to the presence of a functional topoisomerase and not a result of a contaminant from the purification.

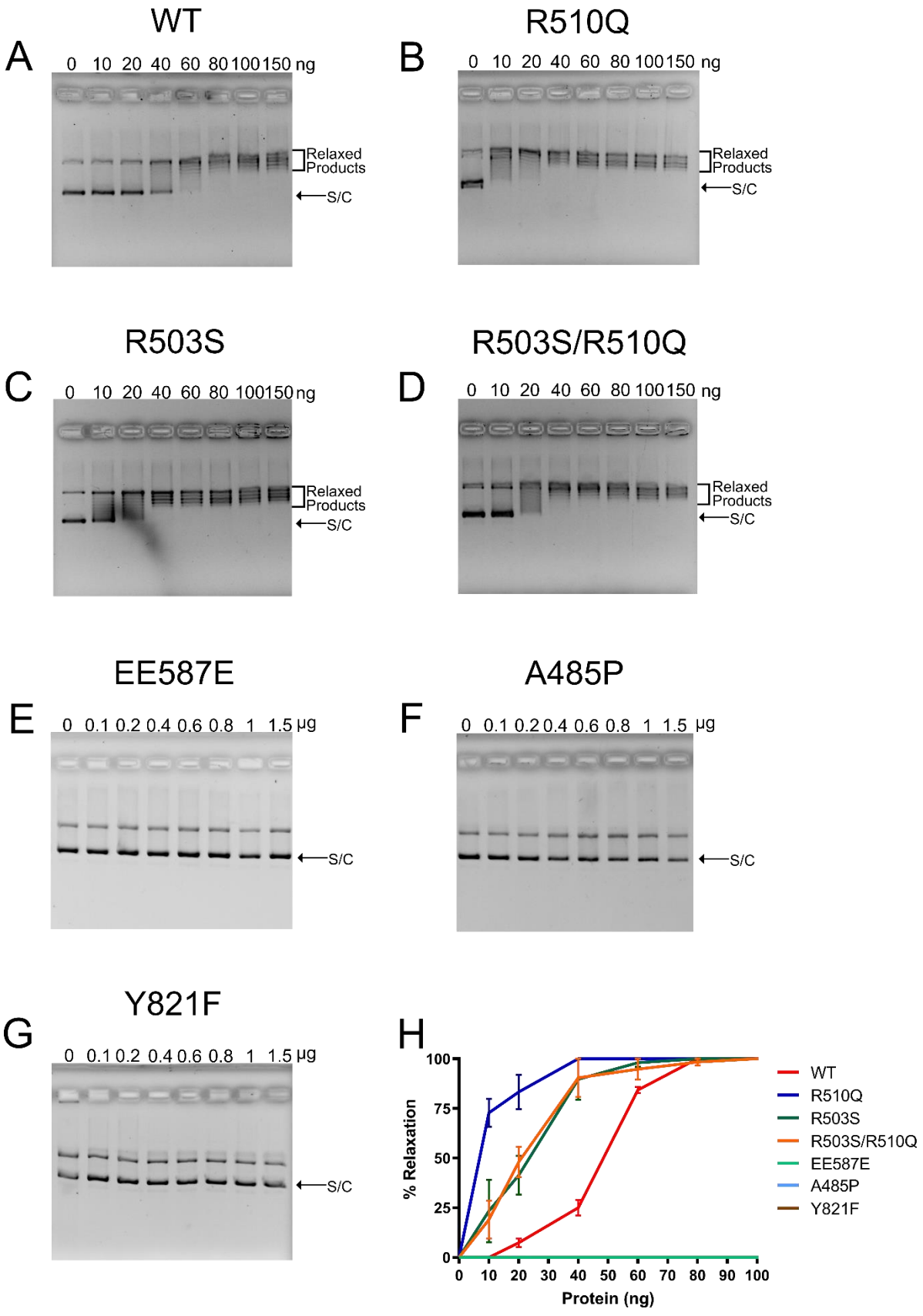

Figure 7-5: Relaxation of supercoiled plasmid DNA by wild type TOP2B and mutated proteins

Increasing amounts of protein (as indicated) were incubated with 10x relaxation buffer, 6.5 µg of TCS1 plasmid DNA and 1 mM ATP at 37 °C for 30 minutes. Relaxed products and supercoiled (S/C) DNA denoted on the right. Compact supercoiled DNA migrates further down the gel compared to relaxed DNA which exhibits a more open conformation. Relaxation activity of all seven TOP2B proteins analysed: wild type TOP2B (WT) (**A**), R510Q (**B**), R503S (**C**), R503S/R510Q (**D**), EE587E (**E**), A485P (**F**), Y821F (**G**). Relaxed products were quantified as a percentage of total DNA for three replicates and error bars represent one standard deviation from the mean (**H**). Note no relaxation activity was detected for EE587E, A485P or Y821F.

7.6.2 Effect of magnesium ions on relaxation activity

Magnesium ions are essential in the catalytic cycle of type II topoisomerases and mutations E477Q and K505E in TOP2B altered the affinity of the protein to magnesium ions (West, Meczes et al. 2000). These mutations are located within the B' domain of TOP2B, which corresponds to the same region of the protein where the patient mutations are located (A485P, R503S, R510Q and EE587E). Therefore, to test the magnesium dependence of the mutated proteins, relaxation was performed with a range of magnesium concentrations. Typically, relaxation reactions are performed with 10 mM $MgCl_2$ however, activity was tested at 0, 10, 20, 30, 40, and 50 mM $MgCl_2$ (Figure 7-6) to determine whether the magnesium dependence of the mutated proteins differed from wild type TOP2B. A485P and EE587E were also included in this analysis in case the proteins were active but required a larger concentration of magnesium for catalysis due to reduced binding or affinity. 100 ng protein was used in the reactions for wild type TOP2B, R503S, R510Q and R503S/R510Q. A larger amount of protein (1.5 µg) was used for A485P, EE587E and Y821F to increase the likelihood of observing relaxation.

For wild type TOP2B, optimal relaxation was with 10 mM $MgCl_2$ although activity was also observed in the presence of 20 mM $MgCl_2$. Likewise, the mutated proteins showed a similar magnesium optimum as wild type TOP2B. None of the proteins could relax in the absence of $MgCl_2$ as type II topoisomerases require magnesium ions for both catalytic reactions: ATP hydrolysis and DNA cleavage-religation. Additionally, extremely high magnesium concentrations (40-50 mM) inhibited relaxation of TOP2B. R510Q and R503S/R510Q were the most tolerant of different magnesium concentrations. Both mutations could relax equally well with 10 or 20 mM $MgCl_2$, and slight relaxation was observed even at 30 mM $MgCl_2$.

Despite changing the magnesium concentration, relaxation activity was still not observed for the Hoffman patient mutations A485P or EE587E. Thus, the lack of activity was not due to the mutations having reduced binding affinity for $MgCl_2$. Likewise, no relaxation was observed with Y821F.

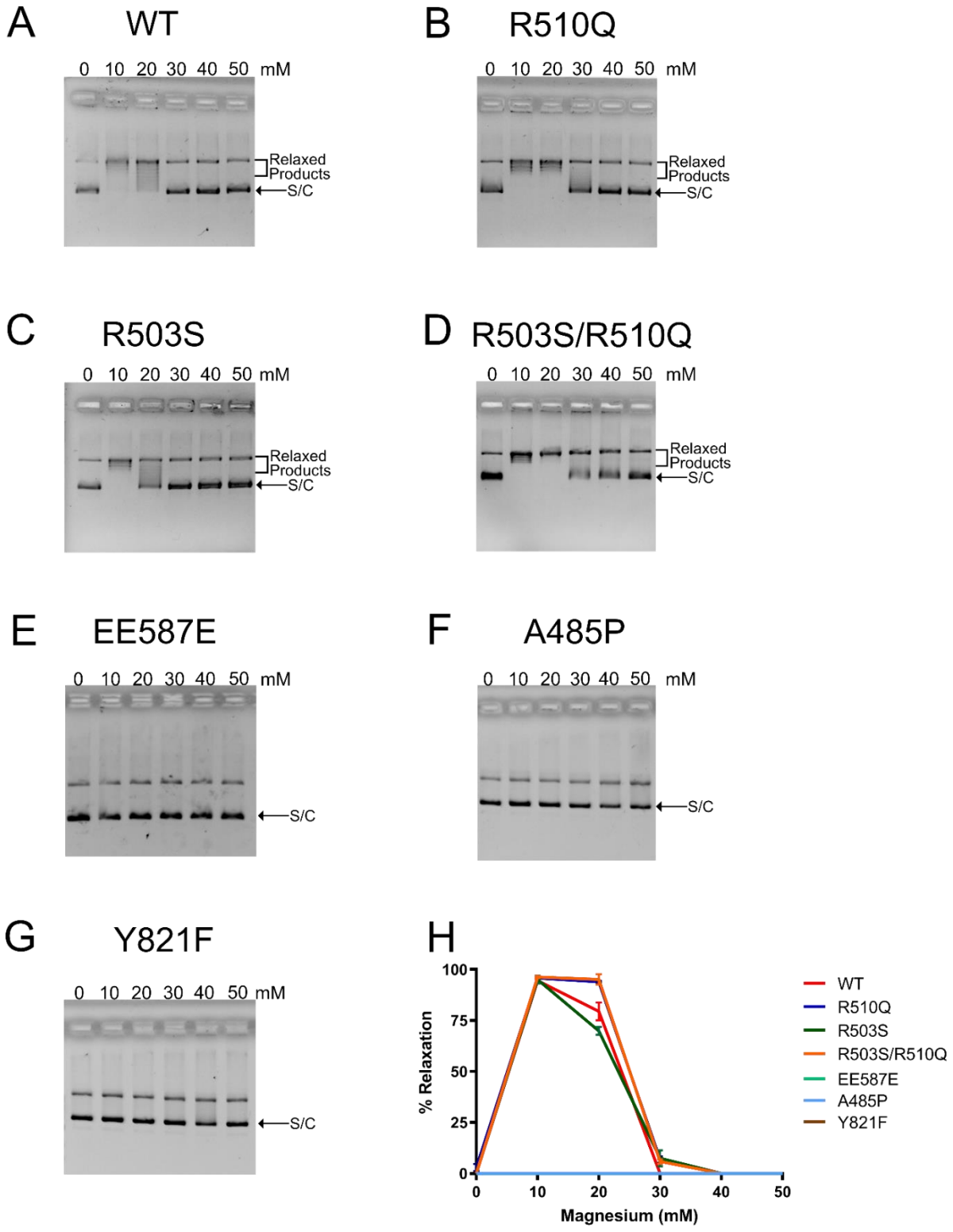

Figure 7-6: Effect of magnesium concentration on relaxation of supercoiled plasmid DNA by wild type TOP2B and mutated proteins

Relaxation of plasmid DNA was carried out at 0, 10, 20, 30, 40 and 50 mM $MgCl_2$. 100 ng of wild type TOP2B (WT) (**A**), R510Q (**B**), R503S (**C**), R503S/R510Q (**D**), and 600 ng of EE587E (**E**), A485P (**F**) and Y821F (**G**) was incubated with 10x

relaxation buffer, 6.5 µg of TCS1 plasmid DNA and 1 mM ATP at 37 °C for 30 minutes. 1 µg EE587E, A485P and Y821F used. Relaxed products and supercoiled (S/C) DNA denoted on the right. Compact supercoiled DNA migrates further down the gel compared to relaxed DNA which exhibits a more open conformation. Relaxed products were quantified as a percentage of total DNA for three replicates and error bars represent one standard deviation from the mean (**H**). Note no relaxation activity was detected for EE587E, A485P or Y821F.

7.6.3 Decatenation of Kinetoplast DNA

Decatenation is another method of testing strand passage activity of type II topoisomerases but in contrast to DNA relaxation, decatenation is specific to topoisomerase II activity. Decatenation of kDNA results in the release of individual minicircles from the kDNA network which can be visualised by gel electrophoresis. The same concentration of protein was used for decatenation as was used previously for the relaxation assays (Figure 7-7A-F) and the amount of decatenation was quantified and the data represented in (Figure 7-7H).

Wild type TOP2B began to decatenate kDNA in the presence of 40 ng protein and 80 ng of protein was required for the kDNA to become fully decatenated. Whereas the mutated proteins displayed greater decatenation activity compared to wild type TOP2B reaching significance at specific protein concentrations. Minicircles were first observed with 10 ng of R510Q and in the presence of 40 ng almost all the kDNA was decatenated. Consequently, at the protein concentrations 10-60 ng, R510Q was significantly more active than wild type TOP2B ($P < 0.001$). Moreover, the difference in decatenation activity between R503S and wild type TOP2B was significant at protein concentrations 10-40 ng, with the R503S mutation increasing the decatenation activity of topoisomerase II. Minicircles were first detected in the presence of 10 ng of R503S, but for complete decatenation 80 ng of protein was necessary. The double mutation, R503S/R510Q possessed a very similar decatenation profile to R503S with the only significant difference occurring at 40 ng protein ($P < 0.001$). At this protein concentration the individual R503S mutation was more active than the double mutation. As was the case with relaxation, there was no detectable decatenation activity for A485P, EE587E and Y821F.

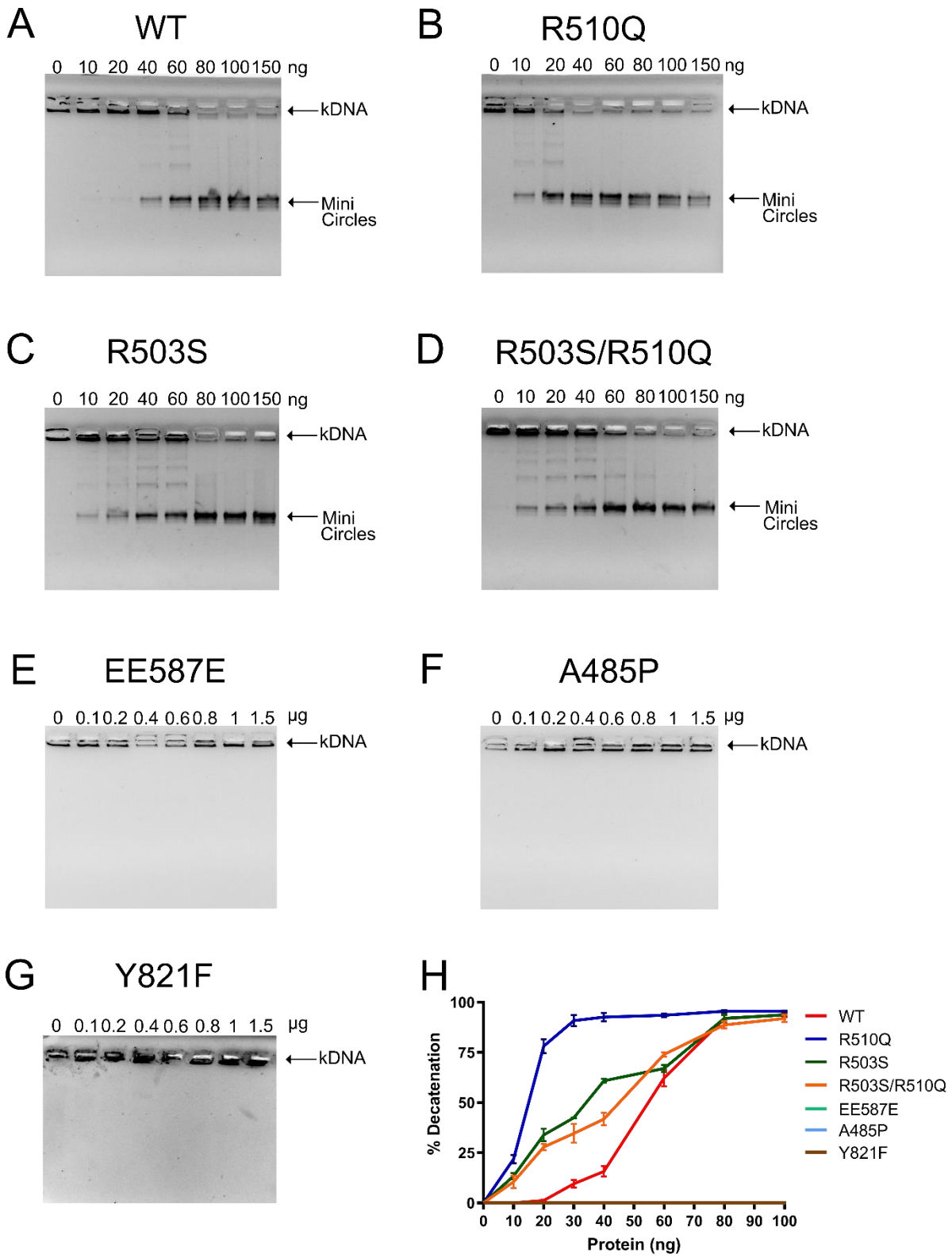

Figure 7-7: Decatenation of kDNA by wild type TOP2B and mutated proteins

Increasing amounts of protein (as indicated) were incubated with 10x relaxation buffer, 1 mM ATP, and 0.2 µg kDNA per reaction. Reactions were incubated at 37 °C

for 30 minutes and stopped by addition of loading buffer. kDNA and minicircles denoted on the right. Catenated kDNA is too large to enter the agarose gel but on addition of protein minicircles are released which can be visualised after electrophoresis. Increasing protein concentration increased the number of minicircles as they were decatenated from the kDNA. Decatenation activity of all seven TOP2B proteins analysed: wild type TOP2B (WT) (**A**), R510Q (**B**), R503S (**C**), R503S/R510Q (**D**), EE587E (**E**), A485P (**F**), Y821F (**G**). Released minicircles were quantified as a percentage of total kDNA for three replicates and error bars represent one standard deviation from the mean (**H**). Note no decatenation activity was detected for EE587E, A485P or Y821F.

7.7 *In Vitro* DNA Cleavage

The cleavage-religation equilibrium of topoisomerase II can be studied *in vitro* by adding SDS to the reaction after DNA cleavage has occurred. SDS denatures the topoisomerase protein, freezing the equilibrium and preventing religation of the cleaved products. The cleaved DNA products can then be analysed by electrophoresis as the DNA substrate is end labelled with fluorophores. DNA cleavage can occur in the presence of different cations although, magnesium is the physiological ion for topoisomerase II catalysis. However, *in vitro* the percentage of cleavage complexes observed in the presence of magnesium is very low. Instead, cleavage can be stimulated *in vitro* with calcium ions. Moreover, topoisomerase II targeting drugs such as topoisomerase II poisons stabilise the cleavage complex thereby greatly increasing the amount of cleavage products observed *in vitro.*

The DNA substrate used in the cleavage assays was a double-stranded oligonucleotide that is 5' end labelled with a RDye700 (Chapter 2, Figure 2-5). The oligonucleotide contains a single cleavage site that is positioned asymmetrically so that upon topoisomerase cleavage two products are observed which can be easily quantified by fluorescence imaging (Li-Cor Odyssey). Cleavage of the top and bottom strand can be studied simultaneously as the products are of different lengths (15 and 21 nucleotides). However, only the products containing the 5' end are visualised on the gel due to the 3' end being unlabeled. Cleavage of the oligonucleotide can be dramatically stimulated in the presence of mAMSA, with very little cleavage observed in its absence.

The cleavage-religation equilibrium of the TOP2B mutated proteins were analysed with the mAMSA oligonucleotide described above in the presence of magnesium and calcium ions with and without the topoisomerase II poison mAMSA to determine their cleavage activity and response to drug. Cleavage of each of the TOP2B mutated proteins was analysed with a constant amount of topoisomerase II protein per reaction (1.2 µg) as previously reported (Leontiou, Lakey et al. 2004). To calculate the percentage cleavage activity for each of the mutations, the cleavage products (bands at 15 and 21 nt) were quantified and expressed as a percentage of total DNA (Chapter 2, Section 2.22.4). Statistical analysis of the mutated proteins was performed by a two-way ANOVA and Bonferroni post-test.

7.7.1 DNA Cleavage Activity on Wild Type and Mutated TOP2B Proteins

Wild type TOP2B displays a DNA cleavage profile aligned with previous results. Topoisomerase cleavage is stimulated in the presence of mAMSA as shown by the increase in intensity of the cleaved products in Figure 7-8A. Ca^{2+} ions enhance cleavage to a greater extent than Mg^{2+} ions with little cleavage observed in the presence of Mg^{2+} without drug. These trends were also observed with all the mutated proteins (R503S, R510Q and R503S/R510Q) and there was no significant difference in cleavage between wild type TOP2B and the mutations in the absence of drug ($P > 0.05$). However, in the presence of mAMSA R510Q was stimulated the most and cleaved significantly more than all other proteins studied ($P < 0.001$). Whilst the cleavage activity of R503S was not significantly different to wild type TOP2B under all conditions tested. Interestingly mutating R503 to a serine changed the cleavage site specificity observed in the presence of Mg^{2+} and mAMSA as a faint smaller cleavage product (~12 nt) was observed which wasn't seen with the other proteins. In the absence of drug R503S/R510Q cleavage was comparable to R503S not reaching significance in the presence of Ca^{2+} and Mg^{2+}. However, upon addition of mAMSA in the presence of Ca^{2+}, R503S/R510Q had activity more comparable to R510Q. Cleavage by the double mutation was stimulated to a greater extent in the presence of Ca^{2+} and mAMSA compared to the individual R503S mutation ($P < 0.01$).

A485P and EE587E behaved similar to the negative control protein Y821F with no functional topoisomerase cleavage activity detected under any of the conditions trialed.

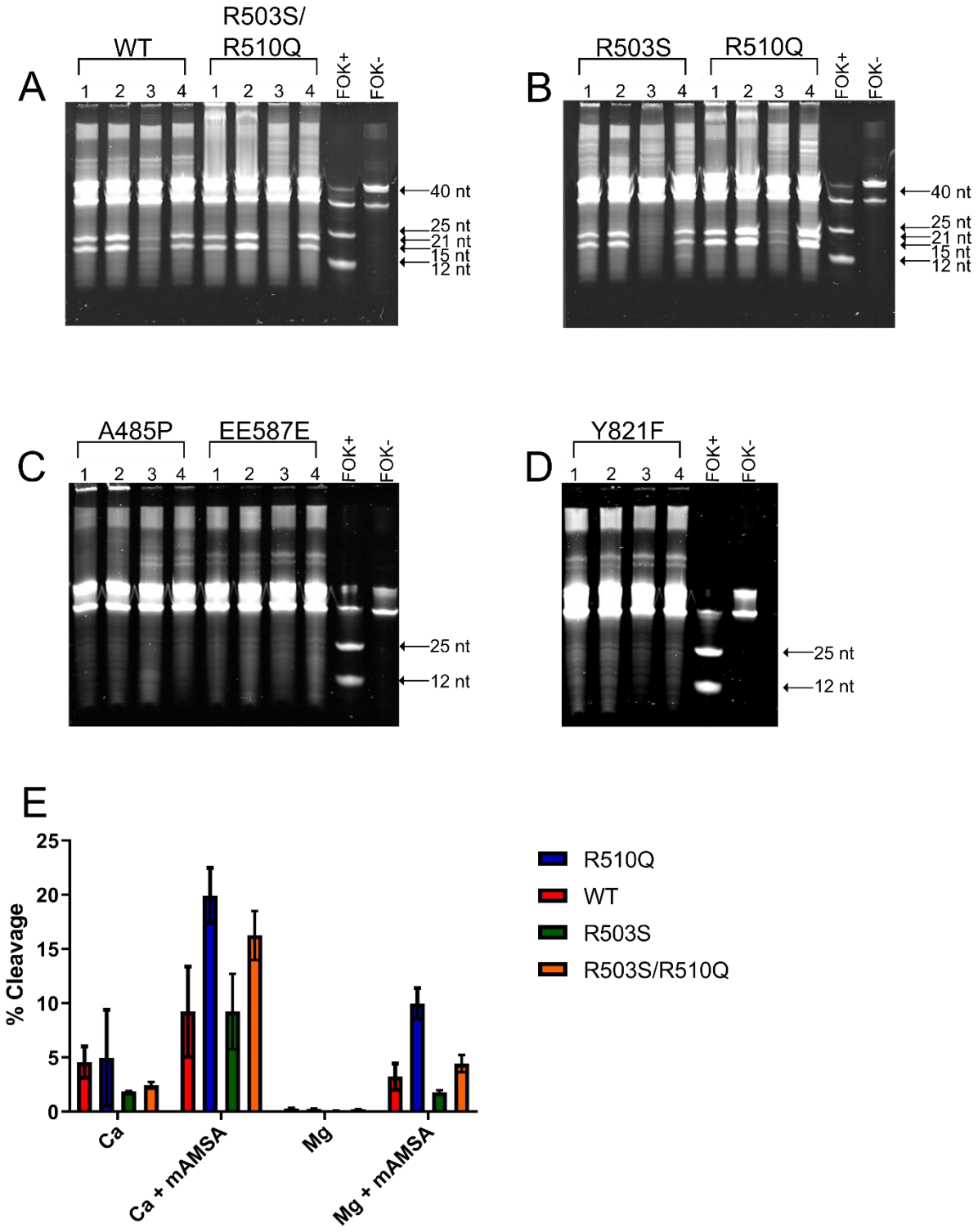

Figure 7-8: Cleavage of mAMSA oligonucleotide by wild type TOP2B and mutated TOP2B proteins

Cleavage reactions were carried out with 1.2 µg protein for all TOP2B proteins: wild type TOP2B (WT) and R503S/R510Q (**A**), R503S and R510Q (**B**), A485P and EE587E (**C**) and Y821F (**D**). Cleavage by each protein was assayed in the presence of 1 µM mAMSA oligo, 1 mM ATP, 10 mM Ca^{2+} (lane 1), 10 mM Ca^{2+} and 0.01 µg

mAMSA (lane 2), 10 mM Mg^{2+} (lane 3) or 10 mM Mg^{2+} and 0.01 µg mAMSA (lane 4) per reaction. Fok digest (FOK+) and uncut oligo (FOK -) included in the last two wells. Arrows indicate the 15 and 21 nucleotide cleavage products produced from the double labelled substrate (40 nucleotide oligo) and the Fok digest products (25 and 12 nucleotides). Cleaved products were quantified as a percentage of total oligonucleotide for three replicates and error bars represent one standard deviation from the mean (**E**).

7.7.2 Comparison of DNA Cleavage Activity Between Wild Type and Mutated TOP2B Proteins

The DNA cleavage for each mutation, relative to wild type TOP2B was calculated for every condition and wild type TOP2B cleavage activity was set to 100% in each case (Figure 7-9). The R510Q mutation resulted in a protein that was consistently more active than wild type TOP2B and the other studied mutated proteins. Moreover, R510Q had by far the greatest stimulation in cleavage in the presence of Mg^{2+} and mAMSA, displaying over 3 times as much cleavage compared to wild type TOP2B. Interestingly, despite the wild type TOP2B being less active in relaxation and decatenation assays, compared to R503S it generally cleaved the mAMSA oligo to a greater extent. R503S was less active in DNA cleavage compared to wild type TOP2B for all conditions apart from Ca^{2+} and mAMSA where it showed comparable activity. The double mutation was less active than wild type TOP2B in the absence of drug, however upon addition of mAMSA, R503S/R510Q became more active compared to wild type TOP2B.

A

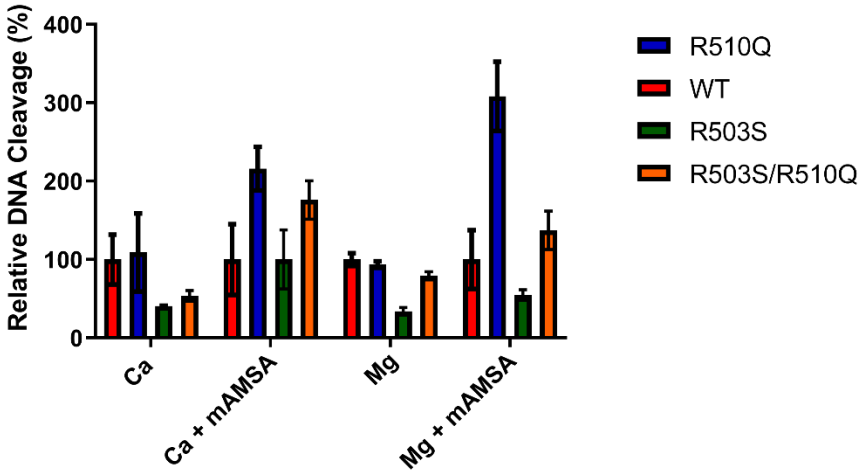

B

Protein	Ca^{2+}	Ca^{2+} and mAMSA	Mg^{2+}	Mg^{2+} and mAMSA
Wildtype (WT)	100.0 +/- 31.8	100.0 +/- 45.1	100.0 +/- 8.3	100.0 +/- 37.5
R510Q	109.0 +/- 49.7	216.0 +/- 27.7	93.7 +/- 4.3	308.3 +/- 44.2
R503S	40.6 +/- 2.5	100.2 +/- 65.4	33.9 +/- 8.4	54.8 +/- 11.8
R503S/R510Q	53.6 +/- 11.8	176.1 +/- 42.3	79.3 +/- 8.8	137.3 +/- 42.4

+/- Standard Error

Figure 7-9: Relative DNA cleavage by wild type and mutated TOP2B proteins

(**A**) Comparison of relative DNA cleavage activities of wild type TOP2B and mutations R510Q, R503S and R503S/R510Q in the presence of Ca^{2+}, Ca^{2+} and mAMSA, Mg^{2+} and Mg^{2+} and mAMSA. For each condition, the mean for wild type TOP2B cleavage activity was set to 100%. Results shown are the means of three replicates expressed as a percentage of cleavage by wild type TOP2B for that particular condition. Error bars represent one standard deviation from the mean and the results are tabulated in **B**.

7.8 Discussion

Wild type TOP2B and seven mutated proteins were assayed *in vitro* for catalytic activity. Strand passage activity was assessed using relaxation and decatenation experiments and DNA cleavage activity was assessed by topoisomerase II cleavage of a fluorescently labelled oligonucleotide. By comparing the mutated proteins to wild type TOP2B, it is possible to understand the impact of the mutation. All TOP2B mutated proteins studied in this chapter were functional *in vivo* by complementing the temperature-sensitive yeast strain JN394 (Chapter 6).

It should be noted that in the experiments performed in this chapter, wild type TOP2B was less active than previous studies (West and Austin 1999, West, Meczes et al. 2000, Leontiou, Lakey et al. 2004, Leontiou, Lakey et al. 2006, Leontiou, Watters et al. 2007). This was still the case after performing four independent wild type TOP2B purifications. There are several important differences in how the proteins were prepared which could explain this discrepancy. Firstly, a different construct was used. In the experiments reported here the protein was expressed as a 6xHis fusion protein from the 12UraB vector, whereas previous studies have expressed the protein without a tag from the YEphTOP2βKLM vector. Consequently, the proteins were purified differently and at different pHs. Here the yeast cells were lysed with mechanical disruption, at 37 kPSI in a buffer containing Tris HCl pH 8.5. Protease inhibitors were included during cell lysis but were absent at all further stages. Protein purification was performed at room temperature with buffers and samples kept on ice. The first column used was nickel affinity, followed by a heparin column then a Q column. In contrast, other studies have lysed cells by the glass bead method (Leontiou, Lakey et al. 2006, Leontiou, Watters et al. 2007) and included protease inhibitors throughout the purification protocol. Previously, proteins were purified at a pH of 7.5 by ammonium sulphate precipitation, phosphocellulose chromatography and then a Q column. Purification was performed at 4 °C throughout and took a considerably longer amount of time (2 days with untagged protein vs 6 hours with tagged protein). Earlier studies have shown that the pH conditions can impact TOP2B binding to DNA (West and Austin 1999) and thus purifying with buffers at different pHs may impact topoisomerase II activity. Moreover, the presence of a 6xHis N-terminal tag which remained in place during these assays may alter the catalytic activity. Consequently, some of the TOP2B mutations studied in this chapter appear more active than wild

type TOP2B, however caution should be applied when interpreting the results. Instead, attention should be focused on whether the proteins display catalytic activity rather than comparing the relative levels to wild type TOP2B.

7.8.1 R510Q

In vitro R510Q was extremely active and consistently the most active TOP2B protein studied. R510Q could effectively relax supercoiled plasmid DNA at protein concentrations as low as 10 ng (Figure 7-5), whilst it possessed a more sigmoidal character during the decatenation of kDNA akin to wild type TOP2B (Figure 7-7). In decatenation assays the topoisomerase enzyme only has a limited number of interlinks to remove before the minicircle is released from the network. After which, the enzyme must bind to another kDNA minicircle to continue catalysis. Whereas relaxation is more processive, with the enzyme potentially remaining bound to the same DNA molecule for multiple catalytic cycles or until all supercoils have been released, before dissociating from the DNA. Thus, the rate of DNA binding is more likely to impact catalysis in decatenation assays compared to relaxation, and the sigmoidal behaviour during decatenation could be due to cooperative DNA binding. In the absence of drug, R510Q cleaved the mAMSA oligonucleotide substrate comparable to wild type TOP2B. However, upon addition of the topoisomerase II poison, mAMSA, cleavage was dramatically stimulated in the presence of both Mg^{2+} and Ca^{2+} ions (Figure 7-9A). From the structural visualisation in Figure 7-2, the R510Q change results in the side chain of glutamine (Q) now pointing towards the DNA and being in much closer proximity than the wild type TOP2B structure. Therefore, this amino acid change could contribute an additional hydrogen bond to DNA accounting for the increase in DNA cleavage activity and ultimately strand passage activity. As such, performing DNA binding affinity experiments with R510Q compared to wild type TOP2B would be valuable.

The patient that possesses the R510Q mutation has no wild type copies of TOP2B due to also possessing the R503S mutation. Thus, it was not surprising that the R510Q mutated protein retained catalytic activity *in vitro* as the patient is alive despite having disabilities. Moreover, an arginine to glutamine mutation is a relatively conserved substitution and R510Q was able to complement extremely well *in vivo* using the yeast temperature-sensitive JN394 strain (Chapter 6).

7.8.2 R503S

R503S is the second mutation in TOP2B that the patient possesses and has previously not been studied. In strand passage assays, R503S was functional but displayed less activity than R510Q but more activity compared to wild type TOP2B (Figure 7-5 and Figure 7-7). It also differed from the R510Q mutation in that it did not display sigmoidal character during the decatenation of kDNA and was less tolerant of the magnesium concentration during relaxation (Figure 7-6).

An arginine to serine amino acid change is more dramatic compared to the R510Q mutation with a large difference in side chain branching. Furthermore, the amino acid R503 is absolutely conserved throughout evolution and is present even in *E. coli* parE whereas the equivalent R510 residue is a glutamate in bacteria. *In vitro* DNA cleavage experiments with R503S were comparable to wild type TOP2B with no significant difference under any of the conditions trialled. Consequently, for there to be a significant difference in strand passage activity between R503S and wild type, but no significant difference in DNA cleavage activity it is possible that the R503S mutation results in a more active ATPase domain. Therefore, it would be interesting to study the ATP hydrolysis activity of R503S compared to wild type TOP2B.

7.8.3 R503S/R510Q

When both patient mutations were present within the same protein, R503S/R510Q the result was the same *in vitro* properties as R503S. During strand passage, activity was not significantly different to the individual R503S mutation (Figure 7-5 and Figure 7-7) and the presence of a mutation at R510 to a glutamine didn't increase the activity. Similarly, cleavage was not significantly different to wild type TOP2B and R503S in the presence of Ca^{2+}, Mg^{2+} and Mg^{2+} and mAMSA. Only in the presence of Ca^{2+} and mAMSA was cleavage significantly increased compared to wild type TOP2B and R503S, however this increase was still significantly less than cleavage by R510Q. Although, the magnesium dependence of R503S/R510Q was equivalent to R510Q as the double mutation could relax at higher magnesium concentrations (Figure 7-6).

Even when both patient mutations (R510Q and R503S) were present within the same protein, the protein retained activity *in vitro.* Consequently, the patient phenotype must be due to another physiological function of TOP2B. For example, the mutations could

impact TOP2B's role in the maintenance of chromatin structure or in the transcriptional regulation of certain developmentally regulated genes. However, as the double mutated protein could still perform the catalytic reaction, it provides an explanation for why the patient is alive.

7.8.4 A485P

A485P is a mutation in TOP2B that has been reported to give rise to Hoffman syndrome. In total there are six patients with this mutation from two independent families. The patients are heterozygous, possessing one wild type copy of TOP2B and one mutated copy. The patients lack circulating B cells but possess normal T cell responses. In both families, A485P initially arose due to *a de novo* mutation, but has since been inherited by offspring (Papapietro, Chandra et al. 2020).

The purification protocol for wild type TOP2B was followed for each of the mutated proteins, however there was no visible protein band on the SDS-PAGE for the A485P mutated protein. Proline mutations are known for destabilising proteins due to the unusual side chain which bonds with the backbone nitrogen forming a ring structure. This places steric constraints on proline and neighbouring residues that can hinder secondary structure formation (Choi and Mayo 2006). Indeed, when A485P was previously purified from HEK293 cells, a lower molecular weight band was observed suggesting degradation of A485P had occurred (Papapietro, Chandra et al. 2020). Although, there were no lower molecular weight products in the final purified A485P fractions from *S. cerevisiae* (Figure 7-4) it is possible that the protein degraded earlier on in the purification and the smaller fragments were lost in the flow through. Thus, it is likely that the lack of visible protein on the gel is due to the A485P mutation destabilising the protein.

Even though no TOP2B protein could be detected for A485P on the SDS-PAGE gel, strand passage activity was still measured because it is more sensitive than SDS-PAGE and there was a small UV peak during elution of the final column. However, A485P showed no topoisomerase II activity in relaxation, decatenation or DNA cleavage experiments (Figure 7-5-Figure 7-8). When A485P was expressed and purified from HEK293 cells, the heterodimer possessed relaxation and decatenation activity though it was reduced compared to wild type TOP2B. Moreover, the study showed that an A485P homodimer is even less active than the A485P heterodimer.

The main difference between protein expression with a yeast system such as *S. cerevisiae* and mammalian cells such as HEK293 are the type of posttranslational modifications that can occur. Expressing a human protein with a human expression system like HEK293 cells is advantageous over expression with yeast because the correct posttranslational modifications can occur (Jenkins, Murphy et al. 2008, Khan 2013). Consequently, the difference in activity between A485P purified from HEK293 cells and the mutated protein expressed from *S. cerevisiae* reported here could be due to differences in the expression host and purification protocol. In addition, the 6xHis N-terminal tag was not cleaved off during the experiments performed in this chapter which could also hinder topoisomerase activity. Therefore, to be certain that A485P expressed from *S. cerevisiae* is inactive the purification would need to be repeated and optimised so that a topoisomerase II protein band is observed on the SDS-PAGE gel. Then, strand passage activity should be analysed in the presence and absence of the 6xHis N-terminal tag. Furthermore, it would be useful to determine whether A485P still retains functional ATP hydrolysis activity, as the mutation lies just outside of the ATPase domain.

7.8.5 EE587E

The TOP2B mutation EE587E is another Hoffman syndrome mutation. To date two patients have been identified with the in-frame deletion of glutamate 587 and both patients are heterozygous (Broderick, Yost et al. 2019, Erdős, Lányi et al. 2021). EE587E expressed from S. cerevisiae was purified to high purity and there was a strong topoisomerase II protein band in the eluted Q fractions (Figure 7-4). However, despite this there was no observed catalytic activity for the mutated protein. Even at protein concentrations as high as 2 µg strand passage activity was not observed (Figure 7-5-Figure 7-7) and no cleavage was observed in the presence of mAMSA (Figure 7-8). This was surprising because the protein could complement in the temperature-sensitive JN394 strain, albeit weakly. However, different plasmids were used in complementation compared to the plasmids used in this chapter for the expression and purification of TOP2B proteins. During complementation the YEphTOP2βKLM plasmid was used which encodes an untagged TOP2B protein, whereas the proteins expressed for in vitro analysis contain a 6xHis tag. It is possible that the tag could reduce topoisomerase II activity and if the mutation EE587E already has a low level of activity, when the protein is coupled with the 6xHis tag the activity

may fall below the level of detection. Whereas other mutations studied here such as R503S and R510Q may have less of a severe impact on TOP2B function such that even in the presence of a 6xHis tag activity was still observed. Consequently, investigating ATP hydrolysis activity as well as strand passage and DNA cleavage activity of EE587E in the presence and absence of the N-terminal 6xHis tag would also be valuable to better understand if it is the TOP2B mutation that inhibits catalysis or the presence of a 6xHis tag.

The work presented in this chapter is the first study of the EE587E mutated protein *in vitro* as a homodimer. The previous study with nuclear fractions from haploid yeast strains heterozygous for EE587E showed the heterozygous protein could decatenate kDNA but less effectively than wild type TOP2B. In fact, the EE587E exhibited a partial dominant negative effect with the strain possessing only one copy of wild type topoisomerase II decatenating kDNA better (Broderick, Yost et al. 2019). Moreover, mice that were homozygous for EE587E were non-viable which could suggest that the patients may only be alive as a result of possessing a wild type copy of TOP2B and an EE587E homodimer has too little topoisomerase II activity to carry out the catalytic mechanism.

Chapter 8 Summary and Future Work

8.1 TOP2B ATPase Domain

The ATPase domain of type II topoisomerase enzymes are vital for binding and hydrolysing ATP which provides the energy to resolve topological problems in DNA. The structure of the ATPase domain of human TOP2A and yeast TOP2 have previously been determined (Classen, Olland et al. 2003, Wei, Ruthenburg et al. 2005), and the ATPase activity for the isolated TOP2A ATPase domain and yeast ATPase domain have been reported (Campbell and Maxwell 2002, Schmidt, Osheroff et al. 2012). However, less is known about the ATPase domain of TOP2B despite this region of the protein being targeted therapeutically. Therefore, the first aim of this study was to express the ATPase domain of human TOP2B and determine the tertiary structure.

The ATPase domain of human TOP2B (45-444) was crystallised in the presence of the non-hydrolysable ATP analogue AMPPNP and the ATP hydrolysis product ADP. In the presence of AMPPNP, the ATPase domain was in the restrained conformation previously described for bacterial DNA Gyrase (Stanger, Dehio et al. 2014), and the nucleotide binding site was sequestered from solvent. Whereas upon hydrolysis of ATP the QTK loop from the transducer domain moved away from the active site in order to create space for inorganic phosphate release. A catalytic magnesium ion was observed in both protein conformations, bound to either AMPPNP or ADP, coordinated by the catalytic base E103. Indeed, when E103 was mutated to an alanine in biochemical studies, ATP hydrolysis activity was abolished further confirming the function of this residue.

Intriguingly, the full-length ATPase domain of TOP2B (1-444) was significantly less active in hydrolysing ATP compared to the N-terminal truncated protein used for crystallography (45-444). Similarly the alternative splice variant of TOP2B that contains an additional five amino acids after valine 23 (1-449) also had reduced ATPase activity. It is possible that the first 44 amino acids in the N-terminal strap are inhibitory to ATP hydrolysis due to a regulatory mechanism. Likewise the ATP hydrolysis activity of the isolated ATPase domain proteins was stimulated in the presence of nucleic acid, as previously reported for human TOP2A and *S. cerevisiae* TOP2 (Campbell and Maxwell 2002, Schmidt, Osheroff et al. 2012). By coupling DNA

binding to ATPase stimulation, the enzyme has a regulatory mechanism which prevents ATP from being hydrolysed unnecessarily when there is no DNA substrate in proximity.

As the ATPase domain of human TOP2B is the clinical target of bisdioxopiperazines, the structure of TOP2B in complex with ICRF193 was solved. The drug binding site was identified between the dimer interface in the same location as reported for the *S. cerevisiae* ATPase domain in complex with ICRF187 (Classen, Olland et al. 2003). The availability of these high-resolution crystal structures will provide a valuable resource to study mutations within the ATPase domain of human TOP2B and will be a valuable tool in future drug design.

8.1.1 Future Work

The biochemical characterisation of the ATPase domain in Chapter 3 determined that the N-terminal strap had a function *in vitro.* Therefore, a eukaryotic ATPase domain structure containing the complete N-terminal strap would be valuable to further understand the purpose of the N-terminal strap. It would also be of interest to determine the structure of a eukaryotic ATPase domain protein in the presence of nucleic acid to identify the specific DNA binding residues.

As topoisomerase II is a large multidomain protein that undergoes allosteric conformational changes, studying isolated protein domains has limitations. To understand how the conformational changes of the ATPase domain are transduced to the breakage reunion core, a tertiary structure spanning both domains is necessary. This has been achieved for the *S. cerevisiae* TOP2 protein (Schmidt, Osheroff et al. 2012) and a cryoEM structure of human TOP2A (Vanden Broeck, Lotz et al. 2021) has been reported, although no full-length structure for the TOP2B isoform is available. As the two human isoforms have differing functions and share only ~78% overall similarity it would be of interest to obtain a human TOP2B structure comprising multiple domains to provide information on the allosteric movements of the enzyme.

8.2 Complementation

In a previous study, mutated TOP2B proteins were generated in a drug resistance screen (Leontiou, Watters et al. 2007). Interestingly, in three of these proteins the mutated residue (H514Y, G550R and A596T) was adjacent to a lysine residue that is frequently ubiquitinated (K515, K551 and K595) and in the case of K595 can also be SUMOylated (Hendriks, D'Souza et al. 2014). Therefore, to investigate whether the lysine residue is required for *in vivo* drug resistance, lysine to alanine mutations were generated (K515A, K551A and K595A). The *in vivo* functionality of the mutated proteins was analysed in the yeast temperature-sensitive system (JN394t2-4) and compared to the original mutated proteins H514Y, G550R and A596T selected for drug resistance. All three lysine to alanine mutated proteins were able to complement indicating the lysine residue was not necessary for type II topoisomerase function *in vivo.* Similarly, two of the mutated proteins (K515A and K551A) displayed drug resistance to topoisomerase II poisons. Whereas K595A was not resistant to any of the drugs tested.

Eight patient mutations in TOP2B were also studied in this project. Biallelic mutations R503S and R510Q could both complement as homodimers at the non-permissive temperature in the yeast strain JN394t2-4. To investigate the function of residue R503 further, three more mutations were generated: R503A, R503E and R503K. Mutation of arginine to a glutamic acid (R503E) is a severe amino acid change where a basic residue is replaced with an acidic residue and as a result, R503E could not complement *in vivo* as previously reported (West, Meczes et al. 2000). Whilst mutation of R503 to a lysine residue (R503K) which conserves the amino acid properties, allowed growth of the temperature-sensitive yeast strain at the non-permissive temperature. Similarly, R503A could complement albeit not as well as wild type TOP2B because an alanine residue is non-polar rather than possessing a positive charge like an arginine residue. These results suggest that position 503 is important for type II topoisomerase function as a dramatic amino acid change abolishes topoisomerase II activity.

Mutations K172R and L1146V result in only slight differences in the amino acid side chains and both proteins could complement *in vivo.* It is not yet known whether these mutations are causative for the observed patient phenotype, though the results derived

from this study indicate either mutation maintains a functional type II topoisomerase enzyme. Likewise, when the mutation K172R was generated in the isolated ATPase domain protein (Chapter 3), ATP hydrolysis activity was observed. It is possible that residues K172 and L1146 are not essential for topoisomerase II catalytic mechanism.

Four Hoffman syndrome mutations were also studied *in vivo.* Patients exhibit autosomal dominant B cell immunodeficiency combined with facial and limb abnormalities. The patients all possess a causative, heterozygous mutation in TOP2B which involves either a *de novo* missense mutation (S483L, G633S, A485P) or a *de novo* in-frame deletion (EE587E) (Broderick, Yost et al. 2019, Papapietro, Chandra et al. 2020). Two of the Hoffman syndrome mutations (A485P and EE587E) could rescue the temperature-sensitive phenotype *in vivo* whilst no growth was detected for S483L or G633S.

8.2.1 Future Work

The use of yeast as a model organism to study human proteins is advantageous because genetic manipulation of yeast cells is much quicker and cheaper than genetically modifying mammalian cells. Moreover, many human genes have a yeast homologue making yeast a valuable tool. However, in the case of heterozygous mutations, using a haploid yeast model has limitations. For example, the mutated TOP2B proteins in this study were homodimers whereas patients possess TOP2B heterodimers, containing one wild type copy and one mutated copy. Consequently, in the future it would be interesting to investigate the impact of the TOP2B mutations as heterodimers and observe whether the temperature-sensitive phenotype of S483L and G633S could be rescued in the presence of one wild type copy of TOP2B.

8.3 *In Vitro* Activity

A subset of the human TOP2B patient mutations analysed via the complementation assay were then studied *in vitro* to understand the impact of the amino acid change on enzyme function. The catalytic activity of the biallelic mutations R503S and R510Q was investigated as well as the two Hoffman syndrome mutated proteins that could complement (A485P and EE587E). The proteins were overexpressed in yeast as an N-terminal 6xHis fusion protein and purified through a combination of affinity and ion

exchange chromatography. Determination of the catalytic activity *in vitro* involved strand passage assessment through relaxation and decatenation assays, in addition to DNA cleavage reactions in the presence and absence of the topoisomerase II poison, mAMSA.

The two biallelic mutations, R503S and R510Q were extremely active *in vitro* demonstrating significant strand passage and DNA cleavage activity. This could provide an explanation as to how the patient can survive without any wild type TOP2B protein. In addition, when both patient mutations were present within the same protein (R503S/R510Q) type II topoisomerase activity was retained and was comparable to R503S. Whilst the single R510Q mutation was consistently the most active TOP2B protein studied.

Surprisingly for the two Hoffman mutations that could complement *in vivo* (A485P and EE587E) no detectable topoisomerase II activity was observed in any of the *in vitro* assays. The major difference between the two assays is the nature of the plasmid used. For *in vivo* analysis a plasmid was utilised that encodes an untagged TOP2B protein (YEphTOP2βKLM), whereas the proteins expressed for *in vitro* analysis contain a 6xHis tag (12UraB) to aid purification.

8.3.1 Future Work

To further analyse the mutations R503S and R510Q, it would be interesting to observe the kinetics of the cleavage complexes using either TARDIS or RADAR assay. Although, the results presented in this study show that the enzymes are functional in cleaving DNA, the mutation could have an effect on the duration or stability of the cleavage complexes. Alternatively, the patient phenotype may arise due to the mutations affecting TOP2B's transcriptional regulation of genes required during development. Consequently, investigating the impact of the TOP2B mutations on gene expression via RNA seq would be valuable to understand whether any proteins are up or downregulated as a result of the TOP2B amino acid changes.

As A485P and EE587E were functional *in vivo,* it was unusual that no detectable topoisomerase II catalytic activity was observed *in vitro.* It is possible that the N-terminal 6xHis tag has an inhibitory effect on topoisomerase II activity therefore, future work should investigate the catalytic activity after cleavage of the 6xHis tag.

Alternatively, the mutations could reduce the stability of the enzyme such that by the time purification is achieved the enzyme is inactive. Consequently, structural analysis of the mutated proteins via circular dichroism or differential scanning fluorimetry would be interesting to see whether the mutations reduce the thermal stability of the enzyme.

8.4 Summary

Overall, the work presented in this thesis has provided knowledge on the tertiary structure of the ATPase domain of human TOP2B and identified conformational changes that occur within the protein during ATP hydrolysis. In addition, interesting results were obtained for the mutated TOP2B proteins. The fact that some Hoffman syndrome proteins can complement whilst others can't despite the patients being alive with such mutations is intriguing. Moreover, how these specific amino acid changes in a type II topoisomerase enzyme can cause such a severe phenotype is an active area of research with much still to be answered.

Appendices

Appendix 1: Summary of the eukaryotic topoisomerase II crystal structures solved to date. Details provided include: protein name, residue numbers included in the structure, crystallisation condition, protein condition, crystal resolution, PDB number and primary reference.

Appendix 2: Details of the crystallography screens and conditions used during the project. Information includes the type of salt and concentration, buffer type and pH, and the precipitant type and concentration for screens: JCSG Plus (**A**), PACT Premier (**B**), Structure (**C**), Index (**D**), Morpheus II (**E**).

Appendix 1: Summary of the eukaryotic topoisomerase II structures solved to date

Protein	Residues	Species	Crystallisation Condition	Protein Condition	Comment	PDB Code	Reference
TOP2A ATPase domain with AMPPNP	29-428	Human	4-8% PEG6000, 10mM β-mercaptoethanol	8 mg/mL protein, 20mM Tris-HCl pH 7.4, 5mM $MgCl_2$, 1mM dithiothreitol, 1mM AMPPNP	Crystals grew at 4 °C to 150 x 150 x 1000µm in 2 days. 1.87 Å resolution.	1ZXM	Wei *et al.*, 2005
TOP2A ATPase domain with ADP	29-428	Human	21% PEG1500, 35mM ammonium sulphate, 100mM Tris-HCl pH 8.0	8 mg/mL protein, 20mM Tris-HCl pH 7.4, 5mM $MgCl_2$, 1mM dithiothreitol, 5mM ADP	Crystals grew at 20 °C to 120 x 120 x 50µm in 2 days. 2.41 Å resolution.	1ZXN	Wei *et al*., 2005
TOP2A Core	431-1193	Human	10% PEG3000, 200mM $MgCl_2$, 100mM Na-cacodylate (pH 6.5)	5 mg/mL protein/DNA complex, 20mM Tris-HCl pH 7.9, 10 mM $MgCl_2$, 100mM KCl	Crystals grew at 18 °C in 1 day. 2.9 Å resolution.	4FM9	Wendorff *et al.*, 2012
TOP2A in complex with DNA and Etoposide	429–1188	Human	100mM magnesium acetate, 50mM 2-(N-morpholino) ethanesulfonic acid pH 5.6 and 26% 2-methyl-2,4-pentanediol (MPD)	5 mg/ml protein, 1mM etoposide, ~34µM 20 bp dsDNA substrate, 50mM Tris–HCl pH 7.0, 200mM KCl, 5 M $MnCl_2$, 1mM EDTA, 2mM β-mercaptoethanol	Crystals grew at 4 °C within 2 weeks in hanging drops. 3.15 Å resolution.	5GWK	Wang *et al.*, 2017
TOP2B Core in complex with Etoposide	445-1201	Human	100mM magnesium acetate, 50mM 2-(N-morpholino) ethanesulfonic acid pH 5.8, and 22% 2-methyl-2,4-pentanediol (MPD)	6.5mg/ml protein, 2mM etoposide and DNA substrate at 1.2-fold molar ratio to protein, 30mM Tris-HCl pH 7.5, 70mM NaCl, 2mM	Crystals grew at 4 °C within 1 week in hanging drops. 2.16 Å resolution.	3QX3	Wu *et al.*, 2011

Protein	Residues	Species	Crystallisation Condition	Protein Condition	Comment	PDB Code	Reference
				βmercaptoethanol, and 1mM EDTA			
TOP2B Core with mAMSA	445-1201	Human	Post-crystallisation drug replacement. hTop2βcore–DNA–etoposide crystal transferred to 100mM magnesium acetate, 50mM 2-(N-morpholino) ethanesulfonic acid (pH 5.8) and 30% 2-methyl-2,4-pentanediol. Then 1 mM mAMSA added.	6.5mg/ml protein, 2mM etoposide and DNA substrate at 1.2-fold molar ratio to protein, 30mM Tris-HCl pH 7.5, 70mM NaCl, 2mM βmercaptoethanol, and 1mM EDTA	Crystals grew at 4 °C within 1 week in hanging drops. 2.70 Å resolution.	4G0U	Wu *et al.*, 2013
TOP2B Core with Mitoxantrone	445-1201	Human	Post-crystallisation drug replacement. hTop2βcore–DNA–etoposide crystal transferred to 100mM magnesium acetate, 50mM 2-(N-morpholino)ethanesulfonic acid (pH 5.8) and 30% 2-methyl-2,4-pentanediol. Then 1mM Mitoxantrone added.	6.5mg/ml protein, 2mM etoposide and DNA substrate at 1.2-fold molar ratio to protein, 30mM Tris-HCl pH 7.5, 70mM NaCl, 2mM βmercaptoethanol, and 1mM EDTA	Crystals grew at 4 °C within 1 week in hanging drops. 2.55 Å resolution.	4G0V	Wu *et al.*, 2013
TOP2B Core with Ametantrone	445-1201	Human	Post-crystallisation drug replacement. hTop2βcore–DNA–etoposide crystal transferred to 100mM magnesium acetate, 50mM 2-(N-morpholino)ethanesulfonic acid (pH 5.8) and 30% 2-methyl-2,4-pentanediol. Then 1mM Ametantrone added.	6.5mg/ml protein, 2mM etoposide and DNA substrate at 1.2-fold molar ratio to protein, 30mM Tris-HCl pH 7.5, 70mM NaCl, 2mM βmercaptoethanol, and 1mM EDTA	Crystals grew at 4 °C within 1 week in hanging drops. 2.70 Å resolution.	4G0W	Wu *et al.*, 2013

Protein	Residues	Species	Crystallisation Condition	Protein Condition	Comment	PDB Code	Reference
TOP2B Core with organoplatinum compound, etoplatin-N2β	445–1201	Human	Post-crystallisation drug replacement. hTop2βcore–DNA–etoposide crystal transferred to mother liquor containing 30% MPD at 4 °C. Then 1mM Etoplatin-N2β was added.	5 mg/ml protein, 1mM etoposide, ~34μM 20 bp dsDNA substrate, 50mM Tris–HCl pH 7.0, 200mM KCl, 5 M $MnCl_2$, 1mM EDTA, 2mM β-mercaptoethanol	Crystals grew at 4 °C within 2 weeks in hanging drops. 2.57 Å resolution.	5GWJ	Wang *et al.*, 2017
TOP2B Core with organoplatinum compound, etoplatin-N2α	445–1201	Human	Post-crystallisation drug replacement. hTop2βcore–DNA–etoposide transferred to mother liquor containing 30% MPD at 4 °C. Then 1mM Etoplatin-N2α added.	5 mg/ml protein, 1mM etoposide, ~34μM 20 bp dsDNA substrate, 50mM Tris–HCl pH 7.0, 200mM KCl, 5 M $MnCl_2$, 1mM EDTA, 2mM β-mercaptoethanol	Crystals grew at 4 °C within 2 weeks in hanging drops. 2.74 Å resolution.	5GWI	Wang *et al.*, 2017
TOP2B Core with G-DNA in open conformation	445-1201	Human	100mM magnesium acetate, 50mM 2-(N-morpholino) ethanesulfonic acid pH 5.8, 22% 2-methyl-2,4-pentanediol	5 mg/mL protein, 2mM etoposide or doxorubicin, 34μM DNA substrate, 30mM Tris HCl pH 7.0, 70mM NaCl, 2mM $MnCl_2$, 1mM EDTA, 2mM β-mercaptoethanol	Crystals grew at 4 °C within 2 weeks. 2.75 Å resolution.	5ZEN	Chen *et al.*, 2018
Yeast ATPase with ADPNP	1-413	*S. cerevisiae*	22% PEG1500, 50mM sodium cacodylate pH 6.5, 100mM KCl, 10% glycerol	12 mg/mL protein, 5mM Tris-HCl pH 7.5, 100mM KCl, 2mM ADPNP, 5mM $MgCl_2$	Crystals grew at 20 °C to 200 x 50 x 50μm after 4-6 days. 1.75 Å resolution.	1PVG	Classen *et al.,* 2003

Protein	Residues	Species	Crystallisation Condition	Protein Condition	Comment	PDB Code	Reference
Yeast ATPase with ICRF-187	1-413	*S. cerevisiae*	22% PEG1500, 50mM sodium cacodylate pH 6.5, 100mM KCl, 10% glycerol	12 mg/mL protein, 5mM Tris-HCl pH 7.5, 100mM KCl, 5mM ICRF-187, 2mM ADPNP, 5mM $MgCl_2$	Crystals grew at 20 °C to 200 x 50 x 50µm after 4-6 days. 1.90 Å resolution.	1QZR	Classen *et al.,* 2003
Yeast Core (T2O structure)	410-1202	*S. cerevisiae*	0.4% PEG3350, 30mM Cacodylate pH 6.4, 8mM $MgCl_2$, 290mM NaCl	12 mg/mL protein, 10mM HEPES pH 7.4, 270mM KCl, 0.1mM β-mercaptoethanol, 1µM leupeptin, 1µM pepstatin-A	Crystals grew at 4 °C to 250 x 250 x 150µM. 2.70 Å resolution.	1BGW	Berger *et al.,* 1996
Yeast Core (T2M structure)	410-1202	*S. cerevisiae*	1-2% PEG3350, 20-40mM Tris-HCl pH 8.0	12 mg/mL protein, 400mM ammonium acetate, 10mM Tris-HCl pH	Crystals grew at 4 °C to 100 x 200 x 400µM in 2-3 weeks. 2.50 Å resolution.	1BJT	Fass *et al.,* 1999
Yeast Core (bound to G-DNA)	408-1177	*S. cerevisiae*	12–20% PEG 1000, 100–250mM $MgCl_2$ and 100mM sodium cacodylate, pH 7.0	7.5 mg/mL protein, 1mM sodium orthovanadate and annealed DNA duplexes at a 1:1.3 monomer:DNA ratio in 50mM Tris 7.5, 200mM KCl and 2mM $MgCl_2$ buffer	Crystals grew at 4 °C in hanging drops. 3.00 Å resolution.	2RGR	Berger *et al.,* 2007
Yeast Apo Core (covalently linked to DNA)	408-1177	*S. cerevisiae*	1µL protein solution mixed with 1µL well solution containing 20% 1,4-butanediol and 100 mM sodium acetate (pH 4.5)	3.5–6mg/mL protein–DNA complex, 100mM KCl, 10mM Tris (pH 7.9) and 5mM $MnCl_2$. Oligonucleotides added at 1:1 molar ratio with protein.	Crystals grew at 18 °C in hanging drops. 2.50 Å resolution.	3L4J	Schmidt *et al.,* 2010

Protein	Residues	Species	Crystallisation Condition	Protein Condition	Comment	PDB Code	Reference
Yeast Core (bound to Zn)	408-1177	*S. cerevisiae*	Apo crystals soaked with metal ions. Apo crystals cross-linked by 0.09% glutaraldehyde. Crystal pH changed to pH 6.5 by adjusting the acetate buffer. Metal salt solutions added.	3.5–6mg/mL protein–DNA complex, 100mM KCl, 10mM Tris (pH 7.9) and 5 mM $MnCl_2$. Oligonucleotides added at 1:1 molar ratio with protein.	Crystals grew at 18 °C in hanging drops. 3.00 Å resolution.	3L4K	Schmidt *et al.,* 2010
Yeast ATPase and Core	1-1177	*S. cerevisiae*	23% PEG300, 100 mM Tris pH 8.0	5 mg/mL protein-DNA complex, 1mM AMPPNP, 20 mM Tris pH 7.9, 100 mM KCl and 5 mM $MgCl_2$	Crystals grew at 18 °C in hanging drops. 4.41 Å resolution.	4GFH	Schmidt *et al.,* 2012

Appendix 2A: Details of the conditions for the crystallography screen JCSG Plus

Number	Salt	Buffer	Precipitant
1	0.2 M lithium sulphate	0.1 M sodium acetate pH 4.5	50% w/v PEG 400
2	N/A	0.1 M sodium citrate pH 5.5	20% w/v PEG 3000
3	0.2 M ammonium citrate dibasic	N/A	20% w/v PEG 3350
4	0.02 M calcium chloride dihydrate	0.1 M sodium acetate pH 4.6	30% v/v MPD
5	0.2 M magnesium formate dihydrate	N/A	20% w/v PEG 3350
6	0.2 M lithium sulphate	0.1 M phosphate citrate pH 4.2	20% w/v PEG 1000
7	N/A	0.1 M CHES pH 9.5	20% w/v PEG 8000
8	0.2 M ammonium formate	N/A	20% w/v PEG 3350
9	0.2 M ammonium chloride	N/A	20% w/v PEG 3350
10	0.2 M potassium formate	N/A	20% w/v PEG 3350
11	0.2 M ammonium phosphate monobasic	0.1 M tris pH 8.5	50% v/v MPD
12	0.2 M potassium nitrate	N/A	20% w/v PEG 3350
13	0.8 M ammonium sulphate	0.1 M citrate pH 4.0	N/A
14	0.2 M sodium thiocyanate	N/A	20% w/v PEG 3350
15	N/A	0.1 M BICINE pH 9.0	20% w/v PEG 6000
16	N/A	0.1 M HEPES pH 7.5	10% w/v PEG 8000 8% v/v ethylene glycol

Number	Salt	Buffer	Precipitant
17	N/A	0.1 M sodium cacodylate pH 6.5	40% v/v MPD
			5% w/v PEG 8000
18	N/A	0.1 M phosphate citrate pH 4.2	40% v/v ethanol
			5% w/v PEG 1000
19	N/A	0.1 M sodium acetate pH 4.6	8% w/v PEG 4000
20	0.2 M magnesium chloride hexahydrate	0.1 M tris pH 7.0	10% w/v PEG 8000
21	N/A	0.1 M citrate pH 5.0	20% w/v PEG 6000
22	0.2 M magnesium chloride hexahydrate	0.1 M sodium cacodylate pH 6.5	50% v/v PEG 200
23	1.6 M sodium citrate tribasic dihydrate	N/A	N/A
24	0.2 M potassium citrate tribasic monohydrate	N/A	20% w/v PEG 3350
25	0.2 M sodium chloride	0.1 M phosphate citrate pH 4.2	20% w/v PEG 8000
26	1 M lithium chloride	0.1 M citrate pH 4.0	20% w/v PEG 6000
27	0.2 M ammonium nitrate	N/A	20% w/v PEG 3350
28	N/A	0.1 M HEPES pH 7.0	10% w/v PEG 6000
29	0.8 M sodium phosphate monobasic monohydrate	0.1 M sodium HEPES pH 7.5	N/A
	0.8 M potassium phosphate monobasic		
30	N/A	0.1 M phosphate citrate pH 4.2	40% v/v PEG 300
31	0.2 M zinc acetate dihydrate	0.1 M sodium acetate pH 4.5	10% w/v PEG 3000

Number	Salt	Buffer	Precipitant
32	N/A	0.1 M tris pH 8.5	20% v/v ethanol
33	N/A	0.1 M sodium potassium phosphate pH 6.2	25% v/v 1,2-Propanediol
			10% v/v glycerol
34	N/A	0.1 M BICINE pH 9.0	10% w/v PEG 20,000
			2% v/v 1,4-Dioxane
35	2 M ammonium sulphate	0.1 M sodium acetate pH 4.6	N/A
36	N/A	N/A	10% w/v PEG 1000
			10% w/v PEG 8000
37	N/A	N/A	24% w/v PEG 1500
			20% v/v Glycerol
38	0.2 M magnesium chloride hexahydrate	0.1 M sodium HEPES pH 7.5	30% v/v PEG 400
39	0.2 M sodium chloride	0.1 M sodium potassium phosphate pH 6.2	50% v/v PEG 200
40	0.2 M lithium sulphate	0.1 M sodium acetate pH 4.5	30% w/v PEG 8000
41	N/A	0.1 M HEPES pH 7.5	70% v/v MPD
42	0.2 M magnesium chloride hexahydrate	0.1 M tris pH 8.5	20% w/v PEG 8000
43	0.2 M lithium sulphate	0.1 M tris pH 8.5	40% v/v PEG 400
44	N/A	0.1 M tris pH 8.0	40% v/v MPD
45	0.17 M ammonium sulphate	N/A	25.5% w/v PEG 4000
			15% v/v glycerol

Number	Salt	Buffer	Precipitant
46	0.2 M calcium acetate hydrate	0.1 M sodium cacodylate pH 6.5	40% v/v PEG 300
47	0.14 M calcium chloride dihydrate	0.07 M sodium acetate pH 4.6	14% v/v 2-Propanol
			30% v/v glycerol
48	0.04 M potassium phosphate monobasic	N/A	16% w/v PEG 8000
			20% v/v glycerol
49	1 M sodium citrate tribasic dihydrate	0.1 M sodium cacodylate pH 6.5	N/A
50	2 M ammonium sulphate	0.1 M sodium cacodylate pH 6.5	N/A
	0.2 M sodium chloride		
51	0.2 M sodium chloride	0.1 M HEPES pH 7.5	10% v/v 2-Propanol
52	1.26 M ammonium sulphate	0.1 M tris pH 8.5	N/A
	0.2 M lithium sulphate		
53	N/A	0.1 M CAPS pH 10.5	40% v/v MPD
54	0.2 M zinc acetate dihydrate	0.1 M imidazole pH 8.0	20% w/v PEG 3000
55	0.2 M zinc acetate dihydrate	0.1 M sodium cacodylate pH 6.5	10% v/v 2-Propanol
56	1 M ammonium phosphate dibasic	0.1 M sodium acetate pH 4.5	N/A
57	1.6 M magnesium sulphate heptahydrate	0.1 M MES pH 6.5	N/A
58	N/A	0.1 M BICINE pH 9.0	10% w/v PEG 6000
59	0.16 M calcium acetate hydrate		14.4% w/v PEG 8000

Number	Salt	Buffer	Precipitant
		0.08 M sodium cacodylate pH 6.5	20% v/v glycerol
60	N/A	0.1 M imidazole pH 8.0	10% w/v PEG 8000
61	0.05 M caesium chloride	0.1 M MES pH 6.5	30% v/v Jeffamine M-600
62	3.2 M ammonium sulphate	0.1 M citrate pH 5.0	None
63	N/A	0.1 M tris pH 8.0	20% v/v MPD
64	N/A	0.1 M HEPES pH 7.5	20% v/v Jeffamine M-600
65	0.2 M magnesium chloride hexahydrate	0.1 M tris pH 8.5	50% v/v ethylene glycol
66	N/A	0.1 M BICINE pH 9.0	10% v/v MPD
67	0.8 M succinic acid	N/A	N/A
68	2.1 M DL-Malic acid	N/A	N/A
69	2.4 M sodium malonate dibasic monohydrate	N/A	N/A
70	1.1 M sodium malonate dibasic monohydrate	0.1 M HEPES pH 7.0	0.5% v/v Jeffamine ED-2003
71	1 M succinic acid	0.1 M HEPES pH 7.0	1% w/v PEG 2000 MME
72	N/A	0.1 M HEPES pH 7.0	30% v/v Jeffamine M-600
73	N/A	0.1 M HEPES pH 7.0	30% v/v Jeffamine ED-2003
74	0.02 M magnesium chloride hexahydrate	0.1 M HEPES pH 7.5	22% w/v Poly (acrylic acid sodium salt) 5100
75	0.01 M cobalt (II) chloride hexahydrate	0.1 M tris pH 8.5	20% w/v polyvinylpyrolidone

Number	Salt	Buffer	Precipitant
76	0.2 M TMAO	0.1 M tris pH 8.5	20% w/v PEG 2000 MME
77	0.005 M cobalt (II) chloride hexahydrate	0.1 M HEPES pH 7.5	12% w/v PEG 3350
	0.005 M cadmium chloride hemi(pentahydrate)		
	0.005 M magnesium chloride hexahydrate		
	0.005 M nickel (II) chloride hexahydrate		
78	0.2 M sodium malonate dibasic monohydrate	N/A	20% w/v PEG 3350
79	0.1 M succinic acid	N/A	15% w/v PEG 3350
80	0.15 M DL-Malic acid	N/A	20% w/v PEG 3350
81	0.1 M potassium thiocyanate	N/A	30% w/v PEG 2000 MME
82	0.15 M potassium bromide	N/A	30% w/v PEG 2000 MME
83	2 M ammonium sulphate	0.1 M Bis-Tris pH 5.5	N/A
84	3 M sodium chloride	0.1 M Bis-Tris pH 5.5	N/A
85	0.3 M magnesium formate dihydrate	0.1 M Bis-Tris pH 5.5	N/A
86	1 M ammonium sulphate	0.1 M Bis-Tris pH 5.5	1% w/v PEG 3350
87	N/A	0.1 M Bis-Tris pH 5.5	25% w/v PEG 3350
88	0.2 M calcium chloride dihydrate	0.1 M Bis-Tris pH 5.5	45% v/v MPD
89	0.2 M ammonium acetate	0.1 M Bis-Tris pH 5.5	45% v/v MPD
90	0.1 M ammonium acetate	0.1 M Bis-Tris pH 5.5	17% w/v PEG 10,000
91	0.2 M ammonium sulphate	0.1 M Bis-Tris pH 5.5	25% w/v PEG 3350

Number	Salt	Buffer	Precipitant
92	0.2 M sodium chloride	0.1 M Bis-Tris pH 5.5	25% w/v PEG 3350
93	0.2 M lithium sulphate	0.1 M Bis-Tris pH 5.5	25% w/v PEG 3350
94	0.2 M ammonium acetate	0.1 M Bis-Tris pH 5.5	25% w/v PEG 3350
95	0.2 M magnesium chloride hexahydrate	0.1 M Bis-Tris pH 5.5	25% w/v PEG 3350
96	0.2 M ammonium acetate	0.1 M HEPES pH 7.5	45% v/v MPD

Appendix 2B: Details of the conditions for the crystallography screen PACT Premier

Number	Salt	Buffer	Precipitant
1	N/A	0.1 M SPG pH 4.0	25% w/v PEG 1500
2	N/A	0.1 M SPG pH 5.0	25% w/v PEG 1500
3	N/A	0.1 M SPG pH 6.0	25% w/v PEG 1500
4	N/A	0.1 M SPG pH 7.0	25% w/v PEG 1500
5	N/A	0.1 M SPG pH 8.0	25% w/v PEG 1500
6	N/A	0.1 M SPG pH 9.0	25% w/v PEG 1500
7	0.2 M sodium chloride	0.1 M sodium acetate pH 5.0	20% w/v PEG 6000
8	0.2 M ammonium chloride	0.1 M sodium acetate pH 5.0	20% w/v PEG 6000
9	0.2 M lithium chloride	0.1 M sodium acetate pH 5.0	20% w/v PEG 6000
10	0.2 M magnesium chloride hexahydrate	0.1 M sodium acetate pH 5.0	20% w/v PEG 6000
11	0.2 M calcium chloride dihydrate	0.1 M sodium acetate pH 5.0	20% w/v PEG 6000
12	0.01 M zinc chloride	0.1 M sodium acetate pH 5.0	20% w/v PEG 6000
13	N/A	0.1 M MIB pH 4.0	25% w/v PEG 1500
14	N/A	0.1 M MIB pH 5.0	25% w/v PEG 1500
15	N/A	0.1 M MIB pH 6.0	25% w/v PEG 1500
16	N/A	0.1 M MIB pH 7.0	25% w/v PEG 1500
17	N/A	0.1 M MIB pH 8.0	25% w/v PEG 1500

Number	Salt	Buffer	Precipitant
18	N/A	0.1 M MIB pH 9.0	25% w/v PEG 1500
19	0.2 M sodium chloride	0.1 M MES pH 6.0	20% w/v PEG 6000
20	0.2 M ammonium chloride	0.1 M MES pH 6.0	20% w/v PEG 6000
21	0.2 M lithium chloride	0.1 M MES pH 6.0	20% w/v PEG 6000
22	0.2 M magnesium chloride hexahydrate	0.1 M MES pH 6.0	20% w/v PEG 6000
23	0.2 M calcium chloride dihydrate	0.1 M MES pH 6.0	20% w/v PEG 6000
24	0.01 M zinc chloride	0.1 M MES pH 6.0	20% w/v PEG 6000
25	N/A	0.1 M PCTP pH 4.0	25% w/v PEG 1500
26	N/A	0.1 M PCTP pH 5.0	25% w/v PEG 1500
27	N/A	0.1 M PCTP pH 6.0	25% w/v PEG 1500
28	N/A	0.1 M PCTP pH 7.0	25% w/v PEG 1500
29	N/A	0.1 M PCTP pH 8.0	25% w/v PEG 1500
30	N/A	0.1 M PCTP pH 9.0	25% w/v PEG 1500
31	0.2 M sodium chloride	0.1 M HEPES pH 7.0	20% w/v PEG 6000
32	0.2 M ammonium chloride	0.1 M HEPES pH 7.0	20% w/v PEG 6000
33	0.2 M lithium chloride	0.1 M HEPES pH 7.0	20% w/v PEG 6000
34	0.2 M magnesium chloride hexahydrate	0.1 M HEPES pH 7.0	20% w/v PEG 6000
35	0.2 M calcium chloride hexahydrate	0.1 M HEPES pH 7.0	20% w/v PEG 6000
36	0.01 M zinc chloride	0.1 M HEPES pH 7.0	20% w/v PEG 6000
37	N/A	0.1 M MMT pH 4.0	25% w/v PEG 1500

Number	Salt	Buffer	Precipitant
38	N/A	0.1 M MMT pH 5.0	25% w/v PEG 1500
39	N/A	0.1 M MMT pH 6.0	25% w/v PEG 1500
40	N/A	0.1 M MMT pH 7.0	25% w/v PEG 1500
41	N/A	0.1 M MMT pH 8.0	25% w/v PEG 1500
42	N/A	0.1 M MMT pH 9.0	25% w/v PEG 1500
43	0.2 M sodium chloride	0.1 M tris pH 8.0	20% w/v PEG 6000
44	0.2 M ammonium chloride	0.1 M tris pH 8.0	20% w/v PEG 6000
45	0.2 M lithium chloride	0.1 M tris pH 8.0	20% w/v PEG 6000
46	0.2 M magnesium chloride hexahydrate	0.1 M tris pH 8.0	20% w/v PEG 6000
47	0.2 M calcium chloride dihydrate	0.1 M tris pH 8.0	20% w/v PEG 6000
48	0.002 M zinc chloride	0.1 M tris pH 8.0	20% w/v PEG 6000
49	0.2 M sodium fluoride	N/A	20% w/v PEG 3350
50	0.2 M sodium bromide	N/A	20% w/v PEG 3350
51	0.2 M sodium iodide	N/A	20% w/v PEG 3350
52	0.2 M potassium thiocyanate	N/A	20% w/v PEG 3350
53	0.2 M sodium nitrate	N/A	20% w/v PEG 3350
54	0.2 M sodium formate	N/A	20% w/v PEG 3350
55	0.2 M sodium acetate trihydrate	N/A	20% w/v PEG 3350
56	0.2 M sodium sulphate	N/A	20% w/v PEG 3350
57	0.2 M potassium sodium tartrate tetrahydrate	N/A	20% w/v PEG 3350

Number	Salt	Buffer	Precipitant
58	0.02 M sodium potassium phosphate	N/A	20% w/v PEG 3350
59	0.2 M sodium citrate tribasic dihydrate	N/A	20% w/v PEG 3350
60	0.2 M sodium malonate dibasic monohydrate	N/A	20% w/v PEG 3350
61	0.2 M sodium fluoride	0.1 M Bis-Tris propane pH 6.5	20% w/v PEG 3350
62	0.2 M sodium bromide	0.1 M Bis-Tris propane pH 6.5	20% w/v PEG 3350
63	0.2 M sodium iodide	0.1 M Bis-Tris propane pH 6.5	20% w/v PEG 3350
64	0.2 M potassium thiocyanate	0.1 M Bis-Tris propane pH 6.5	20% w/v PEG 3350
65	0.2 M sodium nitrate	0.1 M Bis-Tris propane pH 6.5	20% w/v PEG 3350
66	0.2 M sodium formate	0.1 M Bis-Tris propane pH 6.5	20% w/v PEG 3350
67	0.2 M sodium acetate trihydrate	0.1 M Bis-Tris propane pH 6.5	20% w/v PEG 3350
68	0.2 M sodium sulphate	0.1 M Bis-Tris propane pH 6.5	20% w/v PEG 3350
69	0.2 M potassium sodium tartrate tetrahydrate	0.1 M Bis-Tris propane pH 6.5	20% w/v PEG 3350
70	0.02 M sodium potassium phosphate	0.1 M Bis-Tris propane pH 6.5	20% w/v PEG 3350
71	0.2 M sodium citrate tribasic dihydrate	0.1 M Bis-Tris propane pH 6.5	20% w/v PEG 3350
72	0.2 M sodium malonate dibasic monohydrate	0.1 M Bis-Tris propane pH 6.5	20% w/v PEG 3350
73	0.2 M sodium fluoride	0.1 M Bis-Tris propane pH 7.5	20% w/v PEG 3350
74	0.2 M sodium bromide	0.1 M Bis-Tris propane pH 7.5	20% w/v PEG 3350
75	0.2 M sodium iodide	0.1 M Bis-Tris propane pH 7.5	20% w/v PEG 3350

Number	Salt	Buffer	Precipitant
76	0.2 M potassium thiocyanate	0.1 M Bis-Tris propane pH 7.5	20% w/v PEG 3350
77	0.2 M sodium nitrate	0.1 M Bis-Tris propane pH 7.5	20% w/v PEG 3350
78	0.2 M sodium formate	0.1 M Bis-Tris propane pH 7.5	20% w/v PEG 3350
79	0.2 M sodium acetate trihydrate	0.1 M Bis-Tris propane pH 7.5	20% w/v PEG 3350
80	0.2 M sodium sulphate	0.1 M Bis-Tris propane pH 7.5	20% w/v PEG 3350
81	0.2 M potassium sodium tartrate tetrahydrate	0.1 M Bis-Tris propane pH 7.5	20% w/v PEG 3350
82	0.02 M sodium potassium phosphate	0.1 M Bis-Tris propane pH 7.5	20% w/v PEG 3350
83	0.2 M sodium citrate tribasic dihydrate	0.1 M Bis-Tris propane pH 7.5	20% w/v PEG 3350
84	0.2 M sodium malonate dibasic monohydrate	0.1 M Bis-Tris propane pH 7.5	20% w/v PEG 3350
85	0.2 M sodium fluoride	0.1 M Bis-Tris propane pH 8.5	20% w/v PEG 3350
86	0.2 M sodium bromide	0.1 M Bis-Tris propane pH 8.5	20% w/v PEG 3350
87	0.2 M sodium iodide	0.1 M Bis-Tris propane pH 8.5	20% w/v PEG 3350
88	0.2 M potassium thiocyanate	0.1 M Bis-Tris propane pH 8.5	20% w/v PEG 3350
89	0.2 M sodium nitrate	0.1 M Bis-Tris propane pH 8.5	20% w/v PEG 3350
90	0.2 M sodium formate	0.1 M Bis-Tris propane pH 8.5	20% w/v PEG 3350
91	0.2 M sodium acetate trihydrate	0.1 M Bis-Tris propane pH 8.5	20% w/v PEG 3350
92	0.2 M sodium sulphate	0.1 M Bis-Tris propane pH 8.5	20% w/v PEG 3350
93	0.2 M potassium sodium tartrate tetrahydrate	0.1 M Bis-Tris propane pH 8.5	20% w/v PEG 3350

Number	Salt	Buffer	Precipitant
94	0.02 M sodium potassium phosphate	0.1 M Bis-Tris propane pH 8.5	20% w/v PEG 3350
95	0.2 M sodium citrate tribasic dihydrate	0.1 M Bis-Tris propane pH 8.5	20% w/v PEG 3350
96	0.2 M sodium malonate dibasic monohydrate	0.1 M Bis-Tris propane pH 8.5	20% w/v PEG 3350

Appendix 2C: Details of the conditions for the crystallography screen Structure

Number	Salt	Buffer	Precipitant
1	0.02 M calcium chloride dihydrate	0.1 M sodium acetate pH 4.6	30% v/v MPD
2	0.2 M ammonium acetate	0.1 M sodium acetate pH 4.6	30% w/v PEG 4000
3	0.2 M ammonium sulphate	0.1 M sodium acetate pH 4.6	25% w/v PEG 4000
4	2 M sodium formate	0.1 M sodium acetate pH 4.6	N/A
5	2 M ammonium sulphate	0.1 M sodium acetate pH 4.6	N/A
6	N/A	0.1 M sodium acetate pH 4.6	8% w/v PEG 4000
7	0.2 M ammonium acetate	0.1 M sodium citrate pH 5.6	30% w/v PEG 4000
8	0.2 M ammonium acetate	0.1 M sodium citrate pH 5.6	30% v/v MPD 20% v/v 2-Propanol
9	N/A	0.1 M sodium citrate pH 5.6	20% w/v PEG 4000
10	1 M ammonium phosphate monobasic	0.1 M sodium citrate pH 5.6	N/A
11	0.2 M calcium chloride dihydrate	0.1 M sodium acetate pH 4.6	20% v/v 2-Propanol
12	1.4 M sodium acetate trihydrate	0.1 M sodium cacodylate pH 6.5	N/A
13	0.2 M sodium citrate tribasic dihydrate	0.1 M sodium cacodylate pH 6.5	30% v/v 2-Propanol
14	0.2 M ammonium sulphate	0.1 M sodium cacodylate pH 6.5	30% w/v PEG 8000

Number	Salt	Buffer	Precipitant
15	0.2 M magnesium acetate tetrahydrate	0.1 M sodium cacodylate pH 6.5	20% w/v PEG 8000
16	0.2 M magnesium acetate tetrahydrate	0.1 M sodium cacodylate pH 6.5	30% v/v MPD
17	1 M sodium acetate trihydrate	0.1 M imidazole pH 6.5	N/A
18	0.2 M sodium acetate trihydrate	0.1 M sodium cacodylate pH 6.5	30% w/v PEG 8000
19	0.2 M zinc acetate dihydrate	0.1 M sodium cacodylate pH 6.5	18% w/v PEG 8000
20	0.2 M calcium acetate hydrate	0.1 M sodium cacodylate pH 6.5	18% w/v PEG 8000
21	0.2 M sodium citrate tribasic dihydrate	0.1 M sodium HEPES pH 7.5	30% v/v MPD
22	0.2 M magnesium chloride hexahydrate	0.1 M sodium HEPES pH 7.5	30% v/v 2-Propanol
23	0.2 M calcium chloride dihydrate	0.1 M sodium HEPES pH 7.5	28% v/v PEG 400
24	0.2 M magnesium chloride hexahydrate	0.1 M sodium HEPES pH 7.5	30% v/v PEG 400
25	0.2 M sodium citrate tribasic dihydrate	0.1 M sodium HEPES pH 7.5	20% v/v 2-Propanol
26	0.8 M potassium sodium tartrate tetrahydrate	0.1 M sodium HEPES pH 7.5	N/A
27	1.5 M lithium sulphate	0.1 M sodium HEPES pH 7.5	N/A
28	0.8 M sodium phosphate monobasic monohydrate	0.1 M sodium HEPES pH 7.5	N/A
29	1.4 M sodium citrate tribasic dihydrate	0.1 M sodium HEPES pH 7.5	N/A

Number	Salt	Buffer	Precipitant
30	2 M ammonium sulphate	0.1 M sodium HEPES pH 7.5	2% v/v PEG 400
31	N/A	0.1 M sodium HEPES pH 7.5	20% w/v PEG 4000 10% v/v 2-Propanol
32	2 M ammonium sulphate	0.1 M tris pH 8.5	N/A
33	0.2 M magnesium chloride hexahydrate	0.1 M tris pH 8.5	30% w/v PEG 4000
34	0.2 M sodium citrate tribasic dihydrate	0.1 M tris pH 8.5	30% v/v PEG 400
35	0.2 M lithium sulphate	0.1 M tris pH 8.5	30% w/v PEG 4000
36	0.2 M ammonium acetate	0.1 M tris pH 8.5	30% v/v 2-Propanol
37	0.2 M sodium acetate trihydrate	0.1 M tris pH 8.5	30% w/v PEG 4000
38	N/A	0.1 M tris pH 8.5	8% w/v PEG 8000
39	2 M ammonium phosphate monobasic	0.1 M tris pH 8.5	N/A
40	0.4 M potassium sodium tartrate tetrahydrate	N/A	N/A
41	0.4 M ammonium phosphate monobasic	N/A	N/A
42	0.2 M ammonium sulphate	N/A	30% w/v PEG 8000
43	0.2 M ammonium sulphate	N/A	30% w/v PEG 4000
44	2 M ammonium sulphate	N/A	N/A
45	4 M sodium formate	N/A	N/A
46	0.05 M potassium phosphate monobasic	N/A	N/A
47	N/A	N/A	30% w/v PEG 1500
48	0.2 M magnesium formate dihydrate	N/A	N/A

Number	Salt	Buffer	Precipitant
49	1 M lithium sulphate	N/A	2% w/v PEG 8000
50	0.5 M lithium sulphate	N/A	15% w/v PEG 8000
51	0.1 M sodium chloride	0.1 M BICINE pH 9.0	30% v/v PEG 500 MME
52	2 M magnesium chloride hexahydrate	0.1 M BICINE pH 9.0	N/A
53	N/A	0.1 M BICINE pH 9.0	10% w/v PEG 20000
54	N/A	0.1 M tris pH 8.5	3.4 M 1,6-Hexanediol
55	N/A	0.1 M tris pH 8.5	25% v/v tert-Butanol
56	1 M lithium sulphate	0.1 M tris pH 8.5	N/A
57	1.5 M ammonium sulphate	0.1 M tris pH 8.5	12% v/v glycerol
58	0.2 M ammonium phosphate monobasic	0.1 M tris pH 8.5	50% v/v MPD
59	N/A	0.1 M tris pH 8.5	20% v/v ethanol
60	0.01 M nickel (II) chloride hexahydrate	0.1 M tris pH 8.5	20% w/v PEG 2000 MME
61	0.5 M ammonium sulphate	0.1 M sodium HEPES pH 7.5	30% v/v MPD
62	N/A	0.1 M sodium HEPES pH 7.5	10% w/v PEG 6000
63	N/A	0.1 M sodium HEPES pH 7.5	20% v/v Jeffamine M-600
64	1.6 M ammonium sulphate	0.1 M sodium HEPES pH 7.5	N/A
65	2 M ammonium formate	0.1 M sodium HEPES pH 7.5	N/A
66	1 M sodium acetate trihydrate	0.1 M sodium HEPES pH 7.5	N/A
67	N/A	0.1 M sodium HEPES pH 7.5	70% v/v MPD
68	4.3 M sodium chloride	0.1 M sodium HEPES pH 7.5	N/A

Number	Salt	Buffer	Precipitant
69	N/A	0.1 M sodium HEPES pH 7.5	10% w/v PEG 8000
70	1.6 M magnesium sulphate heptahydrate	0.1 M MES pH 6.5	N/A
71	2 M sodium chloride	0.1 M MES pH 6.5	N/A
72	N/A	0.1 M MES pH 6.5	12% w/v PEG 20000
73	1.6 M ammonium sulphate	0.1 M MES pH 6.5	10% v/v 1,4-Dioxane
74	0.05 M caesium chloride	0.1 M MES pH 6.5	30% v/v Jeffamine M-600
75	0.01 M cobalt (II) chloride hexahydrate	0.1 M MES pH 6.5	N/A
76	0.2 M ammonium sulphate	0.1 M MES pH 6.5	30% w/v PEG 5000 MME
77	0.01 M zinc sulphate heptahydrate	0.1 M MES pH 6.5	25% v/v PEG 500 MME
78	N/A	0.1 M sodium HEPES pH 7.5	20% w/v PEG 10000
79	2 M ammonium sulphate	0.1 M sodium citrate pH 5.6	N/A
80	1 M lithium sulphate	0.1 M sodium citrate pH 5.6	N/A
81	0.5 M sodium chloride	0.1 M sodium citrate pH 5.6	4% v/v Polyethyleneimine
82	N/A	0.1 M sodium citrate pH 5.6	35% v/v tert-Butanol
83	0.01 M iron (III) chloride hexahydrate	0.1 M sodium citrate pH 5.6	10% v/v Jeffamine M-600
84	N/A	0.1 M sodium citrate pH 5.6	2.5 M 1,6-Hexanediol
85	2 M sodium chloride	0.1 M sodium acetate pH 4.6	N/A
86	0.2 M sodium chloride	0.1 M sodium acetate pH 4.6	30% v/v MPD
87	0.01 M cobalt (II) chloride hexahydrate	0.1 M sodium acetate pH 4.6	1 M 1,6-Hexanediol
88	0.1 M cadmium chloride hemi(pentahydrate)	0.1 M sodium acetate pH 4.6	30% v/v PEG 400

Number	Salt	Buffer	Precipitant
89	0.2 M ammonium sulphate	0.1 M sodium acetate pH 4.6	30% w/v PEG 2000 MME
90	2 M sodium chloride	N/A	10% w/v PEG 6000
91	0.5 M sodium chloride	N/A	25% v/v ethylene glycol
92	N/A	N/A	35% v/v 1,4-Dioxane
93	2 M ammonium sulphate	N/A	5% v/v 2-Propanol
94	N/A	1 M imidazole pH 7.0	10% w/v PEG 1000
95	1.5 M sodium chloride	N/A	N/A
96	N/A	1.6 M sodium citrate pH 6.5	10% v/v ethanol

Appendix 2D: Details of the conditions for the crystallography screen Index

Number	Salt	Buffer	Precipitant
1	2.0 M ammonium sulphate	0.1 M citric acid pH 3.5	N/A
2	2.0 M ammonium sulphate	0.1 M sodium acetate trihydrate pH 4.5	N/A
3	2.0 M ammonium sulphate	0.1 M BIS-TRIS pH 5.5	N/A
4	2.0 M ammonium sulphate	0.1 M BIS-TRIS pH 6.5	N/A
5	2.0 M ammonium sulphate	0.1 M HEPES pH 7.5	N/A
6	2.0 M ammonium sulphate	0.1 M tris pH 8.5	N/A
7	3.0 M sodium chloride	0.1 M citric acid pH 3.5	N/A
8	3.0 M sodium chloride	0.1 M sodium acetate trihydrate pH 4.5	N/A
9	3.0 M sodium chloride	0.1 M BIS-TRIS pH 5.5	N/A
10	3.0 M sodium chloride	0.1 M BIS-TRIS pH 6.5	N/A
11	3.0 M sodium chloride	0.1 M HEPES pH 7.5	N/A
12	3.0 M sodium chloride	0.1 M tris pH 8.5	N/A
13	0.3 M magnesium formate dihydrate	0.1 M BIS-TRIS pH 5.5	N/A
14	0.5 M magnesium formate dihydrate	0.1 M BIS-TRIS pH 6.5	N/A
15	0.5 M magnesium formate dihydrate	0.1 M HEPES pH 7.5	N/A
16	0.3 M magnesium formate dihydrate	0.1 M tris pH 8.5	N/A

Number	Salt	Buffer	Precipitant
17	1.26 M sodium phosphate monobasic monohydrate	N/A	N/A
18	0.14 M potassium phosphate dibasic	N/A	N/A
19	0.49 M sodium phosphate monobasic monohydrate	N/A	N/A
20	0.91 M potassium phosphate dibasic	0.1 M HEPES pH 7.5	N/A
21	0.056 M sodium phosphate monobasic monohydrate	N/A	N/A
22	1.344 M potassium phosphate dibasic	N/A	N/A
23	1.4 M sodium citrate tribasic dihydrate	N/A	N/A
24	1.8 M ammonium citrate tribasic pH 7.0	N/A	N/A
25	0.8 M succinic acid pH 7.0	N/A	N/A
26	2.1 M DL-Malic acid pH 7.0	N/A	N/A
27	2.8 M sodium acetate trihydrate pH 7.0	N/A	N/A
28	3.5 M sodium formate pH 7.0	N/A	N/A
29	1.1 M ammonium tartrate dibasic pH 7.0	N/A	N/A
30	2.4 M sodium malonate pH 7.0 0.1 M sodium chloride	0.1 M BIS-TRIS pH 6.5	N/A
31	0.8 M potassium sodium tartrate tetrahydrate	0.1 M tris pH 8.5	35% v/v Tacsimate TM pH 7.0
32	1.0 M ammonium sulphate	0.1 M BIS-TRIS pH 5.5	60% v/v Tacsimate TM pH 7.0
33	1.1 M sodium malonate pH 7.0	0.1 M HEPES pH 7.0	

Number	Salt	Buffer	Precipitant
	1.5 M ammonium sulphate		
34	1.0 M succinic acid pH 7.0	0.1 M HEPES pH 7.0	0.5% w/v PEG Monomethyl Ether 5000
35	1.0 M ammonium sulphate	0.1 M HEPES pH 7.0	1% w/v PEG 3350
36	15% v/v Tacsimate TM pH 7.0	0.1 M HEPES pH 7.0	0.5% v/v Jeffamine ED-2001 pH 7.0
37	N/A	N/A	1% w/v PEG Monomethyl Ether 2000
38	N/A	0.1 M HEPES pH 7.0	0.5% w/v PEG 8000
39	N/A	0.1 M HEPES pH 7.0	2% w/v PEG 3350
40	N/A	0.1 M citric acid pH 3.5	25% w/v PEG 1500
41	N/A	0.1 M sodium acetate trihydrate pH 4.5	30% v/v Jeffamine M-600 ® pH 7.0
42	N/A	0.1 M BIS-TRIS pH 5.5	30% v/v Jeffamine ED-2001 pH 7.0
43	N/A	0.1 M BIS-TRIS pH 6.5	25% w/v PEG 3350
44	N/A	0.1 M HEPES pH 7.5	25% w/v PEG 3350
45	N/A	0.1 M tris pH 8.5	25% w/v PEG 3350
46	N/A	0.1 M BIS-TRIS pH 6.5	25% w/v PEG 3350
47	N/A	0.1 M BIS-TRIS pH 6.5	25% w/v PEG 3350
48	0.2 M calcium chloride dihydrate	0.1 M BIS-TRIS pH 5.5	25 % w/v PEG 3350 20% w/v PEG Monomethyl Ether 5000 28% w/v PEG Monomethyl Ether 2000 45% v/v (+/-)-2-Methyl-2,4-pentanediol
49	0.2 M calcium chloride dihydrate	0.1 M BIS-TRIS pH 6.5	45% v/v (+/-)-2-Methyl-2,4-pentanediol

Number	Salt	Buffer	Precipitant
50	0.2 M ammonium acetate	0.1 M BIS-TRIS pH 5.5	45% v/v (+/-)-2-Methyl-2,4-pentanediol
51	0.2 M ammonium acetate	0.1 M BIS-TRIS pH 6.5	45% v/v (+/-)-2-Methyl-2,4-pentanediol
52	0.2 M ammonium acetate	0.1 M HEPES pH 7.5	45% v/v (+/-)-2-Methyl-2,4-pentanediol
53	0.2 M ammonium acetate	0.1 M tris pH 8.5	45% v/v (+/-)-2-Methyl-2,4-pentanediol
54	0.05 M calcium chloride dihydrate	0.1 M BIS-TRIS pH 6.5	30% v/v PEG Monomethyl Ether 550
55	0.05 M magnesium chloride hexahydrate	0.1 M HEPES pH 7.5	30% v/v PEG Monomethyl Ether 550
56	0.2 M potassium chloride	0.05 M HEPES pH 7.5	35% v/v Pentaerythritol Propoxylate (5/4 PO/OH)
57	0.05 M ammonium sulphate	0.05 M BIS-TRIS pH 6.5	30% v/v Pentaerythritol Ethoxylate (15/4 EO/OH)
58	N/A	0.1 M BIS-TRIS pH 6.5	45% v/v PEG 400
59	0.02 M magnesium chloride hexahydrate	0.1 M HEPES pH 7.5	22% w/v Poly (acrylic acid sodium salt) 5100
60	0.01 M cobalt (II) chloride hexahydrate	0.1 M tris pH 8.5	20% w/v Polyvinylpyrrolidone K 15
61	0.2 M L-Proline	0.1 M HEPES pH 7.5	10% w/v PEG 3350
62	0.2 M Trimethylamine N-oxide Dihydrate	0.1 M tris pH 8.5	20% w/v PEG Monomethyl Ether 2000
63	5 % v/v Tacsimate TM pH 7.0	0.1 M HEPES pH 7.0	10% w/v PEG Monomethyl Ether 5000
64	0.005 M cobalt (II) chloride hexahydrate	0.1 M HEPES pH 7.5	12% w/v PEG 3350
65	0.005 M nickel (II) chloride hexahydrate	0.1 M BIS-TRIS pH 5.5	17% w/v PEG 10000
66	0.005 M cadmium chloride hydrate	0.1 M BIS-TRIS pH 5.5	25% w/v PEG 3350
67	0.005 M magnesium chloride hexahydrate	0.1 M BIS-TRIS pH 6.5	25% w/v PEG 3350

Number	Salt	Buffer	Precipitant
68	0.1 M ammonium acetate	0.1 M HEPES pH 7.5	25% w/v PEG 3350
69	0.2 M ammonium sulphate	0.1 M tris pH 8.5	25% w/v PEG 3350
70	0.2 M ammonium sulphate	0.1 M BIS-TRIS pH 5.5	25% w/v PEG 3350
71	0.2 M ammonium sulphate	0.1 M BIS-TRIS pH 6.5	25% w/v PEG 3350
72	0.2 M ammonium sulphate	0.1 M HEPES pH 7.5	25% w/v PEG 3350
73	0.2 M sodium chloride	0.1 M tris pH 8.5	25% w/v PEG 3350
74	0.2 M sodium chloride	0.1 M BIS-TRIS pH 5.5	25% w/v PEG 3350
75	0.2 M sodium chloride	0.1 M BIS-TRIS pH 6.5	25% w/v PEG 3350
76	0.2 M sodium chloride	0.1 M HEPES pH 7.5	25% w/v PEG 3350
77	0.2 M lithium sulphate monohydrate	0.1 M tris pH 8.5	25% w/v PEG 3350
78	0.2 M lithium sulphate monohydrate	0.1 M BIS-TRIS pH 5.5	25% w/v PEG 3350
79	0.2 M lithium sulphate monohydrate	0.1 M BIS-TRIS pH 6.5	25% w/v PEG 3350
80	0.2 M lithium sulphate monohydrate	0.1 M HEPES pH 7.5	25% w/v PEG 3350
81	0.2 M ammonium acetate	0.1 M tris pH 8.5	25% w/v PEG 3350
82	0.2 M ammonium acetate	0.1 M BIS-TRIS pH 5.5	25% w/v PEG 3350
83	0.2 M ammonium acetate	0.1 M BIS-TRIS pH 6.5	25% w/v PEG 3350
84	0.2 M ammonium acetate	0.1 M HEPES pH 7.5	25% w/v PEG 3350
85	0.2 M magnesium chloride hexahydrate	0.1 M tris pH 8.5	25% w/v PEG 3350
86	0.2 M magnesium chloride hexahydrate	N/A	20% w/v PEG 3350
87	0.2 M magnesium chloride hexahydrate	N/A	20% w/v PEG 3350

Number	Salt	Buffer	Precipitant
88	0.2 M magnesium chloride hexahydrate	N/A	20% w/v PEG 3350
89	0.2 M potassium sodium tartrate tetrahydrate	N/A	15% w/v PEG 3350
90	0.2 M sodium malonate pH 7.0	N/A	20% w/v PEG 3350
91	0.2 M ammonium citrate tribasic pH 7.0	N/A	20% w/v PEG 3350
92	0.1 M succinic acid pH 7.0	N/A	15% w/v PEG 3350
93	0.2 M sodium formate	N/A	20% w/v PEG 3350
94	0.15 M DL-Malic acid pH 7.0	N/A	20% w/v PEG 3350
95	0.1 M magnesium formate dihydrate	N/A	30% w/v PEG Monomethyl Ether 2000
96	0.05 M zinc acetate dihydrate 0.2 M sodium citrate tribasic dihydrate 0.1 M potassium thiocyanate 0.15 M potassium bromide	N/A	30% w/v PEG Monomethyl Ether 2000

Appendix 2E: Details of the conditions for the crystallography screen Morpheus II

Number	Salt	Buffer	Precipitant
1	N/A	0.1 M HEPES pH 6	50% v/v polypropylene glycol 400 %% v/v dimethyl sulfoxide
2	N/A	0.1 M MES pH 5.5	12% w/v polyvinylpyrrolidone
3	N/A	0.1 M HEPES pH 6.5	45% w/v poly(acrylic acid sodium salt) 2100
4	N/A	N/A	14% v/v poly(acrylic acid-co-maleic acid)
5	0.5 M ammonium phosphate monobasic	N/A	12.5% w/v poly(acrylic acid sodium salt) 2100
6	N/A	0.1 M tris pH 8.5	19% v/v poly(acrylic acid-co-maleic acid)
7	N/A	N/A	10% v/v polypropylene glycol 400
8	N/A	N/A	5% w/v poly(acrylic acid sodium salt) 2100
9	N/A	0.1 M MES pH 6.0	25% v/v pentaerythritol propoxylate (5/4 PO/OH)
10	0.1 M sodium sulphate	N/A	24% w/v polyvinylpyrrolidone
11	0.2 M calcium chloride dihydrate	0.1 M HEPES pH 6.5	35% v/v pentaerythritol ethoxylate (15/4 EO/OH)
12	N/A	0.1 M potassium sodium phosphate pH 7.0	35% v/v polypropylene glycol 400
13	0.1 M sodium formate	N/A	20% w/v SOKALAN CP 45

Number	Salt	Buffer	Precipitant
14	0.2 M sodium thiocyanate	0.1 M HEPES pH 7.0	15% v/v pentaerythritol propoxylate (5/4 PO/OH)
15	0.1 M sodium chloride	0.1 M HEPES pH 7.0	25% w/v SOKALAN PA 25 CL
16	0.2 M sodium chloride	0.1 M MES pH 6.0	45% v/v pentaerythritol propoxylate (5/4 PO/OH)
17	N/A	0.1 M HEPES pH 7.0	8% w/v polyvinyl alcohol 10% v/v 1-Propanol
18	0.1 M lithium sulphate	0.1 M HEPES pH 7.0	30% w/v polyvinylpyrrolidone
19	N/A	0.2 M imidazole pH 7.0	40% v/v polypropylene glycol 400
20	0.06 M lithium sulphate	0.1 M HEPES pH 7.5	8% v/v poly(acrylic acid-co-maleic acid) 3% v/v pentaerythritol ethoxylate (3/4 EO/OH)
21	0.1 M sodium tartrate dibasic dihydrate	0.1 M HEPES pH 7.0	20% w/v SOKALAN PA 25 CL
22	N/A	N/A	30% v/v Jeffamine M-600 10% v/v Dimethyl Sulfoxide
23	N/A	N/A	20% v/v polypropylene glycol 400 10% v/v 1-Propanol
24	N/A	0.1 M HEPES pH 6.5	28% v/v poly(acrylic acid-co-maleic acid)
25	N/A	N/A	15% v/v Jeffamine ED-2003 10% v/v ethanol
26	0.2 M sodium chloride	0.1 M MES pH 6.0	30% v/v Jeffamine ED-2003
27	0.1 M sodium malonate dibasic monohydrate	0.1 M MES pH 5.5	25% w/v SOKALAN CP 45

Number	Salt	Buffer	Precipitant
28	0.2 M sodium chloride	0.1 M MES pH 6.0	15% v/v pentaerythritol propoxylate (5/4 PO/OH)
29	0.2 M magnesium chloride hexahydrate	magnesium chloride hexahydrate	35% v/v pentaerythritol ethoxylate (3/4 EO/OH)
30	N/A	N/A	40% v/v pentaerythritol propoxylate (5/4 PO/OH) 15% v/v ethanol
31	N	0.1 M tris pH 8.0	50% v/v pentaerythritol propoxylate (5/4 PO/OH)
32	0.2 M sodium chloride	0.1 M tris pH 8.0	12.5% w/v polyvinylpyrrolidone 10% w/v PEG 4000
33	0.1 M sodium chloride	N/A	25% v/v pentaerythritol propoxylate (5/4 PO/OH) 10% v/v dimethyl sulfoxide
34	0.2 M ammonium sulphate	0.1 M HEPES pH 7.5	35% w/v poly(acrylic acid sodium salt) 2100
35	0.1 M magnesium formate dihydrate	0.1 M tris pH 8.5	30% v/v pentaerythritol ethoxylate (15/4 EO/OH)
36	0.2 M potassium acetate	N/A	24% v/v poly(acrylic acid-co-maleic acid)
37	N/A	0.1 M tris pH 8.0	60% v/v polypropylene glycol 400
38	N/A	0.1 M HEPES pH 7.5	30% v/v pentaerythritol ethoxylate (15/4 EO/OH) 6% w/v polyvinylpyrrolidone
39	N/A	N/A	45% v/v polypropylene glycol 400

Number	Salt	Buffer	Precipitant
			10% v/v ethanol
40	N/A	N/A	10% v/v pentaerythritol ethoxylate (3/4 EO/OH) 10% v/v 1-Butanol
41	N/A	0.1 M HEPES pH 7.0	12.5% w/v poly(acrylic acid sodium salt) 2100 6% v/v PPGBA 2000
42	N/A	0.1 M HEPES pH 6.5	6% w/v polyvinylpyrrolidone
43	N/A	0.1 M HEPES pH 6.5	20% v/v Jeffamine ED-2003
44	N/A	0.1 M tris pH 8.0	20% v/v glycerol ethoxylate 10% v/v tetrahydrofuran
45	N/A	0.2 M imidazole pH 7.0	25% v/v PPGBA 2000
46	0.2 M potassium chloride	0.1 M HEPES pH 6.5	30% v/v PPGBA 230
47	0.1 M sodium chloride	N/A	30% v/v polypropylene glycol 400
48	N/A	N/A	20% v/v PPGBA 400 15% v/v 1-Propanol
49	0.1 M lithium citrate tribasic tetrahydrate	0.1 M tris pH 8.5	15% v/v PPGBA 400
50	0.2 M potassium acetate	N/A	35% v/v pentaerythritol propoxylate (5/4 PO/OH)
51	0.2 M potassium chloride	0.1 M glycine pH 9.5	20% v/v pentaerythritol ethoxylate (15/4 EO/OH)
52	0.2 M sodium thiocyanate	0.1 M HEPES pH 7.0	40% v/v pentaerythritol propoxylate (5/4 PO/OH)

Number	Salt	Buffer	Precipitant
53	N/A	N/A	25% w/v SOKALAN CP 45
54	0.2 M potassium acetate	0.1 M MES pH 6.0	15% v/v pentaerythritol ethoxylate (15/4 EO/OH)
55	0.1 M sodium malonate dibasic monohydrate	0.1 M HEPES pH 7.0	30% w/v poly(acrylic acid sodium salt) 2100
56	N/A	N/A	10% v/v PPGBA 230 10% v/v Jeffamine M-600
57	0.1 M lithium sulphate	0.1 M tris pH 8.0	25% v/v Jeffamine ED-2003
58	N/A	0.1 M tris pH 8.0	20% w/v SOKALAN PA 25 CL
59	0.1 M lithium sulphate	0.1 M HEPES pH 6.5	25% w/v poly(acrylic acid sodium salt) 2100
60	0.2 M magnesium chloride hexahydrate	0.1 M HEPES pH 7.5	15% w/v poly(acrylic acid sodium salt) 2100
61	N/A	0.1 M HEPES pH 6.5	40% v/v PPGBA 2000
62	0.5 M sodium chloride	0.1 M tris pH 8.0	10% w/v poly(acrylic acid sodium salt) 2100
63	N/A	0.1 M potassium sodium phosphate pH 7.0	10% v/v PPGBA 230 15% v/v PPGBA 400
64	0.2 M sodium chloride	0.1 M BICINE pH 9.0	20% w/v poly(acrylic acid sodium salt) 2100
65	0.2 M sodium malonate dibasic monohydrate	0.1 M MES pH 5.5	20% v/v PPGBA 2000
66	0.1 M caesium chloride	N/A	25% w/v SOKALAN CP 45

Number	Salt	Buffer	Precipitant
67	N/A	N/A	25% w/v SOKALAN PA 25 CL
68	0.2 M lithium nitrate	0.1 M Bis-Tris pH 6.5	30% v/v PPGBA 400
69	N/A	0.1 M tris pH 8.0	20% w/v poly(acrylic acid sodium salt) 5100
70	N/A	0.1 M HEPES pH 7.0	28% v/v polyethyleneimine
71	0.1 M ammonium formate	0.1 M HEPES pH 7.0	20% w/v SOKALAN CP 7
72	0.2 M sodium sulphate	0.1 M tris pH 8.0	20% w/v SOKALAN HP 56
73	0.1 M potassium chloride	0.1 M HEPES pH 7.0	25% w/v SOKALAN CP 7
74	0.3 M ammonium formate	0.1 M HEPES pH 7.0	20% w/v SOKALAN CP 5
75	N/A	N/A	40% v/v glycerol ethoxylate
76	N/A	0.1 M tris pH 8.5	30% v/v glycerol ethoxylate
77	N/A	N/A	55% v/v polypropylene glycol 400
78	0.2 M lithium citrate tribasic tetrahydrate	N/A	35% v/v glycerol ethoxylate
79	0.2 M ammonium acetate	0.1 M MES pH 6.5	30% v/v glycerol ethoxylate
80	N/A	0.1 M tris pH 8.0	20% w/v SOKALAN CP 42 5% v/v methanol
81	N/A	0.1 M tris pH 7.0	25% w/v SOKALAN CP 42 10% v/v tetrahydrofuran
82	0.1 M lithium acetate dihydrate	0.1 M Bis-Tris pH 6.0	20% w/v SOKALAN CP 42
83	0.1 M sodium chloride	0.1 M Bis-Tris pH 5.5	20% v/v PPGBA 400
84	N/A	0.1 M Bis-Tris pH 6.0	15% w/v SOKALAN CP 5

Number	Salt	Buffer	Precipitant
85	N/A	0.1 M Bis-Tris pH 6.0	25% w/v SOKALAN CP 42
86	0.2 M ammonium formate	N/A	25% v/v PPGBA 400
87	N/A	0.1 M tris pH 8.5	20% v/v glycerol ethoxylate 3% v/v polyethyleneimine
88	0.2 M ammonium chloride	0.1 M HEPES pH 7.5	25% v/v glycerol ethoxylate
89	N/A	0.1 M Tris pH 8.5	10% w/v SOKALAN CP 42
90	N/A	0.1 M MES pH 6.0	30% w/v poly(acrylic acid sodium salt) 5100 10% v/v ethanol
91	0.2 M potassium citrate tribasic monohydrate	N/A	15% w/v SOKALAN CP 42
92	N/A	0.1 M tris pH 8.5	30% w/v SOKALAN CP 42
93	0.2 M ammonium acetate	0.1 M HEPES pH 7.0	25% w/v SOKALAN HP 56
94	N/A	0.1 M tris pH 8.5	25% w/v SOKALAN CP 5
95	0.2 M ammonium formate	N/A	10% w/v polyvinylpyrrolidone 20% w/v PEG 4000
96	N/A	0.1 M tris pH 8.0	15% w/v polyvinylpyrrolidone 25% w/v PEG 5000 MME

References

Ackerman, P., C. Glover and N. Osheroff (1985). "Phosphorylation of DNA topoisomerase II by casein kinase II: modulation of eukaryotic topoisomerase II activity in vitro." Proceedings of the National Academy of Sciences **82**(10): 3164-3168.

Ackerman, P., C. V. Glover and N. Osheroff (1988). "Phosphorylation of DNA topoisomerase II in vivo and in total homogenates of Drosophila Kc cells. The role of casein kinase II." J Biol Chem **263**(25): 12653-12660.

Adachi, N., M. Miyaike, S. Kato, R. Kanamaru, H. Koyama and A. Kikuchi (1997). "Cellular distribution of mammalian DNA topoisomerase II is determined by its catalytically dispensable C-terminal domain." Nucleic Acids Res **25**(15): 3135-3142.

Adachi, Y., M. Luke and U. K. Laemmli (1991). "Chromosome assembly in vitro: topoisomerase II is required for condensation." Cell **64**(1): 137-148.

Adams, D. E., E. M. Shekhtman, E. L. Zechiedrich, M. B. Schmid and N. R. Cozzarelli (1992). "The role of topoisomerase IV in partitioning bacterial replicons and the structure of catenated intermediates in DNA replication." Cell **71**(2): 277-288.

Adolph, K., S. Cheng, J. Paulson and U. Laemmli (1977). "Isolation of a protein scaffold from mitotic HeLa cell chromosomes." Proceedings of the National Academy of Sciences **74**(11): 4937-4941.

Agostinho, M., V. Santos, F. Ferreira, R. Costa, J. Cardoso, I. Pinheiro, J. Rino, E. Jaffray, R. T. Hay and J. Ferreira (2008). "Conjugation of human topoisomerase 2 alpha with small ubiquitin-like modifiers 2/3 in response to topoisomerase inhibitors: cell cycle stage and chromosome domain specificity." Cancer Res **68**(7): 2409-2418.

Akimitsu, N., N. Adachi, H. Hirai, M. S. Hossain, H. Hamamoto, M. Kobayashi, Y. Aratani, H. Koyama and K. Sekimizu (2003). "Enforced cytokinesis without complete nuclear division in embryonic cells depleting the activity of DNA topoisomerase IIalpha." Genes Cells **8**(4): 393-402.

Ali, J. A., A. P. Jackson, A. J. Howells and A. Maxwell (1993). "The 43-kilodalton N-terminal fragment of the DNA gyrase B protein hydrolyzes ATP and binds coumarin drugs." Biochemistry **32**(10): 2717-2724.

Aoyama, M., D. R. Grabowski, G. R. Dubyak, A. I. Constantinou, L. A. Rybicki, R. M. Bukowski, M. K. Ganapathi, I. D. Hickson and R. Ganapathi (1998). "Attenuation of drug-stimulated topoisomerase II-DNA cleavable complex formation in wild-type HL-60 cells treated with an intracellular calcium buffer is correlated with decreased cytotoxicity and site-specific hypophosphorylation of topoisomerase IIalpha." Biochem J **336 (Pt 3)**(Pt 3): 727-733.

Aravind, L., D. D. Leipe and E. V. Koonin (1998). "Toprim--a conserved catalytic domain in type IA and II topoisomerases, DnaG-type primases, OLD family nucleases and RecR proteins." Nucleic Acids Res **26**(18): 4205-4213.

Arndt-Jovin, D. J., A. Udvardy, M. M. Garner, S. Ritter and T. M. Jovin (1993). "Z-DNA binding and inhibition by GTP of Drosophila topoisomerase II." Biochemistry **32**(18): 4862-4872.

Asano, T., K. Nakamura, H. Fujii, N. Horichi, T. Ohmori, K. Hasegawa, T. Isoe, M. Adachi, N. Otake and Y. Fukunaga (2005). "Altered expression of topoisomerase IIalpha contributes to cross-resistant to etoposide K562/MX2 cell line by aberrant methylation." Br J Cancer **92**(8): 1486-1492.

Atwal, M., R. L. Swan, C. Rowe, K. C. Lee, D. C. Lee, L. Armstrong, I. G. Cowell and C. A. Austin (2019). "Intercalating TOP2 Poisons Attenuate Topoisomerase Action at Higher Concentrations." Mol Pharmacol **96**(4): 475-484.

Austin, C. A., I. G. Cowell, M. M. Khazeem, D. Lok and H. T. Ng (2021). "TOP2B's contributions to transcription." Biochem Soc Trans **49**(6): 2483-2493.

Austin, C. A. and L. M. Fisher (1990). "Isolation and characterization of a human cDNA clone encoding a novel DNA topoisomerase II homologue from HeLa cells." FEBS Lett **266**(1-2): 115-117.

Austin, C. A., K. L. Marsh, R. A. Wasserman, E. Willmore, P. J. Sayer, J. C. Wang and L. M. Fisher (1995). "Expression, domain structure, and enzymatic properties of an active recombinant human DNA topoisomerase IIβ." Journal of Biological Chemistry **270**(26): 15739-15746.

Austin, C. A., J. H. Sng, S. Patel and L. M. Fisher (1993). "Novel HeLa topoisomerase II is the II beta isoform: complete coding sequence and homology with other type II topoisomerases." Biochim Biophys Acta **1172**(3): 283-291.

Azuma, Y., A. Arnaoutov, T. Anan and M. Dasso (2005). "PIASy mediates SUMO-2 conjugation of Topoisomerase-II on mitotic chromosomes." Embo j **24**(12): 2172-2182.

Baguley, B. C. and L. R. Ferguson (1998). "Mutagenic properties of topoisomerase-targeted drugs." Biochimica et Biophysica Acta (BBA)-Gene Structure and Expression **1400**(1-3): 213-222.

Baird, C. L., T. T. Harkins, S. K. Morris and J. E. Lindsley (1999). "Topoisomerase II drives DNA transport by hydrolyzing one ATP." Proc Natl Acad Sci U S A **96**(24): 13685-13690.

Ban, C. and W. Yang (1998). "Crystal structure and ATPase activity of MutL: implications for DNA repair and mutagenesis." Cell **95**(4): 541-552.

Bansal, N., C. Joshi, M. J. Adams, K. Hutchins, A. Ray and S. E. Lipshultz (2021). "Cardiotoxicity in pediatric lymphoma survivors." Expert Rev Cardiovasc Ther **19**(11): 957-974.

Barnard, F. M. and A. Maxwell (2001). "Interaction between DNA gyrase and quinolones: effects of alanine mutations at GyrA subunit residues Ser(83) and Asp(87)." Antimicrob Agents Chemother **45**(7): 1994-2000.

Bartlett, J., J. Blagojevic, D. Carter, C. Eskiw, M. Fromaget, C. Job, M. Shamsher, I. F. Trindade, M. Xu and P. R. Cook (2006). "Specialized transcription factories." Biochem Soc Symp(73): 67-75.

Bates, A. D. and A. Maxwell (2005). DNA topology, Oxford University Press, USA.

Bauer, W. R., F. H. Crick and J. H. White (1980). "Supercoiled DNA." Sci Am **243**(1): 100-113.

Baxter, J. and L. Aragón (2012). "A model for chromosome condensation based on the interplay between condensin and topoisomerase II." Trends Genet **28**(3): 110-117.

Bedez, C., C. Lotz, C. Batisse, A. V. Broeck, R. H. Stote, E. Howard, K. Pradeau-Aubreton, M. Ruff and V. Lamour (2018). "Post-translational modifications in DNA topoisomerase 2α highlight the role of a eukaryote-specific residue in the ATPase domain." Scientific Reports **8**(1): 9272.

Been, M. D. and J. J. Champoux (1981). "DNA breakage and closure by rat liver type 1 topoisomerase: separation of the half-reactions by using a single-stranded DNA substrate." Proceedings of the National Academy of Sciences **78**(5): 2883-2887.

Berger, J. M., D. Fass, J. C. Wang and S. C. Harrison (1998). "Structural similarities between topoisomerases that cleave one or both DNA strands." Proceedings of the National Academy of Sciences **95**(14): 7876.

Berger, J. M., S. J. Gamblin, S. C. Harrison and J. C. Wang (1996). "Structure and mechanism of DNA topoisomerase II." Nature **379**(6562): 225-232.

Bergerat, A., B. de Massy, D. Gadelle, P. C. Varoutas, A. Nicolas and P. Forterre (1997). "An atypical topoisomerase II from Archaea with implications for meiotic recombination." Nature **386**(6623): 414-417.

Bergerat, A., D. Gadelle and P. Forterre (1994). "Purification of a DNA topoisomerase II from the hyperthermophilic archaeon Sulfolobus shibatae. A thermostable enzyme with both bacterial and eucaryal features." Journal of Biological Chemistry **269**(44): 27663-27669.

Berman, H. M. (1977). "Biochemical Method: Protein Crystallography T. L. Blundell and L. N. Johnson. Academic Press, New York, 1976. Molecular Biology." Science **196**(4285): 50-50.

Berrios, M., N. Osheroff and P. A. Fisher (1985). "In situ localization of DNA topoisomerase II, a major polypeptide component of the Drosophila nuclear matrix fraction." Proceedings of the National Academy of Sciences **82**(12): 4142-4146.

Bessette, P. H., F. Aslund, J. Beckwith and G. Georgiou (1999). "Efficient folding of proteins with multiple disulfide bonds in the Escherichia coli cytoplasm." Proc Natl Acad Sci U S A **96**(24): 13703-13708.

Bjergbaek, L., P. Kingma, I. S. Nielsen, Y. Wang, O. Westergaard, N. Osheroff and A. H. Andersen (2000). "Communication between the ATPase and cleavage/religation domains of human topoisomerase IIalpha." J Biol Chem **275**(17): 13041-13048.

Blower, T. R., A. Bandak, A. S. Y. Lee, C. A. Austin, J. L. Nitiss and J. M. Berger (2019). "A complex suite of loci and elements in eukaryotic type II topoisomerases determine selective sensitivity to distinct poisoning agents." Nucleic acids research **47**(15): 8163-8179.

Brill, S. J. (1987). "DNA Topoisomerase Activity Is Required as a Swivel for DNA Replication and for Ribosomal RNA Transcription1 Steven J. Brill, 2 Stephen DiNardo, 2 3 Karen Voelkel-Meiman, 2 and Rolf Sternglanz24." NCI monographs: a publication of the National Cancer Institute **4**(4): 11-15.

Broderick, L., G. M. Clay, R. H. Blum, Y. Liu, R. McVicar, F. Papes, L. M. Booshehri, I. G. Cowell, C. A. Austin, C. D. Putnam and D. S. Kaufman (2022). "Disease-associated mutations in topoisomerase IIβ result in defective NK cells." J Allergy Clin Immunol **149**(6): 2171-2176.e2173.

Broderick, L., S. Yost, D. Li, M. D. McGeough, L. M. Booshehri, M. Guaderrama, S. D. Brydges, K. Kucharova, N. C. Patel, M. Harr, H. Hakonarson, E. Zackai, I. G. Cowell, C. A. Austin, B. Hügle, C. Gebauer, J. Zhang, X. Xu, J. Wang, B. A. Croker, K. A. Frazer, C. D. Putnam and H. M. Hoffman (2019). "Mutations in topoisomerase IIβ result in a B cell immunodeficiency." Nature Communications **10**(1): 3644.

Bromberg, K. D., C. Hendricks, A. B. Burgin and N. Osheroff (2002). "Human topoisomerase IIalpha possesses an intrinsic nucleic acid specificity for DNA ligation. Use of 5' covalently

activated oligonucleotide substrates to study enzyme mechanism." J Biol Chem **277**(34): 31201-31206.

Brown, P. and N. Cozzarelli (1979). "A sign inversion mechanism for enzymatic supercoiling of DNA." Science **206**(4422): 1081-1083.

Bugg, B. Y., M. K. Danks, W. T. Beck and D. P. Suttle (1991). "Expression of a mutant DNA topoisomerase II in CCRF-CEM human leukemic cells selected for resistance to teniposide." Proc Natl Acad Sci U S A **88**(17): 7654-7658.

Burden, D. A. and N. Osheroff (1998). "Mechanism of action of eukaryotic topoisomerase II and drugs targeted to the enzyme." Biochim Biophys Acta **1400**(1-3): 139-154.

Burden, D. A. and N. Osheroff (1999). "In vitro evolution of preferred topoisomerase II DNA cleavage sites." J Biol Chem **274**(8): 5227-5235.

Burden, D. A. and D. M. Sullivan (1994). "Phosphorylation of the alpha- and beta-isoforms of DNA topoisomerase II is qualitatively different in interphase and mitosis in Chinese hamster ovary cells." Biochemistry **33**(49): 14651-14655.

Buss, J. L. and B. B. Hasinoff (1993). "The one-ring open hydrolysis product intermediates of the cardioprotective agent ICRF-187 (dexrazoxane) displace iron from iron-anthracycline complexes." Agents Actions **40**(1-2): 86-95.

Campbell, S. and A. Maxwell (2002). "The ATP-operated clamp of human DNA topoisomerase IIalpha: hyperstimulation of ATPase by "piggy-back" binding." J Mol Biol **320**(2): 171-188.

Canela, A., Y. Maman, S. Jung, N. Wong, E. Callen, A. Day, K. R. Kieffer-Kwon, A. Pekowska, H. Zhang, S. S. P. Rao, S. C. Huang, P. J. McKinnon, P. D. Aplan, Y. Pommier, E. L. Aiden, R. Casellas and A. Nussenzweig (2017). "Genome Organization Drives Chromosome Fragility." Cell **170**(3): 507-521.e518.

Capranico, G., S. Tinelli, C. A. Austin, M. L. Fisher and F. Zunino (1992). "Different patterns of gene expression of topoisomerase II isoforms in differentiated tissues during murine development." Biochim Biophys Acta **1132**(1): 43-48.

Cardenas, M. E., Q. Dang, C. Glover and S. M. Gasser (1992). "Casein kinase II phosphorylates the eukaryote-specific C-terminal domain of topoisomerase II in vivo." The EMBO Journal **11**(5): 1785-1796.

Cardenas, M. E. and S. M. Gasser (1993). "Regulation of topoisomerase II by phosphorylation: a role for casein kinase II." J Cell Sci **104 (Pt 2)**: 219-225.

Caron, P. R., P. Watt and J. C. Wang (1994). "The C-terminal domain of Saccharomyces cerevisiae DNA topoisomerase II." Mol Cell Biol **14**(5): 3197-3207.

Carpenter, A. J. and A. C. G. Porter (2004). "Construction, Characterization, and Complementation of a Conditional-Lethal DNA Topoisomerase IIα Mutant Human Cell Line." Molecular Biology of the Cell **15**(12): 5700-5711.

Cavalli, G., D. Bachmann and F. Thoma (1996). "Inactivation of topoisomerases affects transcription-dependent chromatin transitions in rDNA but not in a gene transcribed by RNA polymerase II." Embo j **15**(3): 590-597.

Chaly, N. and D. L. Brown (1996). "Is DNA topoisomerase IIβ a nucleolar protein?" Journal of Cellular Biochemistry **63**(2): 162-173.

Champoux, J. J. (2001). "DNA topoisomerases: structure, function, and mechanism." Annu Rev Biochem **70**: 369-413.

Champoux, J. J. and R. Dulbecco (1972). "An activity from mammalian cells that untwists superhelical DNA--a possible swivel for DNA replication (polyoma-ethidium bromide-mouse-embryo cells-dye binding assay)." Proc Natl Acad Sci U S A **69**(1): 143-146.

Champoux, J. J. and R. Dulbecco (1972). "An Activity from Mammalian Cells That Untwists Superhelical DNA—A Possible Swivel For DNA Replication." Proceedings of the National Academy of Sciences **69**(1): 143-146.

Chang, C. J., S. Goulding, W. C. Earnshaw and M. Carmena (2003). "RNAi analysis reveals an unexpected role for topoisomerase II in chromosome arm congression to a metaphase plate." J Cell Sci **116**(Pt 23): 4715-4726.

Chen, A. Y. and L. F. Liu (1994). "DNA topoisomerases: essential enzymes and lethal targets." Annu Rev Pharmacol Toxicol **34**: 191-218.

Chen, S. F., N. L. Huang, J. H. Lin, C. C. Wu, Y. R. Wang, Y. J. Yu, M. K. Gilson and N. L. Chan (2018). "Structural insights into the gating of DNA passage by the topoisomerase II DNA-gate." Nat Commun **9**(1): 3085.

Chikamori, K., D. R. Grabowski, M. Kinter, B. B. Willard, S. Yadav, R. H. Aebersold, R. M. Bukowski, I. D. Hickson, A. H. Andersen, R. Ganapathi and M. K. Ganapathi (2003). "Phosphorylation of serine 1106 in the catalytic domain of topoisomerase II alpha regulates enzymatic activity and drug sensitivity." J Biol Chem **278**(15): 12696-12702.

Choi, E. J. and S. L. Mayo (2006). "Generation and analysis of proline mutants in protein G." Protein Eng Des Sel **19**(6): 285-289.

Chung, T., F. H. Drake, K. Tan, S. R. Per, S. T. Crooke and C. K. Mirabelli (1989). "Characterization and immunological identification of cDNA clones encoding two human DNA topoisomerase II isozymes." Proceedings of the National Academy of Sciences **86**(23): 9431-9435.

Chung, T. D., F. H. Drake, K. B. Tan, S. R. Per, S. T. Crooke and C. K. Mirabelli (1989). "Characterization and immunological identification of cDNA clones encoding two human DNA topoisomerase II isozymes." Proc Natl Acad Sci U S A **86**(23): 9431-9435.

Clague, M. J., I. Barsukov, J. M. Coulson, H. Liu, D. J. Rigden and S. Urbé (2013). "Deubiquitylases From Genes to Organism." Physiological Reviews **93**(3): 1289-1315.

Clark, K. L., E. D. Halay, E. Lai and S. K. Burley (1993). "Co-crystal structure of the HNF-3/fork head DNA-recognition motif resembles histone H5." Nature **364**(6436): 412-420.

Classen, S., S. Olland and J. M. Berger (2003). "Structure of the topoisomerase II ATPase region and its mechanism of inhibition by the chemotherapeutic agent ICRF-187." Proceedings of the National Academy of Sciences **100**(19): 10629-10634.

Coldwell, K. E., S. M. Cutts, T. J. Ognibene, P. T. Henderson and D. R. Phillips (2008). "Detection of Adriamycin-DNA adducts by accelerator mass spectrometry at clinically relevant Adriamycin concentrations." Nucleic Acids Res **36**(16): e100.

Conde-Estévez, D., S. Saumell, A. Salar and J. Mateu-de Antonio (2010). "Successful dexrazoxane treatment of a potentially severe extravasation of concentrated doxorubicin." Anticancer Drugs **21**(8): 790-794.

Consortium, G. (2020). "The GTEx Consortium atlas of genetic regulatory effects across human tissues." Science **369**(6509): 1318-1330.

Constantinou, A., R. Mehta, C. Runyan, K. Rao, A. Vaughan and R. Moon (1995). "Flavonoids as DNA topoisomerase antagonists and poisons: structure-activity relationships." J Nat Prod **58**(2): 217-225.

Cook, P. R. and D. Marenduzzo (2018). "Transcription-driven genome organization: a model for chromosome structure and the regulation of gene expression tested through simulations." Nucleic Acids Res **46**(19): 9895-9906.

Corbett, A. H. and N. Osheroff (1993). "When good enzymes go bad: conversion of topoisomerase II to a cellular toxin by antineoplastic drugs." Chem Res Toxicol **6**(5): 585-597.

Corbett, A. H., E. L. Zechiedrich and N. Osheroff (1992). "A role for the passage helix in the DNA cleavage reaction of eukaryotic topoisomerase II. A two-site model for enzyme-mediated DNA cleavage." J Biol Chem **267**(2): 683-686.

Corbett, K. D. and J. M. Berger (2003). "Structure of the topoisomerase VI-B subunit: implications for type II topoisomerase mechanism and evolution." Embo j **22**(1): 151-163.

Corbett, K. D. and J. M. Berger (2004). "Structure, Molecular Mechanisms, and Evolutionary Relationships in DNA Topoisomerases." Annual Review of Biophysics and Biomolecular Structure **33**(1): 95-118.

Cowell, I. G., E. Willmore, D. Chalton, K. L. Marsh, E. Jazrawi, L. M. Fisher and C. A. Austin (1998). "Nuclear distribution of human DNA topoisomerase IIβ: a nuclear targeting signal resides in the 116-residue C-terminal tail." Experimental cell research **243**(2): 232-240.

Craig, N. L. (1988). "The mechanism of conservative site-specific recombination." Annu Rev Genet **22**: 77-105.

Crenshaw, D. G. and T. Hsieh (1993). "Function of the hydrophilic carboxyl terminus of type II DNA topoisomerase from Drosophila melanogaster. I. In vitro studies." Journal of Biological Chemistry **268**(28): 21328-21334.

Crenshaw, D. G. and T. Hsieh (1993). "Function of the hydrophilic carboxyl terminus of type II DNA topoisomerase from Drosophila melanogaster. II. In vivo studies." J Biol Chem **268**(28): 21335-21343.

Cullen, M. E., A. W. Wyke, R. Kuroda and L. M. Fisher (1989). "Cloning and characterization of a DNA gyrase A gene from Escherichia coli that confers clinical resistance to 4-quinolones." Antimicrob Agents Chemother **33**(6): 886-894.

Cuvier, O. and T. Hirano (2003). "A role of topoisomerase II in linking DNA replication to chromosome condensation." The Journal of cell biology **160**(5): 645-655.

D'Arcy, A. (1994). "Crystallizing proteins – a rational approach?" Acta Crystallographica Section D **50**(4): 469-471.

Dale, G. E., C. Oefner and A. D'Arcy (2003). "The protein as a variable in protein crystallization." J Struct Biol **142**(1): 88-97.

Danks, M. K., C. A. Schmidt, M. C. Cirtain, D. P. Suttle and W. T. Beck (1988). "Altered catalytic activity of and DNA cleavage by DNA topoisomerase II from human leukemic cells selected for resistance to VM-26." Biochemistry **27**(24): 8861-8869.

Danks, M. K., J. C. Yalowich and W. T. Beck (1987). "Atypical multiple drug resistance in a human leukemic cell line selected for resistance to teniposide (VM-26)." Cancer Research **47**(5): 1297-1301.

Davies, K. J. and J. H. Doroshow (1986). "Redox cycling of anthracyclines by cardiac mitochondria. I. Anthracycline radical formation by NADH dehydrogenase." J Biol Chem **261**(7): 3060-3067.

Davies, S. L., J. R. Jenkins and I. D. Hickson (1993). "Human cells express two differentially spliced forms of topoisomerase II beta mRNA." Nucleic acids research **21**(16): 3719-3723.

Dereuddre, S., C. Delaporte and A. Jacquemin-Sablon (1997). "Role of Topoisomerase IIβ in the Resistance of 9-OH-ellipticine-resistant Chinese Hamster Fibroblasts to Topoisomerase II Inhibitors." Cancer Research **57**(19): 4301-4308.

Dereuddre, S., S. Frey, C. Delaporte and A. Jacquemin-Sablon (1995). "Cloning and characterization of full-length cDNAs coding for the DNA topoisomerase II beta from Chinese hamster lung cells sensitive and resistant 9-OH-ellipticine." Biochim Biophys Acta **1264**(2): 178-182.

Dessau, M. A. and Y. Modis (2011). "Protein crystallization for X-ray crystallography." J Vis Exp(47).

Deweese, J. E. and N. Osheroff (2009). "The DNA cleavage reaction of topoisomerase II: wolf in sheep's clothing." Nucleic Acids Res **37**(3): 738-748.

Deweese, J. E. and N. Osheroff (2010). "The use of divalent metal ions by type II topoisomerases." Metallomics : integrated biometal science **2**(7): 450-459.

DiGate, R. J. and K. J. Marians (1989). "Molecular cloning and DNA sequence analysis of Escherichia coli topB, the gene encoding topoisomerase III." Journal of Biological Chemistry **264**(30): 17924-17930.

Dikic, I. and V. Dötsch (2009). "Ubiquitin linkages make a difference." Nat Struct Mol Biol **16**(12): 1209-1210.

DiNardo, S., K. Voelkel and R. Sternglanz (1984). "DNA topoisomerase II mutant of Saccharomyces cerevisiae: topoisomerase II is required for segregation of daughter molecules at the termination of DNA replication." Proceedings of the National Academy of Sciences **81**(9): 2616-2620.

Dixon, J. R., S. Selvaraj, F. Yue, A. Kim, Y. Li, Y. Shen, M. Hu, J. S. Liu and B. Ren (2012). "Topological domains in mammalian genomes identified by analysis of chromatin interactions." Nature **485**(7398): 376-380.

Dong, K. C. and J. M. Berger (2007). "Structural basis for gate-DNA recognition and bending by type IIA topoisomerases." Nature **450**(7173): 1201-1205.

Doroshow, J. H. (1983). "Effect of anthracycline antibiotics on oxygen radical formation in rat heart." Cancer Res **43**(2): 460-472.

Dovey, M., E. E. Patton, T. Bowman, T. North, W. Goessling, Y. Zhou and L. I. Zon (2009). "Topoisomerase II alpha is required for embryonic development and liver regeneration in zebrafish." Mol Cell Biol **29**(13): 3746-3753.

Drake, F. H., G. A. Hofmann, H. F. Bartus, M. R. Mattern, S. T. Crooke and C. K. Mirabelli (1989). "Biochemical and pharmacological properties of p170 and p180 forms of topoisomerase II." Biochemistry **28**(20): 8154-8160.

Dröge, P. (1994). "Protein tracking-induced supercoiling of DNA: A tool to regulate DNA transactions in vivo?" Bioessays **16**(2): 91-99.

Dutta, R. and M. Inouye (2000). "GHKL, an emergent ATPase/kinase superfamily." Trends Biochem Sci **25**(1): 24-28.

Earnshaw, W. C. and M. Heck (1985). "Localization of topoisomerase II in mitotic chromosomes." The Journal of cell biology **100**(5): 1716-1725.

Eijdems, E. W., M. de Haas, A. J. Timmerman, G. P. Van der Schans, E. Kamst, J. de Nooij, G. C. Astaldi Ricotti, P. Borst and F. Baas (1995). "Reduced topoisomerase II activity in multidrug-resistant human non-small cell lung cancer cell lines." Br J Cancer **71**(1): 40-47.

Emsley, P., B. Lohkamp, W. G. Scott and K. Cowtan (2010). "Features and development of Coot." Acta Crystallogr D Biol Crystallogr **66**(Pt 4): 486-501.

Erdős, M., Á. Lányi, G. Balázs, J. L. Casanova, B. Boisson and L. Maródi (2021). "Inherited TOP2B Mutation: Possible Confirmation of Mutational Hotspots in the TOPRIM Domain." J Clin Immunol **41**(4): 817-819.

Escargueil, A. E., S. Y. Plisov, O. Filhol, C. Cochet and A. K. Larsen (2000). "Mitotic phosphorylation of DNA topoisomerase II α by protein kinase CK2 creates the MPM-2 phosphoepitope on Ser-1469." Journal of Biological Chemistry **275**(44): 34710-34718.

Espeli, O. and K. J. Marians (2004). "Untangling intracellular DNA topology." Mol Microbiol **52**(4): 925-931.

Evans, P. R. and G. N. Murshudov (2013). "How good are my data and what is the resolution?" Acta Crystallogr D Biol Crystallogr **69**(Pt 7): 1204-1214.

Fachinetti, D., R. Bermejo, A. Cocito, S. Minardi, Y. Katou, Y. Kanoh, K. Shirahige, A. Azvolinsky, V. A. Zakian and M. Foiani (2010). "Replication termination at eukaryotic chromosomes is mediated by Top2 and occurs at genomic loci containing pausing elements." Mol Cell **39**(4): 595-605.

Falaschi, A., G. Abdurashidova, O. Sandoval, S. Radulescu, G. Biamonti and S. Riva (2007). "Molecular and structural transactions at human DNA replication origins." Cell Cycle **6**(14): 1705-1712.

Fass, D., C. E. Bogden and J. M. Berger (1999). "Quaternary changes in topoisomerase II may direct orthogonal movement of two DNA strands." Nat Struct Biol **6**(4): 322-326.

Feldhoff, P. W., S. E. Mirski, S. P. Cole and D. M. Sullivan (1994). "Altered subcellular distribution of topoisomerase IIα in a drug-resistant human small cell lung cancer cell line." Cancer research **54**(3): 756-762.

Fernandes, D. J., M. K. Danks and W. T. Beck (1990). "Decreased nuclear matrix DNA topoisomerase II in human leukemia cells resistant to VM-26 and m-AMSA." Biochemistry **29**(17): 4235-4241.

Fielding, A. B., M. Concannon, S. Darling, E. V. Rusilowicz-Jones, J. J. Sacco, I. A. Prior, M. J. Clague, S. Urbé and J. M. Coulson (2018). "The deubiquitylase USP15 regulates topoisomerase II alpha to maintain genome integrity." Oncogene **37**(17): 2326-2342.

Forrest, R. A., L. P. Swift, A. Rephaeli, A. Nudelman, K. Kimura, D. R. Phillips and S. M. Cutts (2012). "Activation of DNA damage response pathways as a consequence of anthracycline-DNA adduct formation." Biochem Pharmacol **83**(12): 1602-1612.

Fortune, J. M. and N. Osheroff (2000). "Topoisomerase II as a target for anticancer drugs: when enzymes stop being nice." Progress in nucleic acid research and molecular biology **64**: 221-253.

Froelich-Ammon, S. J., K. C. Gale and N. Osheroff (1994). "Site-specific cleavage of a DNA hairpin by topoisomerase II. DNA secondary structure as a determinant of enzyme recognition/cleavage." J Biol Chem **269**(10): 7719-7725.

Froelich-Ammon, S. J., M. W. Patchan, N. Osheroff and R. B. Thompson (1995). "Topoisomerase II binds to ellipticine in the absence or presence of DNA. Characterization of enzyme-drug interactions by fluorescence spectroscopy." J Biol Chem **270**(25): 14998-15004.

Fudenberg, G., M. Imakaev, C. Lu, A. Goloborodko, N. Abdennur and L. A. Mirny (2016). "Formation of Chromosomal Domains by Loop Extrusion." Cell Rep **15**(9): 2038-2049.

Fuxa, M. and M. Busslinger (2007). "Reporter gene insertions reveal a strictly B lymphoid-specific expression pattern of Pax5 in support of its B cell identity function." J Immunol **178**(5): 3031-3037.

Gadelle, D., C. Bocs, M. Graille and P. Forterre (2005). "Inhibition of archaeal growth and DNA topoisomerase VI activities by the Hsp90 inhibitor radicicol." Nucleic Acids Res **33**(7): 2310-2317.

Gadelle, D., J. Filée, C. Buhler and P. Forterre (2003). "Phylogenomics of type II DNA topoisomerases." Bioessays **25**(3): 232-242.

Ganapathi, R., A. Constantinou, N. Kamath, G. Dubyak, D. Grabowski and K. Krivacic (1996). "Resistance to etoposide in human leukemia HL-60 cells: reduction in drug-induced DNA cleavage associated with hypophosphorylation of topoisomerase II phosphopeptides." Mol Pharmacol **50**(2): 243-248.

Gangloff, S., M. R. Lieber and R. Rothstein (1994). "Transcription, topoisomerases and recombination." Experientia **50**(3): 261-269.

Gardiner, L. P., D. I. Roper, T. R. Hammonds and A. Maxwell (1998). "The N-terminal domain of human topoisomerase IIalpha is a DNA-dependent ATPase." Biochemistry **37**(48): 16997-17004.

Gartenberg, M. R. and J. C. Wang (1992). "Positive supercoiling of DNA greatly diminishes mRNA synthesis in yeast." Proc Natl Acad Sci U S A **89**(23): 11461-11465.

Gasser, S., T. Laroche, J. Falquet, E. B. De La Tour and U. Laemmli (1986). "Metaphase chromosome structure: involvement of topoisomerase II." Journal of molecular biology **188**(4): 613-629.

Gasser, S. M. and U. K. Laemmli (1986). "The organisation of chromatin loops: characterization of a scaffold attachment site." The EMBO Journal **5**(3): 511-518.

Gasser, S. M., R. Walter, Q. Dang and M. E. Cardenas (1992). "Topoisomerase II: its functions and phosphorylation." Antonie van Leeuwenhoek **62**(1): 15-24.

Geisberg, C. A. and D. B. Sawyer (2010). "Mechanisms of anthracycline cardiotoxicity and strategies to decrease cardiac damage." Current hypertension reports **12**(6): 404-410.

Gellert, M., K. Mizuuchi, M. H. O'Dea and H. A. Nash (1976). "DNA gyrase: an enzyme that introduces superhelical turns into DNA." Proceedings of the National Academy of Sciences **73**(11): 3872-3876.

Gernert, K. M., R. Smith and D. C. Carter (1988). "A simple apparatus for controlling nucleation and size in protein crystal growth." Anal Biochem **168**(1): 141-147.

Gilbert, N. and J. Allan (2014). "Supercoiling in DNA and chromatin." Curr Opin Genet Dev **25**(100): 15-21.

Gilroy, K. L. and C. A. Austin (2011). "The impact of the C-terminal domain on the interaction of human DNA topoisomerase II α and β with DNA." PLoS One **6**(2): e14693.

Glikin, G. C., T. M. Jovin and D. J. Arndt-Jovin (1991). "Interactions of Drosophila DNA topoisomerase II with left-handed Z-DNA in supercoiled minicircles." Nucleic Acids Res **19**(25): 7139-7144.

Goswami, P. C., J. L. Roti Roti and C. R. Hunt (1996). "The cell cycle-coupled expression of topoisomerase IIalpha during S phase is regulated by mRNA stability and is disrupted by heat shock or ionizing radiation." Mol Cell Biol **16**(4): 1500-1508.

Goto, T. and J. C. Wang (1984). "Yeast DNA topoisomerase II is encoded by a single-copy, essential gene." Cell **36**(4): 1073-1080.

Goto, T. and J. C. Wang (1985). "Cloning of yeast TOP1, the gene encoding DNA topoisomerase I, and construction of mutants defective in both DNA topoisomerase I and DNA topoisomerase II." Proceedings of the National Academy of Sciences **82**(21): 7178-7182.

Haffner, M. C., M. J. Aryee, A. Toubaji, D. M. Esopi, R. Albadine, B. Gurel, W. B. Isaacs, G. S. Bova, W. Liu, J. Xu, A. K. Meeker, G. Netto, A. M. De Marzo, W. G. Nelson and S. Yegnasubramanian (2010). "Androgen-induced TOP2B-mediated double-strand breaks and prostate cancer gene rearrangements." Nat Genet **42**(8): 668-675.

Hallett, P. and A. Maxwell (1991). "Novel quinolone resistance mutations of the Escherichia coli DNA gyrase A protein: enzymatic analysis of the mutant proteins." Antimicrob Agents Chemother **35**(2): 335-340.

Hammonds, T. R. and A. Maxwell (1997). "The DNA dependence of the ATPase activity of human DNA topoisomerase IIalpha." J Biol Chem **272**(51): 32696-32703.

Hammonds, T. R. and A. Maxwell (1997). "The DNA Dependence of the ATPase Activity of Human DNA Topoisomerase IIα." Journal of Biological Chemistry **272**(51): 32696-32703.

Harker, W. G., D. L. Slade, R. L. Parr, P. W. Feldhoff, D. M. Sullivan and M. H. Holguin (1995). "Alterations in the topoisomerase II alpha gene, messenger RNA, and subcellular protein distribution as well as reduced expression of the DNA topoisomerase II beta enzyme in a mitoxantrone-resistant HL-60 human leukemia cell line." Cancer Res **55**(8): 1707-1716.

Harkin, L. F., D. Gerrelli, D. C. Gold Diaz, C. Santos, A. Alzu'bi, C. A. Austin and G. J. Clowry (2016). "Distinct expression patterns for type II topoisomerases IIA and IIB in the early foetal human telencephalon." Journal of Anatomy **228**(3): 452-463.

Harkins, T. T., T. J. Lewis and J. E. Lindsley (1998). "Pre-steady-state analysis of ATP hydrolysis by Saccharomyces cerevisiae DNA topoisomerase II. 2. Kinetic mechanism for the sequential hydrolysis of two ATP." Biochemistry **37**(20): 7299-7312.

Hartsuiker, E., J. Bähler and J. Kohli (1998). "The role of topoisomerase II in meiotic chromosome condensation and segregation in Schizosaccharomyces pombe." Molecular biology of the cell **9**(10): 2739-2750.

Hasinoff, B. B., T. I. Kuschak, J. C. Yalowich and A. M. Creighton (1995). "A QSAR study comparing the cytotoxicity and DNA topoisomerase II inhibitory effects of bisdioxopiperazine analogs of ICRF-187 (dexrazoxane)." Biochem Pharmacol **50**(7): 953-958.

Hasinoff, B. B., D. Patel and X. Wu (2020). "A QSAR study that compares the ability of bisdioxopiperazine analogs of the doxorubicin cardioprotective agent dexrazoxane (ICRF-187) to protect myocytes with DNA topoisomerase II inhibition." Toxicol Appl Pharmacol **399**: 115038.

Hebditch, M., M. A. Carballo-Amador, S. Charonis, R. Curtis and J. Warwicker (2017). "Protein-Sol: a web tool for predicting protein solubility from sequence." Bioinformatics **33**(19): 3098-3100.

Heck, M., W. Hittelman and W. Earnshaw (1989). "In vivo phosphorylation of the 170-kDa form of eukaryotic DNA topoisomerase II. Cell cycle analysis." Journal of Biological Chemistry **264**(26): 15161-15164.

Heck, M. M., W. N. Hittelman and W. C. Earnshaw (1988). "Differential expression of DNA topoisomerases I and II during the eukaryotic cell cycle." Proc Natl Acad Sci U S A **85**(4): 1086-1090.

Hendriks, I. A., R. C. D'Souza, B. Yang, M. Verlaan-de Vries, M. Mann and A. C. Vertegaal (2014). "Uncovering global SUMOylation signaling networks in a site-specific manner." Nat Struct Mol Biol **21**(10): 927-936.

Herzog, C. E., K. A. Holmes, L. M. Tuschong, R. Ganapathi and L. A. Zwelling (1998). "Absence of Topoisomerase IIβ in an Amsacrine-resistant Human Leukemia Cell Line with Mutant Topoisomerase IIα." Cancer Research **58**(23): 5298-5300.

Hiasa, H., R. J. DiGate and K. J. Marians (1994). "Decatenating activity of Escherichia coli DNA gyrase and topoisomerases I and III during oriC and pBR322 DNA replication in vitro." Journal of Biological Chemistry **269**(3): 2093-2099.

Hiasa, H. and K. J. Marians (1994). "Topoisomerase III, but not topoisomerase I, can support nascent chain elongation during theta-type DNA replication." Journal of Biological Chemistry **269**(51): 32655-32659.

Hinds, M., K. Deisseroth, J. Mayes, E. Altschuler, R. Jansen, F. D. Ledley and L. A. Zwelling (1991). "Identification of a point mutation in the topoisomerase II gene from a human leukemia cell line containing an amsacrine-resistant form of topoisomerase II." Cancer Res **51**(17): 4729-4731.

Hiraide, T., S. Watanabe, T. Matsubayashi, K. Yanagi, M. Nakashima, T. Ogata and H. Saitsu (2020). "A de novo TOP2B variant associated with global developmental delay and autism spectrum disorder." Mol Genet Genomic Med **8**(3): e1145.

Hirano, T. and T. J. Mitchison (1993). "Topoisomerase II does not play a scaffolding role in the organization of mitotic chromosomes assembled in Xenopus egg extracts." J Cell Biol **120**(3): 601-612.

Hochstrasser, M. (2000). "Evolution and function of ubiquitin-like protein-conjugation systems." Nat Cell Biol **2**(8): E153-157.

Hoffman, H. M., J. F. Bastian and L. M. Bird (2001). "Humoral immunodeficiency with facial dysmorphology and limb anomalies: a new syndrome." Clin Dysmorphol **10**(1): 1-8.

Holden, J. A., D. H. Rolfson and C. T. Wittwer (1992). "The distribution of immunoreactive topoisomerase II Protein in human tissues and neoplasms." Oncol Res **4**(4-5): 157-166.

Holm, C., T. Goto, J. C. Wang and D. Botstein (1985). "DNA topoisomerase II is required at the time of mitosis in yeast." Cell **41**(2): 553-563.

Holm, C., T. Stearns and D. Botstein (1989). "DNA topoisomerase II must act at mitosis to prevent nondisjunction and chromosome breakage." Mol Cell Biol **9**(1): 159-168.

Hornbeck, P. V., B. Zhang, B. Murray, J. M. Kornhauser, V. Latham and E. Skrzypek (2015). "PhosphoSitePlus, 2014: mutations, PTMs and recalibrations." Nucleic Acids Res **43**(Database issue): D512-520.

Huang, C. C., Y. Hou and J. J. Wang (1973). "Effects of a new antitumor agent, epipodophyllotoxin, on growth and chromosomes in human hematopoietic cell lines." Cancer Res **33**(12): 3123-3129.

Huang, W. C., C. Y. Lee and T. S. Hsieh (2017). "Single-molecule Förster resonance energy transfer (FRET) analysis discloses the dynamics of the DNA-topoisomerase II (Top2) interaction in the presence of TOP2-targeting agents." J Biol Chem **292**(30): 12589-12598.

Hügle, B., H. Hoffman, L. M. Bird, C. Gebauer, P. Suchowerskyj, U. Sack, J. Kohlhase and V. Schuster (2011). "Hoffman syndrome: New patients, new insights." Am J Med Genet A **155a**(1): 149-153.

Hung, F., D. Luo, D. M. Sauvé, M. T. Muller and M. Roberge (1996). "Characterization of topoisomerase II-DNA interaction and identification of a DNA-binding domain by ultraviolet laser crosslinking." FEBS Lett **380**(1-2): 127-132.

Ishida, R., M. Iwai, K. L. Marsh, C. A. Austin, T. Yano, M. Shibata, N. Nozaki and A. Hara (1996). "Threonine 1342 in human topoisomerase IIalpha is phosphorylated throughout the cell cycle." J Biol Chem **271**(47): 30077-30082.

Ishida, R., T. Miki, T. Narita, R. Yui, M. Sato, K. R. Utsumi, K. Tanabe and T. Andoh (1991). "Inhibition of Intracellular Topoisomerase II by Antitumor Bis(2,6-dioxopiperazine) Derivatives: Mode of Cell Growth Inhibition Distinct from that of Cleavable Complex-forming Type Inhibitors." Cancer Research **51**(18): 4909-4916.

Ishida, R., R. Takashima, T. Koujin, M. Shibata, N. Nozaki, M. Seto, H. Mori, T. Haraguchi and Y. Hiraoka (2001). "Mitotic specific phosphorylation of serine-1212 in human DNA topoisomerase IIα." Cell structure and function **26**(4): 215-226.

Isik, S., K. Sano, K. Tsutsui, M. Seki, T. Enomoto, H. Saitoh and K. Tsutsui (2003). "The SUMO pathway is required for selective degradation of DNA topoisomerase IIβ induced by a catalytic inhibitor ICRF-1931." FEBS Letters **546**(2-3): 374-378.

Jackson, D. A., A. B. Hassan, R. J. Errington and P. R. Cook (1993). "Visualization of focal sites of transcription within human nuclei." Embo j **12**(3): 1059-1065.

Jang, Y., H. Son, S. W. Lee, W. Hwang, S. R. Jung, J. A. W. Byl, N. Osheroff and S. Lee (2019). "Selection of DNA Cleavage Sites by Topoisomerase II Results from Enzyme-Induced Flexibility of DNA." Cell Chem Biol **26**(4): 502-511.e503.

Jaworski, A., N. P. Higgins, R. D. Wells and W. Zacharias (1991). "Topoisomerase mutants and physiological conditions control supercoiling and Z-DNA formation in vivo." J Biol Chem **266**(4): 2576-2581.

Jenkins, N., L. Murphy and R. Tyther (2008). "Post-translational modifications of recombinant proteins: significance for biopharmaceuticals." Mol Biotechnol **39**(2): 113-118.

Jensen, L. H., A. Renodon-Corniere, I. Wessel, S. W. Langer, B. Søkilde, E. V. Carstensen, M. Sehested and P. B. Jensen (2002). "Maleimide is a potent inhibitor of topoisomerase II in vitro and in vivo: a new mode of catalytic inhibition." Mol Pharmacol **61**(5): 1235-1243.

Jensen, L. H., I. Wessel, M. Møller, J. L. Nitiss, M. Sehested and P. B. Jensen (2000). "N-terminal and core-domain random mutations in human topoisomerase II alpha conferring bisdioxopiperazine resistance." FEBS Lett **480**(2-3): 201-207.

Jensen, P. B., B. S. Sørensen, M. Sehested, P. Grue, E. J. Demant and H. H. Hansen (1994). "Targeting the cytotoxicity of topoisomerase II-directed epipodophyllotoxins to tumor cells in acidic environments." Cancer research **54**(11): 2959-2963.

Jirkovská, A., G. Karabanovich, J. Kubeš, V. Skalická, I. Melnikova, J. Korábečný, T. Kučera, E. Jirkovský, L. Nováková, H. Bavlovič Piskáčková, J. Škoda, M. Štěrba, C. A. Austin, T. Šimůnek and J. Roh (2021). "Structure–Activity Relationship Study of Dexrazoxane Analogues Reveals ICRF-193 as the Most Potent Bisdioxopiperazine against Anthracycline Toxicity to Cardiomyocytes Due to Its Strong Topoisomerase IIβ Interactions." Journal of Medicinal Chemistry **64**(7): 3997-4019.

Johnson, P. (1949). ""“Crystalline enzymes.” Northrop, Kunitz, and Herriott. Columbia Univ. Press, New York, 1948, 352 pp." Journal of Polymer Science **4**(4): 543-544.

Joshi, R. S., B. Piña and J. Roca (2012). "Topoisomerase II is required for the production of long Pol II gene transcripts in yeast." Nucleic acids research **40**(16): 7907-7915.

Ju, B. G., V. V. Lunyak, V. Perissi, I. Garcia-Bassets, D. W. Rose, C. K. Glass and M. G. Rosenfeld (2006). "A topoisomerase IIbeta-mediated dsDNA break required for regulated transcription." Science **312**(5781): 1798-1802.

Juenke, J. M. and J. A. Holden (1993). "The distribution of DNA topoisomerase II isoforms in differentiated adult mouse tissues." Biochim Biophys Acta **1216**(2): 191-196.

Kallish, S., D. M. McDonald-McGinn, M. M. van Haelst, S. P. Bartlett, J. A. Katowitz and E. H. Zackai (2011). "Ablepharon-Macrostomia syndrome--extension of the phenotype." Am J Med Genet A **155a**(12): 3060-3062.

Kapust, R. B., J. Tözsér, J. D. Fox, D. E. Anderson, S. Cherry, T. D. Copeland and D. S. Waugh (2001). "Tobacco etch virus protease: mechanism of autolysis and rational design of stable mutants with wild-type catalytic proficiency." Protein Eng **14**(12): 993-1000.

Ketron, A. C. and N. Osheroff (2014). "Phytochemicals as Anticancer and Chemopreventive Topoisomerase II Poisons." Phytochemistry reviews : proceedings of the Phytochemical Society of Europe **13**(1): 19-35.

Khan, K. H. (2013). "Gene expression in Mammalian cells and its applications." Adv Pharm Bull **3**(2): 257-263.

Khazeem, M. M., J. W. Casement, G. Schlossmacher, N. S. Kenneth, N. K. Sumbung, J. Y. T. Chan, J. F. McGow, I. G. Cowell and C. A. Austin (2022). "TOP2B Is Required to Maintain the

Adrenergic Neural Phenotype and for ATRA-Induced Differentiation of SH-SY5Y Neuroblastoma Cells." Mol Neurobiol.

Khazeem, M. M., I. G. Cowell, L. F. Harkin, J. W. Casement and C. A. Austin (2020). "Transcription of carbonyl reductase 1 is regulated by DNA topoisomerase II beta." FEBS Lett **594**(20): 3395-3405.

Kimura, K., N. Nozaki, T. Enomoto, M. Tanaka and A. Kikuchi (1996). "Analysis of M phase-specific phosphorylation of DNA topoisomerase II." J Biol Chem **271**(35): 21439-21445.

King, I. F., C. N. Yandava, A. M. Mabb, J. S. Hsiao, H. S. Huang, B. L. Pearson, J. M. Calabrese, J. Starmer, J. S. Parker, T. Magnuson, S. J. Chamberlain, B. D. Philpot and M. J. Zylka (2013). "Topoisomerases facilitate transcription of long genes linked to autism." Nature **501**(7465): 58-62.

Kirkegaard, K. and J. C. Wang (1985). "Bacterial DNA topoisomerase I can relax positively supercoiled DNA containing a single-stranded loop." Journal of Molecular Biology **185**(3): 625-637.

Kornberg, R. D. and Y. Lorch (1999). "Twenty-five years of the nucleosome, fundamental particle of the eukaryote chromosome." Cell **98**(3): 285-294.

Krissinel, E. and K. Henrick (2007). "Inference of macromolecular assemblies from crystalline state." J Mol Biol **372**(3): 774-797.

Kroll, D. J. and T. C. Rowe (1991). "Phosphorylation of DNA topoisomerase II in a human tumor cell line." J Biol Chem **266**(12): 7957-7961.

Kubo, A., A. Yoshikawa, T. Hirashima, N. Masuda, M. Takada, J. Takahara, M. Fukuoka and K. Nakagawa (1996). "Point mutations of the topoisomerase IIalpha gene in patients with small cell lung cancer treated with etoposide." Cancer Res **56**(6): 1232-1236.

Kubo, T., K. Kohno, T. Ohga, K. Taniguchi, K. Kawanami, M. Wada and M. Kuwano (1995). "DNA Topoisomerase IIα Gene Expression under Transcriptional Control in Etoposide/Teniposide-resistant Human Cancer Cells." Cancer Research **55**(17): 3860-3864.

Kusumoto, H., Q. E. Rodgers, F. Boege, S. C. Raimondi and W. T. Beck (1996). "Characterization of Novel Human Leukemic Cell Lines Selected for Resistance to Merbarone, a Catalytic Inhibitor of DNA Topoisomerase II." Cancer Research **56**(11): 2573-2583.

Laemmli, U. K., E. Käs, L. Poljak and Y. Adachi (1992). "Scaffold-associated regions: cis-acting determinants of chromatin structural loops and functional domains." Curr Opin Genet Dev **2**(2): 275-285.

Lam, C. W., W. L. Yeung and C. Y. Law (2017). "Global developmental delay and intellectual disability associated with a de novo TOP2B mutation." Clin Chim Acta **469**: 63-68.

Lamour, V., L. Hoermann, J. M. Jeltsch, P. Oudet and D. Moras (2002). "An open conformation of the Thermus thermophilus gyrase B ATP-binding domain." J Biol Chem **277**(21): 18947-18953.

Landy, A. (1989). "Dynamic, structural, and regulatory aspects of lambda site-specific recombination." Annu Rev Biochem **58**: 913-949.

Laponogov, I., X. S. Pan, D. A. Veselkov, K. E. McAuley, L. M. Fisher and M. R. Sanderson (2010). "Structural basis of gate-DNA breakage and resealing by type II topoisomerases." PLoS One **5**(6): e11338.

Larsen, A. K. and A. Skladanowski (1998). "Cellular resistance to topoisomerase-targeted drugs: from drug uptake to cell death." Biochimica et biophysica acta **1400**(1-3): 257-274.

Lavoie, B. D., E. Hogan and D. Koshland (2002). "In vivo dissection of the chromosome condensation machinery: reversibility of condensation distinguishes contributions of condensin and cohesin." The Journal of cell biology **156**(5): 805-815.

Lavoie, B. D., K. M. Tuffo, S. Oh, D. Koshland and C. Holm (2000). "Mitotic chromosome condensation requires Brn1p, the yeast homologue of Barren." Mol Biol Cell **11**(4): 1293-1304.

Lee, I., K. C. Dong and J. M. Berger (2013). "The role of DNA bending in type IIA topoisomerase function." Nucleic Acids Res **41**(10): 5444-5456.

Lee, J. H., T. J. Wendorff and J. M. Berger (2017). "Resveratrol: A novel type of topoisomerase II inhibitor." J Biol Chem **292**(51): 21011-21022.

Lee, M.-T. and J. Bachant (2009). "SUMO modification of DNA topoisomerase II: trying to get a CENse of it all." DNA repair **8**(4): 557-568.

Lee, M., S. H. Kim and S. C. Hong (2010). "Minute negative superhelicity is sufficient to induce the B-Z transition in the presence of low tension." Proc Natl Acad Sci U S A **107**(11): 4985-4990.

Lee, M. P., M. Sander and T. Hsieh (1989). "Nuclease protection by Drosophila DNA topoisomerase II. Enzyme/DNA contacts at the strong topoisomerase II cleavage sites." J Biol Chem **264**(36): 21779-21787.

Lee, M. S., J. C. Wang and M. Beran (1992). "Two independent amsacrine-resistant human myeloid leukemia cell lines share an identical point mutation in the 170 kDa form of human topoisomerase II." J Mol Biol **223**(4): 837-843.

Leontiou, C., J. H. Lakey and C. A. Austin (2004). "Mutation E522K in Human DNA Topoisomerase IIβ Confers Resistance to Methyl N-(4′-(9-acridinylamino)-phenyl)carbamate hydrochloride and Methyl N-(4′-(9-acridinylamino)-3-methoxy-phenyl) methane sulfonamide but Hypersensitivity to Etoposide." Molecular Pharmacology **66**(3): 430-439.

Leontiou, C., J. H. Lakey, R. Lightowlers, R. M. Turnbull and C. A. Austin (2006). "Mutation P732L in Human DNA Topoisomerase IIβ Abolishes DNA Cleavage in the Presence of Calcium and Confers Drug Resistance." Molecular Pharmacology **69**(1): 130-139.

Leontiou, C., G. P. Watters, K. L. Gilroy, P. Heslop, I. G. Cowell, K. Craig, R. N. Lightowlers, J. H. Lakey and C. A. Austin (2007). "Differential Selection of Acridine Resistance Mutations in Human DNA Topoisomerase IIβ Is Dependent on the Acridine Structure." Molecular Pharmacology **71**(4): 1006-1014.

Leppard, J. B. and J. J. Champoux (2005). "Human DNA topoisomerase I: relaxation, roles, and damage control." Chromosoma **114**(2): 75-85.

Li, H., Y. Wang and X. Liu (2008). "Plk1-dependent phosphorylation regulates functions of DNA topoisomerase IIalpha in cell cycle progression." J Biol Chem **283**(10): 6209-6221.

Li, W. and J. C. Wang (1997). "Footprinting of yeast DNA topoisomerase II lysyl side chains involved in substrate binding and interdomainal interactions." J Biol Chem **272**(49): 31190-31195.

Lindsey, R. H., Jr., K. D. Bromberg, C. A. Felix and N. Osheroff (2004). "1,4-Benzoquinone is a topoisomerase II poison." Biochemistry **43**(23): 7563-7574.

Lindsley, J. E. and J. C. Wang (1991). "Proteolysis patterns of epitopically labeled yeast DNA topoisomerase II suggest an allosteric transition in the enzyme induced by ATP binding." Proceedings of the National Academy of Sciences of the United States of America **88**(23): 10485-10489.

Lindsley, J. E. and J. C. Wang (1993). "On the coupling between ATP usage and DNA transport by yeast DNA topoisomerase II." J Biol Chem **268**(11): 8096-8104.

Liu, L. F., T. C. Rowe, L. Yang, K. M. Tewey and G. L. Chen (1983). "Cleavage of DNA by mammalian DNA topoisomerase II." J Biol Chem **258**(24): 15365-15370.

Liu, L. F. and J. C. Wang (1987). "Supercoiling of the DNA template during transcription." Proceedings of the National Academy of Sciences **84**(20): 7024-7027.

Lotz, C., V. Lamour and C. D. Resistance (2020). "The interplay between DNA topoisomerase 2α post-translational modifications and drug resistance." **3**: 86-97.

Luft, J. R., S. V. Arakali, M. J. Kirisits, J. Kalenik, I. Wawrzak, V. Cody, W. A. Pangborn and G. T. DeTitta (1994). "A macromolecular crystallization procedure employing diffusion cells of varying depths as reservoirs to tailor the time course of equilibration in hanging- and sitting-drop vapor-diffusion and microdialysis experiments." Journal of Applied Crystallography **27**(4): 443-452.

Lund, K., A. H. Andersen, K. Christiansen, J. Q. Svejstrup and O. Westergaard (1990). "Minimal DNA requirement for topoisomerase II-mediated cleavage in vitro." J Biol Chem **265**(23): 13856-13863.

Lyu, Y. L., C. P. Lin, A. M. Azarova, L. Cai, J. C. Wang and L. F. Liu (2006). "Role of topoisomerase IIbeta in the expression of developmentally regulated genes." Mol Cell Biol **26**(21): 7929-7941.

Lyu, Y. L. and J. C. Wang (2003). "Aberrant lamination in the cerebral cortex of mouse embryos lacking DNA topoisomerase IIbeta." Proc Natl Acad Sci U S A **100**(12): 7123-7128.

Madabhushi, R., F. Gao, A. R. Pfenning, L. Pan, S. Yamakawa, J. Seo, R. Rueda, T. X. Phan, H. Yamakawa, P. C. Pao, R. T. Stott, E. Gjoneska, A. Nott, S. Cho, M. Kellis and L. H. Tsai (2015). "Activity-Induced DNA Breaks Govern the Expression of Neuronal Early-Response Genes." Cell **161**(7): 1592-1605.

Manville, C. M., K. Smith, Z. Sondka, H. Rance, S. Cockell, I. G. Cowell, K. C. Lee, N. J. Morris, K. Padget, G. H. Jackson and C. A. Austin (2015). "Genome-wide ChIP-seq analysis of human TOP2B occupancy in MCF7 breast cancer epithelial cells." Biol Open **4**(11): 1436-1447.

Mao, Y., S. D. Desai and L. F. Liu (2000). "SUMO-1 conjugation to human DNA topoisomerase II isozymes." J Biol Chem **275**(34): 26066-26073.

Mao, Y., C. Yu, T. S. Hsieh, J. L. Nitiss, A. A. Liu, H. Wang and L. F. Liu (1999). "Mutations of human topoisomerase II alpha affecting multidrug resistance and sensitivity." Biochemistry **38**(33): 10793-10800.

Marcelino, A. M. and L. M. Gierasch (2008). "Roles of beta-turns in protein folding: from peptide models to protein engineering." Biopolymers **89**(5): 380-391.

McClendon, A. K. and N. Osheroff (2007). "DNA topoisomerase II, genotoxicity, and cancer." Mutat Res **623**(1-2): 83-97.

McCoy, A. J., R. W. Grosse-Kunstleve, P. D. Adams, M. D. Winn, L. C. Storoni and R. J. Read (2007). "Phaser crystallographic software." J Appl Crystallogr **40**(Pt 4): 658-674.

McPherson, A. (1990). "Current approaches to macromolecular crystallization." Eur J Biochem **189**(1): 1-23.

McPherson, A. and J. A. Gavira (2014). "Introduction to protein crystallization." Acta Crystallogr F Struct Biol Commun **70**(Pt 1): 2-20.

Meczes, E. L., K. L. Gilroy, K. L. West and C. A. Austin (2008). "The Impact of the Human DNA Topoisomerase II C-Terminal Domain on Activity." PLOS ONE **3**(3): e1754.

Meczes, E. L., K. L. Marsh, L. M. Fisher, M. P. Rogers and C. A. Austin (1997). "Complementation of temperature-sensitive topoisomerase II mutations in Saccharomyces cerevisiae by a human TOP2 beta construct allows the study of topoisomerase II beta inhibitors in yeast." Cancer Chemother Pharmacol **39**(4): 367-375.

Meyer, K. N., E. Kjeldsen, T. Straub, B. R. Knudsen, I. D. Hickson, A. Kikuchi, H. Kreipe and F. Boege (1997). "Cell cycle-coupled relocation of types I and II topoisomerases and modulation of catalytic enzyme activities." The Journal of cell biology **136**(4): 775-788.

Mirski, S. E., J. C. Bielawski and S. P. Cole (2003). "Identification of functional nuclear export sequences in human topoisomerase IIα and β." Biochemical and biophysical research communications **306**(4): 905-911.

Mirski, S. E., C. D. Evans, K. C. Almquist, M. L. Slovak and S. P. Cole (1993). "Altered topoisomerase II alpha in a drug-resistant small cell lung cancer cell line selected in VP-16." Cancer Res **53**(20): 4866-4873.

Mirski, S. E., J. H. Gerlach and S. P. Cole (1999). "Sequence determinants of nuclear localization in the α and β isoforms of human topoisomerase II." Experimental cell research **251**(2): 329-339.

Mirski, S. E., K. E. Sparks, Q. Yu, A. J. Lang, N. Jain, B. G. Campling and S. P. Cole (2000). "A truncated cytoplasmic topoisomerase IIalpha in a drug-resistant lung cancer cell line is encoded by a TOP2A allele with a partial deletion of exon 34." Int J Cancer **85**(4): 534-539.

Mitchell, J. A. and P. Fraser (2008). "Transcription factories are nuclear subcompartments that remain in the absence of transcription." Genes Dev **22**(1): 20-25.

Mogk, A., M. P. Mayer and E. Deuerling (2002). "Mechanisms of protein folding: molecular chaperones and their application in biotechnology." Chembiochem **3**(9): 807-814.

Mondal, N. and J. D. Parvin (2001). "DNA topoisomerase IIalpha is required for RNA polymerase II transcription on chromatin templates." Nature **413**(6854): 435-438.

Montecucco, A., F. Zanetta and G. Biamonti (2015). "Molecular mechanisms of etoposide." Excli j **14**: 95-108.

Moreira, F., M. Arenas, A. Videira and F. Pereira (2022). "Evolutionary History of TOPIIA Topoisomerases in Animals." Journal of Molecular Evolution **90**(2): 149-165.

Mouchel, N. A. and J. R. Jenkins (2006). "The identification of a functional interaction between PKC and topoisomerase II." FEBS Lett **580**(1): 51-57.

Mueller-Planitz, F. and D. Herschlag (2006). "Interdomain communication in DNA topoisomerase II. DNA binding and enzyme activation." J Biol Chem **281**(33): 23395-23404.

Mueller-Planitz, F. and D. Herschlag (2007). "DNA topoisomerase II selects DNA cleavage sites based on reactivity rather than binding affinity." Nucleic Acids Res **35**(11): 3764-3773.

Murshudov, G. N., P. Skubák, A. A. Lebedev, N. S. Pannu, R. A. Steiner, R. A. Nicholls, M. D. Winn, F. Long and A. A. Vagin (2011). "REFMAC5 for the refinement of macromolecular crystal structures." Acta Crystallogr D Biol Crystallogr **67**(Pt 4): 355-367.

Myers, C. (1998). "The role of iron in doxorubicin-induced cardiomyopathy." Semin Oncol **25**(4 Suppl 10): 10-14.

Nakagawa, M., E. Schneider, K. H. Dixon, J. Horton, K. Kelley, C. Morrow and K. H. Cowan (1992). "Reduced intracellular drug accumulation in the absence of P-glycoprotein (mdr1) overexpression in mitoxantrone-resistant human MCF-7 breast cancer cells." Cancer Res **52**(22): 6175-6181.

Nakazawa, N., O. Arakawa, M. Ebe and M. Yanagida (2019). "Casein kinase II-dependent phosphorylation of DNA topoisomerase II suppresses the effect of a catalytic topo II inhibitor, ICRF-193, in fission yeast." J Biol Chem **294**(10): 3772-3782.

Naughton, C., N. Avlonitis, S. Corless, J. G. Prendergast, I. K. Mati, P. P. Eijk, S. L. Cockroft, M. Bradley, B. Ylstra and N. Gilbert (2013). "Transcription forms and remodels supercoiling domains unfolding large-scale chromatin structures." Nat Struct Mol Biol **20**(3): 387-395.

Nelson, H. C. (1995). "Structure and function of DNA-binding proteins." Curr Opin Genet Dev **5**(2): 180-189.

Newport, J. and T. Spann (1987). "Disassembly of the nucleus in mitotic extracts: membrane vesicularization, lamin disassembly, and chromosome condensation are independent processes." Cell **48**(2): 219-230.

Nitiss, J. and J. C. Wang (1988). "DNA topoisomerase-targeting antitumor drugs can be studied in yeast." Proc Natl Acad Sci U S A **85**(20): 7501-7505.

Nitiss, J. L. (1998). "Investigating the biological functions of DNA topoisomerases in eukaryotic cells." Biochim Biophys Acta **1400**(1-3): 63-81.

Nitiss, J. L. (2009). "Targeting DNA topoisomerase II in cancer chemotherapy." Nature reviews. Cancer **9**(5): 338-350.

Nitiss, J. L., Y. X. Liu, P. Harbury, M. Jannatipour, R. Wasserman and J. C. Wang (1992). "Amsacrine and etoposide hypersensitivity of yeast cells overexpressing DNA topoisomerase II." Cancer Res **52**(16): 4467-4472.

Niwa, T., B. W. Ying, K. Saito, W. Jin, S. Takada, T. Ueda and H. Taguchi (2009). "Bimodal protein solubility distribution revealed by an aggregation analysis of the entire ensemble of Escherichia coli proteins." Proc Natl Acad Sci U S A **106**(11): 4201-4206.

Noble, C. G. and A. Maxwell (2002). "The role of GyrB in the DNA cleavage-religation reaction of DNA gyrase: a proposed two metal-ion mechanism." J Mol Biol **318**(2): 361-371.

Nora, E. P., B. R. Lajoie, E. G. Schulz, L. Giorgetti, I. Okamoto, N. Servant, T. Piolot, N. L. van Berkum, J. Meisig, J. Sedat, J. Gribnau, E. Barillot, N. Blüthgen, J. Dekker and E. Heard (2012). "Spatial partitioning of the regulatory landscape of the X-inactivation centre." Nature **485**(7398): 381-385.

Nur, E. K. A., S. Meiners, I. Ahmed, A. Azarova, C. P. Lin, Y. L. Lyu and L. F. Liu (2007). "Role of DNA topoisomerase IIbeta in neurite outgrowth." Brain Res **1154**: 50-60.

Nutt, S. L., B. Heavey, A. G. Rolink and M. Busslinger (1999). "Commitment to the B-lymphoid lineage depends on the transcription factor Pax5." Nature **401**(6753): 556-562.

Odaimi, M., B. S. Andersson, K. B. McCredie and M. Beran (1986). "Drug sensitivity and cross-resistance of the 4'-(9-acridinylamino)methanesulfon-m-anisidide-resistant subline of HL-60 human leukemia." Cancer Res **46**(7): 3330-3333.

Oestergaard, V. H., L. Giangiacomo, L. Bjergbaek, B. R. Knudsen and A. H. Andersen (2004). "Hindering the strand passage reaction of human topoisomerase IIalpha without disturbing DNA cleavage, ATP hydrolysis, or the operation of the N-terminal clamp." J Biol Chem **279**(27): 28093-28099.

Okada, Y., Y. Ito, A. Kikuchi, Y. Nimura, S. Yoshida and M. Suzuki (2000). "Assignment of functional amino acids around the active site of human DNA topoisomerase IIalpha." J Biol Chem **275**(32): 24630-24638.

Okada, Y., A. Tosaka, Y. Nimura, A. Kikuchi, S. Yoshida and M. Suzuki (2001). "Atypical multidrug resistance may be associated with catalytically active mutants of human DNA topoisomerase II alpha." Gene **272**(1-2): 141-148.

Olland, S. and J. C. Wang (1999). "Catalysis of ATP hydrolysis by two NH(2)-terminal fragments of yeast DNA topoisomerase II." J Biol Chem **274**(31): 21688-21694.

Onoda, A., O. Hosoya, K. Sano, K. Kiyama, H. Kimura, S. Kawano, R. Furuta, M. Miyaji, K. Tsutsui and K. M. Tsutsui (2014). "Nuclear dynamics of topoisomerase IIβ reflects its catalytic activity that is regulated by binding of RNA to the C-terminal domain." Nucleic Acids Res **42**(14): 9005-9020.

Osheroff, N. (1986). "Eukaryotic topoisomerase II. Characterization of enzyme turnover." Journal of Biological Chemistry **261**(21): 9944-9950.

Osheroff, N. (1987). "Role of the divalent cation in topoisomerase II mediated reactions." Biochemistry **26**(20): 6402-6406.

Osheroff, N. and E. L. Zechiedrich (1987). "Calcium-promoted DNA cleavage by eukaryotic topoisomerase II: trapping the covalent enzyme-DNA complex in an active form." Biochemistry **26**(14): 4303-4309.

Pang, B., X. Qiao, L. Janssen, A. Velds, T. Groothuis, R. Kerkhoven, M. Nieuwland, H. Ovaa, S. Rottenberg, O. van Tellingen, J. Janssen, P. Huijgens, W. Zwart and J. Neefjes (2013). "Drug-induced histone eviction from open chromatin contributes to the chemotherapeutic effects of doxorubicin." Nat Commun **4**: 1908.

Papapietro, O., A. Chandra, D. Eletto, S. Inglott, V. Plagnol, J. Curtis, M. Maes, A. Alisaac, A. S. Albuquerque, E. Basseres, O. Hermine, C. Picard, A. Fischer, A. Durandy, S. Kracker, S. O. Burns, D. Cuchet-Lourenco, K. Okkenhaug and S. Nejentsev (2020). "Topoisomerase 2β mutation impairs early B-cell development." Blood **135**(17): 1497-1501.

Parvin, J. D. and P. A. Sharp (1993). "DNA topology and a minimal set of basal factors for transcription by RNA polymerase II." Cell **73**(3): 533-540.

Patel, S., E. Jazrawi, A. M. Creighton, C. A. Austin and L. M. Fisher (2000). "Probing the Interaction of the Cytotoxic Bisdioxopiperazine ICRF-193 with the Closed Enzyme Clamp of Human Topoisomerase IIα." Molecular Pharmacology **58**(3): 560-568.

Patel, S., B. A. Keller and L. M. Fisher (2000). "Mutations at arg486 and glu571 in human topoisomerase IIalpha confer resistance to amsacrine: relevance for antitumor drug resistance in human cells." Mol Pharmacol **57**(4): 784-791.

Pendleton, M., R. H. Lindsey, Jr., C. A. Felix, D. Grimwade and N. Osheroff (2014). "Topoisomerase II and leukemia." Ann N Y Acad Sci **1310**(1): 98-110.

Perillo, B., M. N. Ombra, A. Bertoni, C. Cuozzo, S. Sacchetti, A. Sasso, L. Chiariotti, A. Malorni, C. Abbondanza and E. V. Avvedimento (2008). "DNA oxidation as triggered by H3K9me2 demethylation drives estrogen-induced gene expression." Science **319**(5860): 202-206.

Pommier, Y. (1993). "DNA topoisomerase I and II in cancer chemotherapy: update and perspectives." Cancer Chemother Pharmacol **32**(2): 103-108.

Pommier, Y. (2013). "Drugging topoisomerases: lessons and challenges." ACS Chem Biol **8**(1): 82-95.

Pommier, Y., G. Capranico, A. Orr and K. W. Kohn (1991). "Local base sequence preferences for DNA cleavage by mammalian topoisomerase II in the presence of amsacrine or teniposide." Nucleic Acids Res **19**(21): 5973-5980.

Pommier, Y., E. Leo, H. Zhang and C. Marchand (2010). "DNA Topoisomerases and Their Poisoning by Anticancer and Antibacterial Drugs." Chemistry & Biology **17**(5): 421-433.

Potterton, L., J. Agirre, C. Ballard, K. Cowtan, E. Dodson, P. R. Evans, H. T. Jenkins, R. Keegan, E. Krissinel, K. Stevenson, A. Lebedev, S. J. McNicholas, R. A. Nicholls, M. Noble, N. S. Pannu, C. Roth, G. Sheldrick, P. Skubak, J. Turkenburg, V. Uski, F. von Delft, D. Waterman, K. Wilson, M. Winn and M. Wojdyr (2018). "CCP4i2: the new graphical user interface to the CCP4 program suite." Acta Crystallogr D Struct Biol **74**(Pt 2): 68-84.

Prosperi, E., C. Negri, G. Marchese and G. C. Ricotti (1994). "Expression of the 170-kDa and 180-kDa isoforms of DNA topoisomerase II in resting and proliferating human lymphocytes." Cell Prolif **27**(5): 257-267.

Qi, X., S. Hou, A. Lepp, R. Li, Z. Basir, Z. Lou and G. Chen (2011). "Phosphorylation and stabilization of topoisomerase IIα protein by p38γ mitogen-activated protein kinase sensitize breast cancer cells to its poisons." J Biol Chem **286**(41): 35883-35890.

Rao, S. S., M. H. Huntley, N. C. Durand, E. K. Stamenova, I. D. Bochkov, J. T. Robinson, A. L. Sanborn, I. Machol, A. D. Omer, E. S. Lander and E. L. Aiden (2014). "A 3D map of the human genome at kilobase resolution reveals principles of chromatin looping." Cell **159**(7): 1665-1680.

Raran-Kurussi, S., J. Tözsér, S. Cherry, J. E. Tropea and D. S. Waugh (2013). "Differential temperature dependence of tobacco etch virus and rhinovirus 3C proteases." Analytical biochemistry **436**(2): 142-144.

Rattner, J. B., M. J. Hendzel, C. S. Furbee, M. T. Muller and D. P. Bazett-Jones (1996). "Topoisomerase II alpha is associated with the mammalian centromere in a cell cycle- and species-specific manner and is required for proper centromere/kinetochore structure." J Cell Biol **134**(5): 1097-1107.

Reece, R. J. and A. Maxwell (1989). "Tryptic fragments of the Escherichia coli DNA gyrase A protein." Journal of Biological Chemistry **264**(33): 19648-19653.

Reece, R. J. and A. Maxwell (1991). "DNA gyrase: structure and function." Crit Rev Biochem Mol Biol **26**(3-4): 335-375.

Reid, R. J., P. Benedetti and M. A. Bjornsti (1998). "Yeast as a model organism for studying the actions of DNA topoisomerase-targeted drugs." Biochim Biophys Acta **1400**(1-3): 289-300.

Ritke, M. K., N. R. Murray, W. P. Allan, A. P. Fields and J. C. Yalowich (1995). "Hypophosphorylation of topoisomerase II in etoposide (VP-16)-resistant human leukemia K562 cells associated with reduced levels of beta II protein kinase C." Mol Pharmacol **48**(5): 798-805.

Robinson, M. J. and N. Osheroff (1990). "Stabilization of the topoisomerase II-DNA cleavage complex by antineoplastic drugs: inhibition of enzyme-mediated DNA religation by 4'-(9-acridinylamino) methanesulfon-m-anisidide." Biochemistry **29**(10): 2511-2515.

Robinson, M. J. and N. Osheroff (1991). "Effects of antineoplastic drugs on the post-strand-passage DNA cleavage/religation equilibrium of topoisomerase II." Biochemistry **30**(7): 1807-1813.

Roca, J. (1995). "The mechanisms of DNA topoisomerases." Trends Biochem Sci **20**(4): 156-160.

Roca, J., J. M. Berger, S. C. Harrison and J. C. Wang (1996). "DNA transport by a type II topoisomerase: direct evidence for a two-gate mechanism." Proc Natl Acad Sci U S A **93**(9): 4057-4062.

Roca, J., R. Ishida, J. M. Berger, T. Andoh and J. C. Wang (1994). "Antitumor bisdioxopiperazines inhibit yeast DNA topoisomerase II by trapping the enzyme in the form of a closed protein clamp." Proceedings of the National Academy of Sciences of the United States of America **91**(5): 1781-1785.

Roca, J. and J. C. Wang (1992). "The capture of a DNA double helix by an ATP-dependent protein clamp: a key step in DNA transport by type II DNA topoisomerases." Cell **71**(5): 833-840.

Roca, J. and J. C. Wang (1994). "DNA transport by a type II DNA topoisomerase: evidence in favor of a two-gate mechanism." Cell **77**(4): 609-616.

Rose, D. and C. Holm (1993). "Meiosis-specific arrest revealed in DNA topoisomerase II mutants." Mol Cell Biol **13**(6): 3445-3455.

Rose, D., W. Thomas and C. Holm (1990). "Segregation of recombined chromosomes in meiosis I requires DNA topoisomerase II." Cell **60**(6): 1009-1017.

Rule, C. S., M. Patrick and M. Sandkvist (2016). "Measuring In Vitro ATPase Activity for Enzymatic Characterization." J Vis Exp(114).

Rupp, B. (2010). "Biomolecular Crystallography: Principles, Practice, and Applications to Structural Biology. New York: Garland Science, Taylor and Francis Group, 2010. ." Acta Crystallographica Section D **66**(5): 640-641.

Saijo, M., T. Enomoto, F. Hanaoka and M. Ui (1990). "Purification and characterization of type II DNA topoisomerase from mouse FM3A cells: phosphorylation of topoisomerase II and modification of its activity." Biochemistry **29**(2): 583-590.

Sakaguchi, A. and A. Kikuchi (2004). "Functional compatibility between isoform α and β of type II DNA topoisomerase." Journal of Cell Science **117**(7): 1047-1054.

Sambrook, J. (1989). Molecular cloning: a laboratory manual. Molecular cloning :. Cold Spring Harbor, N.Y. :**:** 1244-1249.

Samejima, K., I. Samejima, P. Vagnarelli, H. Ogawa, G. Vargiu, D. A. Kelly, F. de Lima Alves, A. Kerr, L. C. Green, D. F. Hudson, S. Ohta, C. A. Cooke, C. J. Farr, J. Rappsilber and W. C. Earnshaw (2012). "Mitotic chromosomes are compacted laterally by KIF4 and condensin and axially by topoisomerase IIα." Journal of Cell Biology **199**(5): 755-770.

Schebesta, A., S. McManus, G. Salvagiotto, A. Delogu, G. A. Busslinger and M. Busslinger (2007). "Transcription factor Pax5 activates the chromatin of key genes involved in B cell signaling, adhesion, migration, and immune function." Immunity **27**(1): 49-63.

Schein, C. H. (1989). "Production of soluble recombinant proteins in bacteria." Bio/technology **7**(11): 1141-1149.

Schmidt, B. H., A. B. Burgin, J. E. Deweese, N. Osheroff and J. M. Berger (2010). "A novel and unified two-metal mechanism for DNA cleavage by type II and IA topoisomerases." Nature **465**(7298): 641-644.

Schmidt, B. H., N. Osheroff and J. M. Berger (2012). "Structure of a topoisomerase II-DNA-nucleotide complex reveals a new control mechanism for ATPase activity." Nat Struct Mol Biol **19**(11): 1147-1154.

Schoeffler, A. J. and J. M. Berger (2005). "Recent advances in understanding structure-function relationships in the type II topoisomerase mechanism." Biochem Soc Trans **33**(Pt 6): 1465-1470.

Schultz, M. C., S. J. Brill, Q. Ju, R. Sternglanz and R. H. Reeder (1992). "Topoisomerases and yeast rRNA transcription: negative supercoiling stimulates initiation and topoisomerase activity is required for elongation." Genes Dev **6**(7): 1332-1341.

Schultz, S. C., G. C. Shields and T. A. Steitz (1991). "Crystal structure of a CAP-DNA complex: the DNA is bent by 90 degrees." Science **253**(5023): 1001-1007.

Sehested, M. and P. B. Jensen (1996). "Mapping of DNA topoisomerase II poisons (etoposide, clerocidin) and catalytic inhibitors (aclarubicin, ICRF-187) to four distinct steps in the topoisomerase II catalytic cycle." Biochem Pharmacol **51**(7): 879-886.

Sehested, M., I. Wessel, L. H. Jensen, B. Holm, R. S. Oliveri, S. Kenwrick, A. M. Creighton, J. L. Nitiss and P. B. Jensen (1998). "Chinese hamster ovary cells resistant to the topoisomerase II catalytic inhibitor ICRF-159: a Tyr49Phe mutation confers high-level resistance to bisdioxopiperazines." Cancer Res **58**(7): 1460-1468.

Sexton, T., E. Yaffe, E. Kenigsberg, F. Bantignies, B. Leblanc, M. Hoichman, H. Parrinello, A. Tanay and G. Cavalli (2012). "Three-dimensional folding and functional organization principles of the Drosophila genome." Cell **148**(3): 458-472.

Shapiro, A. B. and C. A. Austin (2014). "A high-throughput fluorescence anisotropy-based assay for human topoisomerase II β-catalyzed ATP-dependent supercoiled DNA relaxation." Anal Biochem **448**: 23-29.

Shelton, E. R., N. Osheroff and D. L. Brutlag (1983). "DNA topoisomerase II from Drosophila melanogaster. Purification and physical characterization." J Biol Chem **258**(15): 9530-9535.

Sherman, F. (2002). "Getting started with yeast." Methods Enzymol **350**: 3-41.

Shuman, S. and B. Moss (1987). "Identification of a vaccinia virus gene encoding a type I DNA topoisomerase." Proceedings of the National Academy of Sciences **84**(21): 7478-7482.

Sigrist, C. J. A., E. de Castro, L. Cerutti, B. A. Cuche, N. Hulo, A. Bridge, L. Bougueleret and I. Xenarios (2012). "New and continuing developments at PROSITE." Nucleic Acids Research **41**(D1): D344-D347.

Singh, B. and R. S. Gupta (1983). "Mutagenic responses of thirteen anticancer drugs on mutation induction at multiple genetic loci and on sister chromatid exchanges in Chinese hamster ovary cells." Cancer Res **43**(2): 577-584.

Slesarev, A. I., G. I. Belova, J. A. Lake and S. A. Kozyavkin (2001). "Topoisomerase V from Methanopyrus kandleri." Methods Enzymol **334**: 179-192.

Slesarev, A. I., K. O. Stetter, J. A. Lake, M. Gellert, R. Krah and S. A. Kozyavkin (1993). "DNA topoisomerase V is a relative of eukaryotic topoisomerase I from a hyperthermophilic prokaryote." Nature **364**(6439): 735-737.

Smiley, R. D., T. R. Collins, G. G. Hammes and T. S. Hsieh (2007). "Single-molecule measurements of the opening and closing of the DNA gate by eukaryotic topoisomerase II." Proc Natl Acad Sci U S A **104**(12): 4840-4845.

Smith, C. V. and A. Maxwell (1998). "Identification of a residue involved in transition-state stabilization in the ATPase reaction of DNA gyrase." Biochemistry **37**(27): 9658-9667.

Sng, J. H., V. J. Heaton, M. Bell, P. Maini, C. A. Austin and L. M. Fisher (1999). "Molecular cloning and characterization of the human topoisomerase IIalpha and IIbeta genes: evidence for isoform evolution through gene duplication." Biochim Biophys Acta **1444**(3): 395-406.

Sobreira, N., F. Schiettecatte, D. Valle and A. Hamosh (2015). "GeneMatcher: a matching tool for connecting investigators with an interest in the same gene." Hum Mutat **36**(10): 928-930.

Sørensen, B. S., J. Sinding, A. H. Andersen, J. Alsner, P. B. Jensen and O. Westergaard (1992). "Mode of action of topoisomerase II-targeting agents at a specific DNA sequence. Uncoupling the DNA binding, cleavage and religation events." J Mol Biol **228**(3): 778-786.

Sørensen, H. P. and K. K. Mortensen (2005). "Soluble expression of recombinant proteins in the cytoplasm of Escherichia coli." Microb Cell Fact **4**(1): 1.

Sperling, A. S., K. S. Jeong, T. Kitada and M. Grunstein (2011). "Topoisomerase II binds nucleosome-free DNA and acts redundantly with topoisomerase I to enhance recruitment of RNA Pol II in budding yeast." Proc Natl Acad Sci U S A **108**(31): 12693-12698.

Spitzner, J. R. and M. T. Muller (1988). "A consensus sequence for cleavage by vertebrate DNA topoisomerase II." Nucleic Acids Res **16**(12): 5533-5556.

Stanger, F. V., C. Dehio and T. Schirmer (2014). "Structure of the N-terminal Gyrase B fragment in complex with ADP·Pi reveals rigid-body motion induced by ATP hydrolysis." PLoS One **9**(9): e107289.

Strumberg, D., J. L. Nitiss, J. Dong, K. W. Kohn and Y. Pommier (1999). "Molecular analysis of yeast and human type II topoisomerases. Enzyme-DNA and drug interactions." J Biol Chem **274**(40): 28246-28255.

Strumberg, D., J. L. Nitiss, A. Rose, M. C. Nicklaus and Y. Pommier (1999). "Mutation of a conserved serine residue in a quinolone-resistant type II topoisomerase alters the enzyme-DNA and drug interactions." J Biol Chem **274**(11): 7292-7301.

Takano, H., K. Kohno, M. Ono, Y. Uchida and M. Kuwano (1991). "Increased phosphorylation of DNA topoisomerase II in etoposide-resistant mutants of human cancer KB cells." Cancer Res **51**(15): 3951-3957.

Tan, K. B., T. E. Dorman, K. M. Falls, T. D. Y. Chung, C. K. Mirabelli, S. T. Crooke and J.-i. Mao (1992). "Topoisomerase IIα and Topoisomerase IIβ Genes: Characterization and Mapping to Human Chromosomes 17 and 3, Respectively." Cancer Research **52**(1): 231-234.

Tasaki, T., S. M. Sriram, K. S. Park and Y. T. Kwon (2012). "The N-end rule pathway." Annu Rev Biochem **81**: 261-289.

Tewey, K. M., T. C. Rowe, L. Yang, B. D. Halligan and L. F. Liu (1984). "Adriamycin-induced DNA damage mediated by mammalian DNA topoisomerase II." Science **226**(4673): 466-468.

Thakurela, S., A. Garding, J. Jung, D. Schübeler, L. Burger and V. K. Tiwari (2013). "Gene regulation and priming by topoisomerase IIα in embryonic stem cells." Nat Commun **4**: 2478.

Thomas, W., R. M. Spell, M. E. Ming and C. Holm (1991). "Genetic analysis of the gyrase A-like domain of DNA topoisomerase II of Saccharomyces cerevisiae." Genetics **128**(4): 703-716.

Tiwari, V. K., L. Burger, V. Nikoletopoulou, R. Deogracias, S. Thakurela, C. Wirbelauer, J. Kaut, R. Terranova, L. Hoerner, C. Mielke, F. Boege, R. Murr, A. H. Peters, Y. A. Barde and D. Schübeler (2012). "Target genes of Topoisomerase IIβ regulate neuronal survival and are defined by their chromatin state." Proc Natl Acad Sci U S A **109**(16): E934-943.

Travers, A. and G. Muskhelishvili (2007). "A common topology for bacterial and eukaryotic transcription initiation?" EMBO Rep **8**(2): 147-151.

Trotter, K. W., H. A. King and T. K. Archer (2015). "Glucocorticoid Receptor Transcriptional Activation via the BRG1-Dependent Recruitment of TOP2β and Ku70/86." Mol Cell Biol **35**(16): 2799-2817.

Tsai-Pflugfelder, M., L. F. Liu, A. A. Liu, K. M. Tewey, J. Whang-Peng, T. Knutsen, K. Huebner, C. M. Croce and J. C. Wang (1988). "Cloning and sequencing of cDNA encoding human DNA topoisomerase II and localization of the gene to chromosome region 17q21-22." Proc Natl Acad Sci U S A **85**(19): 7177-7181.

Tse-Dinh, Y. C. (1986). "Uncoupling of the DNA breaking and rejoining steps of Escherichia coli type I DNA topoisomerase. Demonstration of an active covalent protein-DNA complex." Journal of Biological Chemistry **261**(23): 10931-10935.

Turnbull, R. M., E. L. Meczes, M. Perenna Rogers, R. B. Lock, D. M. Sullivan, G. J. Finlay, B. C. Baguley and C. A. Austin (1999). "Carbamate analogues of amsacrine active against non-cycling cells: relative activity against topoisomerases IIalpha and beta." Cancer Chemother Pharmacol **44**(4): 275-282.

Turner, J. G., R. Engel, J. A. Derderian, R. Jove and D. M. Sullivan (2004). "Human topoisomerase IIα nuclear export is mediated by two CRM-1-dependent nuclear export signals." Journal of cell science **117**(14): 3061-3071.

Uemura, T., H. Ohkura, Y. Adachi, K. Morino, K. Shiozaki and M. Yanagida (1987). "DNA topoisomerase II is required for condensation and separation of mitotic chromosomes in S. pombe." Cell **50**(6): 917-925.

Uemura, T. and M. Yanagida (1984). "Isolation of type I and II DNA topoisomerase mutants from fission yeast: single and double mutants show different phenotypes in cell growth and chromatin organization." Embo j **3**(8): 1737-1744.

Uusküla-Reimand, L., H. Hou, P. Samavarchi-Tehrani, M. V. Rudan, M. Liang, A. Medina-Rivera, H. Mohammed, D. Schmidt, P. Schwalie, E. J. Young, J. Reimand, S. Hadjur, A. C. Gingras and M. D. Wilson (2016). "Topoisomerase II beta interacts with cohesin and CTCF at topological domain borders." Genome Biol **17**(1): 182.

Vagin, A. and A. Teplyakov (1997). "MOLREP: an Automated Program for Molecular Replacement." Journal of Applied Crystallography **30**(6): 1022-1025.

van Dalen, E. C., H. N. Caron, H. O. Dickinson and L. C. Kremer (2011). "Cardioprotective interventions for cancer patients receiving anthracyclines." Cochrane Database Syst Rev **2011**(6): Cd003917.

Vanden Broeck, A., C. Lotz, R. Drillien, L. Haas, C. Bedez and V. Lamour (2021). "Structural basis for allosteric regulation of Human Topoisomerase IIα." Nat Commun **12**(1): 2962.

Vanden Broeck, A., C. Lotz, J. Ortiz and V. Lamour (2019). "Cryo-EM structure of the complete E. coli DNA gyrase nucleoprotein complex." Nature Communications **10**(1): 4935.

Varshavsky, A. (1997). "The N-end rule pathway of protein degradation." Genes Cells **2**(1): 13-28.

Vassetzky, Y. S., G. C. Alghisi and S. M. Gasser (1995). "DNA topoisomerase II mutations and resistance to anti-tumor drugs." Bioessays **17**(9): 767-774.

Vélez-Cruz, R., J. N. Riggins, J. S. Daniels, H. Cai, F. P. Guengerich, L. J. Marnett and N. Osheroff (2005). "Exocyclic DNA lesions stimulate DNA cleavage mediated by human topoisomerase II alpha in vitro and in cultured cells." Biochemistry **44**(10): 3972-3981.

Vella, F. (1992). "Introduction to protein structure. By C Branden and J Tooze. pp 302. garland publishing, New York. 1991 ISBN 0–8513–0270–3 (pbk)." Biochemical Education **20**(2): 121-122.

Vologodskii, A. V. and N. R. Cozzarelli (1994). "Conformational and thermodynamic properties of supercoiled DNA." Annu Rev Biophys Biomol Struct **23**: 609-643.

Walker, J. E., M. Saraste, M. J. Runswick and N. J. Gay (1982). "Distantly related sequences in the alpha- and beta-subunits of ATP synthase, myosin, kinases and other ATP-requiring enzymes and a common nucleotide binding fold." Embo j **1**(8): 945-951.

Wallis, J. W., G. Chrebet, G. Brodsky, M. Rolfe and R. Rothstein (1989). "A hyper-recombination mutation in S. cerevisiae identifies a novel eukaryotic topoisomerase." Cell **58**(2): 409-419.

Wang, J. C. (1969). "Variation of the average rotation angle of the DNA helix and the superhelical turns of covalently closed cyclic λ DNA." Journal of Molecular Biology **43**(1): 25-39.

Wang, J. C. (1971). "Interaction between DNA and an Escherichia coli protein ω." Journal of Molecular Biology **55**(3): 523-IN516.

Wang, J. C. (1996). "DNA topoisomerases." Annu Rev Biochem **65**: 635-692.

Wang, J. C. (1998). "Moving one DNA double helix through another by a type II DNA topoisomerase: the story of a simple molecular machine." Q Rev Biophys **31**(2): 107-144.

Wang, J. C. (2002). "Cellular roles of DNA topoisomerases: a molecular perspective." Nat Rev Mol Cell Biol **3**(6): 430-440.

Wang, J. C., P. R. Caron and R. A. Kim (1990). "The role of DNA topoisomerases in recombination and genome stability: a double-edged sword?" Cell **62**(3): 403-406.

Wang, J. C. and L. F. Liu (1979). Chapter II - DNA Topoisomerases: Enzymes That Catalyze the Concerted Breaking and Rejoining of DNA Backbone Bonds. Molecular Genetics. J. H. Taylor, Academic Press**:** 65-88.

Wansink, D. G., W. Schul, I. van der Kraan, B. van Steensel, R. van Driel and L. de Jong (1993). "Fluorescent labeling of nascent RNA reveals transcription by RNA polymerase II in domains scattered throughout the nucleus." J Cell Biol **122**(2): 283-293.

Wasserman, R. A., C. A. Austin, L. M. Fisher and J. C. Wang (1993). "Use of yeast in the study of anticancer drugs targeting DNA topoisomerases: expression of a functional recombinant human DNA topoisomerase II alpha in yeast." Cancer Res **53**(15): 3591-3596.

Wasserman, R. A. and J. C. Wang (1994). "Mechanistic studies of amsacrine-resistant derivatives of DNA topoisomerase II. Implications in resistance to multiple antitumor drugs targeting the enzyme." Journal of Biological Chemistry **269**(33): 20943-20951.

Watanabe, M., K. Tsutsui, K. Tsutsui and Y. Inoue (1994). "Differential expressions of the topoisomerase II alpha and II beta mRNAs in developing rat brain." Neurosci Res **19**(1): 51-57.

Wei, H., A. J. Ruthenburg, S. K. Bechis and G. L. Verdine (2005). "Nucleotide-dependent domain movement in the ATPase domain of a human type IIA DNA topoisomerase." J Biol Chem **280**(44): 37041-37047.

Wells, N., C. Addison, A. Fry, R. Ganapathi and I. Hickson (1994). "Serine 1524 is a major site of phosphorylation on human Topoisomerase IIα protein in vivo and is a substrate for casein kinase II in vitro." The Journal of biological chemistry **269**: 29746-29751.

Wells, N. J., A. M. Fry, F. Guano, C. Norbury and I. D. Hickson (1995). "Cell cycle phase-specific phosphorylation of human topoisomerase II alpha. Evidence of a role for protein kinase C." J Biol Chem **270**(47): 28357-28363.

Wells, N. J. and I. D. Hickson (1995). "Human Topoisomerase IIα is Phosphorylated in a Cell-Cycle Phase-Dependent Manner by a Proline-Directed Kinase." European Journal of Biochemistry **231**(2): 491-497.

Wendorff, T. J., B. H. Schmidt, P. Heslop, C. A. Austin and J. M. Berger (2012). "The structure of DNA-bound human topoisomerase II alpha: conformational mechanisms for coordinating inter-subunit interactions with DNA cleavage." J Mol Biol **424**(3-4): 109-124.

Wessel, I., L. H. Jensen, P. B. Jensen, J. Falck, A. Rose, M. Roerth, J. L. Nitiss and M. Sehested (1999). "Human small cell lung cancer NYH cells selected for resistance to the bisdioxopiperazine topoisomerase II catalytic inhibitor ICRF-187 demonstrate a functional R162Q mutation in the Walker A consensus ATP binding domain of the alpha isoform." Cancer Res **59**(14): 3442-3450.

Wessel, I., L. H. Jensen, A. Renodon-Corniere, T. K. Sorensen, J. L. Nitiss, P. B. Jensen and M. Sehested (2002). "Human small cell lung cancer NYH cells resistant to the

bisdioxopiperazine ICRF-187 exhibit a functional dominant Tyr165Ser mutation in the Walker A ATP binding site of topoisomerase II alpha." FEBS Lett **520**(1-3): 161-166.

Wessel, I., P. B. Jensen, J. Falck, S. E. Mirski, S. P. Cole and M. Sehested (1997). "Loss of amino acids 1490Lys-Ser-Lys1492 in the COOH-terminal region of topoisomerase IIα in human small cell lung cancer cells selected for resistance to etoposide results in an extranuclear enzyme localization." Cancer research **57**(20): 4451-4454.

West, K. L. and C. A. Austin (1999). "Human DNA topoisomerase IIβ binds and cleaves four-way junction DNA in vitro." Nucleic Acids Research **27**(4): 984-992.

West, K. L., E. L. Meczes, R. Thorn, R. M. Turnbull, R. Marshall and C. A. Austin (2000). "Mutagenesis of E477 or K505 in the B' domain of human topoisomerase II beta increases the requirement for magnesium ions during strand passage." Biochemistry **39**(6): 1223-1233.

West, K. L., R. M. Turnbull, E. Willmore, J. H. Lakey and C. A. Austin (2002). "Characterisation of the DNA-dependent ATPase activity of human DNA topoisomerase IIbeta: mutation of Ser165 in the ATPase domain reduces the ATPase activity and abolishes the in vivo complementation ability." Nucleic acids research **30**(24): 5416-5424.

White, J. H. and N. R. Cozzarelli (1984). "A simple topological method for describing stereoisomers of DNA catenanes and knots." Proc Natl Acad Sci U S A **81**(11): 3322-3326.

Wigley, D. B., G. J. Davies, E. J. Dodson, A. Maxwell and G. Dodson (1991). "Crystal structure of an N-terminal fragment of the DNA gyrase B protein." Nature **351**(6328): 624-629.

Wilkins, M. R., E. Gasteiger, A. Bairoch, J. C. Sanchez, K. L. Williams, R. D. Appel and D. F. Hochstrasser (1999). "Protein identification and analysis tools in the ExPASy server." Methods Mol Biol **112**: 531-552.

Williams, C. J., J. J. Headd, N. W. Moriarty, M. G. Prisant, L. L. Videau, L. N. Deis, V. Verma, D. A. Keedy, B. J. Hintze, V. B. Chen, S. Jain, S. M. Lewis, W. B. Arendall, 3rd, J. Snoeyink, P. D. Adams, S. C. Lovell, J. S. Richardson and D. C. Richardson (2018). "MolProbity: More and better reference data for improved all-atom structure validation." Protein Sci **27**(1): 293-315.

Willmott, C. J. and A. Maxwell (1993). "A single point mutation in the DNA gyrase A protein greatly reduces binding of fluoroquinolones to the gyrase-DNA complex." Antimicrobial Agents and Chemotherapy **37**(1): 126-127.

Winter, G., C. M. Lobley and S. M. Prince (2013). "Decision making in xia2." Acta Crystallogr D Biol Crystallogr **69**(Pt 7): 1260-1273.

Winter, G., D. G. Waterman, J. M. Parkhurst, A. S. Brewster, R. J. Gildea, M. Gerstel, L. Fuentes-Montero, M. Vollmar, T. Michels-Clark, I. D. Young, N. K. Sauter and G. Evans (2018). "DIALS: implementation and evaluation of a new integration package." Acta Crystallogr D Struct Biol **74**(Pt 2): 85-97.

Wittig, B., S. Wölfl, T. Dorbic, W. Vahrson and A. Rich (1992). "Transcription of human c-myc in permeabilized nuclei is associated with formation of Z-DNA in three discrete regions of the gene." Embo j **11**(12): 4653-4663.

Woessner, R. D., T. D. Chung, G. A. Hofmann, M. R. Mattern, C. K. Mirabelli, F. H. Drake and R. K. Johnson (1990). "Differences between normal and ras-transformed NIH-3T3 cells in expression of the 170kD and 180kD forms of topoisomerase II." Cancer Res **50**(10): 2901-2908.

Woessner, R. D., M. R. Mattern, C. K. Mirabelli, R. K. Johnson and F. H. Drake (1991). "Proliferation- and cell cycle-dependent differences in expression of the 170 kilodalton and 180 kilodalton forms of topoisomerase II in NIH-3T3 cells." Cell Growth Differ **2**(4): 209-214.

Wong, R. H., I. Chang, C. S. Hudak, S. Hyun, H. Y. Kwan and H. S. Sul (2009). "A role of DNA-PK for the metabolic gene regulation in response to insulin." Cell **136**(6): 1056-1072.

Worland, S. T. and J. C. Wang (1989). "Inducible overexpression, purification, and active site mapping of DNA topoisomerase II from the yeast Saccharomyces cerevisiae." J Biol Chem **264**(8): 4412-4416.

Wu, C. C., T. K. Li, L. Farh, L. Y. Lin, T. S. Lin, Y. J. Yu, T. J. Yen, C. W. Chiang and N. L. Chan (2011). "Structural basis of type II topoisomerase inhibition by the anticancer drug etoposide." Science **333**(6041): 459-462.

Wu, C. C., Y. C. Li, Y. R. Wang, T. K. Li and N. L. Chan (2013). "On the structural basis and design guidelines for type II topoisomerase-targeting anticancer drugs." Nucleic Acids Res **41**(22): 10630-10640.

Xia, W., J. Hu, J. Ma, J. Huang, T. Jing, L. Deng, J. Zhang, N. Jiang, D. Ma and Z. Ma (2019). "Mutations in TOP2B cause autosomal-dominant hereditary hearing loss via inhibition of the PI3K-Akt signalling pathway." FEBS Letters **593**(15): 2008-2018.

Yang, X., W. Li, E. D. Prescott, S. J. Burden and J. C. Wang (2000). "DNA topoisomerase IIbeta and neural development." Science **287**(5450): 131-134.

Yoshida, M. M. and Y. Azuma (2016). "Mechanisms behind Topoisomerase II SUMOylation in chromosome segregation." Cell cycle (Georgetown, Tex.) **15**(23): 3151-3152.

Yu, X., J. W. Davenport, K. A. Urtishak, M. L. Carillo, S. J. Gosai, C. P. Kolaris, J. A. W. Byl, E. F. Rappaport, N. Osheroff, B. D. Gregory and C. A. Felix (2017). "Genome-wide TOP2A DNA cleavage is biased toward translocated and highly transcribed loci." Genome Res **27**(7): 1238-1249.

Zechiedrich, E. L., K. Christiansen, A. H. Andersen, O. Westergaard and N. Osheroff (1989). "Double-stranded DNA cleavage/religation reaction of eukaryotic topoisomerase II: evidence for a nicked DNA intermediate." Biochemistry **28**(15): 6229-6236.

Zechiedrich, E. L., A. B. Khodursky and N. R. Cozzarelli (1997). "Topoisomerase IV, not gyrase, decatenates products of site-specific recombination inEscherichia coli." Genes & development **11**(19): 2580-2592.

Zhang, S., X. Liu, T. Bawa-Khalfe, L. S. Lu, Y. L. Lyu, L. F. Liu and E. T. Yeh (2012). "Identification of the molecular basis of doxorubicin-induced cardiotoxicity." Nat Med **18**(11): 1639-1642.

Zheng, H., D. R. Cooper, P. J. Porebski, I. G. Shabalin, K. B. Handing and W. Minor (2017). "CheckMyMetal: a macromolecular metal-binding validation tool." Acta Crystallogr D Struct Biol **73**(Pt 3): 223-233.